

EUROPEAN MASS SPECTROMETRY

THE INTERNATIONAL JOURNAL IN MOLECULAR SCIENCE

IN THIS ISSUE:

REARRANGEMENT BY INTERMEDIATE ION/NEUTRAL COMPLEXES

DYNAMICAL PARAMETERS OF ION EJECTION AND ION FORMATION IN MALDI

β -CYCLODEXTRIN NON-COVALENT INCLUSION COMPLEXES

VOLUME 1 NUMBER 1

JANUARY/FEBRUARY 1995

ISSN 1356-1049

IMPublications

EUROPEAN MASS SPECTROMETRY

IM Publications, 6 Charlton Mill, Charlton, Chichester,
West Sussex PO18 0HY, United Kingdom.

Tel: +44(0)1243-811334, Fax: +44(0)1243-811711,
E-mail: 100136,1577 (CompuServe), ian.michael@
impub.demon.co.uk (Internet).

Editorial Advisory Board

Professor A. Benninghoven (*Munster*)
Professor U. Boesl (*Munich*)
Dr R.D. Bowen (*Bradford*)
Dr F.H. Cottee (*SmithKline Beecham*)
Professor C.E. Costello (*Boston, MA*)
Professor J.H. Futrell (*Delaware*)
Dr S. Hammerum (*Copenhagen*)
Professor V. Hanus (*Prague*)
Professor R. Kaufmann (*Dusseldorf*)
Professor H. Nakata (*Aichi Kyoiku*)
Professor M. Przybylski (*Konstanz*)
Professor L. Radom (*Canberra*)
Professor B. Rozynov (*US EPA*)
Professor D.H. Russell (*Texas A&M, TX*)
Professor J. Scrivens (*ICI Wilton*)
Professor A. Selva (*Milan*)
Dr M. Sheil (*Wollongong*)
Professor J.F.J. Todd (*Kent*)
Professor A. Tatematsu (*Nagoya*)
Professor J.K. Terlouw (*Hamilton, ON*)
Professor J.C. Traeger (*La Trobe*)
Professor P. Traldi (*Padua*)
Professor M. Tsuchiya (*Yokohama*)
Professor V.G. Zaikin (*Russian Academy of Sciences*)

Managing Board

Chairman

Professor Allan Maccoll
*Department of Chemistry, University College London,
20 Gordon Street, London WC1H 0AJ, UK.*

Deputy Chairman

Professor Hans-Friedrich Grützmacher*
*Fakultät für Chemie, Universität Bielefeld, Postfach 10
01 31, D-33501 Bielefeld, Germany.*

Professor Oleg S. Chizhov*

*N.D. Zelinsky Institute of Organic Chemistry, Russian
Academy of Sciences, Leninsky Prospekt 47, 117334
Moscow, Russia.*

Professor Peter J. Derrick*

*Institute of Mass Spectrometry and Department of
Chemistry, University of Warwick, Coventry CV4 7AL,
UK.*

Professor Jürgen Grotemeyer*

*Institut für Physikalische Chemie, Universität Wür-
zburg, Marcusstrasse 9/11, D-97070 Würzburg, Ger-
many.*

Professor John L. Holmes*

*Department of Chemistry, University of Ottawa, 10
Marie Curie, PO Box 450 Stn A, Ottawa, ON K1N 6N5,
Canada.*

Professor Keith R. Jennings

*Institute of Mass Spectrometry and Department of
Chemistry, University of Warwick, Coventry CV4 7AL,
UK.*

Professor Mamoru Ôhashi*

*Department of Chemistry, University of Electro-Com-
munications, 1-5-1 Chofugaoka, Chofu, Tokyo 182,
Japan*

Professor Jean-Claude Promé

*Institut de Pharmacologie et de Biologie Structurale,
CNRS, 205 Route de Narbonne, F-31077 Toulouse
Cedex, France.*

Professor Douglas P. Ridge*

*Department of Chemistry and Biochemistry, University
of Delaware, Newark, Delaware 19716, USA.*

Professor Einar Uggerud*

*Kjemisk Institutt, Universitetet i Oslo, Postboks 1033,
Blindern, N-0315 Oslo, Norway.*

Submission of articles

Authors intending to submit an article for publication should consult the Instructions for Authors available from the Publisher, members of the Managing Board or printed in the first issue of every volume. Manuscripts may be sent to any of the Managing Board operating an Editorial Office (indicated by an asterisk in the list above).



EUROPEAN MASS SPECTROMETRY

Aims and scope

European Mass Spectrometry (EMS) is devoted to the rapid publication of original research papers concerned with the mass spectrometry of biological, inorganic and organic samples. The scope of the journal encompasses: molecular ionisation and fragmentation, gas-phase ion chemistry, ion–molecule reactions and collisions, spectroscopy of gaseous ions, instrumentation, computers in mass spectrometry and original applications in the life sciences, environmental science and industry.

Topics of interest include experimental and theoretical studies of structures, energetics and reactions of gaseous ions, ion formation from biological solids, determination of structure of biomolecules, mechanisms of ionic reactions, ionisation phenomena, electrospray ionisation (ESI), matrix-assisted laser desorption ionisation (MALDI), mass spectrometry of polymers, reactions of metal ions, reactions of ions at surfaces, multi-photon ionisation and dissociation, time-of-flight (TOF), tandem mass spectrometry, Fourier transform ion cyclotron resonance (FT-ICR) and theories of ion formation, structures and reactions.

© IM Publications 1995

All rights reserved. Apart from any fair dealing for the purposes of research or private study, or criticism or review, as permitted under the UK's Copyright, Designs and Patents Act 1988, this publication may be reproduced, stored or transmitted, in any form or by any means, only with the prior permission in writing of the publishers, or in the case of reprographic reproduction, in accordance with the terms of licences issued by the Copyright Licensing Agency. Enquiries concerning reproduction outside those terms should be sent to the publishers at the address above.

Subscription Details

European Mass Spectrometry is published six times a year. The subscription rates are £250.00 (delivery addresses in Europe) or US\$450.00 (delivery addresses outside Europe) for 1995. Subscriptions can only be accepted for a full calendar year, and should be ordered from the publishers, IM Publications, 6 Charlton Mill, Charlton, Chichester, West Sussex PO18 0HY, UK, Tel: +44(0)1243-811334, Fax: +44(0)1243-811711, or from your subscription agent.

Advertising

Advertising is accepted in *European Mass Spectrometry*, further details can be obtained from the Advertisement Manager, IM Publications, 6 Charlton Mill, Charlton, Chichester, West Sussex PO18 0HY, UK, Tel: +44 (0)1243-811334, Fax: +44 (0)1243-811711.

Imagesetting by Phil Payter Graphics, Portsmouth, UK. Printed in the UK by Selsey Press, Selsey.

Table of Contents

Editorial	1
Allan Maccoll	
Rearrangement by intermediate ion/neutral complexes during the McLafferty fragmentation of unsaturated ketones.....	3
Silvia Dohmeier-Fischer, Nicolai Krämer and Hans-Friedrich Grützmacher	
Positive-ion fast atom bombardment tandem mass spectrometry for characterization of sulfated unsaturated disaccharides from heparin and heparan sulfate	11
Tadashi Ii, Masayuki Kubota, Satoshi Okuda, Takashi Hirano and Mamoru Ohashi	
Collision-induced photon emissions from 8 keV polyatomic ions of composition $C_2H_4O^{+*}$ and $C_2H_5Cl^{+*}$	23
J.L. Holmes and P.M. Mayer	
The mechanism of alkene elimination from the oxonium ions $(CH_3CH_2)_2C=OH^+$, $CH_3CH_2CH_2(CH_3)C=OH^+$ and $(CH_3CH_2CH_2)_2C=OH^+$	33
Richard D. Bowen, Dennis Suh and Johan K. Terlouw	
Time-dependent mass spectra and breakdown graphs. 18. pyrene	41
Yun Ling, Yehiel Gotkis and Chava Lifshitz	
A mass spectral investigation of ethylenediaminetetraacetic acid	51
M.F. Duarte and M.H. Florêncio	
Fast atom bombardment and electrospray tandem mass spectrometry. Some fragmentation reactions in cyclic nitramines studied using collision-induced dissociation	59
Veronica Borrett, Ian J. Dagley, Michael Kony and Thomas Blumenthal	
Fast atom bombardment mass spectrometry of new polydentate Schiff bases. 3. The case of mono- and bis aldimine containing benzo-5-crown-5 groups.....	65
Elvio Bullita, Sergio Tamburini, Pietro Alessandro Vigato, Massimo Carbini, Silvia Catinella and Piero Traldi	
A new general fragmentation reaction in mass spectrometry: The hydrogen-carbon, carbon-carbon double rearrangement of 2-heteroalkyl substituted diphenylmethyl cations	73
Maria Concetta Natoli, Pasquale Agozzino, Leopoldo Ceraulo, Mirella Ferrugia and Liliana Lamartina	
Dynamical parameters of ion ejection and ion formation in matrix-assisted laser desorption/ionization	81
Volker Bökelmann, Bernhard Spengler and Raimund Kaufmann	
Cluster formation of biomolecules in the gas phase	95
Michael Dey and Jürgen Grotemeyer	
Letter: Support for the proposed observation by ionspray mass spectrometry of piroxicam/β-cyclodextrin and terfenadine/β-cyclodextrin non-covalent inclusion complexes	105
Antonio Selva, Enrico Redenti, Margherita Zanol, Paolo Ventura and Bruno Casetta	
Comment: A Reply to the comment on "Isodesmic reactions and thermochemistry of ions"	107
V.V. Takhistov and D.A. Ponomarev	

An asterisk* against the name of an author on the first page of a paper indicates the author to whom correspondence should be directed.

Editorial

“What! Another mass spectroscopic Journal” some readers will say. Yes it is. And here is the reason why. It is felt that there is a place for a journal of independent spirit, born in a mature cultural tradition, and that is just what *European Mass Spectrometry (EMS)* is going to provide. The unique organisation of the Journal will ensure, through its Managing Board, close contact between the Publisher and the authors and readers. Although European in conception, its aim is to publish original and important papers from every continent. A glance at the membership of the Managing Board, the Editorial Advisory Board and at the authors of the papers will show the international nature of the Journal.

The present time is redolent of the heady days of the winter of 1968 when the first mass spectrometric journal was launched. As Editor-in-Chief, along with an enthusiastic band of Regional Editors and of members of the Editorial Advisory Board, I was responsible for guiding the Journal for the first 22 years. On relinquishing the post, I was given the title of Founder Editor-in-Chief and so continued my association with the Journal. The years were happy ones, though not without stress at times. Journal publishing is strongly quantised. There are only two states—insufficient papers to fill a respectable issue or so many as to entail a backlog.

What are the differences between 1968 and 1995? In my first Editorial I commented upon the then state-of-the-art. Organic mass spectrometry reached maturity when the well-established concepts of mechanistic physical organic chemistry were applied to the interpretation of fragmentation behaviour under electron impact. In addition, at that time, “one of the very attractive features of the field of mass spectrometry ... was the camaraderie that existed between workers in the field”. The situation has now changed. In the first place the development of new ionization techniques such as neutralization–reionization multi-sector experiments, fast atom bombardment, electrospray and so on has radically extended

the range of compounds that can be subjected to mass spectrometric investigation. Much of the work involves analysis of compounds sometimes with little attention, unfortunately, being paid to the physics/chemistry of the underlying processes. While all such papers are of considerable practical importance some may contribute less to the understanding of mass spectrometric processes. Second, the number of workers in the field has expanded enormously—to such an extent that it is no longer easy to keep abreast of what other workers are doing, except in fields closely related to one’s own. This makes the literature of extreme importance. Significantly, where there is not a difference between 1968 and 1995 is in the need for the recognition of mass spectrometry as a scholarly pursuit of high repute. Multi-disciplinary fields in all areas of science pose a special challenge of maintaining standards. To adapt the old adage a mass spectrometrists could be said to “talk chemistry to physicists and physics to chemists”. While amusing, this contains more than a grain of truth. Meeting this challenge of maintaining an objective evaluation of material submitted will be the primary object of the editorial team. And I am confident, knowing the people involved, that it will be met.

European Mass Spectrometry has assembled a group of Editors and an Editorial Advisory Board all members of which have had wide experience in editing and advising. The team is enthusiastic and hard working which bodes well for the success of the Journal. We have a publisher who is sympathetic to the needs of the mass spectrometric community and who is forward looking. So all is set fair for the success of *EMS*. But in the long run this success depends on you, the authors and readers of the journal.

Allan Maccoll
Chairman, Managing Board

Rearrangement by intermediate ion/neutral complexes during the McLafferty fragmentation of unsaturated ketones

Silvia Dohmeier-Fischer, Nicolai Krämer and Hans-Friedrich Grützmacher*

Lehrstuhl I für Organische Chemie, Fakultät für Chemie der Universität Bielefeld, PO Box 10 01 31, D-33501 Bielefeld, Germany.

The fragmentation of 1-phenylhex-5-ene-1-one **1** was studied by mass analyzed ion kinetic energy spectrometry of its deuterium and ^{13}C carbon labelled derivatives as a further example of interactions within ion/neutral complexes. The analysis of the MIKE spectra demonstrate two important reaction channels of metastable molecular ions. The first one is a McLafferty rearrangement by elimination of a 1,3-butadiene molecule. The second energetically even more favoured fragmentation corresponds to the loss of an ethyl radical. The MIKE spectra of labelled molecular ions, especially that of the ^{13}C carbon labelled compound, indicate a skeletal rearrangement specifically of the butenyl moiety of the alkyl side chain by interchanging the terminal carbon atoms C-6 and C-5 with the inner C atoms C-3 and C-4 prior to the loss of the ethyl radical. This specific skeletal rearrangement is explained by an internal return within an intermediate ion/neutral complex **f**, consisting of the acetophenone enol radical cation and the neutral butadiene, by addition of the enol radical cation to the remote double bond of the diene. The second reaction channel is the irreversible cyclization of an intermediate distonic ion **c** leading to the formation of an ionized ethyl- α -dihydronaphthol **d**. This ion is stabilized by loss of an ethyl radical resulting in protonated α -naphthol **e**.

Introduction

The fragmentation of radical cations of carbonyl compounds by transfer of a hydrogen atom from the γ -position to the carbonyl-O and cleavage of the α,β -bond, i.e. the *McLafferty rearrangement*,¹ is one of the most reliable and useful mass spectrometric fragmentation mechanisms for structural analysis of organic compounds. The mechanism of this fragmentation has been studied much in detail,² and it has been shown that typically the fragmentation occurs by at least two reaction steps, the transfer of the γ -hydrogen atom to the carbonyl oxygen resulting in a γ -distonic ion and the subsequent bond cleavage to an enol and an alkene with the charge residing at the product of lowest ionization energy. The formation of an intermediate γ -distonic ion during the process provides a rationale for the apparent loss of site specificity of the hydrogen atom transferred in long-lived radical cations fragmenting as metastable ions in the mass spectrometer.

In 1980 Longevialle and Botter³ described the fragmentation of molecular ions of amino steroids via a complex of the ionized and neutral fragment resulting from the mass spectrometric bond cleavages. In the mean time there is overwhelming experimental evidence⁴ for fragmentations via intermediate ion/neutral complexes in particular of long-lived and low energy ions studied by metastable ion techniques,⁵

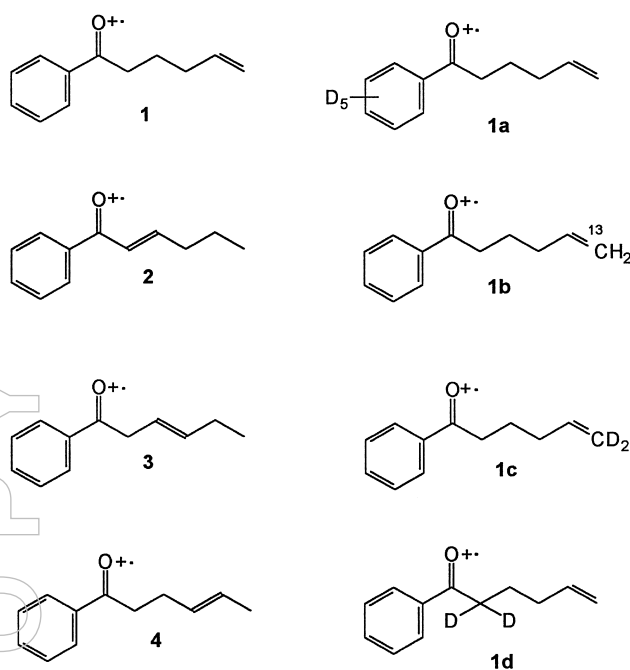
and the conditions essential for an intercession of these complexes in the course of unimolecular fragmentations of gaseous ions have been discussed thoroughly.⁶ It has also been shown that similar intramolecular reactions can be observed in molecular clusters after photoionization.⁷ The mobility of the components within low energy ion/neutral complexes arising from unimolecular fragmentations of metastable ions is apparently quite large. Although most of the mass spectrometric fragmentations mediated by ion/neutral complexes are hydrogen abstractions by a leaving radical next to the point of initial bond cleavage⁸ the observation of Longevialle and co-workers^{3,9} as well as examples reported by Audier *et al.*,¹⁰ Kuck *et al.*¹¹ and by our group¹² clearly demonstrate long-range interactions by rotations of the components within the ion/neutral complex. These results prove that the ion explores distant regions of the neutral component for energetically favourable reactions.

The bond breaking step of the γ -distonic ion during the McLafferty rearrangement of a ketone molecular ion may result in an ion/neutral complex consisting of an enol and an alkene with the charge residing on the component with the lowest ionization energy. Fast bimolecular addition reactions are observed between the radical cations of enol ethers and alkenes.¹³ Thus, an "internal return" of the components of the

intermediate ion/neutral complex of a McLafferty rearrangement yielding the original γ -distonic ion as well as a rearranged new γ -distonic ion is feasible. Following our first report¹⁴ of an internal return of intermediate enol radical cation/alkene complexes the role of intermediate ion/neutral complexes generated by the McLafferty rearrangement has been confirmed¹⁵ and has been examined in detail by theoretical and experimental methods.^{16,17} Although these studies clearly show that ionized enols add to alkenes forming γ -distonic ions or even ionized cyclobutanols¹⁷ the rearrangement of ketone molecular ions by a formal 1,2-enol shift can also be described by conventional mechanisms.¹⁸ It is therefore of interest to look for examples where the enol shift has to occur over larger molecular distances. Candidates for this type of *long-range* rearrangement are molecular ions of unsaturated carbonyl compounds which fragment to an ionized enol and a diene (Scheme 1). Internal return of the corresponding ion/neutral complex may occur by reaction at the distant carbon double bond giving rise to a rearranged γ -distonic ion. After a preliminary inspection of some unsaturated ketones and esters we chose 1-phenylhex-5-ene-1-one (**1**) as a model compound. There is only one aliphatic chain involved in the McLafferty rearrangement of the molecular ions of this aromatic ketone giving rise to the enol of acetophenone and butadiene with the charge clearly staying with the aromatic enol. However, double bond migration along an aliphatic chain prior to decomposition is well known for alkene molecular ions, hence we included the double bond isomers **2**, **3** and **4** in this study. The course of the fragmentations of the molecular ions of **1** was observed by labelling with ¹³C and D and by using metastable ion techniques. The results show that the molecular ions of **1** fragment indeed after deep-sited rearrangements including an interchange of internal and terminal carbon atoms of the pentenyl side chain.

Experimental

The EI mass spectra were obtained by a Finnigan MAT CH5 D double focussing mass spectrometer¹⁹ using 70 eV electron energy, accelerating voltage 3 kV and a heated batch inlet system. The structures of compounds synthesized as described below were confirmed by ¹H NMR spectrometry

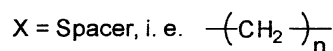
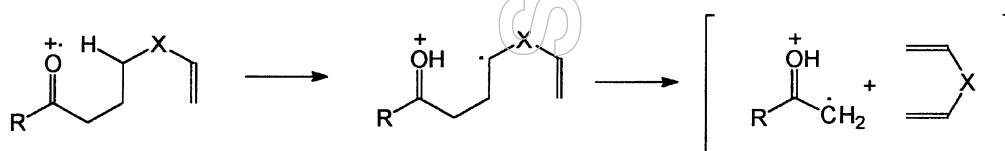


Structures.

using a Bruker AM 300 instrument²⁰ and CD₃Cl as solvent. All compounds were purified by distillation or column chromatography on silica gel (KG 60; 0.063–0.200 mm) with a mixture of petroleum ether/ethyl acetate (20 : 1) as eluents.

Compounds

1-Phenylhex-5-ene-1-one (1) was prepared by Grignard reaction of phenylmagnesium bromide with hex-5-enoic acid chloride in the presence of 3 mol% Fe(III)-acetyl-acetonate.²¹ ¹H NMR (CDCl₃): δ = 1.83 (2H, quint., ³J = 7 Hz, CH₂), 2.15 (2H, q., ³J = 7 Hz, CH₂), 2.99 (2H, t., ³J = 7 Hz, CH₂), 5.01 (2H, m., CH₂=CH), 5.68 (1H, m., CH₂=CH), 7.43 (2H, m., arom. H), 7.53 (1H, m., arom. H), 7.94 (2H, m., arom. H). MS (70 eV) see Table 1.



Scheme 1.

1-Phenylhex-2-ene-1-one (2) was obtained by aldol condensation of acetophenone and butanal²². ¹H NMR (CDCl₃): δ = 0.98 (3H, t., ³J = 7 Hz, CH₃), 1.57 (2H, sext., ³J = 7 Hz, CH₂), 2.30 (2H, dq., ³J = 7 Hz, ⁴J = 1 Hz, CH₂), 6.89 (1H, dt., ³J = 15 Hz, ⁴J = 1 Hz, CO–CH=CH–CH₂), 7.06 (1H, dt., ³J = 15 Hz, ³J = 7 Hz, CO–CH=CH–CH₂), 7.44–7.59 (3H, m., arom. H), 7.93 (2H, m., arom. H). MS (70 eV) see Table 1.

1-Phenylhex-3-ene-1-one (3) was synthesized by Grignard reaction of phenylmagnesium bromide with hex-3-enoic acid chloride in the presence of 3 mol% Fe(III)-acetylacetonate. CH₂Cl₂ was used for chromatography in this case. ¹H NMR (CDCl₃): δ = 0.99 (2H, t., ³J = 7 Hz, CH₃), 2.08 (2H, m., CH₂–CH=CH), 3.70 (2H, m., CH₂–CO), 5.67 (2H, m., CH=CH), 7.44–7.57 (3H, m., arom. H), 7.97 (2H, m. arom. H). MS (70 eV) see Table 1.

1-Phenylhex-4-ene-1-one (4) was prepared by heating methylvinylcarbinyl benzoylacetate for three hours at 240°C.²³ ¹H NMR (CDCl₃): δ = 1.65 (3H, m., CH₃), 2.43 (2H, m., CH₂–CH=CH), 3.04 (2H, t., ³J = 7 Hz CH₂–CO), 5.51 (2H, m., CH=C–H), 7.44–7.59 (3H, m., arom. H), 7.97 (2H, m., arom. H). MS (70 eV) see Table 1.

Labelled compounds

1-Pentadeuterophenylhex-5-ene-1-one (1a) was obtained analogously to **1** but by using pentadeuterophenylmagnesium bromide. %D-content >96% (by ¹H NMR).

6-¹³C-1-phenylhex-5-ene-1-one (1b) was synthesized by a Wittig reaction of 2-phenyl-2-(4-oxobutyl)-1,3-dioxolane and ¹³C-methylphosphonium iodide in THF using NaH as a base. Mol% ¹³C (by mass spectrometry): >90% ¹³C₁.

6-Dideutero-1-phenylhex-5-ene-1-one (1c) was prepared analogously to **1b** but by using trideuteromethylphosphonium iodide. Mol% D (by mass spectrometry): 42% d₂, 43% d₁, 15% d₀.

2-Dideutero-1-phenylhex-5-ene-1-one (1d) was obtained by exchanging the acidic H atoms next to the carbonyl group of **1** by treatment of **1** three times with excess D₂O/NaOD in THF. Mol% D (by mass spectrometry): 89% d₂, 10.5% d₁, 0.5% d₀.

MIKE spectra of the parent and fragment ions were measured by a Fisons VG ZAB 2F double focussing mass spectrometer²⁴ using 70 eV electron energy, electron trap current 100 μ A, 6 kV accelerating voltage and introduction of the samples by a home-made direct inlet system at ambient temperatures. The ions studied were focussed magnetically into the second field free region (2nd FFR) of the instrument and the ions arising in the 2nd FFR by unimolecular fragmentations were recorded by scanning the voltage across the electrostatic analyzer. Three spectra were measured to get the average intensities.

CA spectra were measured by a Fisons VG ZAB 2F Instrument and/or by a Fisons AutoSpec mass spectrometer²⁴ under the usual conditions. The ions studied were focussed magnetically into the field free region following the magnetic sector and were activated by collisions with Ar in the collision cell of that region. The pressure of the collision gas was adjusted

so that the main beam of ions was attenuated to 50%. The CID product ions were recorded by scanning the voltage across the electrostatic analyzer following the collision cell.

Results and discussion

The 70 eV EI mass spectra of the phenylketones **1–4** are shown in Table 1. As expected the signal of the benzoyl ions, *m/z* 105, is always the base peak in the mass spectra, and the decomposition of metastable ions show that the benzoyl ions are formed by α -cleavage of the molecular ions as well as by methyl loss from the McLafferty product ions at *m/z* 120. Besides the signals of this McLafferty product ion, *m/z* 120, and the molecular ions, *m/z* 174, the mass spectra exhibit distinct peaks of fragment ions *m/z* 159 and *m/z* 145 arising from losses of methyl and ethyl radicals, respectively, from the molecular ions. The formation of the McLafferty product ions from **2** and **3** entails H migration and double bond shifts along the pentenyl side chain of the ketone. Similarly, the elimination of an ethyl radical from **1** and **4** is only possible after rearrangements. The different relative abundances of these fragment ions, however, can be easily correlated with the fragmentation abilities of the original structures of the compounds. Thus, the rates of rearrangement by H migration and by fragmentation are similar for the molecular ions decomposing in the ion source.

Competition between rearrangement and fragmentation is corroborated by the MIKE spectra of **1–4** listed in Table 2. For convenience the relative intensities were normalized to the

Table 1. 70 eV mass spectra, characteristic signals of compounds **1** to **4**, relative intensities (%).

Compounds		1	2	3	4
M ⁺	<i>m/z</i> 174	17	28	16	11
M ⁺ –2	<i>m/z</i> 172	—	10	7	—
M ⁺ –15	<i>m/z</i> 159	1	5	5	3
M ⁺ –17	<i>m/z</i> 157	—	19	15	2
M ⁺ –29	<i>m/z</i> 145	2	10	7	5
M ⁺ –43	<i>m/z</i> 131	1	6	4	4
M ⁺ –54	<i>m/z</i> 120	48	7	1	8
M ⁺ –69	<i>m/z</i> 105	100	100	100	100
M ⁺ –77	<i>m/z</i> 77	46	51	36	33

intensity of ions *m/z* 105. The formation of this ion *m/z* 105 by α -cleavage is not influenced much by the specific structure of the pentenyl chain. Therefore, a normalization of the other fragment ion intensities to the ion *m/z* 105 intensity reflects clearly structural effects on the other fragmentation reactions. With the exception of **4** the MIKE spectra display a prominent

peak of the McLafferty product ion at m/z 120 of similar intensity. Further, the relative abundances of the ions m/z 145 formed by ethyl loss have increased considerably compared to the EI mass spectra proving that the loss of the ethyl radical from the molecular ions needs less energy than the McLafferty rearrangement. Both fragmentations require hydrogen migrations *prior* to decomposition and are expected to be more advanced in metastable ions but the distinct differences in the MIKE spectra of **1–4** show that an equilibrium mixture of ion structures is not achieved.

To detect fragmentations of the molecular ions of **1** by intermediate ion/neutral complexes the MIKE spectra of the labelled 1-phenylhex-5-ene-1-ones **1a–1d** were analyzed (Ta-

Table 2. MIKE spectra of the compounds **1–4**, relative peak intensities (%).

	1	T_{50}^a	2	T_{50}^a	3	T_{50}^a	4	T_{50}^a
m/z 173	108±4		204±9		95±9		19±1	
m/z 159	6±3		32±5		18±4		5±1	
m/z 156	3±2		—		—		2±1	50
m/z 145	42±3	65	156±5	61	120±17	33	32±3	50
m/z 133	10±3		9±1		5±2		—	
m/z 132	3±1		9±1		4±2		—	
m/z 131	3±1		9±1		6±3		3	±1
m/z 120	39±6	49	58±3	57	33±5	35	4±1	—
m/z 105	100±3	51	100±17	32	100±16	29	100±7	19

^aKinetic energy release (meV) determined at 50% peak height.

ble 3). In the MIKE spectrum of the pentadeuterophenyl derivative **1a** all peaks are clearly shifted by five mass units. Thus, the hydrogen atoms at the aromatic ring are not involved in the rearrangements and fragmentations. However, in the case of the derivatives **1c** and **1d** deuterated specifically at the pentenyl chain the MIKE spectra expose the expected H/D-migrations within the aliphatic moiety. In view of these hydrogen migrations the MIKE spectrum of the ¹³C-labelled compound **1b** is of special interest and more easy to analyze. This spectrum shows complete loss of the ¹³C-label for ions m/z 105, m/z 120 and m/z 133 as expected for α -cleavage at the carbonyl group, McLafferty rearrangement and allylic bond cleavage, respectively. Unexpectedly, however, the peaks due to loss of a methyl radical and an ethyl radical originally at m/z 159 and m/z 145 are split 1 : 1 into peaks at m/z 159/160 and at m/z 145/146. Obviously the ¹³C atom has migrated from its terminal position into an inner position of the pentenyl chain. For a perception of this rearrangement the structure of the $[M-C_2H_5]^+$ must be known.

In view of the energetically favourable transfer of an allylic hydrogen atom in the McLafferty rearrangement² and the

Table 3. MIKE spectra of the metastable molecular ions of the ketones **1a–1e** [relative to (m/z 105) peak intensities, %].

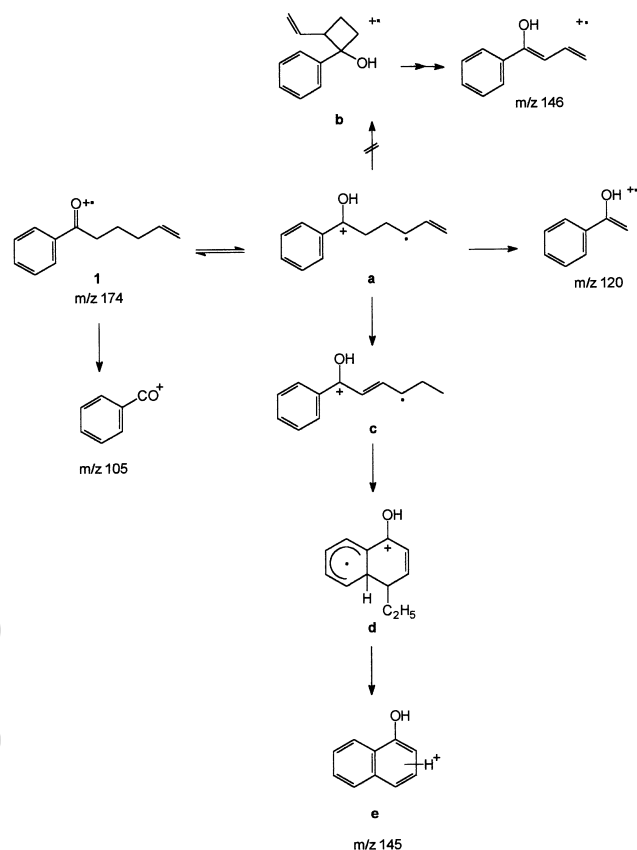
m/z	1a	1b	1c	1d	1e
105	100		100	100	100
110		100			
120	39		52	28	14
121				31	18
122					9
125		45			
131	3		4	6	1
132	3		3	4	4
133	10		12	6	4
134				9	6
135					1
136		6			
138		11			
145	42		17	15	15
146			17	17	10
147				7	8
150		34			
156	3				
157			2		1
158					3
159	6		3	5	1
160			3		3
161				5	
164		9			
173	108				
174			151		
175				132	132
177		25			
178		24			

stability of both rearrangement products the strong competition by the loss of an ethyl radical from metastable molecular ions of **1** is only possible if a stable ion m/z 145 is formed. It is known that the γ -distonic ion generated in the first step of a McLafferty rearrangement may rearrange further by a cyclization step. A cyclization of the phenyl substituted γ -distonic

ion **a** (Scheme 2) derived from the molecular ion **1** to an ionized cyclobutanol²⁵ **b** can be excluded because the expected fragmentation^{25d} of **b** into ions m/z 146 is not observed. However, it has been suggested that the molecular ions of alkyl phenyl ketones and of 1-tetralol interconvert²⁶ via the γ -distonic ion.^{26b} The cyclization of the phenyl substituted γ -distonic ions by attack of the phenyl group is followed by elimination of H_2O . Indeed, the MIKE spectrum of **1** exhibits a small peak at m/z 156 due to loss of H_2O . However, hydrogen rearrangements either before or after the cyclization of the γ -distonic ion **a** (Scheme 2) result eventually in an ionized ethyl- α -dihydronaphthol **d** which eliminates the ethyl side chain to form the very stable protonated α -naphthol **e**, m/z 145. It is significant that the ions $[\text{M}-\text{C}_2\text{H}_5]^+$ are particularly abundant in the MIKE spectra of **2** and **3** yielding α,β -unsaturated enol ions **c** (Scheme 2) prepared for the cyclization by less hydrogen migration steps from the respective molecular ions than **1**. Protonated α -naphthol **e** is the most stable ion m/z 145 which can be generated from **a**, and the formation of very stable ions by rearrangements is typical of the fragmentations of metastable ions.

To prove the structure of the $[\text{M}-\text{C}_2\text{H}_5]^+$ the CA spectra of this ion generated from **1** and of authentic protonated naphthol are compared in Figure 1. The CA spectrum of the $[\text{M}-\text{C}_2\text{H}_5]^+$ ions exhibits a better resolution owing to an increased total intensity, but otherwise both spectra are identical within the limits of error showing abundant losses of H_2O (m/z 127), of CO (m/z 117) and H_2CO (m/z 115). Clearly, protonated α -naphthol **e**, m/z 145, is eventually formed from the γ -distonic ion **a** by the route depicted in Scheme 2. Consequently, the result of the ^{13}C labelling showing an 1 : 1 loss of C_2H_5 and $^{13}\text{CCH}_3$ from metastable ions **1b** proves unequivocally an exchange of the atoms C(3)–C(6) of the pentenyl group in the γ -distonic ion **a**. Definitely no ^{13}C incorporation is observed for the McLafferty product ion m/z 120, so the terminal $^{13}\text{C}(6)$ atom of **1b** must have exchanged either with C(3) or C(4) to yield the statistical label distribution. This is convincingly explained only by an internal return of an intermediate ion/neutral complex **f** (Scheme 3) consisting of the enol radical cation of acetophenone and butadiene, the products of the McLafferty rearrangement shown in Scheme 3. Obviously, those ion/neutral complexes **f** decomposing slowly because of a small internal energy prefer the internal return to the γ -distonic ion **a** and fragment eventually via the cyclization mechanism of Scheme 2 by loss of an ethyl radical. On route, the butadiene in the intermediate ion/neutral complex **f** must have been rotated freely so that addition of the acetophenone enol radical cation occurs with equal probability at both double bonds (Scheme 3). To our knowledge this is the first example of an enol radical cation shift along a polyene chain, as anticipated by the peculiar properties of ion/neutral complexes as intermediates of unimolecular fragmentations of metastable ions.

A MNDO calculation of the enthalpies of the competing reactions shows that the formation of protonated naphthol **e** by loss of an ethyl radical from **1** needs indeed distinctly less



Scheme 2.

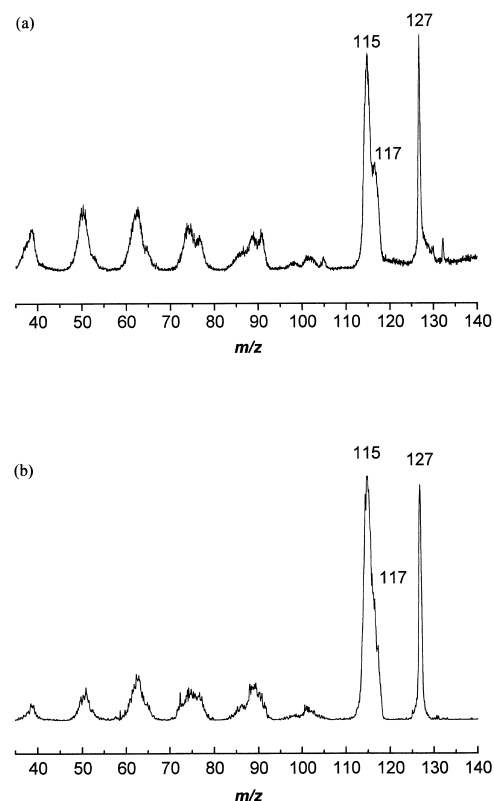
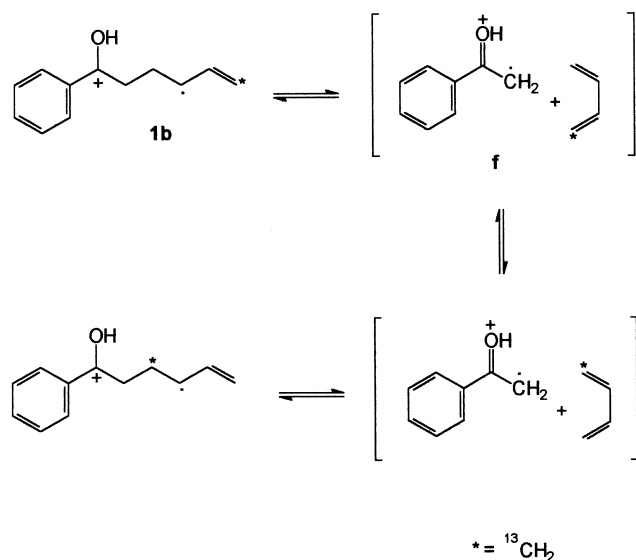


Figure 1. (a) CA spectrum of the $[\text{M}-\text{C}_2\text{H}_5]^+$ ion (m/z 145) generated from **1**. (b) CA spectrum of m/z 145 generated from protonated α -Naphthol.



Scheme 3.

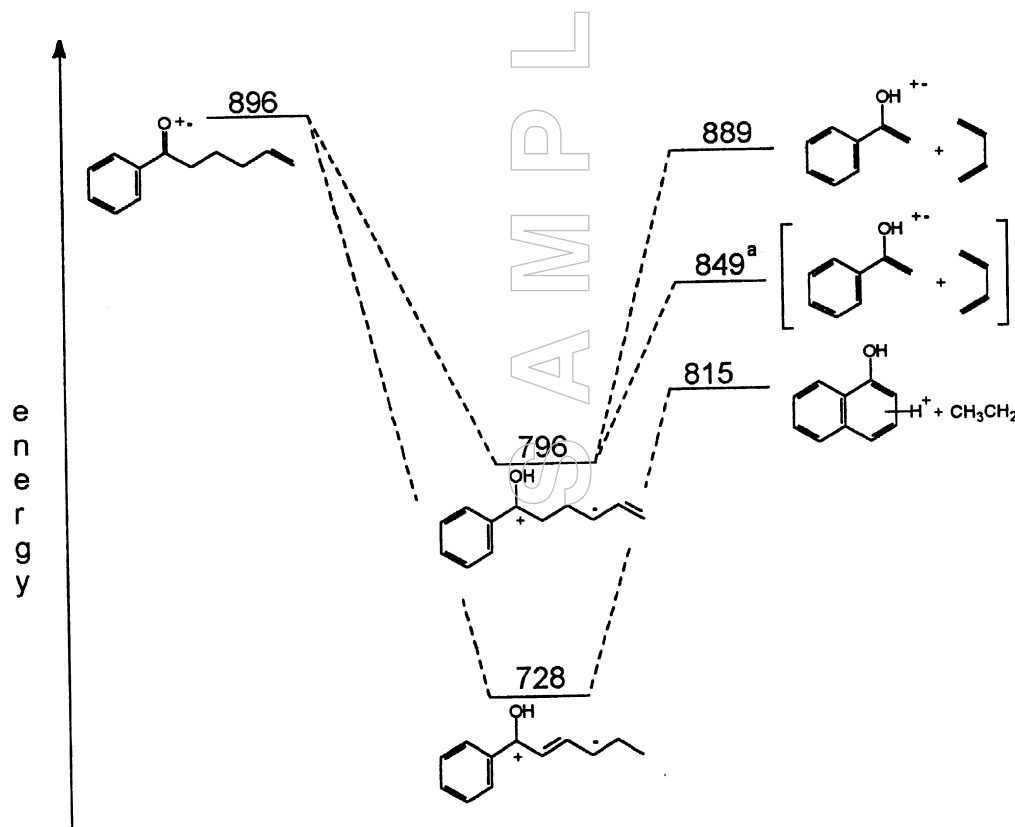
Table 4. Enthalpies of formation (kJ mol^{-1}).

	ΔH_f^a	ΔH_f
1	896	
Butadiene		110 ^b
Ethyl radical		117 ^b
α -naphthol/ H^+	698	623 ^c
Acetophenone enol ⁺⁺	779	731 ^d
Distonic ion a	796	
Radical cation c	728	

^aCalculated by MNDO, ^bexperimental, ²⁸ ^cestimated by isodesmic reactions and ^dexperimental.²⁷

energy than the McLafferty rearrangement (Scheme 4). The calculated ΔH_f of relevant distonic ions **a**, **c**, protonated naphthol **e** and acetophenone enol radical cation are listed in Table 4. For the latter ion ΔH_f is available from experiments,^{27,28} and ΔH_f (Naphthol/ H^+) can be estimated from the experimental proton affinity of phenol via isodesmic reactions. In both cases the experimentally based ΔH_f values are

significantly lower. However, the *relative* ΔH_f are expected to be more reliable and more practical for a discussion of competing reactions. The difference between the reactions enthalpies of the McLafferty and of the loss of an ethyl radical from molecular ions of **1** is 101 kJ mol^{-1} by the experimental data and 74 kJ mol^{-1} by calculation in favor of the ethyl loss. Even taking into account an electrostatic stabilization energy of 40



Scheme 4. MNDO calculated enthalpies of reaction (kJ mol^{-1}). ^aThe energy of the complex is calculated by the Average Dipole Orientation theory, assuming a distance of 3.5 Å.

kJ mol^{-1} of the intermediate ion/neutral complex (calculated by the ADO potential for a distance of 3.5 Å between center of the acetophenone enol radical ion and the butadiene) the loss of ethyl and formation of protonated naphthol **e** from the ion/neutral complex is still exothermic. Furthermore, the distonic ion **a**, which is the first intermediate of the McLafferty rearrangement, is clearly more stable than the molecular ion of **1**, and the McLafferty reaction products. This latter situation favors an internal return of intermediate ion/neutral complexes of low internal energy. Finally, the MNDO calculation reveals that a rearrangement of the distonic ion **a** to the radical cation **c** by hydrogen migrations is distinctly exothermic. Ion **c** is the key intermediate for the formation of the protonated naphthol **e** via a cyclization of **c** to a dihydronaphthalene structure. Thus, the MNDO calculation corroborates the fragmentation mechanism depicted in Scheme 2 and the transposition of the pentenyl side chain by an internal return within an intermediate complex of the ionized acetophenone enol and neutral 1,3-butadiene.

The interpretation of the results of the D-labelling experiments is more elaborate. As mentioned before the H(D) atoms at the aromatic ring do not exchange with H(D) atoms of the pentenyl moiety. This means that the cyclization step to the intermediate ions **d** is very likely irreversible and that H(D) migrations to generate the ethyl group eventually eliminated have to occur in **a** or **c** before cyclization. Otherwise H(D) atoms of the phenyl group should appear in the ethyl radical because in **d** the H(D) atoms at the phenyl group are expected to take part in the hydrogen shifts. This is not observed, however. The MIKE spectrum of **1c** deuterated at the terminal C(6) (Table 3) shows the formation of the nondeuterated and monodeuterated McLafferty product ions m/z 120 and m/z 121 in a ratio of 1 : 1.1 but no dideuterated ion at m/z 122. This establishes clearly a reversible formation of the γ -distonic ion **a** by a sequence of 1,5- and 1,7-H(D) shifts equilibrating the CH_2 groups at C(4) and the terminal C(6) by the delocalized allylic radical site of **a**. In contrast to this regiospecific H/D-exchange the loss of the ethyl radical is accompanied by more extensive H/D-exchanges. The most simple mechanism to generate a terminal ethyl group is a *specific* migration of one H atom from each of the C atoms in α - and β -position to the carbonyl-C atom of the γ -distonic ion **a** to the terminal vinyl group without any H/D-exchange. In this case the H/D-scrambling between C(4) and C(6) discussed before and the additional scrambling by internal return within the ion/neutral complex **f** (Scheme 3) would result in the loss of C_2H_5 , $\text{C}_2\text{H}_4\text{D}$ and $\text{C}_2\text{H}_3\text{D}_2$ in the ratio 5% : 47.5% : 47.5%. This is obviously not the case. Instead, the ratio 18% : 44% : 38% observed for the loss of C_2H_5 , $\text{C}_2\text{H}_4\text{D}$ and $\text{C}_2\text{H}_3\text{D}_2$ indicates much more H/D scrambling although the ratio 16.7% : 55.5% : 27.8% calculated for a statistical distribution of the two D in the pentenyl group is not reached *prior* to decomposition. These excessive H/D-exchanges have to take place in intermediates following the formation of the γ -distonic ion **a** and the ion/neutral complex **f** to account for the specific H/D exchange during the McLafferty rearrangement of **1c**. Likely candidates are ions **c**

and **d** with insufficient internal energy to decompose by the McLafferty reaction but still with enough energy to fragment by loss of an ethyl radical. This picture gets even more complicated if the results from the MIKE spectrum (Table 3) of **1d** deuterated at C(2) in α -position of the carbonyl group are included. Again the loss of the ethyl radical is accompanied by extensive H/D exchanges as in the case of **1c**, in agreement with H/D migrations in intermediates **c** and/or **d**. However, this time H/D exchanges precede also the McLafferty rearrangement although the H atoms at C(2) are not involved in this process and other H/D migrations within the ions of **1d** decomposing by the McLafferty reaction are in conflict with the results from **1c**. This dissension can be settled only by analyzing derivative specifically deuterated at all different positions of the pentenyl group and in addition by the “inversely” deuterated derivatives, because the results obtained here can be untangled only by assuming a strong influence of H/D isotope effects on the H/D exchange processes. Thus it appears, that the 1-phenylhexene-1-ones **1–4** are further examples of the complex rearrangements observed in ketone radical cations.

Conclusion

The analysis of the EI mass spectra and MIKE spectra of 1-phenylhexene-1-one **1**, of its isomers **2–4**, and of the deuterated derivatives **1a**, **1c** and **1d** show clearly extensive H migrations within the pentenyl group *prior* to a decomposition by α -cleavage forming a benzoyl ion, by a McLafferty rearrangement, and by loss of an ethyl radical. The extent of H/D migration observed during the McLafferty rearrangement and the ethyl elimination differ distinctly proving irreversible branching between the two reaction channels. The loss of the ethyl radical corresponds to the energetically very favourable formation of a protonated α -naphthol predominating particularly in the MIKE spectra of **2** and **3**. An irreversible cyclization by attack of the pentenyl side chain on the phenyl group of the enol radical cations **c** arising from **a** by hydrogen migrations within the pentenyl group is proposed as the key step for this process.

Even more important, however, is the observation from the MIKE spectrum of the ^{13}C labelled derivative **1b** proving unambiguously a specific skeletal rearrangement of the pentenyl side chain of the 1-phenylhexene-1-one radical cation preceding the ethyl loss. In line with earlier observations of intermediate ion/neutral complexes^{14,15} during the McLafferty rearrangement the obvious explanation for this skeletal reorganization is an internal return within the ion/neutral complex formed by the McLafferty products of **1**, the enol radical cation of acetophenone and 1,3-butadiene. In this complex attack of the radical cation to restore the γ -distonic ion **a** occurs equally at both double bonds of the 1,3-butadiene leading eventually to an equilibration between C(3) and the terminal C(6) of the hexenone **1**. Rearrangement of the equilibrated γ -distonic ion **a** into the more stable ion **c** and cyclization of this ion eventually give rise to the observed 1 : 1 loss of ethyl

and ^{13}C -ethyl from **1b**. Thus, the fragmentations of the radical cations derived from 1-phenylhexene-1-ones are a further example of the Longevialle–Botter mechanisms including an intermediate ion/neutral complex with freely rotating components.

Acknowledgement

The financial assistance of the Fonds der Chemischen Industrie is gratefully acknowledged.

References

1. a) F.W. McLafferty, *Chem. Ind.* (London), 1366 (1958); b) F.W. McLafferty, *Anal. Chem.* **31**, 82 (1959).
2. a) W. Carpenter, A.M. Duffield and C. Djerassi, *J. Am. Chem. Soc.* **90**, 160 (1968); b) H. Budzikiewicz, C. Djerassi and D.H. Williams, *Mass Spectrometry of Organic Compounds*. Holden Day, Inc., San Francisco, CA, USA, Ch. 3 a. 4 (1967).
3. P. Longevialle and R. Botter, *J. Chem. Soc., Chem. Commun.*, 823 (1980).
4. a) D.J. McAdoo, *Mass Spectrom. Rev.* **7**, 363 (1988); b) P. Longevialle, *Mass Spectrom. Rev.* **11**, 157 (1992).
5. see *Tandem Mass Spectrometry* (Ed. by F.W. McLafferty). John Wiley & Sons, New York (1983).
6. T.H. Morton, *Org. Mass Spectrom.* **27**, 353 (1992).
7. a) A.W. Castleman Jr, W.B. Tzeng, S. Wei and S. Morgan, *J. Chem. Soc. Faraday Trans.* **86**, 13, 2417 (1990); b) B. Brutschy, *J. Phys. Chem.* **94**, 8637 (1990); c) B. Brutschy, J. Eggert, C. Janes and H. Baumgärtel, *J. Phys. Chem.* **95**, 5041 (1991).
8. a) S. Hammerum and H.E. Audier, *Adv. Mass Spectrom.* **11A**, 894 (1988); b) J.C. Traeger, C.E. Hudson and D.J. McAdoo, *Int. J. Mass Spectrom. Ion Processes* **82**, 101 (1988).
9. P. Longevialle and R. Botter, *Int. J. Mass Spectrom. Ion Physics* **47**, 179 (1983).
10. H.E. Audier, C. Monteiro, P. Mourgues and D. Berthomieu, *Org. Mass Spectrom.* **25**, 245 (1990).
11. C. Matthias and D. Kuck, *Org. Mass Spectrom.* **28**, 1073 (1993).
12. a) U. Filges and H.-F. Grützmacher, *Int. J. Mass Spectrom. Ion Processes* **83**, 93 (1988); b) U. Zalfen and H.-F. Grützmacher, *Org. Mass Spectrom.* **25**, 323 (1990); c) G. Thielking and H.-F. Grützmacher, *J. Am. Chem. Mass Spectrom.* **3**, 417 (1992).
13. G.S. Groenewold and M.L. Gross, *J. Am. Chem. Soc.* **106**, 6575 (1984).
14. M. Masur, A. Sprafke and H.-F. Grützmacher, *Org. Mass Spectrom.* **22**, 307 (1987).
15. a) G. Bouchoux, J. Tortajada, J. Dagaut and J. Filiaux, *Org. Mass Spectrom.* **22**, 451 (1987); b) G. Bouchoux, F. Bidault, F. Djazi, B. Nicod and J. Tortajada, *Org. Mass Spectrom.* **22**, 748 (1987). c) C.E. Hudson, T. Lin and D.J. McAdoo, *Org. Mass Spectrom.* **22**, 311 (1988).
16. a) G. Bouchoux, Y. Hoppillard and J. Tortajada, *Int. J. Mass Spectrom. Ion Processes* **90**, 197 (1989); b) D.J. McAdoo, C.E. Hudson, C.E. Skyiepal, E. Broido and L.L. Griffin, *J. Am. Chem. Soc.* **109**, 7648 (1987).
17. a) P. Mourgues, C. Monteiro and H.E. Audier, *Org. Mass Spectrom.* **25**, 389 (1990); b) F. Berruyer and G. Bouchoux, *Rapid Commun. Mass Spectrom.* **4**, 476 (1990).
18. a) T. Weiske, H. Halim and H. Schwarz, *Chem. Ber.* **118**, 323 (1983); b) C.E. Hudson and D.J. McAdoo, *Org. Mass Spectrom.* **20**, 402 (1985); c) G. Bouchoux and Y. Hoppiliard, *Int. J. Mass Spectrom. Ion Phys.* **55**, 47 (1983).
19. Finnigan MAT GmbH, Bremen, Germany.
20. Bruker Analytische Meßtechnik GmbH, Rheinstetten/Karlsruhe, Germany.
21. V. Flandese, G. Marchese and L. Ronzini, *Tetrahedron Lett.*, 4850 (1984).
22. see H.G.O. Becker u.a., *Organikum* (19 Ed.). Barth, Dt. Verl. der Wiss., Leipzig, p. 469 (1993).
23. W. Kiemel and A.C. Cope, *J. Am. Chem. Soc.* **65**, 1992 (1943).
24. Fisons Instruments, VG Analytical, Manchester M23 9LE, GB.
25. a) H.E. Audier and C. Moustapha, *New J. Chem.* **6**, 101 (1982); b) P. Mourgues, C. Monteiro, H.E. Audier and S. Hammerum, *Org. Mass Spectrom.* **25**, 389 (1990); c) F. Berruyer and G. Bouchoux, *Rapid Commun. Mass Spectrom.* **4**, 476 (1990); d) J.-F. Rontani and C. Aubert, *Org. Mass Spectrom.* **28**, 795 (1993).
26. a) M.L. Gross, E. Chiu, D. Polorny and F.L. DeRoos, *Org. Mass Spectrom.* **12**, 55 (1977); b) P. Mourgues, J.P. Denhez, H.E. Audier and S. Hammerum, *Org. Mass Spectrom.* **28**, 193 (1993).
27. J.W. Dallinger, N.M.M. Nibbering and G.J. Louter, *Org. Mass Spectrom.* **16**, 183 (1981).
28. S.G. Lias, J.E. Liebman, J.L. Holmes, R.D. Levin and W.G. Mallard, *J. Phys. Chem. Ref. Data* **17**, Suppl. 1 (1988).

Received: 7 December 1994

Accepted: 7 January 1995

Positive-ion fast atom bombardment tandem mass spectrometry for characterization of sulfated unsaturated disaccharides from heparin and heparan sulfate

Tadashi Ii,^a Masayuki Kubota,^b Satoshi Okuda,^c Takashi Hirano^b and Mamoru Ohashi^{b*}

^aResearch and Development Laboratories, Soda Aromatic Co., Ltd, Noda-shi, Chiba 270-02, Japan.

^bDepartment of Applied Physics and Chemistry, The University of Electro-Communications, Chofu, Tokyo 182, Japan.

^cSchool of Agricultural Science, Nagoya University, Chikusa-ku, Nagoya 464-01, Japan.

Positive-ion fast atom bombardment tandem mass spectrometry has been used in the characterization of non-, mono-, di- and trisulfated disaccharides from heparin and heparan sulfate. The positional isomers of sulfate groups of monosulfated disaccharides have been distinguished from each other by positive-ion fast atom bombardment tandem mass spectra, which provide an easy way of identifying the positional isomers. The fast atom bombardment collision-induced dissociation mass spectrometry/mass spectrometry technique was also applied successfully to the characterization of di- and trisulfated disaccharides.

Introduction

Fast atom bombardment mass spectrometry (FABMS) is now a well-established method for the analysis of large and polar molecules, including glycoconjugates.^{1–3} Recently the tandem mass spectrometry (MS/MS) technique has also proven to be very useful in the structural analyses of glycoconjugates, providing information on sugar sequences and linkage positions.¹

Because of the acidic nature of sulfated saccharides, the negative-ion FABMS has been widely used in the structural studies of these compounds.^{5–10} However, several papers dealing with the analysis of sulfated oligosaccharides by positive-ion FABMS have been published.^{5,6,10} It has been reported that in positive-ion FABMS, CID (collision-induced dissociation)-MS/MS of lithiated disaccharide gave useful information on the differentiation of the linkage position in the five isomeric sugars.¹¹ Previously, we have successfully used CID-MS/MS in the positive-ion as well as the negative-ion modes for characterization of non-, mono-, di- and trisulfated disaccharides from chondroitin sulfate (CS), dermatan sulfate (DS) and hyaluronan (HA), having (1→3)-glycosidic bonds.¹⁰

In a proceeding paper, we have shown that the negative-ion FAB CID-MS/MS was very useful in the characterization of unsaturated disaccharide from heparin (Hep) and heparan sulfate (HS).¹² Here we report the characterization of a series of non-, mono-, di- and trisulfated unsaturated disaccharides from Hep and HS and three *N*-desulfated derivatives based on the positive-ion FAB CID-MS/MS.

Experimental

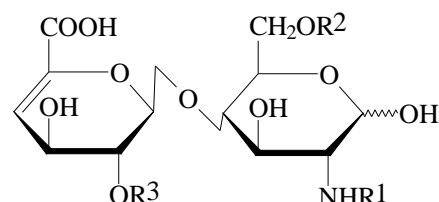
The unsaturated disaccharides investigated [2-acetamido-2-deoxy-4-*O*-(β -D-glucopyranosyluronic acid)-D-glucose (Δ UA(1→4)GlcNAc), 2-acetamido-2-deoxy-4-*O*-(β -D-glucopyranosyluronic acid)-6-*O*-sulfo-D-glucose (Δ UA(1→4)GlcNAc6S), 2-acetamido-2-deoxy-4-*O*-(2-*O*-sulfo- β -D-glucopyranosyluronic acid)-D-glucose (Δ UA2S(1→4)GlcNAc), 2-acetamido-2-deoxy-4-*O*-(2-*O*-sulfo- β -D-glucopyranosyluronic acid)-6-*O*-sulfo-D-glucose (Δ UA2S(1→4)GlcNAc6S), 2-amino-2-deoxy-4-*O*-(2-*O*-sulfo- β -D-glucopyranosyluronic acid)-6-*O*-sulfo-D-glucose (Δ UA(1→4)GlcN6S), 2-amino-2-deoxy-4-*O*-(2-*O*-sulfo- β -D-glucopyranosyluronic acid)-D-glucose (Δ UA2S(1→4)GlcN), 2-amino-2-deoxy-4-*O*-(2-*O*-sulfo- β -D-glucopyranosyluronic acid)-6-*O*-sulfo-D-glucose (Δ UA2S(1→4)GlcN6S), 2-deoxy-2-sulfamino-4-*O*-(β -D-glucopyranosyluronic acid)-D-glucose (Δ UA(1→4)GlcNS), 2-deoxy-2-sulfamino-4-*O*-(β -D-glucopyranosyluronic acid)-6-*O*-sulfo-D-glucose (Δ UA(1→4)GlcNS6S), 2-deoxy-2-sulfamino-4-*O*-(2-*O*-sulfo- β -D-glucopyranosyluronic acid)-D-glucose (Δ UA2S(1→4)GlcNS), 2-deoxy-2-sulfamino-4-*O*-(2-*O*-sulfo- β -D-glucopyranosyluronic acid)-6-*O*-sulfo-D-glucose (Δ UA2S(1→4)GlcNS6S)], are listed in Table 1. All compounds (sodium salts) were obtained from Sigma Chemical Co. (USA) and used without further purification.

Mass spectra were recorded on a Finnigan MAT TSQ 700 triple stage quadrupole mass spectrometer equipped with an

Table 1. Compounds investigated.

Compound	RMM ^a	R ¹	R ²	R ³
Unsaturated disaccharides from heparin/heparan sulfate				
a) GlcNAc-containing disaccharide				
ΔUA(1→4)GlcNAc	379	Ac	H	H
ΔUA(1→4)GlcNAc6S	459	Ac	SO ₃ H	H
ΔUA2S(1→4)GlcNAc	459	Ac	H	SO ₃ H
ΔUA2S(1→4)GlcNAc6S	539	Ac	SO ₃ H	SO ₃ H
b) GlcNS-containing disaccharide				
ΔUA(1→4)GlcNS	417	SO ₃ H	H	H
ΔUA(1→4)GlcNS6S	497	SO ₃ H	SO ₃ H	H
ΔUA2S(1→4)GlcNS	497	SO ₃ H	H	SO ₃ H
ΔUA2S(1→4)GlcNS6S	577	SO ₃ H	SO ₃ H	SO ₃ H
c) GlcN-containing disaccharide derivative				
ΔUA(1→4)GlcN6S	417	H	SO ₃ H	H
ΔUA2S(1→4)GlcN	417	H	H	SO ₃ H
ΔUA2S(1→4)GlcN6S	497	H	SO ₃ H	SO ₃ H

^aRMM represents the relative molecular mass of the free acid.



Ion Tech FAB gun. A xenon beam with an energy of 8 keV was used. About a 1 μ l aliquot of an aqueous sample solution (c. 1.0 mg in 50 μ l) was mixed with 1 μ l of glycerol or thioglycerol as the matrices and then placed on the FAB target. CID-MS/MS spectra were taken using argon as the collision gas at typically 1.0 mTorr to reduce the beam of parent ions by approximately 30%. Collision energies were used at 30 eV. At least 10 scans were averaged to obtain each MS/MS spectrum.

Results and discussions

Positive-ion FAB mass spectra of non-, mono-, di- and trisulfated unsaturated disaccharides

As summarized in Table 2, the positive-ion FAB spectra of non-(ΔUA(1→4)GlcNAc), mono-(ΔUA(1→4)GlcNAc6S, ΔUA2S(1→4)GlcNAc, ΔUA(1→4)GlcNS, ΔUA(1→4)GlcN6S and ΔUA2S(1→4)GlcN), di-(ΔUA2S(1→4)GlcNAc6S, ΔUA(1→4)GlcNS6S, ΔUA2S(1→4)GlcNS and ΔUA2S(1→4)GlcN6S) and trisulfated (ΔUA2S(1→4)GlcNS6S) unsaturated disaccharides exhibited unambiguously the peaks of molecule related ions, $[M + H]^+$ and/or $[M - nH + (n + 1)Na]^+$ (where $n = 0-3$), as reported earlier.^{5,6,10} M represents the fully protonated molecule throughout this article. The spectra of the D-glucosamine (GlcN)-containing disaccharides such as ΔUA(1→4)GlcN6S showed the sodium adduct ions to be less abundant than those of N-acetylated GlcN (GlcNAc)- and N-sulfo GlcN (GlcNS)-containing disaccharides,

which may be caused by an amphoteric electrolyte of the GlcN-containing disaccharides.¹²

The losses of sodium sulfite with hydrogen transfer (i.e. $-NaSO_3 + H$), resulting in intense peaks down 102 units from the molecule related ions for di- and trisulfated unsaturated disaccharides were also commonly observed (Table 2).^{5,6,10,13} This elimination for GlcNS-containing disaccharides was more pronounced than that for GlcNAc- and GlcN-containing disaccharides. In the positive-ion FABMS of GlcNAc-containing disaccharides, the fragment ions produced by the elimination of AcNHCHCHOH, derived by the cleavage of GlcNAc residue at the reducing end, as found in the negative ion mode,¹² were not observed.

These results show that it is impossible to distinguish between the disaccharides obtained from Hep/HS and those from CS/DS, and to distinguish between the positional isomers of the mono- or disulfated derivatives from these positive-ion FABMS. However, CID-MS/MS turned out to be quite useful for differentiation of these isomers from each other.

CID-MS/MS spectra of the positive-ion FAB of GlcNAc-containing unsaturated disaccharides

Non-sulfated disaccharide

As a typical example for unsaturated disaccharides having a (1→4)-glycosidic bond, the CID-MS/MS of non-sulfated disaccharide ΔUA(1→4)GlcNAc was examined at first. The spectra of the $[M + H]^+$ ion (m/z 380), (data not shown), and the $[M + Na]^+$ ion (m/z 402) [Figure 1(a)] of ΔUA

Table 2. Molecule related and major fragment ions (*m/z*) and relative peak intensities (%) in the positive-ion FAB/MS of non-, mono-, di- and trisulfated unsaturated disaccharides from heparin/heparan sulfate.

Compound ^a	Molecule related ions ^{b,c}						Major fragment ions
	[M + H] ⁺	[M + Na] ⁺	[M - H + 2Na] ⁺	[M - 2H + 3Na] ⁺	[M - 3H + 4Na] ⁺	[M - 3H + 4Na] ⁺	
ΔUA(1→4)GlcNAc	380 (24)	402 (100)	424 (20)				
ΔUA(1→4)GlcNAc6S		482 (43)	504 (100)	526 (15)			402 (75) [(M - H + 2Na) - NaSO ₃ + H] ⁺
ΔUA2S(1→4)GlcNAc		482 (11)	504 (100)	526 (30)			402 (43) [(M - H + 2Na) - NaSO ₃ + H] ⁺
ΔUA2S(1→4)GlcNAc6S			584 (55)	606 (55)	628 (14)		504 (100) [(M - 2H + 3Na) - NaSO ₃ + H] ⁺
ΔUA(1→4)GlcNS		440 (50)	462 (100)	484 (19)			360 (73) [(M - H + 2Na) - NaSO ₃ + H] ⁺
ΔUA(1→4)GlcNS6S			542 (38)	564 (82)	586 (31)		462 (94) [(M - 2H + 3Na) - NaSO ₃ + H] ⁺
ΔUA2S(1→4)GlcNS			542 (19)	564 (100)	586 (6)		462 (100) [(M - 2H + 3Na) - NaSO ₃ + H] ⁺
ΔUA2S(1→4)GlcNS6S				644 (32)	666 (100)		564 (87) [(M - 3H + 4Na) - NaSO ₃ + H] ⁺
ΔUA(1→4)GlcN6S	418 (100)	440 (80)	462 (33)				360 (97) [(M - H + 2Na) - NaSO ₃ + H] ⁺
ΔUA2S(1→4)GlcN	418 (72)	440 (46)	462 (45)				360 (100) [(M - H + 2Na) - NaSO ₃ + H] ⁺
ΔUA2S(1→4)GlcN6S		520 (26)	542 (40)	564 (12)			462 (100) [(M - 2H + 3Na) - NaSO ₃ + H] ⁺

^aSee Table 1 for structures.^bM represents the fully protonated acid.^cPeaks are normalized to the base peak.

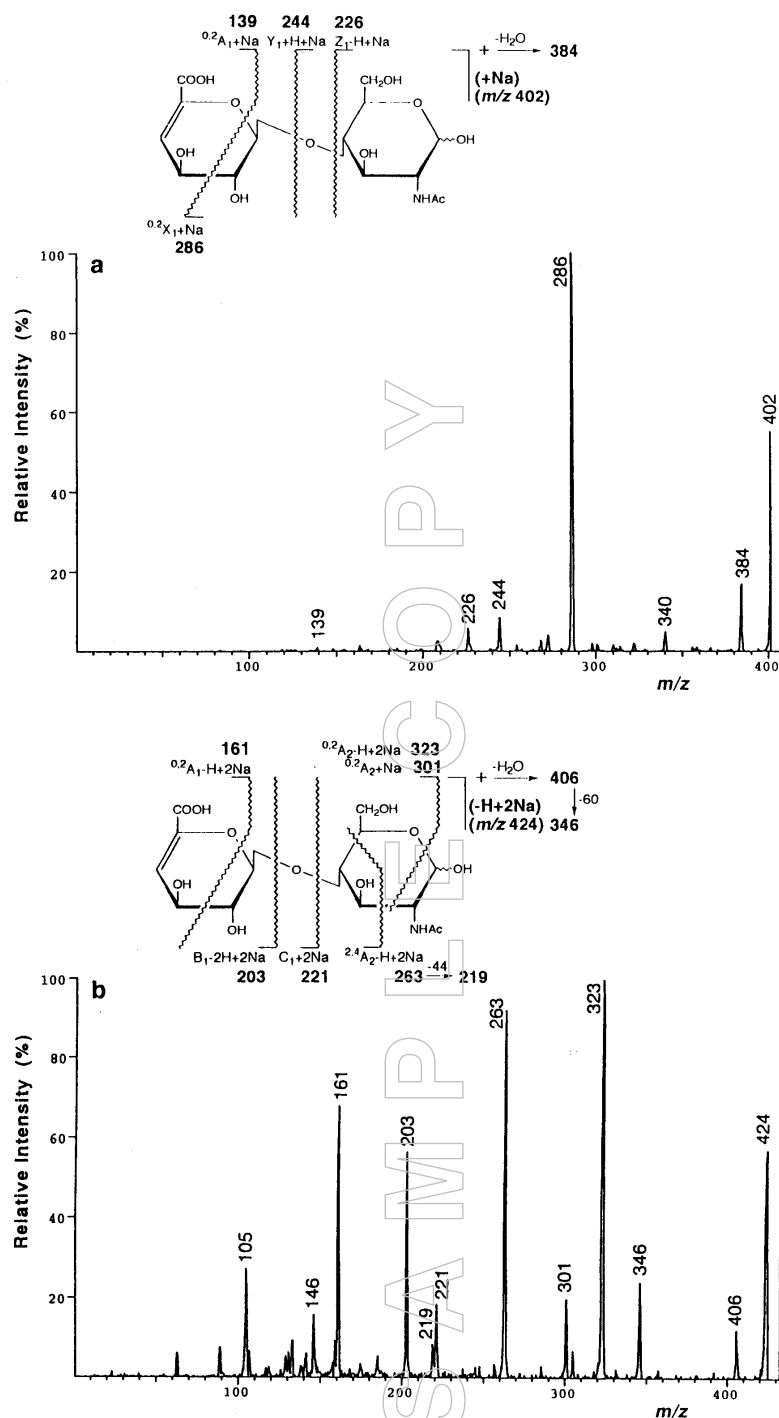


Figure 1. MS/MS spectra of non-sulfated unsaturated disaccharides $\Delta UA(1 \rightarrow 4)GlcNAc$. (a) the $[M + Na]^+$ ion (m/z 402) as the parent ion, (b) the $[M - H + 2Na]^+$ ion (m/z 424) as the parent ion.

(1 \rightarrow 4)GlcNAc are similar to those of $\Delta UA(1 \rightarrow 3)GlcNAc$ obtained from CS and DS,¹⁰ which do not give any information characteristic of the isomers. However, the spectrum of the $[M - H + 2Na]^+$ ion (m/z 424), as shown in Figure 1(b), gave not only intense peaks at m/z 221, 203 and 161 corresponding to $[C_1 + 2Na]^+$, $[B_1 - 2H + 2Na]^+$ and $[^{0,2}A_1 - H + 2Na]^+$ ions, respectively, but also characteristic peaks at m/z 323, 301 and 263 corresponding to $[^{0,2}A_2 - H + 2Na]^+$, $[^{0,2}A_2$

$+ Na]^+$ and $[^{2,4}A_2 - H + 2Na]^+$ ions, respectively. To describe the fragment ions drawn in each figure, we use the nomenclature, shown in Scheme 1, proposed by Domon and Costello.¹⁴ On the basis of the presence of these $^{0,2}A_2^-$ and $^{2,4}A_2^-$ -type ions, derived by the ring cleavage of the GlcNAc residue, it is possible to distinguish the non-sulfated disaccharide having (1 \rightarrow 4)-glycosidic bond from those isomers having (1 \rightarrow 3)-glycosidic bond.

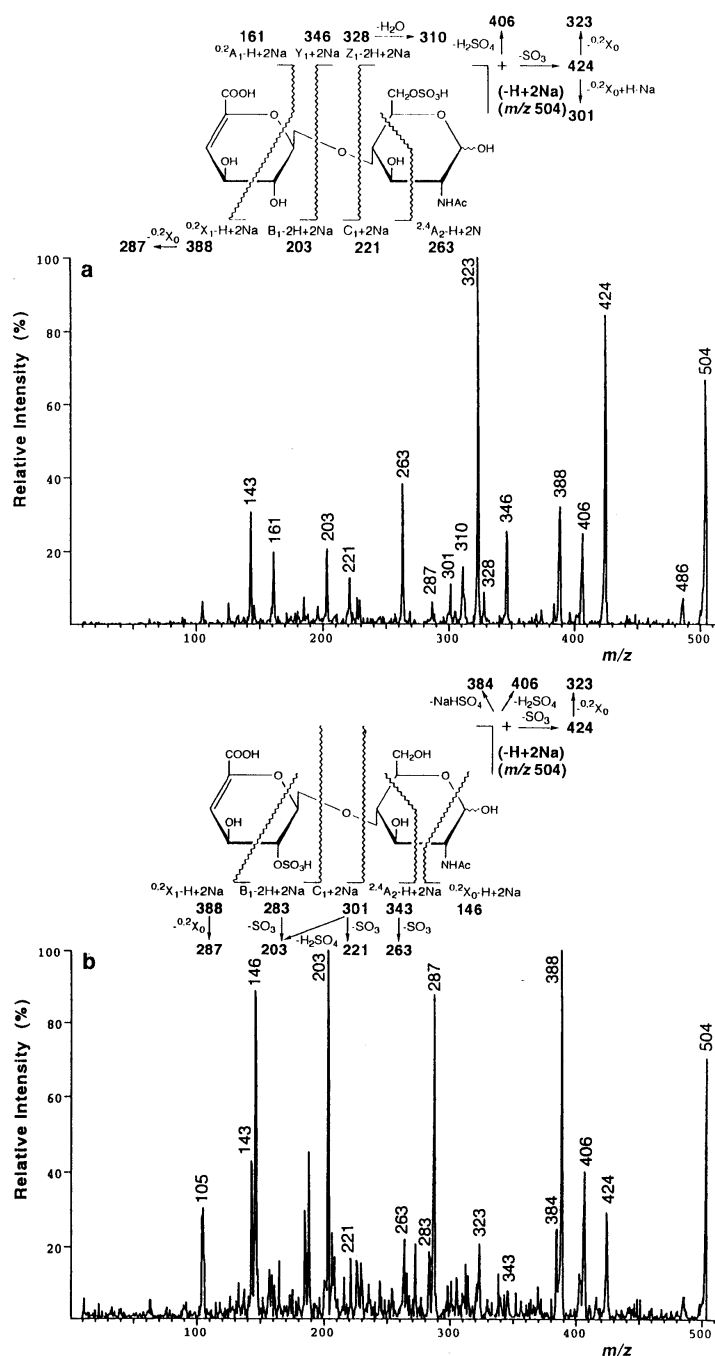
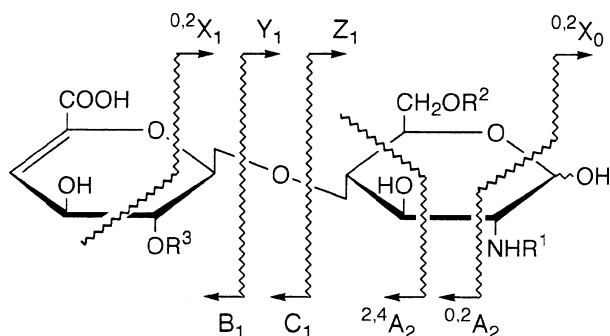


Figure 2. MS/MS spectra of monosulfated unsaturated disaccharides having $[M - H + 2Na]^+$ ions (m/z 504), as the parent ion. (a) Δ UA(1 \rightarrow 4)GlcNAc6S, (b) Δ UA2S(1 \rightarrow 4)GlcNAc.



Scheme 1. The nomenclature for disaccharide fragmentation proposed by Domon and Costello.¹⁴

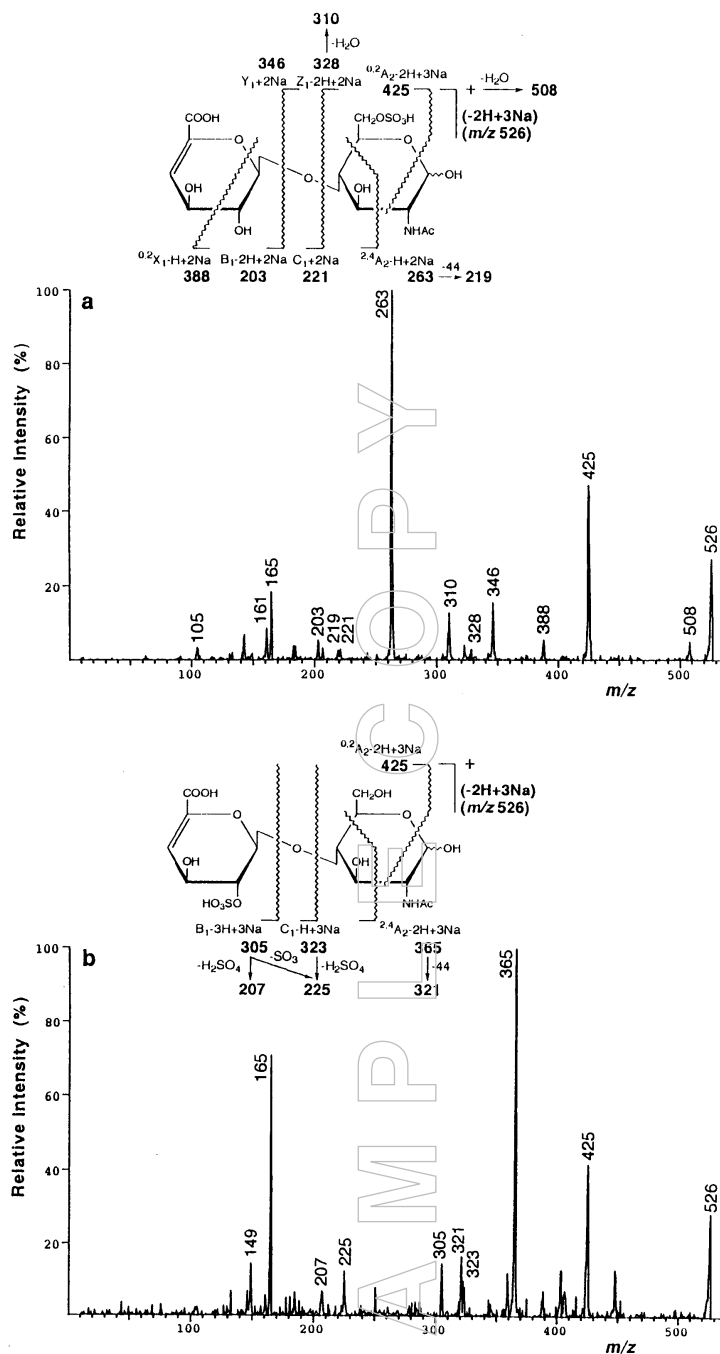


Figure 3. MS/MS spectra of monosulfated unsaturated disaccharides having $[M - 2H + 3Na]^+$ ions (m/z 526), as the parent ion. (a) $\Delta UA(1 \rightarrow 4)GlcNAc6S$, (b) $\Delta UA2S(1 \rightarrow 4)GlcNAc$.

Monosulfated disaccharides

The positive-ion CID-MS/MS spectra of $[M - H + 2Na]^+$ ions provide sufficient information on distinguishing the positional isomers of monosulfated disaccharides. MS/MS spectra of $[M - H + 2Na]^+$ ions (m/z 504) of $\Delta UA(1 \rightarrow 4)GlcNAc6S$ and $\Delta UA2S(1 \rightarrow 4)GlcNAc$ are shown in Figure 2. In the spectrum of $\Delta UA(1 \rightarrow 4)GlcNAc6S$, the predominant peaks at m/z 424 and 323 corresponding to the $[(M - H + 2Na) - SO_3]^+$ and $[(M - H + 2Na) - SO_3 - 0.2X_0]^+$ ions, respectively, were observed. The glycosidic bond cleavage also yielded the peaks

at m/z 346 ($[Y_1 + 2Na]^+$), 328 ($[Z_1 - 2H + 2Na]^+$), 221 ($[C_1 + 2Na]^+$) and 203 ($[B_1 - 2H + 2Na]^+$). Two intense peaks at m/z 388 and 263 correspond to the $[0.2X_1 - H + 2Na]^+$ and $[2.4A_2 - H + 2Na]^+$ ions, respectively. The origins of other peaks were rationalized as illustrated in Figure 2(a). In the spectrum of $\Delta UA2S(1 \rightarrow 4)GlcNAc$ [Figure 2(b)], characteristic peaks were observed at m/z 323 and 287, produced by the elimination of $0.2X_0$ from the peaks at m/z 424 ($[(M - H + 2Na) - SO_3]^+$) and 388 ($[0.2X_1 - H + 2Na]^+$), respectively. In the upper mass region, the relative intensities of peaks at m/z 424, 406,

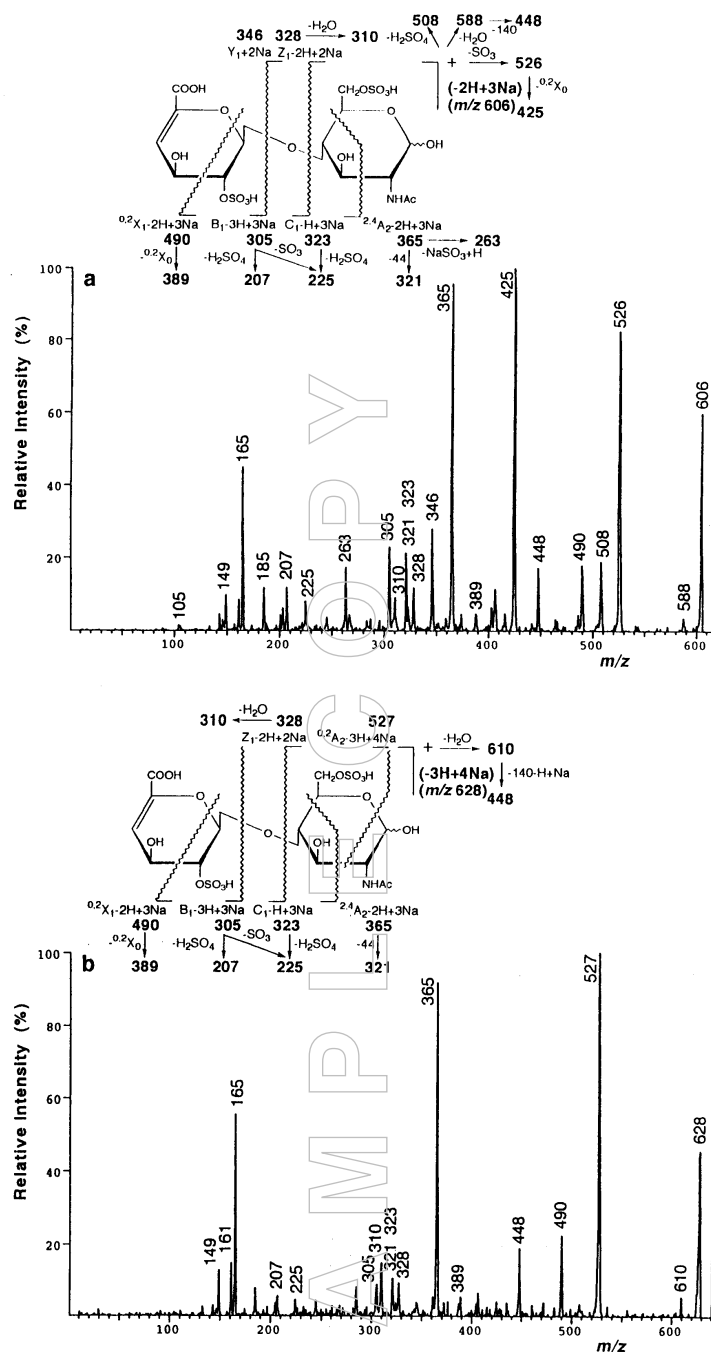


Figure 4. MS/MS spectra of disulfated unsaturated disaccharides $\Delta\text{UA}2\text{S}(1\rightarrow4)\text{GlcNAc}6\text{S}$. (a) the $[M - 2H + 3Na]^+$ ion (m/z 606) as the parent ion, (b) the $[M - 3H + 4Na]^+$ ion (m/z 628) as the parent ion.

388 and 384 are similar to those of $\Delta\text{UA}2\text{S}(1\rightarrow3)\text{GalNAc}$ having the sulfated D-glucosyl-4-enepyransyluronic acid (ΔUA) moiety. The behavior of fragmentation of monosulfated disaccharides, $\Delta\text{UA}(1\rightarrow4)\text{GlcNAc}6\text{S}$ and $\Delta\text{UA}2\text{S}(1\rightarrow4)\text{GlcNAc}$, is similar to that of monosulfated disaccharides from CS and DS, but the former are clearly differentiated from the latter on the basis of the observations of the peaks due to $^{2,4}\text{A}_2$ -type ions and the loss of $^{0,2}\text{X}_0$ residue in the former.

The CID-MS/MS spectra of the $[M - 2H + 3Na]^+$ ions (m/z 526) of $\Delta\text{UA}(1\rightarrow4)\text{GlcNAc}6\text{S}$ and $\Delta\text{UA}2\text{S}(1\rightarrow4)\text{GlcNAc}$ are shown in Figure 3, where more pronounced differences between these isomers are observed. In both spectra, the most predominant peaks at m/z 263 [Figure 3(a)] and m/z 365 [Figure 3(b)], corresponding to the $[^{2,4}\text{A}_2 - H + 2Na]^+$ and $[^{2,4}\text{A}_2 - 2H + 3Na]^+$ ions, respectively, produced by the ring cleavage of GlcNAc were observed. The ring cleavage of GlcNAc also yielded the intense peaks at m/z 425 in these

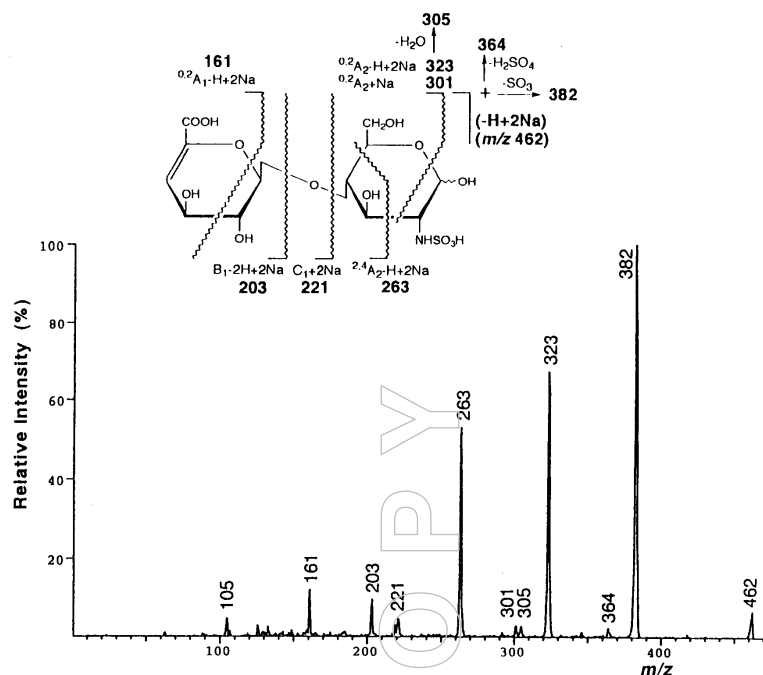


Figure 5. MS/MS spectrum of monosulfated unsaturated disaccharide Δ UA(1 \rightarrow 4)GlcNS having $[M - H + 2Na]^+$ ions (m/z 462), as the parent ion.

spectra. In the spectrum of Δ UA(1 \rightarrow 4)GlcNAc6S, the weak peaks were observed at m/z 388, 346 and 303 corresponding to the $[^{0.2}X_1 - H + 2Na]^+$, $[Y_1 + 2Na]^+$ and $[B_1 - 2H + 2Na]^+$ ions, respectively. Another peak at m/z 310 is assigned as the novel fragment ion derived by the loss of H_2O from the $[Z_1 - 2H + 2Na]^+$ ion (m/z 328). In the spectrum of Δ UA2S(1 \rightarrow 4)GlcNAc, an intense peak at m/z 165 corresponding to $[Na_3SO_4]^+$ ion and four weak peaks at m/z 323, 305, 225 and 207 were observed and rationalized as illustrated in Figure 3(b).

Disulfated disaccharide

As shown in Figure 4(a), the CID-MS/MS spectrum of $[M - 2H + 3Na]^+$ (m/z 606) ion of disulfated disaccharide Δ UA2S(1 \rightarrow 4)GlcNAc6S characteristically exhibits three dominant peaks at m/z 526, 425 and 365 corresponding to $[(M - 2H + 3Na) - SO_3]^+$, $[(M - 2H + 3Na) - SO_3 - ^{0.2}X_0]^+$ and $[^{2.4}A_2 - 2H + 3Na]^+$, respectively. The other peaks similar to those of $[M - 2H + 3Na]^+$ ion of Δ UA2S(1 \rightarrow 3)GalNAc6S obtained from CS and DS¹⁰ are illustrated in this Figure.

The CID-MS/MS of $[M - 3H + 4Na]^+$ ion (m/z 628) of Δ UA2S(1 \rightarrow 4)GlcNAc6S, as shown in Figure 4(b), is rather simple, showing not only the dominant peak at m/z 365 ($[^{2.4}A_2 - 2H + 3Na]^+$), but also a peak at m/z 527 ($[^{0.2}A_2 - 3H + 4Na]^+$). The origin of the other peaks are rationalized as illustrated in the Figure.

These results indicate that CID-MS/MS can be used for identification of Δ UA2S(1 \rightarrow 4)GlcNAc6S, in addition to distinguishing this disulfated disaccharide from other isomers,

such as Δ UA2S(1 \rightarrow 3)GalNAc6S having (1 \rightarrow 3)-glycosidic bond obtained from CS and DS.

CID-MS/MS spectra of the positive-ion FAB of GlcNS-containing unsaturated disaccharides

Monosulfated disaccharide

In the CID-MS/MS spectrum of the $[M + Na]^+$ ion of Δ UA(1 \rightarrow 4)GlcNS, an ion derived by the loss of SO_3 was predominantly observed, but no significant fragment ions (data not shown).

The CID-MS/MS spectrum of $[M - H + 2Na]^+$ ion (m/z 462), as shown in Figure 5, gave intense peaks at m/z 382, 323 and 263 corresponding to the $[(M - H + 2Na) - SO_3]^+$, $[^{0.2}A_2 - H + 2Na]^+$ and $[^{2.4}A_2 - H + 2Na]^+$ ions, respectively, together with several weak peaks at m/z 305 ($[^{0.2}A_2 - H + 2Na - H_2O]^+$), 301 ($[^{0.2}A_2 + Na]^+$), 221 ($[C_1 + 2Na]^+$) and 203 ($[B_1 - 2H + 2Na]^+$), which all derived from the non-reducing end residue.

Disulfated disaccharides

In the CID-MS/MS spectra of $[M - H + 2Na]^+$ ions of Δ UA(1 \rightarrow 4)GlcNS6S and Δ UA2S(1 \rightarrow 4)GlcNS, predominant peaks derived by the loss of SO_3 and H_2SO_4 were observed and no significant differences between them were observed (data not shown).

However, the results of the CID-MS/MS of $[M - 2H + 3Na]^+$ ions (m/z 564) of Δ UA(1 \rightarrow 4)GlcNS6S and Δ UA2S(1 \rightarrow 4)GlcNS, indicate dramatically the possibility of distinguishing between these isomers. The CID-MS/MS of

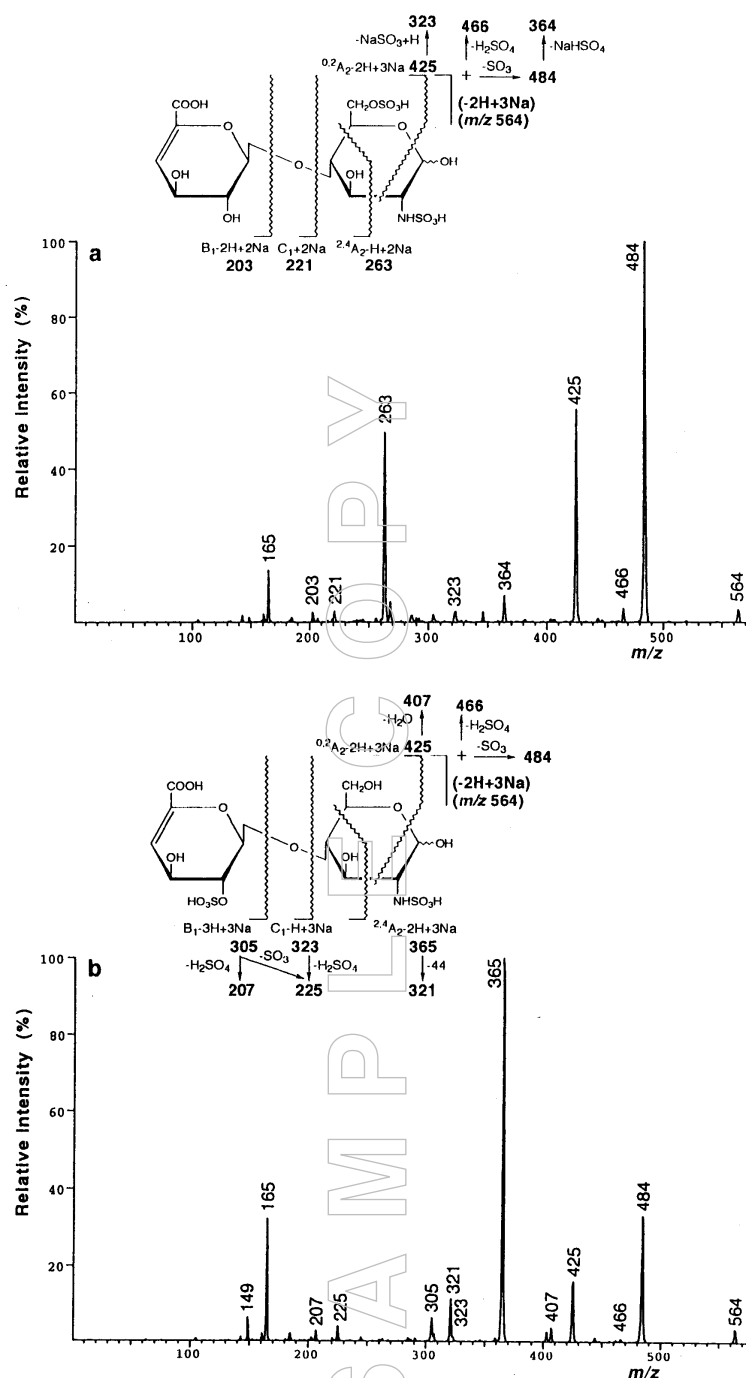


Figure 6. MS/MS spectra of disulfated unsaturated disaccharides having $[\text{M} - 2\text{H} + 3\text{Na}]^+$ ions (m/z 564), as the parent ion. (a) $\Delta\text{UA}(1\rightarrow4)\text{GlcNS6S}$, (b) $\Delta\text{UA}2\text{S}(1\rightarrow4)\text{GlcNS}$.

the $[\text{M} - 2\text{H} + 3\text{Na}]^+$ ion (m/z 564) of $\Delta\text{UA}(1\rightarrow4)\text{GlcNS6S}$, as shown in Figure 6(a), gave the predominant peak at m/z 484 derived by the loss of SO_3 , and also the characteristic other fragment ions similar to those observed in that of $[\text{M} - 2\text{H} + 3\text{Na}]^+$ ion of $\Delta\text{UA}(1\rightarrow4)\text{GlcNAc6S}$ [Figure 3(a)]. The origin of these fragment ions are rationalized as illustrated in the Figure. The feature of the spectra of the $[\text{M} - 2\text{H} + 3\text{Na}]^+$ ion of $\Delta\text{UA}2\text{S}(1\rightarrow4)\text{GlcNS}$, as shown in Figure 6(b), is also

similar to that of $\Delta\text{UA}2\text{S}(1\rightarrow4)\text{GlcNAc6S}$ mentioned above, except for the observation of an intense peak at m/z 484 corresponding to the $[(\text{M} - 2\text{H} + 3\text{Na}) - \text{SO}_3]^+$ ion. The fragment ions are assigned as illustrated in Figure 6(b). This behavior of the fragmentation indicates that the sulfate group at C-2 of GlcN residue may not be sodiated.

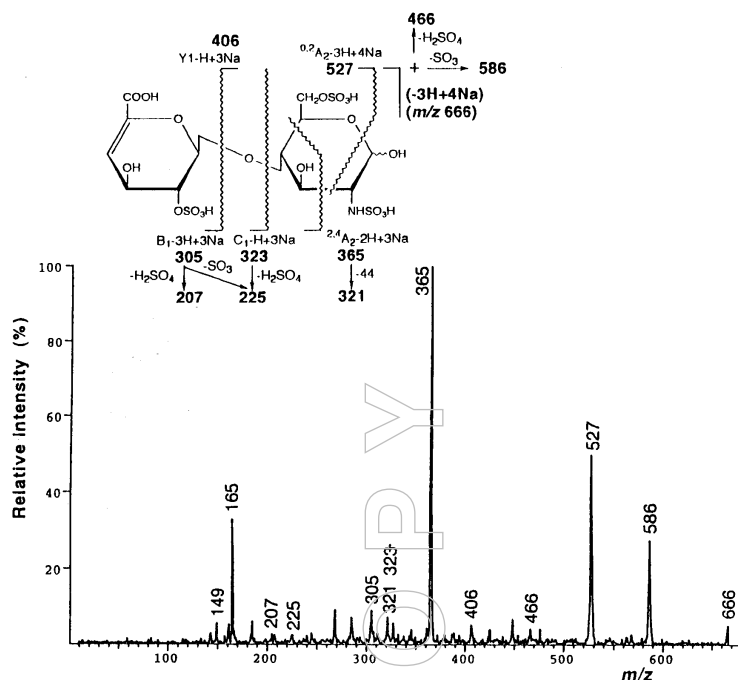


Figure 7. MS/MS spectrum of trisulfated unsaturated disaccharide Δ UA2S(1 \rightarrow 4)GlcNS6S having $[M - 3H + 4Na]^+$ ions (m/z 666), as the parent ion.

These observations show that the CID-MS/MS of $[M - 2H + 3Na]^+$ ions of disulfated GlcNS-containing disaccharides provide an easy way of identifying the positional isomers.

The spectra of CID-MS/MS of the $[M - 3H + 4Na]^+$ ions of Δ UA(1 \rightarrow 4)GlcNS6S and Δ UA2S(1 \rightarrow 4)GlcNS are rather simple, showing predominant peaks derived by the loss of H_2O from Z-type ions, in addition to the fragment ions observed in the spectra of $[M - 2H + 3Na]^+$ ions mentioned above (data not shown).

Trisulfated disaccharides

As shown in Figure 7, the CID-MS/MS spectrum of the $[M - 3H + 4Na]^+$ ion (m/z 666) of trisulfated disaccharide Δ UA2S(1 \rightarrow 4)GlcNS6S exhibits the dominant peaks at m/z 586, 527 and 365 corresponding to $[(M - 3H + 4Na) - SO_3]^+$, $[^{0.2}A_2 - 3H + 4Na]^+$ and $[^{2.4}A_2 - 2H + 3Na]^+$ ions, respectively. Other characteristic peaks are assigned as illustrated in the Figure. These observations indicate that the spectrum can be used for identification of the structure of this trisulfate.

CID-MS/MS spectra of the positive-ion FAB of GlcN-containing unsaturated disaccharides

Monosulfated disaccharides

In the CID-MS/MS spectra of the $[M + H]^+$ and $[M + Na]^+$ ions of Δ UA(1 \rightarrow 4)GlcN6S and Δ UA2S(1 \rightarrow 4)GlcN, no significant differences between the positional isomers were observed (data not shown).

The results of the CID-MS/MS of the $[M - H + 2Na]^+$ ions (m/z 462) of isomeric monosulfated disaccharides, Δ UA(1 \rightarrow 4)GlcN6S and Δ UA2S(1 \rightarrow 4)GlcN, indicate that it is possible to distinguish between the positional isomers of

GlcN-containing disaccharides. The CID-MS/MS of the $[M - H + 2Na]^+$ ion (m/z 462) of Δ UA(1 \rightarrow 4)GlcN6S, as shown in Figure 8(a), gave characteristic fragment ions similar to that observed in those of $[M - H + 2Na]^+$ (m/z 504) of Δ UA(1 \rightarrow 4)GlcNAc6S [Figure 2(a)]. Significant differences between them are that only in the spectrum of Δ UA(1 \rightarrow 4)GlcN6S, two peaks at m/z 403 and 245 corresponding to the $[^{0.2}A_2 - H + 2Na]^+$ and $[(Y_1 + 2Na) - ^{0.2}X_0]^+$ ions, respectively, were observed. Moreover, the CID-MS/MS spectra of the $[M - H + 2Na]^+$ ions of Δ UA2S(1 \rightarrow 4)GlcN [Figure 8(b)] and Δ UA2S(1 \rightarrow 4)GlcNAc [Figure 2(b)] closely resemble each other except for the presence of a predominant peak at m/z 403 ($[^{0.2}A_2 - H + 2Na]^+$) in the former spectrum. The fragment ions, produced by the cleavage of $^{0.2}A_2$ -type, are characteristic of the GlcN-containing disaccharides. These observations show that the CID-MS/MS of $[M - H + 2Na]^+$ ions of monosulfated GlcN-containing disaccharides provide an easy way of not only distinguishing GlcN- from GlcNAc-containing disaccharides, but also identifying the positional isomers of GlcN-containing derivatives.

Disulfated disaccharide

As shown in Figure 9, the CID-MS/MS spectrum of the $[M - 2H + 3Na]^+$ (m/z 564) ion of Δ UA2S(1 \rightarrow 4)GlcN6S gives characteristically the A, B, C, X, Y and Z-type fragment ions. The assignment of the fragment ions are illustrated in the Figure. It is noted that all eliminations of sulfates and sulfites are observed from the ions including the sulfated Δ UA residue of the non-reducing end, which suggests that the sulfate group at C-2 of Δ UA may eliminate more easily than that at C-6 of the GlcNAc residue. These observations indicate that CID-

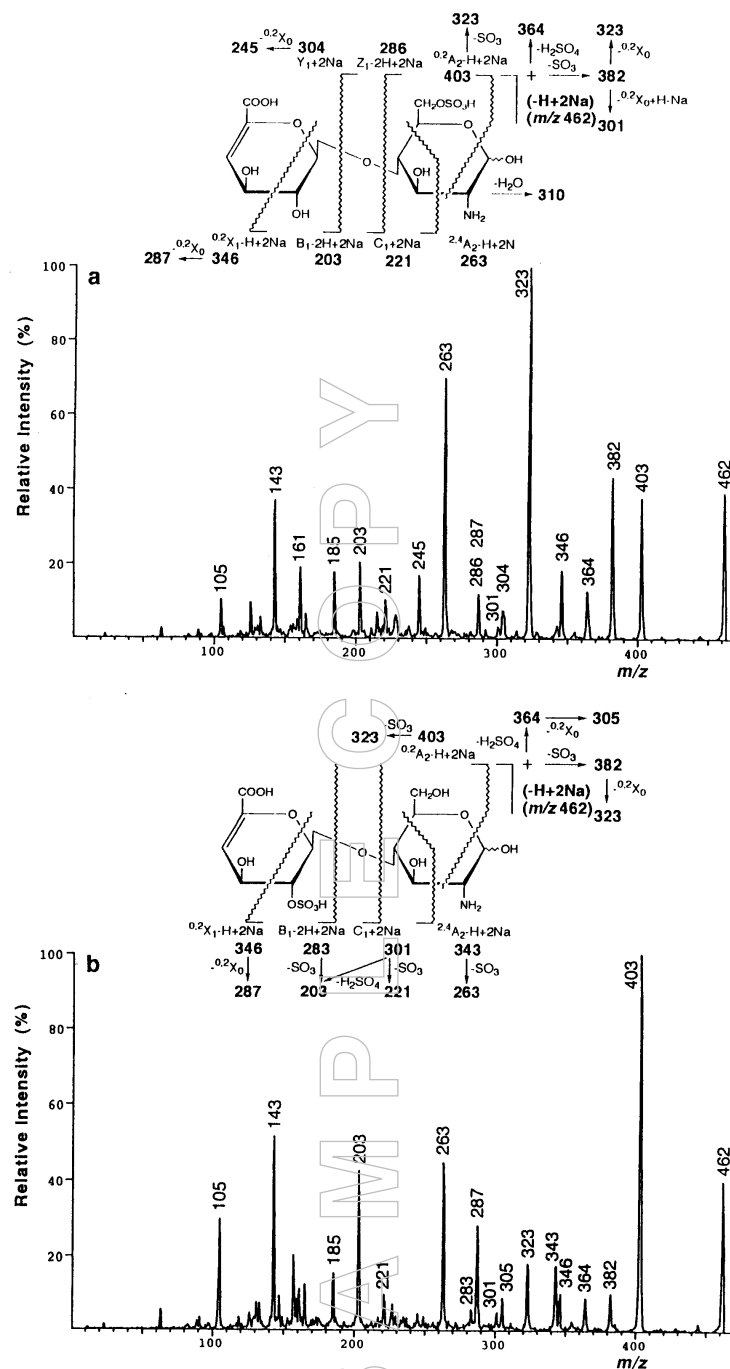


Figure 8. MS/MS spectra of monosulfated unsaturated disaccharides having $[M - H + 2Na]^+$ ions (m/z 462), as the parent ion. (a): $\Delta UA(1 \rightarrow 4)GlcN6S$, (b): $\Delta UA2S(1 \rightarrow 4)GlcN$.

MS/MS is also useful in the identification of the structure of the disulfated compounds.

Conclusion

Positive-ion FAB mass spectra of the sodium salts of eight disaccharides from Hep and HS and three derivatives show distinct molecule related ions, giving only molecular weight

information. The CID-MS/MS spectra of the selected molecule related ions can be used to differentiate between the respective two positional isomers of monosulfated disaccharides, and also provide an easy way of identifying positional isomers. Tandem FABMS also provides useful information on the identification of the di- and trisulfated disaccharide. Our results suggest that tandem FABMS will provide a new rapid tool for the analysis of disaccharides from Hep and HS.

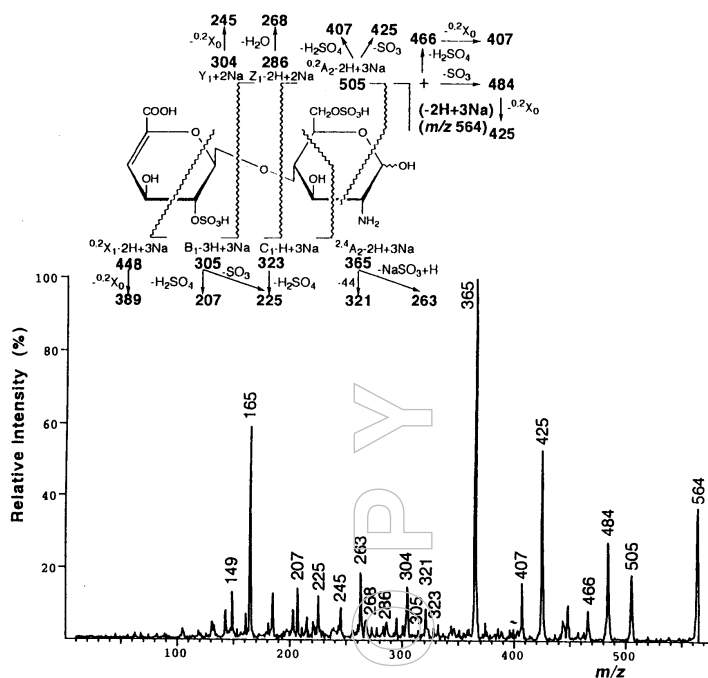


Figure 9. MS/MS spectrum of disulfated unsaturated disaccharide Δ UA2S(1 \rightarrow 4)GlcN6S having $[M - 2H + 3Na]^+$ ions (m/z 564), as the parent ion.

Although negative-ion tandem FABMS has been widely used in the structural studies of these sulfated saccharides, our results indicate that positive-ion tandem FABMS of sodiated molecule related ions is also useful for characterization of these compounds, as we previously succeeded in characterization of nine unsaturated disaccharides from CS, DS and HA.¹⁰ It will be very useful for characterization of many disaccharides isomers from glycosaminoglycans in various biological materials. We are currently extending our studies to the characterizations of sulfated disaccharides from keratan sulfate, and tetrasaccharides from chondroitin sulfate and keratan sulfate.

Acknowledgments

This work was partially supported by the Grant-in-Aid for Scientific Research on Priority Areas No. 06240247 from the Ministry of Education, Science and Culture, Japan.

References

1. J.A. McCloskey (Ed.), *Methods In Enzymology*. Volume 193. Academic Press (1990).
2. A. Dell, *Adv. Carbohydr. Chem. Biochem.* **45**, 19 (1987).
3. H. Egge and J. Peter-Katalinic, *Mass Spectrom. Rev.* **6**, 331 (1987).
4. Y. Kushi, S. Handa and I. Ishizuka, *J. Biochem. (Tokyo)* **97**, 419 (1985).
5. S.A. Carr and V.N. Reinhold, *Carbohydr. Chem.* **3**, 381 (1984).
6. V.N. Reinhold, S.A. Carr, B.N. Green, M. Petitou, J. Choay and P. Sinay, *Carbohydr. Res.* **161**, 305 (1987).
7. L.M. Mallis, H.M. Wang, D. Loganathan and R.J. Linhardt, *Anal. Chem.* **61**, 1453 (1989).
8. R.J. Linhardt, H.M. Wang, D. Loganathan, D.J. Lamb and L.M. Mallis, *Carbohydr. Res.* **225**, 137 (1992).
9. D.J. Lamb, H.M. Wang, L.M. Mallis and R.J. Linhardt, *J. Am. Soc. Mass Spectrom.* **3**, 797 (1992).
10. T. Ii, S. Okuda, T. Hirano and M. Ohashi, *Glycoconjugate J.* **11**, 123 (1994).
11. G.E. Hofmeister, Z. Zhou and J.A. Leary, *J. Am. Chem. Soc.* **113**, 5964 (1991).
12. T. Ii, M. Kubota, S. Okuda, T. Hirano and M. Ohashi, *Glycoconjugate J.*, in press.
13. Y. Ohashi and Y. Nagai, *Carbohydr. Res.* **221**, 235 (1991).
14. B. Domon and C.E. Costello, *Glycoconjugate J.* **5**, 397 (1988).

Received: 15 November 1994

Accepted: 5 January 1995

Collision-induced photon emissions from 8 keV polyatomic ions of composition $C_2H_4O^{+•}$ and $C_2H_5Cl^{+•}$

J.L. Holmes* and P.M. Mayer

Chemistry Department, University of Ottawa, Ottawa, Canada K1N 6N5.

Photon emissions following 8 keV ion beam–target gas collisions of the polyatomic cations of composition $C_2H_4O^{+•}$ and $C_2H_5Cl^{+•}$ were measured and interpreted in conjunction with their collision-induced dissociation (CID) mass spectra. The experiments were performed in a modified analytical VG ZAB-2F mass spectrometer of magnetic sector/electric sector/electric sector (BEE) geometry. The identification of the emission bands in the collision-induced emission (CIE) spectra of oxirane $^{+•}$, acetaldehyde $^{+•}$ and vinyl alcohol $^{+•}$ with helium and argon target gases was assisted by obtaining the CIE spectra of $CO^{+•}$, HCO^{+} and CH_3^{+} . Distinct emission bands due to the HC ($A, B \rightarrow X$), HC^{+} ($B \rightarrow A$ and $A \rightarrow X$) and HO^{+} ($A \rightarrow X$) transitions, as well as atomic C , O^{+} and H^{+} lines, were observed. The emission spectra of 8 keV $CH_3CH_2Cl^{+•}$ and $CH_3ClCH_2^{+•}$ –helium and argon target gas collisions were obtained and analyzed with the aid of the CIE spectra for CCl^{+} and CH_2Cl^{+} . Many of the same bands appeared as for the $C_2H_4O^{+•}$ isomers, with the addition of bands due to the CCl^{+} ($A \rightarrow X$) transition and Cl^{+} atomic lines.

Introduction

Fundamental collision spectroscopy, involving investigations of scattering angle, photon emission and translational energy changes, has led to an understanding of the excitation and dissociation processes occurring in a projectile ion beam–target gas collision event over a wide range of collision energies (thermal to MeV). However, the projectiles and targets have been primarily simple mono-, di- and triatomic ions and neutrals. In contrast, organic mass spectrometry is largely concerned with polyatomic projectile ions. Collisional activation of polyatomic projectiles (eV–keV translational energies) has been used to aid the assigning of structures to ions, to elucidate fragmentation pathways and identify isomers.^{1,2} The method relies on qualitative or semi-quantitative differences between collision-induced dissociation (CID) mass spectra and so the results are treated like any other mass spectrum, i.e. essentially empirically. However, little is known about the excitation and dissociation processes which occur in polyatomic–target gas collisions. This hinders a more detailed interpretation of the results of collision-based experiments such as CID, collision-induced dissociative ionization (CIDI) and neutralization–reionization (NR) mass spectrometry.

Limited qualitative information^{3–5} has been obtained on the effects of projectile translational energy and the nature of the target gas on the internal energy deposited in a projectile ion

undergoing keV collisions. A more objective approach, which does not require the interpretation of yet another mass spectrum, is desirable. In an attempt to obtain information about the internal excitation in both the polyatomic projectile and target in keV collisions a study was undertaken in which photon emission spectroscopy was coupled to a collision cell in a modified sector mass spectrometer.^{6,7}

Recent work on 8 keV $N_2^{+•}$, $O_2^{+•}$ and $CO_2^{+•}$ with a variety of target gases^{8,9} was successful in identifying emitting species in both the ion beam and target. For $N_2^{+•}$ and $CO_2^{+•}$, emissions were predominantly from excited molecular ions, with minor peaks in the spectra due to target and fragment emissions. When O_2 was the *target* in collisions with $N_2^{+•}$, emissions were observed from excited $O_2^{+•}$ and N_2 (formed in a charge exchange reaction between $N_2^{+•}$ and O_2). For $CO_2^{+•}/O_2$ collisions, no emissions were detected from neutral CO_2 . Oxygen molecular ion projectiles exhibited quite different behaviour when helium was used as the target. No $O_2^{+•}$ emissions were observed from the ion beam, instead the spectra consisted of an assortment of fragment O^{+} and O lines and target gas emission bands. This could be attributed to the difference in geometry between ground and excited state $O_2^{+•}$. Vertical excitation in the 8 keV collision event produced excited state $O_2^{+•}$ near or above its dissociation limit and the ions dissociated to produce excited state fragments. When N_2 or CO_2 were the target gas in these experiments, emissions from the $O_2^{+•}$ ion beam were almost undetectable. Spectral bands were

primarily from $\text{N}_2^{+\bullet}$ and $\text{CO}_2^{+\bullet}$ formed in a charge exchange reaction with the ion beam.

The present study extends the technique to 8 keV polyatomic projectile ions of mass spectrometric interest. The collision-induced emission (CIE) spectra of the three $\text{C}_2\text{H}_4\text{O}^{+\bullet}$ isomers oxirane $^{+\bullet}$, acetaldehyde $^{+\bullet}$ and vinyl alcohol $^{+\bullet}$ and the two $\text{C}_2\text{H}_5\text{Cl}^{+\bullet}$ isomers, chloroethane $^{+\bullet}$ and $\text{CH}_3\text{ClCH}_2^{+\bullet}$ have been obtained and analyzed. The interpretation of these emission spectra was aided by the CIE spectra of the smaller fragment ions $\text{CO}^{+\bullet}$, HCO^+ , CH_3^+ , CCl^+ and CH_2Cl^+ . The results have been interpreted in conjunction with the CID mass spectra of these ions.

Experimental

The experiment to detect and analyze light emissions from collisionally activated ion beams has been described in detail elsewhere.⁸ The projectile ions were formed by electron impact ionization in the ion source of a modified three-sector VG ZAB-2F mass spectrometer (BEE geometry). The ions were accelerated to 8 keV translational kinetic energy, selected by the magnet and first electric analyzer and transmitted into the third field-free region (3FFR). An observation cell (OC) is located in the 3FFR underneath a quartz window (fused silica-Optikon W-25). The entrance slit of a scanning wavelength monochromator lies within 30 mm of the ion beam. Collisions performed in the OC yield spectra due to emissions from excited ions and target gas species (in-OC observations). Collisions were also performed in a collision cell (PC) located 1 cm in front of the OC. These experiments will be referred to as post-collision (PC) observations and they allow the analysis of emissions from the ion beam without interference from target gas emissions. However, the radiative lifetimes of species studied in post-collision observations is limited to long-lived metastable states. *Unless stated otherwise*, results are for in-OC collision experiments. The time window of in-OC observations for an ion with m/z 44 is 0–0.11 μs , and that for a post-collision observation is 0.05–0.20 μs .

A scanning monochromator (Acton SpectraPro 275, 27.5 cm focal length, 1200 grooves per mm holographic grating) and cooled photomultiplier, PMT, (Thorn EMI 9635QB, 180–680 nm range, Products For Research Cooler, TE 182TSRF) were used to monitor the emission spectra. The experiments were performed with sufficient target gas pressure to attenuate the ion beam to 60% of its pre-cell flux (unless otherwise stated). The monochromated spectra were obtained by analogue monitoring of the current from the PMT. The resolution used for the monochromated spectra depended on the signal-to-noise of the features in each spectrum. The entrance and exit slits of the monochromator were set to 0.5, 1, 2 or 3 mm depending on the sensitivity required. The full width at half maximum, FWHM, of an atomic line as a function of these slit widths was 1.0, 2.0, 5.5 and 10 nm, respectively.

All compounds used in this study were commercially obtained and of high purity (>99.9%).

Results

Emissions from isomeric $\text{C}_2\text{H}_4\text{O}^{+\bullet}$ ion–target gas collisions

Collision-induced emission (CIE) spectra obtained for the three $\text{C}_2\text{H}_4\text{O}^{+\bullet}$ isomers oxirane $^{+\bullet}$, acetaldehyde $^{+\bullet}$ and vinyl alcohol $^{+\bullet}$ (from electron ionization of cyclobutanol¹⁰) were obtained using He and Ar target gases. The emission levels did not allow high-resolution spectra to be obtained for all three isomers. In order to identify the many possible emitting species, smaller fragment ions were studied independently. As will become evident, it is helpful to start with a description of these smaller projectile ions and build towards the analysis of the polyatomic $\text{C}_2\text{H}_4\text{O}^{+\bullet}$ ions.

The CIE spectrum of 8 keV $\text{CO}^{+\bullet}$ projectile–He target gas collisions is shown in Figure 1(a). Clearly defined are emissions due to the excited $\text{CO}^{+\bullet}$ molecular ion transition $\text{B } ^2\Sigma \rightarrow \text{X } ^2\Sigma$ ($\Delta v = +2, +1, 0, -1$ and -2 at 206, 211, 219, 230 and 246 nm, respectively)¹¹ and less certainly, the $\text{A } ^2\Pi \rightarrow \text{X } ^2\Sigma$ ($\Delta v = +4, +3, +2$ and $+1$ at 403, 426, 458 and 471 nm, respectively)¹¹ and $\text{B } ^2\Sigma \rightarrow \text{A } ^2\Pi$ ($\Delta v = +3, +2$ and $+1$ at 326, 346 and 371 nm, respectively)¹¹ transitions. Also seen are the excited fragments C ($3s \ ^1P^0 \rightarrow 2p \ ^1D$, 193 nm) and O^+ ($4p \ ^2D^0 \rightarrow 2p^4 \ ^2P$, 283.6 nm).¹² Target gas He lines at 388.8 nm and 447.1 nm are also present.¹² When Ar was used as the target, a host of O^+ lines (407 nm, 418 nm, 426 nm, 435 nm and 488 nm) as well as Ar^+ emissions ($4d \ ^2F \rightarrow 4p \ ^2D^0$, 346–356 nm, $5d \ ^2F \rightarrow 4p' \ ^2D^0$, 347, 354 nm and $4p' \ ^2P^0 \rightarrow 3d \ ^2F$, 453 nm)¹³ were identified. With this information emissions appearing in other spectra from excited Ar^+ , He, $\text{CO}^{+\bullet}$, C and O^+ can be identified.

The $\text{CO}^{+\bullet}$ system was extended by one hydrogen atom by studying HCO^+ ions formed from oxirane in the ion source. The ions were also formed from methanol and acetaldehyde and the resulting CIE spectra were identical. The He CIE spectrum is shown in Figure 1(b). Along with the $\text{CO}^{+\bullet}$ ($\text{B} \rightarrow \text{X}$), C, He and O^+ emissions described above, a set of bands corresponding to the HC ($\text{A } ^2\Delta \rightarrow \text{X } ^2\Pi$) and HC^+ ($\text{B } ^1\Delta \rightarrow \text{A } ^1\Pi$) emissions¹¹ and the hydrogen Balmer β line ($n = 4 \rightarrow n = 2$)¹² were also observed. This is in agreement with a previous study of the HCO^+ –target gas collision-induced emission spectrum.¹⁴ With Ar as the target in the OC, the He lines are replaced by Ar^+ lines which overlap the HC^+ ($\text{B} \rightarrow \text{A}$) transition. When the HCO^+ –He collisions were performed in the PC and emissions observed in the OC (post-collision observations), essentially only the emissions from the diatomic species remained and the presence of the HC ($\text{B } ^2\Sigma \rightarrow \text{X } ^2\Pi$) and HC^+ ($\text{A } ^1\Pi \rightarrow \text{X } ^1\Sigma$) transitions between 360 nm and 420 nm were both evident. The time required to traverse the distance between the PC and the OC eliminated atomic emissions which have very short lifetimes.

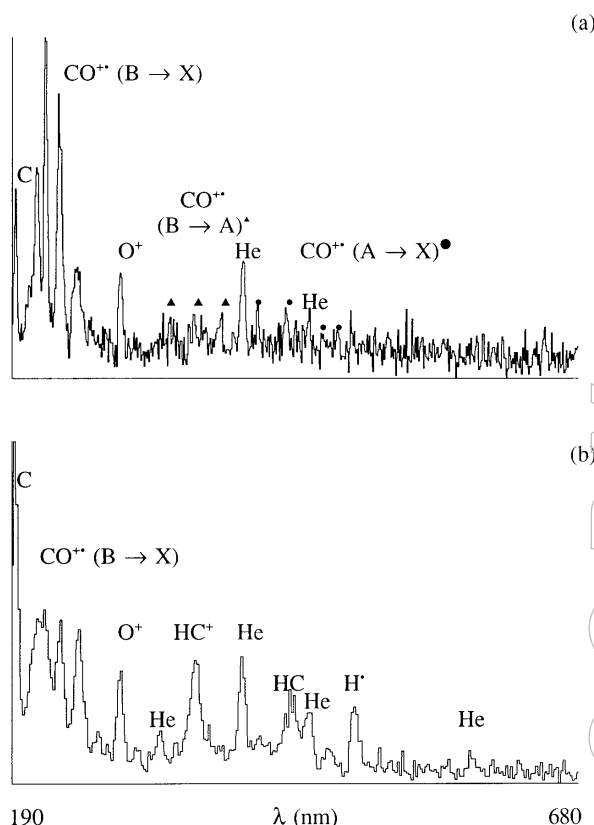


Figure 1. Collision-induced emission spectrum obtained from collisions between (a) $\text{CO}^{+\bullet}$ and He (1.0 mm slits, 1 nm step size, 5 scan average) and (b) HCO^+ and He (2 mm slits, 2 nm step size, 3 scan average).

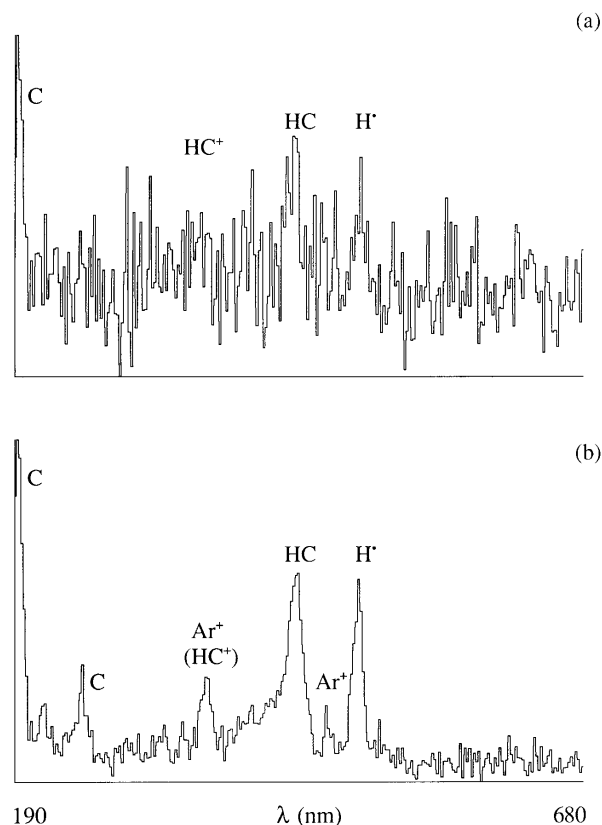


Figure 2. Collision-induced emission spectra obtained from collisions between (a) oxirane $^{+\bullet}$ and He (3 mm slits, 2 nm step size, 13 scan average) and (b) oxirane $^{+\bullet}$ and Ar (3 mm slits, 2 nm step size, 11 scan average).

CH_3^+

Methyl cation (from EI dissociative ionization of methane in the ion source)–He target gas collisions produced a CIE spectrum which exhibited the C, He, $\text{H}^+(4 \rightarrow 2)$, $\text{HC}^+(\text{B} \rightarrow \text{A})$ and $\text{HC}(\text{A} \rightarrow \text{X})$ bands. A previous optical study of high keV H^+ – CH_4 collisions¹⁵ yielded emissions from the $\text{HC}(\text{A}, \text{B})$ and $\text{C} \rightarrow \text{X}$ transitions as well as $\text{HC}^+(\text{A} \rightarrow \text{X})$ and ($\text{b}^3\Sigma \rightarrow \text{a}^3\Pi$) transitions.

Oxirane $^{+\bullet}$

The spectrum obtained from 8 keV oxirane $^{+\bullet}$ –He target gas collisions is shown in Figure 2(a). The spectrum is quite weak but the aforementioned C, H^+ (Balmer- β), $\text{HC}(\text{A} \rightarrow \text{X})$ and $\text{HC}^+(\text{B} \rightarrow \text{A})$ transitions are distinguishable. With Ar as the target, Figure 2(b), most of the above features are enhanced. There was sufficient signal-to-noise in this experiment to measure the post-collision emission spectrum. Only the diatomic $\text{HC}^+(\text{B} \rightarrow \text{A})$, $\text{HC}(\text{A} \rightarrow \text{X})$ and possibly the $\text{HC}(\text{B} \rightarrow \text{X})$ and $\text{HC}^+(\text{A} \rightarrow \text{X})$ transitions remained, together with a small contribution from C. Higher resolution spectra enabled the positive identification of the C and H^+ lines at 193 nm and 486 nm. The oxirane $^{+\bullet}$ –Ar CIE spectrum was also obtainable with 80% ion beam transmission and was identical with the 60% transmission spectrum in Figure 2(b), indicating that

multiple collision events were not responsible for the generation of the emitting species.

Acetaldehyde $^{+\bullet}$

The He CIE spectrum of 8 keV $\text{CH}_3\text{CHO}^{+\bullet}$ projectile ions, Figure 3(a), was similar to that of oxirane $^{+\bullet}$. The same features were present but with two new bands, one at ~283 nm which may be the above mentioned O^+ line (see $\text{CO}^{+\bullet}$ discussion above) and another at ~311 nm. This latter feature may be the $\text{HO}^+(\text{A}^2\Sigma^+ \rightarrow \text{X}^2\Pi) \Delta v = 0$ band common to emissions from flames.¹¹ The spectrum may also include the $\text{CO}^{+\bullet}(\text{B} \rightarrow \text{X})$ bands between 193 and 260 nm.

When Ar was employed as the target, Figure 3(b), all of the above features were observed with the two extra bands at 283 nm and 311 nm decreasing in relative intensity.

Vinyl alcohol $^{+\bullet}$

The CIE spectrum from collisions of 8 keV $\text{CH}_2=\text{CHOH}^{+\bullet}$ projectile ions with He was slightly different from the other two isomers, Figure 4(a). The C, O^+ , He and H^+ (Balmer- β) atomic emissions are present together with the $\text{HC}^+(\text{B} \rightarrow \text{A})$, $\text{HC}(\text{A} \rightarrow \text{X})$ and $\text{HO}^+(\text{A} \rightarrow \text{X})$ bands. The contributions from the O^+ and OH^+ bands are relatively more intense than with either oxirane $^{+\bullet}$ or acetaldehyde $^{+\bullet}$. The Ar CIE spectrum,

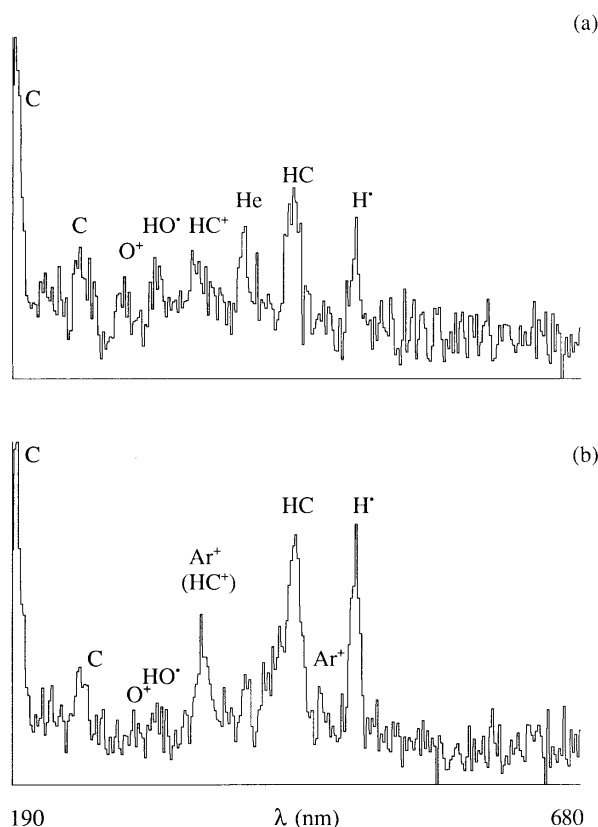


Figure 3. Collision-induced emission spectra obtained from collisions between (a) acetaldehyde⁺ and He (3 mm slits, 2 nm step size, 16 scan average) and (b) acetaldehyde⁺ and Ar (3 mm slits, 2 nm step size, 14 scan average).

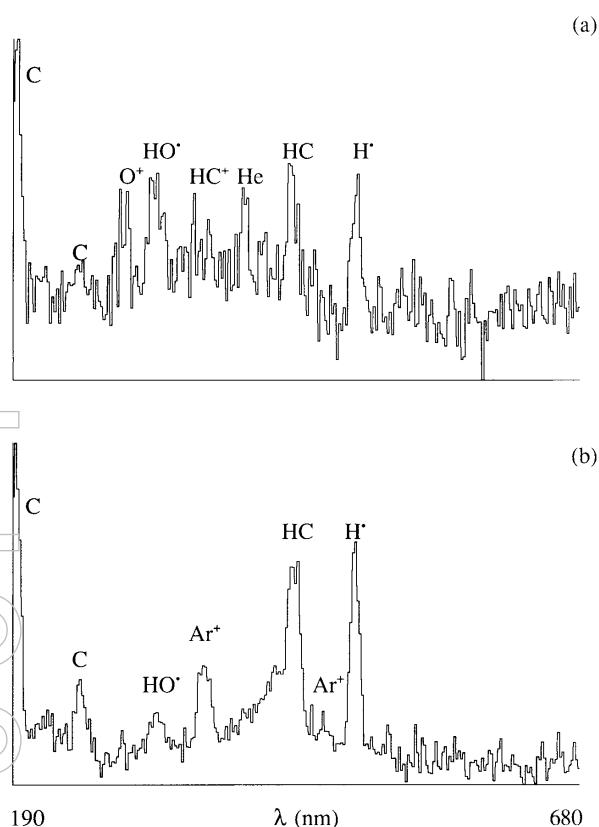


Figure 4. Collision-induced emission spectrum obtained from collisions between vinyl alcohol⁺ and He (3 mm slits, 2 nm step size, 15 scan average) and (b) vinyl alcohol⁺ and Ar (3 mm slits, 2 nm step size, 12 scan average).

Figure 4(b), contained the same peaks, all of which were enhanced in intensity except the O⁺ band at 283 nm.

Emissions from isomeric C₂H₅Cl⁺ ion-target gas collisions

As with the C₂H₄O⁺ isomers, it was helpful to start with smaller fragment ions before attempting to interpret the CIE spectra of the two C₂H₅Cl⁺ isomers.

CCl⁺

The He CIE spectrum of 8 keV CCl⁺ (from electron ionization of CH₂Cl₂ in the ion source) is shown in Figure 5. The dominant feature is the band at 237 nm which corresponds to the A ¹Π → X ¹Σ⁺ transition of CCl⁺.¹⁶ There is also a minor peak at 193 nm which is the same C emission as observed for CO⁺.

CH₂Cl⁺

The chloromethyl cation (from electron ionization of CH₂Cl₂ in the ion source) exhibits several peaks in its helium CIE spectrum, Figure 6(a). Some features are similar to those observed for the C₂H₄O⁺ ions, the C, H• (Balmer-β), HC⁺ (B → A) and HC (A → X) bands. A strong emission arises from

the CCl⁺ (A → X) transition. There are three other bands at ~285, 314 and 389 nm. The feature at 389 nm may be due to the HC (B → X) transition together with the HC⁺ (A → X) transition. These two transitions are more intense than observed in the C₂H₄O⁺ systems described above. When the collisions were performed in the PC, the only bands that remained in the spectrum were the CCl⁺, HC⁺, HC, C (minor) and 285 nm peaks. This suggests that the 285 nm band is *not* atomic and that the 314 nm band *is* atomic in nature.

When Ar was used as the target gas, Figure 6(b), the CIE spectrum showed considerable differences. The C, H•, HC (A → X) and Ar⁺ emissions are present, but the CCl⁺ (A → X) band is considerably less intense than when He was the target. The two minor bands at 285 and 314 nm are still present, along with Cl⁺ emissions¹³ at 384 and 479 nm (which become clearer under higher resolution). Again, when the collisions were performed in the PC, only the non-atomic bands listed above remained to any great extent.

CH₂CH₂Cl⁺

The He CIE spectrum of 8 keV ethyl chloride ions is shown in Figure 7(a). It was a weak spectrum and so only the major components were discernable. The previously described C, H• and HC (A → X) bands are present, together with possibly the CCl⁺ transition at 237 nm. The poor resolution of this spec-

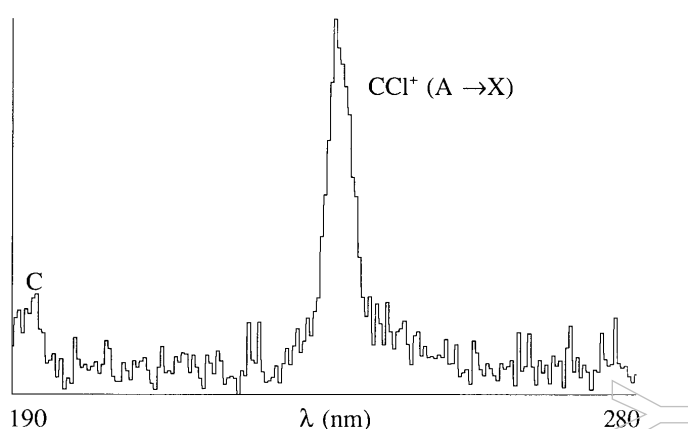


Figure 5. Collision-induced emission spectrum obtained from collisions between CCl^+ and He (1 mm slits, 0.5 nm step size, 3 scan average).

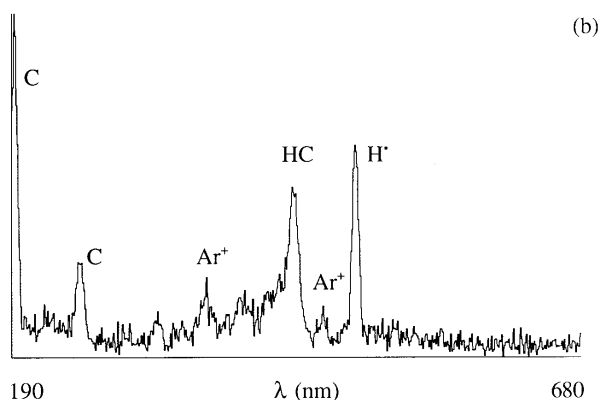
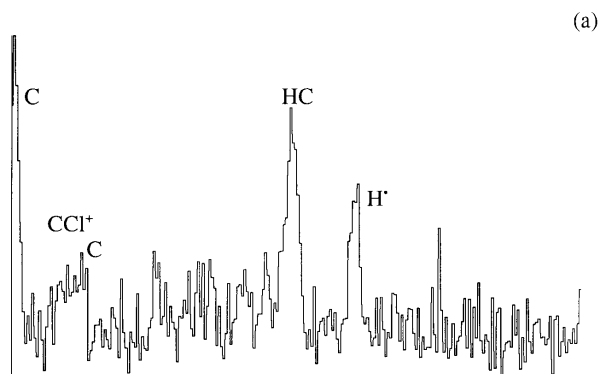


Figure 7. Collision-induced emission spectra obtained from collisions between (a) $\text{CH}_3\text{CH}_2\text{Cl}^{+\bullet}$ and He (3 mm slits, 2 nm step size, 16 scan average) and (b) $\text{CH}_3\text{CH}_2\text{Cl}^{+\bullet}$ and Ar (2 mm slits, 1 nm step size, 5 scan average).

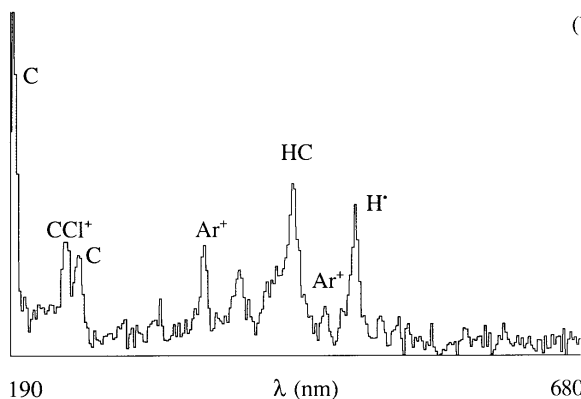
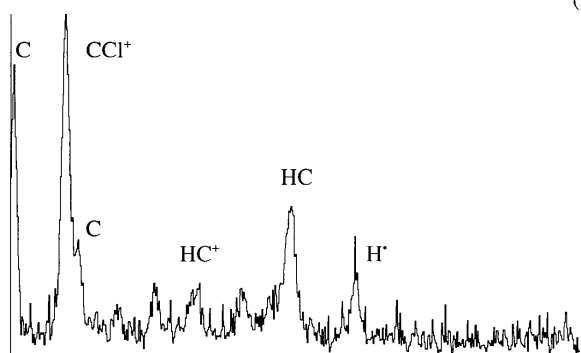
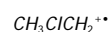


Figure 6. Collision-induced emission spectra obtained from collisions between (a) CH_2Cl^+ and He (2 mm slits, 1 nm step size, 3 scan average) and (b) CH_2Cl^+ and Ar (2 mm slits, 2 nm step size, 8 scan average).

trum does not allow the CCl^+ band to be positively identified. There are possibly several other features between 300 and 420 nm including the above observed band at 314 nm. When Ar was used as the target, Figure 7(b), there was significantly more emission allowing a higher resolution spectrum to be obtained. Similar features were observed, but the CCl^+ band

at 237 nm decreased greatly in intensity. Post-collision observations using Ar target gas identified the HC ($\text{A}, \text{B} \rightarrow \text{X}$) and the HC^+ ($\text{B} \rightarrow \text{A}$ and possibly $\text{A} \rightarrow \text{X}$) transitions as the dominant non-atomic emission sources. The experiment was also performed with sufficient argon to reduce the ion flux to 80% of its pre-cell value, and a weaker CIE spectrum similar to Figure 7(b) was obtained; again, multiple collision processes probably do not contribute to the observed emission.



The ylidion isomer of $\text{CH}_3\text{CH}_2\text{Cl}^{+\bullet}$, $\text{CH}_3\text{ClCH}_2^{+\bullet}$ (formed from electron ionization of $\text{CH}_3\text{OC}(\text{O})\text{CH}_2\text{Cl}$ in the ion source¹⁷) contains the same groups as ethyl chloride and so has a similar CID mass spectrum¹⁷ in spite of the different connectivity of the atoms. Unfortunately, the He CIE spectrum of this ion was extremely weak, owing primarily to a relatively smaller yield of these ions being obtained from the ion source. The Ar CIE spectrum, Figure 8, was more easily interpreted. In many ways it was simpler than the corresponding $\text{CH}_3\text{CH}_2\text{Cl}^{+\bullet}$ spectrum.

Only the two C peaks, the H^+ (Balmer- β) and the HC ($\text{A} \rightarrow \text{X}$) bands were easily observable. There may also be a small band around 308 nm which could be the same as the 314 nm band observed for CH_2Cl^+ and $\text{CH}_3\text{CH}_2\text{Cl}^{+\bullet}$.

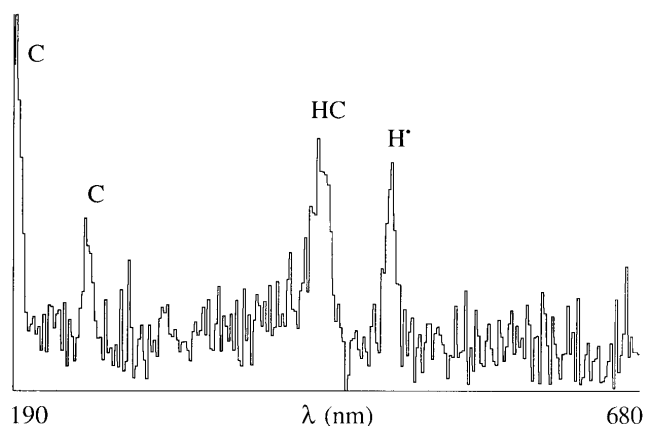


Figure 8. Collision-induced emission spectrum obtained from collisions between $\text{CH}_3\text{ClCH}_2^{+\bullet}$ and Ar (3 mm slits, 2 nm step size, 13 scan average).

Discussion

Information from $\text{C}_2\text{H}_4\text{O}^{+\bullet}$ CIE spectra

No emissions which could be related to intact molecular ions were observed in these experiments (Figures 2–4). In terms of the quasi-equilibrium theory,¹⁸ highly electronically excited polyatomic ions will rapidly undergo radiationless transitions to dissociative states. Such events could lead to only the production of radiatively decaying small fragments, species which are dissociative cul-de-sacs. It may be that when future modifications are made to the observation cell and the detection system, low intensity bands due to emissions from species more complex than atomic and diatomic neutrals and ions will be recognisable, but signal-to-noise in the present experiments precludes their observation. Information *can*, however, be obtained on the minimum excitation of the original $\text{C}_2\text{H}_4\text{O}^{+\bullet}$ ions needed to form the excited atomic and diatomic species responsible for the CIE spectra.

Peak intensities in the CID mass spectra

The He and Ar CID mass spectra of the three isomers, measured under the same conditions as those for the CIE spectra, are listed in Table 1. They are in agreement with those published earlier.^{10,19} In spite of their structural differences, the CID mass spectra of ionized oxirane and acetaldehyde are remarkably similar, both, for example, displaying m/z 15 as a major ion. Differences lie in the C_2H_3^+ and $\text{C}_2\text{H}_2^{+\bullet}$ ion abundances, not surprising for oxirane $^{+\bullet}$ in view of the ease of ring opening¹⁹ to the more stable distonic ion $^{\bullet}\text{CH}_2\text{OCH}_2^+$. Vinyl alcohol ions also display a strong m/z 15 peak but then their rearrangement to ionized methylhydroxycarbene, $\text{CH}_3\text{COH}^{+\bullet}$, is known to precede their fragmentation.²⁰ The strongest distinguishing feature for $\text{CH}_2=\text{CHOH}^{+\bullet}$ is the greater relative intensity of m/z 27 and m/z 26. Distinguishing features of the CIE spectra of the three isomers do not easily relate to fragment peak intensities in the CID mass spectra and, at the present level of sensitivity, they do not permit a ready distinction between ionized oxirane and acetaldehyde.

Table 1. Relative intensities of peaks in the He (Ar) CID mass spectra^a of the three $\text{C}_2\text{H}_4\text{O}^{+\bullet}$ isomers.

m/z	oxirane $^{+\bullet}$		acetaldehyde $^{+\bullet}$		vinyl alcohol $^{+\bullet}$	
43	23	(25)	100	(100)	100	(100)
42	8	(6)	11	(11)	26	(20)
41	0.6	(0.5)	3.6	(3)	5	(3)
40	—	(—)	0.7	(1.1)	1	(0.3)
31	0.6	(1)	—	(—)	—	(—)
30	1.6	(1.8)	0.4	(—)	3	(0.6)
29	100	(100)	53	(80)	53	(26)
28	5	(3)	6	(4)	5	(2)
27	—	(0.5)	3	(2.2)	22	(17)
26	0.6	(0.5)	6.5	(3)	19	(12)
25	—	(—)	3	(0.7)	7	(3)
24	—	(—)	0.7	(—)	1.5	(0.6)
16	3	(4)	1.5	(3)	1	(0.6)
15	14	(16)	13	(15.6)	23	(20)
14	9	(8)	6	(5.5)	9	(6.5)
13	1.3	(1)	2	(1.5)	3	(2)
12	0.4	(0.5)	0.8	(0.7)	1	(0.6)

^aHelium (argon) target gas in the OC, 60% ion beam transmission.

There was almost no detectable ion with m/z 31 (C loss) in the CID spectra to coincide with the large amount of excited atomic C observed in the CIE spectra and it is in any case unlikely to have been formed directly from the molecular ions. Ions with m/z 13 (HC^+) and m/z 30 (HC loss) were relatively minor peaks, though of similar intensities.

Two emission bands possibly directly relate to the CID mass spectra, the bands for O^+ (284 nm) and HO^{\bullet} (312 nm). The counter-ion to HO^{\bullet} formation, C_2H_3^+ , is nearly non-existent in the CID of oxirane $^{+\bullet}$, only 3% of base peak for acetaldehyde $^{+\bullet}$ and about 20% for vinyl alcohol $^{+\bullet}$. This is in keeping with the relatively similar growth of the HO^{\bullet} emission band. On the other hand, the O^+ peak in the CID mass spectra (which may be interfered with by $\text{CH}_4^{+\bullet}$) follows the opposite trend, being most intense for oxirane $^{+\bullet}$ and least intense for vinyl alcohol $^{+\bullet}$. Producing O^+ in the 4d ^2F excited state requires 40 eV, an energy demand which may make it a relatively less likely process for vinyl alcohol $^{+\bullet}$.

Energy deposition

The excited electronic levels of oxirane, acetaldehyde and vinyl alcohol molecular ions are known from photoelectron

Table 2. Minimum precursor excitation in 8 keV $C_2H_4O^{++}$ -target gas collisions.

Excited fragment	Counterpart ^a	Minimum excitation ^b (eV)		
		Oxirane ⁺⁺	Acetaldehyde ⁺⁺	Vinyl alcohol ⁺⁺
C (3s ¹ P ⁰)	$\bullet CH_2OH_2^+$	14.4	15.9	16.5
H [•] (n = 4)	CH_3CO^+	11.7	13.2	13.9
O ⁺ (4p ² D ⁰)	$CH_2=CH_2$	37.4	38.9	39.6
HC ⁺ (B ¹ Δ)	$\bullet CH_2OH$	13.0	14.5	15.2
HC (A ² Δ)	$\bullet CH_2OH$	6.3	7.8	8.5
HO [•] (A ² Σ ⁺)	$C_2H_3^+$	5.9	7.4	8.1

^aLowest possible energy ground state counter-ion/neutral.^bCalculated based on ground state heats of formation of fragment, counterpart and precursor (Reference 22) and excited state energies (References 11 and 12) unless otherwise stated.

spectroscopy.²¹ The highest state observed, the E state, was less than 10 eV above their respective ground states. The excited fragment species observed in the CIE spectra of the three isomers, the lowest energy ground state counter-ions or neutrals and the minimum excitation in each precursor ion required directly to form the products, are listed in Table 2.

All but one of the emissions observed in the CIE spectra were the result of at least 6–14 eV being converted from translational kinetic energy to internal energy of the three molecular ions. However, no emissions were detected due to excitation processes requiring less than 6 eV. If intense emissions only result from very rapid dissociations of the ions having sufficient energy to produce electronically excited atomic and diatomic fragments, then it is not surprising that the less energized ions do not give rise to emissions.

Effect of target gas

The He and Ar CIE spectra of each isomer involved similar excited species but their amounts differed greatly. With Ar, ion beam emissions due to C, HC and H[•] were all enhanced. However, the relative abundance of O⁺ and HO[•] in the CIE spectra of acetaldehyde⁺⁺ and vinyl alcohol⁺⁺ decreased with the introduction of Ar as the target gas. Enhancement of ion beam emissions may be due to the multitude of excited states of Ar which can be easily accessible in interactions with the projectile ion. The exact nature of these interactions could not be determined in this study.

When Ar was the target, emissions from excited state Ar⁺ formed by charge transfer with the projectile ion were observed. The charge transfer reaction from ground state Ar to produce ground state oxirane is endothermic by 5.3 eV and is even more so for acetaldehyde, 5.5 eV, and vinyl alcohol, 6.6 eV. If Ar⁺ was formed in the 4d ²F state, the charge transfer reactions become even more endothermic, 23.3 eV.¹³

Information from $C_2H_5Cl^{++}$ CIE spectra

All of the emissions observed in the CIE spectra of the two $C_2H_5Cl^{++}$ ions were from atomic and diatomic ions and neutrals. The chief surprise was the lack of emissions from Cl containing species, except for a weak CCl⁺ signal in the He- $CH_3CH_2Cl^{++}$ spectrum [Figure 7(a)]. As for the $C_2H_4O^{++}$ ions, the spectra can be used to examine energy deposition in the projectile ions prior to dissociation.

Peak intensities in the CID mass spectra

The He (Ar) CID mass spectra of the two isomers are listed in Table 3. The two CID spectra are easily distinguishable, exhibiting different m/z 49 : m/z 29 peak intensity ratios. The use of Ar as the target does not significantly change the mass spectra. It is evident that most of the atomic and diatomic emitting species observed in the CIE spectra (Figures 7 and 8) do not result from a simple dissociation but rather from at least two consecutive dissociations. The dissociation of a $C_2H_5Cl^{++}$ ion to form a carbon atom would require the formation of an ion of composition $C_2H_5Cl^{++}$, which could only be an ion-neutral complex involving, e.g. CH_4 and HCl . It is therefore unlikely that the C (3s ¹P⁰) atom results from the direct dissociation of the molecular ions but comes rather from secondary fragmentations of smaller ions. As for carbon atom formation, HC⁺ must be produced in a two step process since an intact neutral counterpart of composition C_2H_4Cl would be a hypervalent radical. The generation of HC⁺ (B) may be accompanied by $CH_4 + Cl$ or $CH_3^{\bullet} + HCl$. To form CCl⁺, the two isomers must eliminate CH_5 (another hypervalent radical) or more likely H[•] + CH_4 or similar combination of fragments.

Energy deposition

The excited fragment species observed in the CIE spectra of the two isomers, the lowest energy ground state counter-

Table 3. Relative intensities of the peaks in the He (Ar) CID mass spectra^a of two C₂H₅Cl⁺⁺ isomers.

<i>m/z</i>	CH ₃ CH ₂ Cl ⁺⁺		CH ₃ ClCH ₂ ⁺⁺	
		()		()
63	5	(8)	1.4	(2)
62	1.8	(2)	0.2	(0.3)
61	1.8	(1.4)	2.5	(2)
60	1.2	(0.6)	0.5	(0.2)
59	>0	(>0)	—	(—)
51	—	(—)	0.9	(0.6)
50	—	(—)	5	(3.2)
49	23.4	(23)	100	(100)
48	4	(4)	13	(11.6)
47	4	(4)	11.6	(9)
36	1.2	(1.4)	0.9	(0.6)
35	1.8	(3.4)	0.9	(0.6)
29	100	(100)	62	(48.4)
28	84.5	(88.6)	11.6	(9)
27	26.1	(27)	5.6	(3.2)
26	10.6	(8.6)	2.3	(1)
25	2.1	(1.7)	>0	(—)
24	0.3	(0.3)	—	(—)
16	—	(—)	0.5	(—)
15	0.3	(0.1)	2.8	(1.3)
14	0.3	(0.3)	2.8	(1.3)
13	>0	(0.1)	0.5	(0.3)
12	—	(—)	0.5	(—)

^aHelium (argon) target gas in the OC, 60% ion beam transmission.

ions or neutrals and the minimum excitation in each precursor ion required to form the products are listed in Table 4.

Effect of target gas

One difference between the CIE spectra obtained for CH₃CH₂Cl⁺⁺ and CH₃ClCH₂⁺⁺ using He and Ar target gases, aside from the enhancement of ion beam emissions with Ar, was the abundance of the CCl⁺ (A → X) emission band. There is evidence for this band in the He CIE spectra of both isomers, while it clearly vanishes when Ar was the target.

The same Ar⁺ bands observed in the C₂H₄O⁺⁺ CIE spectra were present in the Ar CIE spectrum of CH₃CH₂Cl⁺⁺, Figure 7(b).

Table 4. Minimum precursor excitation in 8 keV C₂H₅Cl⁺⁺-target gas collisions.

Excited fragment	Counterpart ^a	Minimum excitation ^b (eV)	
		CH ₃ CH ₂ Cl ⁺⁺	CH ₃ ClCH ₂ ⁺⁺¹⁷
C (3s ¹ P ⁰)	CH ₄ ⁺⁺ + HCl	16.9	16.2
H ⁺ (<i>n</i> = 4)	CH ₃ CHCl ⁺	13.8	13.1
HC ⁺ (B ¹ Δ)	CH ₄ + Cl	14.0	13.3
HC (A ² Δ)	CH ₃ ClH ⁺	7.2	6.5
CCl ⁺ (A ¹ Π) ¹⁶	CH ₄ + H ⁺	9.3	8.6

^aLowest possible ground state counter-ion/neutral.

^bCalculated based on ground state heats of formation of fragment, counterpart and precursor (Reference 22) and excited state energies (References 11 and 12) unless otherwise stated.

The charge transfer between Ar and ethyl chloride⁺⁺ is endothermic by 4.78 eV, but will be considerably more so if Ar⁺ is formed in the 4d ²F state. There is no mass spectrometric evidence for the existence of stable neutral CH₃ClCH₂.¹⁷ Interestingly, no Ar⁺ emission bands are obvious in Figure 8, indicating that the charge transfer reaction to form excited Ar⁺ does not occur.

Conclusions

Even though photon emissions from polyatomic projectile-target gas collisions are due (at the present level of sensitivity) only to atomic and diatomic fragments, information can be obtained concerning the amount of translational kinetic energy which is converted into internal energy during the collision event. The CIE spectra obviously represent only a small fraction of the excitation events occurring in the collision cell for polyatomic projectiles. The origin of many of the excited state species observed in the CIE spectra is not a simple one-step dissociation from the molecular ions. Collisional excitation followed by dissociation of the precursor ions may have yielded a wide variety of excited state fragments but these fragments themselves must also dissociate into smaller species until the atomic and diatomic ions and neutrals (typically having large dissociation energies) exhibited in Figures 2–8 were formed. Moreover, for collision processes depositing less energy into the molecular ions, polyatomic fragments which are not electronically but vibrationally excited may be formed.

This technique presents a new look at the processes occurring in the collision event and has provided information on the excitation events which are possible in keV polyatomic projectile-target gas collisions, information unobtainable from experiments which rely on the interpretation of mass spectra. This was a primary purpose for starting this investigation.

Experiments which deserve to be performed are (a) lowering the accelerating voltage to 2 or 3 keV and examining changes in the CIE and CID spectra, (b) studying ions whose neutral counterparts are unstable and examining the changes, if any, in emissions from ionized target gas species formed in charge transfer reactions and (c) changing the PC-to-OC distance to investigate excited state species with longer lifetimes. Other possible experiments are (a) studying neutral polyatomic projectiles after neutralizing charged projectiles in the first 3FFR collision cell and deflecting away the remaining ions with the deflector electrode (Figure 1), (b) studying the CIE spectra of negative ions and (c) ions formed from the dissociation of metastable precursor ions in the 2FFR. These latter experiments will require a more sensitive observation technique (OC, analyzer and detector). Presently, a charge-coupled device array detector is being introduced into the experiment. It should increase the sensitivity enough to perform all of the experiments described above.

Acknowledgements

JLH wishes to thank the Natural Sciences and Engineering Research Council of Canada for continuing financial support and PMM thanks the same organization for a Postgraduate Scholarship during the tenure of which this work was completed.

References

1. R.G. Cooks, *Collision Spectroscopy*. Plenum Press, New York, Ch. 7 (1978).
2. P.J. Todd and F.W. McLafferty, *Tandem Mass Spectrometry*. Wiley-Interscience, New York, Ch. 7. (1983).
3. J.A. Laramee, D. Cameron and R.G. Cooks, *J. Am. Chem. Soc.* **103**, 12 (1981).
4. C.J. Porter, R.P. Morgan and J.H. Beynon, *Int. J. Mass Spectrom. Ion Phys.* **28**, 321 (1978).
5. M.S. Kim and F.W. McLafferty, *J. Am. Chem. Soc.* **100**, 3279 (1978).
6. J.L. Holmes, P.M. Mayer and A.A. Mommers, *J. Am. Chem. Soc.* **113**, 9405 (1991).
7. J.L. Holmes, P.M. Mayer and A.A. Mommers, *Org. Mass Spectrom.* **27**, 537 (1992).
8. J.L. Holmes, P.M. Mayer and A.A. Mommers, *Int. J. Mass Spectrom. Ion Proc.*
9. J.L. Holmes and P.M. Mayer, *Org. Mass Spectrom.*, in press.
10. C.C. Van de Sande and F.W. McLafferty, *J. Am. Chem. Soc.* **97**, 4613 (1975); J.L. Holmes and J.K. Terlouw, *Can. J. Chem.* **53**, 2076 (1975).
11. R.W.B. Pearce and A.G. Gaynon, *The Identification of Molecular Spectra*, 4th Edn. Chapman and Hall, London (1978).
12. S. Bashkin and J.O. Stoner, Jr, *Atomic Energy Levels and Grotrian Diagrams*, Vol. I. North-Holland Publishing Co., New York (1975).
13. S. Bashkin and J.O. Stoner, Jr, *Atomic Energy Levels and Grotrian Diagrams*, Vol. II. North-Holland Publishing Co., New York (1975).
14. A. Michael, P. Misra, A. Farah and V. Kushawaha, *J. Phys. B: At., Mol. Opt. Phys.* **25**, 2343 (1992).
15. M. Carre, *Physica*. **41**, 63 (1969).
16. H. Bredohl, I. Dubois and F. Melen, *J. Mol. Spectrosc.* **98**, 495 (1983).
17. M.C. Blanchette, J.L. Holmes and F.P. Lossing, *Org. Mass Spectrom.* **22**, 701 (1987).
18. H.B. Rosenstock, M.B. Wallenstein, A.L. Wahrhaftig and H. Eyring, *Proc. Nat. Acad. Sci.* **38**, 667 (1952).
19. J.M. Buschek, J.L. Holmes and J.K. Terlouw, *J. Am. Chem. Soc.* **109**, 7321 (1987).
20. J.K. Terlouw, J. Wezenburg, P.C. Burgers and J.L. Holmes, *J. Chem. Soc. Chem. Commun.* 1121 (1983); Y. Apeloig, M. Karni, B. Ciommer, G. Depke, O. Frenking, S. Meyr, J. Schmidt and H. Schwarz, *Int. J. Mass Spectrom. Ion Proc.* **59**, 21 (1984).
21. K. Johnson, I. Powis and C.J. Danby, *Chem. Phys.* **70**, 329 (1982).
22. S.G. Lias, J.E. Bartmess, J.F. Liebman, J.L. Holmes, R.D. Levin and W.G. Mallard, *J. Phys. Chem. Ref. Data* **17**(Suppl. 1) (1988).

Received: 8 November 1994

Accepted: 22 December 1994

The mechanism of alkene elimination from the oxonium ions
 $(\text{CH}_3\text{CH}_2)_2\text{C}=\text{OH}^+$, $\text{CH}_3\text{CH}_2\text{CH}_2(\text{CH}_3)\text{C}=\text{OH}^+$
 and $(\text{CH}_3\text{CH}_2\text{CH}_2)_2\text{C}=\text{OH}^+$

Richard D. Bowen*

Chemistry and Chemical Technology, University of Bradford, Bradford, West Yorkshire BD7 1DP, England.

Dennis Suh and Johan K. Terlouw*

Department of Chemistry, McMaster University, Hamilton, Ontario L8S 4M1, Canada.

The reactions of the metastable oxonium ions $(\text{CH}_3\text{CH}_2)_2\text{C}=\text{OH}^+$, $\text{CH}_3\text{CH}_2\text{CH}_2(\text{CH}_3)\text{C}=\text{OH}^+$ and $(\text{CH}_3\text{CH}_2\text{CH}_2)_2\text{C}=\text{OH}^+$ have been studied by ^{13}C -labelling experiments. The mechanism of alkene elimination from these oxonium ions is discussed in the light of earlier studies on the behaviour of their lower homologues, $(\text{CH}_3)_2\text{C}=\text{OH}^+$ and $\text{CH}_3\text{CH}_2\text{CH}=\text{OH}^+$, which eliminate ethylene. Propene loss from $(\text{CH}_3\text{CH}_2)_2\text{C}=\text{OH}^+$ must entail skeletal rearrangement leading to $\text{CH}_3\text{CH}_2\text{CH}_2(\text{CH}_3)\text{C}=\text{OH}^+$ or related structures. These isomerisation sequences may be formulated in three plausible ways. The first two possibilities involve 1,2-H shifts in conjunction with ring-closures to either protonated oxiranes or oxetanes, followed by ring-opening in the opposite sense, thus breaking the original C–O bond and allowing the hydroxy function to migrate along the carbon chain. Alternatively, a combination of 1,2-H and 1,2-alkyl shifts permits the carbon skeleton to be isomerised via the isomeric oxonium ion, $\text{CH}_3\text{CH}_2(\text{CH}_3)\text{CHCH}=\text{OH}^+$, without disrupting the C–O bond. Both $(\text{CH}_3\text{CH}_2)_2\text{C}=\text{OH}^+$ and $\text{CH}_3\text{CH}_2\text{CH}_2(\text{CH}_3)\text{C}=\text{OH}^+$ lose C_3H_6 with closely similar high selectivities (88 and 89%, respectively). This observation shows that the first two routes compete very poorly with the third pathway in which rearrangement of the carbon skeleton occurs without migration of the oxygen function. Extension of the mechanistic investigation to include propene and butene expulsion from metastable $(\text{CH}_3\text{CH}_2\text{CH}_2)_2\text{C}=\text{OH}^+$ shows that this preference for retaining the initial C–O connection is general: $(\text{CH}_3\text{CH}_2\text{CH}_2)_2\text{C}=\text{OH}^+$ eliminates C_3H_6 and C_4H_8 with extremely high selectivities (~99%).

Introduction

Many members of the important homologous series of oxonium ions, $\text{C}_n\text{H}_{2n+1}\text{O}^+$, have been extensively investigated, especially at low internal energies, thus giving considerable mechanistic insight into their interesting chemistry.¹ A major class of fragmentation is alkene loss, which often may be described by several reasonable mechanisms involving conventional steps and classical intermediates. Thus, metastable $(\text{CH}_3)_2\text{C}=\text{OH}^+$, **1**, and $\text{CH}_3\text{CH}_2\text{CH}=\text{OH}^+$, **2**, eliminate C_2H_4 .^{2,3}

An early study⁴ found that the carbon atoms of the eliminated molecule of ethylene were selected at random in fast fragmentations of ^{13}C -labelled analogues of **1**. However, two subsequent investigations showed that $(\text{CH}_3)_2\text{C}=\text{OH}^+$ lost C_2H_4 with high selectivities in both fast fragmentations in the ion source (89%⁵) and slow dissociations in the field-free regions (99%⁵ and 89%⁶). Consequently, the C–O bond usually remains unbroken when C_2H_4 is eliminated from **1**.^{5,6}

The first study⁶ of ^{13}C -labelled analogues of **2** reported that $\text{CH}_3\text{CH}_2^{13}\text{CH}=\text{OH}^+$ eliminated C_2H_4 and CC^{13}H_4 at almost equal rates (in the ratio 49 : 51). This unexpected result was interpreted by supposing that after two consecutive 1,2-H shifts starting from $\text{CH}_3\text{CH}_2^{13}\text{CH}=\text{OH}^+$, ring closure of the resultant open-chain cation, $^+\text{CH}_2\text{CH}_2^{13}\text{CH}_2\text{OH}$, gives a protonated labelled oxetane, $\text{CH}_2\text{CH}_2^{13}\text{CH}_2\text{OH}^+$, in which the original α - and γ -carbon atoms are equivalent.⁶ Consequently, when this protonated oxetane reopens and ethylene loss occurs by fission of the central C–C bond, C_2H_4 and CC^{13}H_4 are eliminated with equal probabilities by cleavage of $^+\text{CH}_2\text{CH}_2^{13}\text{CH}_2\text{OH}$ and $^{+13}\text{CH}_2\text{CH}_2\text{CH}_2\text{OH}$, respectively. Supporting evidence for this proposal was found in the loss of CC^{13}H_4 with high selectivity (99%) from $\text{CH}_3^{13}\text{CH}_2\text{CH}=\text{OH}^+$.⁶ However, a later investigation⁷ of $\text{CH}_3\text{CH}_2^{13}\text{CH}=\text{OH}^+$ was at variance with the formation of protonated oxetane because it indicated that CC^{13}H_4 elimination was of negligible impor-

tance compared to C_2H_4 loss. A third study⁸ extended the analysis to include $^{13}\text{CH}_3\text{CH}_2\text{CH}=\text{OH}^+$, which was found to expel CC^{13}H_4 with high selectivity, thus confirming that the initial C–O bond in **2** is normally not broken in ethylene elimination. The erroneous early report⁶ of CC^{13}H_4 loss from $\text{CH}_3\text{CH}_2^{13}\text{CH}=\text{OH}^+$ probably arose from confusion caused by an overlapping signal corresponding to C_2H_4 elimination from $\text{CH}_3\text{CH}_2\text{CH}=\text{OH}^+$ generated from residual $\text{CH}_3\text{CH}_2\text{CH}_2\text{OH}$ in the sample of $\text{CH}_3\text{CH}_2^{13}\text{CH}_2\text{OH}$ in which the level of ^{13}C -incorporation was only ~50%.

The most consistent overview of these data is that C_2H_4 loss from **2** takes place after two consecutive 1,2-H shifts, followed by σ -cleavage of $^+\text{CH}_2\text{CH}_2\text{CH}_2\text{OH}$, **3**, without ring closure to $\text{CH}_2\text{CH}_2\text{CH}_2\text{OH}^+$. The rates of these 1,2-H shifts are faster than that of σ -cleavage, thus explaining why the carbon-bound hydrogens of ^2H -labelled analogues of **2** become statistically distributed prior to ethylene loss.⁹ Similarly, fragmentation of **1** proceeds by unidirectional rearrangement to **2**,¹⁰ via a 1,2-H-shift to $^+\text{CH}_2\text{CH}(\text{CH}_3)\text{OH}$, followed by a 1,2-methyl shift, rather than by a route involving formation and subsequent ring opening of the protonated oxirane, $\text{CH}_3\text{CHCH}_2\text{OH}^+$.⁴ The latter alternative [$^+\text{CH}_2\text{CH}(\text{CH}_3)\text{OH} \rightarrow \text{CH}_3\text{CHCH}_2\text{OH}^+ \rightarrow \text{CH}_3\text{CH}^+\text{CH}_2\text{OH}$] is excluded by the ^{13}C -labelling results because migration of the oxygen function would break the original C–O bond. This overall interpretation is consistent with the results of detailed collisional and neutralisation–reionisation studies of $\text{C}_3\text{H}_7\text{O}^+$ ions,^{11,12} which reveal that **2** and $\text{CH}_3\text{CHCH}_2\text{OH}^+$ readily isomerise to form a common structure or mixture of structures that are distinct from **1** and $\text{CH}_2\text{CH}_2\text{CH}_2\text{OH}^+$, both of which are discrete stable species. These results suggest strongly that $\text{CH}_3\text{CHCH}_2\text{OH}^+$ is accessible to **2** via $\text{CH}_3\text{CH}^+\text{CH}_2\text{OH}$, probably on a reversible basis, and that ring-opening of the protonated oxirane at low internal energies always occurs to give the more stable secondary cation, $\text{CH}_3\text{CH}^+\text{CH}_2\text{OH}$, thus conserving the C–O bond in **2**.

A further investigation of the generality of these mechanistic conclusions concerning the mechanism of alkene loss from oxonium ions is now timely. This objective can be achieved by examining the behaviour of the homologous $\text{C}_5\text{H}_{11}\text{O}^+$ ions, which are known to expel C_3H_6 in slow dissociations.^{13,14}

Results and discussion

The oxonium ions $(\text{CH}_3\text{CH}_2)_2\text{C}=\text{OH}^+$, **4**, and $\text{CH}_3\text{CH}_2\text{CH}_2(\text{CH}_3)\text{C}=\text{OH}^+$, **5**, display closely similar reactions that resemble those of $\text{CH}_3\text{CH}_2(\text{CH}_3)\text{CHCH}=\text{OH}^+$, **6**, Table 1. Skeletal isomerisation must precede C_3H_6 elimination from **4** and **6**; moreover, the loss of an appreciable amount of C_3H_6 as well as the expected $\text{C}_3\text{H}_3\text{D}_3$ from $\text{CD}_3\text{CH}_2\text{CH}_2(\text{CH}_3)\text{C}=\text{OH}^+$ shows that propene expulsion cannot be explained unless the initial heavy atom framework of **5** is sometimes reorganised.^{13,14}

Various routes for these skeletal rearrangements have been considered, including migration of the hydroxy function via formation of protonated oxiranes,¹³ Scheme 1, or protonated

Table 1. Reactions of metastable $\text{C}_5\text{H}_{11}\text{O}^+$ ions.

Ion structure	Neutral species lost			
	H_2O		C_3H_6	
	RA^a	T^b	RA	T
$(\text{CH}_3\text{CH}_2)_2\text{C}=\text{OH}^+$	35 ^c 44 ^d 51 ^e 43 ^f	2.2 2.5	65 ^c 56 ^d 49 ^e 57 ^f	1.7
$\text{CH}_3\text{CH}_2\text{CH}_2\text{C}(\text{CH}_3)=\text{OH}^+$	24 ^c 38 ^d 39 ^e 32 ^f	2.2 2.5	76 ^c 62 ^d 61 ^e 68 ^f	1.7
$\text{CH}_3\text{CH}_2\text{CH}(\text{CH}_3)\text{CH}=\text{OH}^+$	49 ^c 70 ^d 71 ^e 58 ^f	1.6 1.8	51 ^c 30 ^d 29 ^e 42 ^f	1.7

^a RA = Relative abundance normalised to a total of 100 units.

^b T = Kinetic energy release (in kJ mol^{-1}) estimated from the width at half-height of the associated metastable peak.

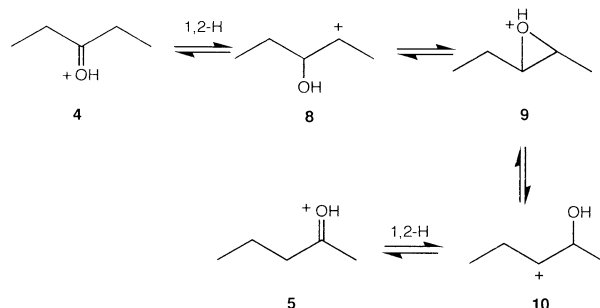
^cMeasured by metastable peak areas arising from dissociation in the second field-free region of the VG Analytical ZAB-R mass spectrometer of ions generated by dissociative ionisation of the appropriate alcohol.

^dMeasured by metastable peak heights arising from dissociation in the second field-free region of an AEI MS 902 mass spectrometer of ions generated by dissociative ionisation of the appropriate alcohol.

^eData from Reference 13 (ions generated by dissociative ionisation of alcohols).

^fData from Reference 14 (ions generated by protonation under chemical ionisation conditions of the appropriate ketone or aldehyde).

oxetanes,¹⁴ Scheme 2. Both these routes involve rupture of the original C–O bond. Alternatively, a series of 1,2-H and 1,2-alkyl shifts could allow **4** and **5** to reach common intermediates accessible to **6**, while maintaining the initial C–O linkage,¹⁴ Scheme 3. The behaviour of ^{13}C -labelled analogues of **4** and **5** unequivocally excludes the first possibility, Table 2. Thus, $(\text{CH}_3\text{CH}_2)_2^{13}\text{C}=\text{OH}^+$ expels C_3H_6 with high selectivity (~88%), but exclusive $\text{C}_2^{13}\text{CH}_6$ elimination would be predicted on the basis of transfer of the oxygen function from C-3



Scheme 1.

Scheme 2.

Scheme 3.

The occurrence of almost identical minor amounts (12% and 11%, respectively) of $\text{C}_2^{13}\text{CH}_6$ expulsion from $(\text{CH}_3\text{CH}_2)_2^{13}\text{C}=\text{OH}^+$ and $\text{CH}_3\text{CH}_2\text{CH}_2(\text{CH}_3)^{13}\text{C}=\text{OH}^+$ points to a common chemistry for these ions in which the C–O bond

Scheme 4.

	Neutral species lost					
	H ₂ O		C ₃ H ₆		C ₂ ¹³ CH ₆	
Ion structure	<i>RA</i> ^a	<i>T</i> ^b	<i>RA</i>	<i>T</i>	<i>RA</i>	<i>T</i>
(CH ₃ CH ₂) ₂ ¹³ C=OH ⁺	33 ^c	2.2	59.1 ^c	1.7	8.2 ^c	1.6
CH ₃ CH ₂ CH ₂ ¹³ C(CH ₃)=OH ⁺	25 ^c	2.3	66.9 ^c	1.7	8.4 ^c	1.5
CH ₃ CH ₂ CH(¹³ CH ₃)CH=OH ⁺	26 ^c	2.3	58.5 ^c	1.7	15.7 ^c	1.5

The loss of a greater proportion (~21%) of $\text{C}_2^{13}\text{CH}_6$ from $\text{CH}_3\text{CH}_2\text{CH}_2(^{13}\text{CH}_3)\text{C}=\text{OH}^+$ suggests strongly that a route other than cyclisation to the protonated oxetane allows the methyl group originally attached to the carbon atom carrying the oxygen function to be transferred to a position from which it can be expelled in the eliminated propene. If rearrangement via the protonated oxetane was the only route for this process, the same percentages of C_3H_6 and $\text{C}_2^{13}\text{CH}_6$ would be lost from $\text{CH}_3\text{CH}_2\text{CH}_2(\text{CH}_3)^{13}\text{C}=\text{OH}^+$ and $\text{CH}_3\text{CH}_2\text{CH}_2(^{13}\text{CH}_3)\text{C}=\text{OH}^+$. A likely explanation is that a small proportion of ions generated as **5** isomerise to **4**, so allowing the two methyl groups to

become equivalent, before dissociation via **11** or **11'** occurs. All the data can be accommodated by Scheme 4: one quarter of the ions which reach structure **11** rearrange to **12**, thus allowing one eighth to expel C_3H_6 after attaining **11'**; similarly, one quarter of ions generated as **5** isomerise via **8** to **4**, so allowing exchange of the two methyl groups to precede formation of **11**.

Scheme 4 also explains some interesting general features of the reactions of **4**, **5** and **6**. Elimination of H_2O competes with C_3H_6 loss more effectively starting from **6** than from **4** or **5**; furthermore, the kinetic energy (KE) release associated with H_2O expulsion from **6** is smaller than those for the corresponding dissociation of **4** and **5**. Thermochemical data¹⁵ indicate that the products given by H_2O loss are $\sim 50 \text{ kJ mol}^{-1}$ more stable than those formed by C_3H_6 expulsion.

These trends reveal that H_2O loss has a lower critical¹⁶ energy than C_3H_6 elimination and that the population of dissociating metastable ions formed as **6** has a lower average^{2,17} internal energy than those generated as **4** or **5**. Isomerisation of **4** and **5** to **7** and other structures accessible to **6** is normally irreversible: these rearranged ions tend to dissociate faster than they revert to **4** or **5**. This finding is in accord with the labelling data. The highest energy species en route to $\text{CH}_3\text{CH}=\text{OH}^+$ and C_3H_6 are probably the secondary cations $\text{CH}_3\text{CH}_2\text{CH}^+\text{CH}(\text{CH}_3)\text{OH}$, **10**, and $\text{CH}_3\text{CH}^+\text{CH}(\text{OH})\text{CH}_2\text{CH}_3$, **8**. These open-chain cations should have appreciably higher enthalpies of formation than the isomeric secondary cation, **11**, because the unfavourable interaction between the electron-withdrawing β -hydroxy group and the nearby charge site will be greater for **8** and **10** than is the case for **11**, which contains a more distant γ -hydroxy substituent.^{18,19} It is significant that the KE releases associated with C_3H_6 loss from **4**, **5** and **6** are the same within experimental error, whereas in H_2O elimination dissociation of **6** has an appreciably lower KE release than those associated with fragmentation of **4** and **5**. This distinction arises because C_3H_6 loss from **4**, **5** and **6** necessarily entails rearrangement to **11** via **10**. However, although **4** and **5** must also isomerise to **8** and/or **10** before expelling H_2O , **6** can undergo this reaction via the more stable tertiary cation $\text{CH}_3\text{CH}_2\text{C}^+(\text{CH}_3)\text{CH}_2\text{OH}$, **7**, without rearranging to either **8** or **10**.

There are clear contrasts between the behaviour of **2** and those of its higher homologues **4**, **5** and **6**. Even at very low internal energies, **2** apparently interconverts freely with the protonated oxirane, $\text{CH}_3\text{CHCH}_2\text{OH}^+$, via $\text{CH}_3\text{CH}^+\text{CH}_2\text{OH}$, as is shown by the close similarity of the collision-induced dissociation (CID) spectra of $\text{C}_3\text{H}_7\text{O}^+$ ions generated by direct protonation of propionaldehyde and methyloxirane, respectively.^{11,12} However, **2** does not rearrange to the protonated oxetane, $\text{CH}_2\text{CH}_2\text{CH}_2\text{OH}^+$, via $^+\text{CH}_2\text{CH}_2\text{CH}_2\text{OH}$, even at the slightly higher internal energies needed to induce C_2H_4 loss.^{7,8} On the other hand, the ^{13}C -labelling results reported in this study establish that **4** and **5** do not interconvert rapidly via the corresponding protonated oxirane, **9**, prior to elimination of C_3H_6 . This finding is consistent with collisional studies^{14,20} of $\text{C}_5\text{H}_{11}\text{O}^+$ ions generated by fragmentation of ionised alcohols

or by protonation of the appropriate $\text{C}_5\text{H}_{10}\text{O}$ precursors: although the reactions of metastable **4** and **5** are essentially identical and similar to those of **6**,^{13,14} each of these three ions displays a distinctive CID spectrum, all of which differ from that of **9**. These results indicate that **4**, **5** and **6** (and probably **9**) exist in discrete potential energy wells, such that there are sizeable barriers for rearrangement of each to any of the others. Nevertheless, at internal energies sufficient to induce dissociation of metastable ions, **4** and **5** are able to reach common intermediates and transition states which are also accessible to **6**. Moreover, the main route for isomerisation of **4** to **5** involves formation of **6**, rather than **9**, because the C–O linkage of **4** is conserved with a selectivity of almost 90% in propene loss. However, both the new ^{13}C -labelling experiments and earlier ^2H -labelling data¹⁴ indicate that a small percentage of ions generated as **5** are able to rearrange to the protonated oxetane, **12**, thus allowing the initial C–O bond to be eventually broken before C_3H_6 is lost.

The greatly reduced degree of interconversion of **4** with **9** can be partly attributed to differences in the energetics of the isomeric $\text{C}_5\text{H}_{11}\text{O}^+$ ions compared to those of the lower homologues in the $\text{C}_3\text{H}_7\text{O}^+$ system. Construction of a potential energy profile²¹ (PEP) for $\text{C}_3\text{H}_7\text{O}^+$ ions reveals that the energies of both $\text{CH}_3\text{CHCH}_2\text{OH}^+$ and $\text{CH}_3\text{CH}^+\text{CH}_2\text{OH}$ are much lower (by 86 and 108 kJ mol^{-1} , respectively²²) than the combined enthalpies of formation of $\text{CH}_2=\text{OH}^+$ and C_2H_4 .

Furthermore, the postulated reacting configuration for C_2H_4 loss ($^+\text{CH}_2\text{CH}_2\text{CH}_2\text{OH}$) lies at an appreciably higher energy than **2**, $\text{CH}_3\text{CHCH}_2\text{OH}^+$ and $\text{CH}_3\text{CH}^+\text{CH}_2\text{OH}$. Consequently, the rate of interconversion of **2** with $\text{CH}_3\text{CHCH}_2\text{OH}^+$ and $\text{CH}_3\text{CH}^+\text{CH}_2\text{OH}$ becomes quite rapid even at energies close to or slightly below those needed to promote C_2H_4 expulsion. In contrast, when the PEP for the analogous $\text{C}_5\text{H}_{11}\text{O}^+$ ions is constructed from known^{15,23–29} or estimated^{18,19,30–32} thermochemical data, Figure 1, it is evident that the corresponding open-chain cations, **8** and **10**, do not lie appreciably below the threshold for C_3H_6 elimination. Moreover, the postulated reacting configuration for C_3H_6 loss (**11**) is lower in energy than **8** and **10**. As a result, the energy needed to promote rearrangement of **4** and **5** to **10** and **8** is comparable to that required to induce C_3H_6 loss. In other words, once **10** has been formed from **5** (or from **4** via isomerisation involving **6**), further rearrangement via the favourable 1,2-H shift to **11** followed by C_3H_6 elimination requires almost no additional energy. Consequently, interconversion of **4** and **5** via any route involving **10** is reduced in efficiency because it must occur in competition with exoergic formation of **11** which leads C_3H_6 loss.

However, even after due allowance for these energetic differences has been made, it appears that another factor must discriminate against ring closure of the α -hydroxy cations to protonated oxiranes. Elimination of C_3H_6 from **4** via either the proposed dominant route (**4**→**8**→**6**→**10**→**11**) or the pathway (**4**→**8**→**9**→**5**→**10**→**11**) involving the protonated oxirane necessarily entails initial formation of the same open-chain cation, **8**. Therefore, the 1,2- C_2H_5 shift which converts **8** into

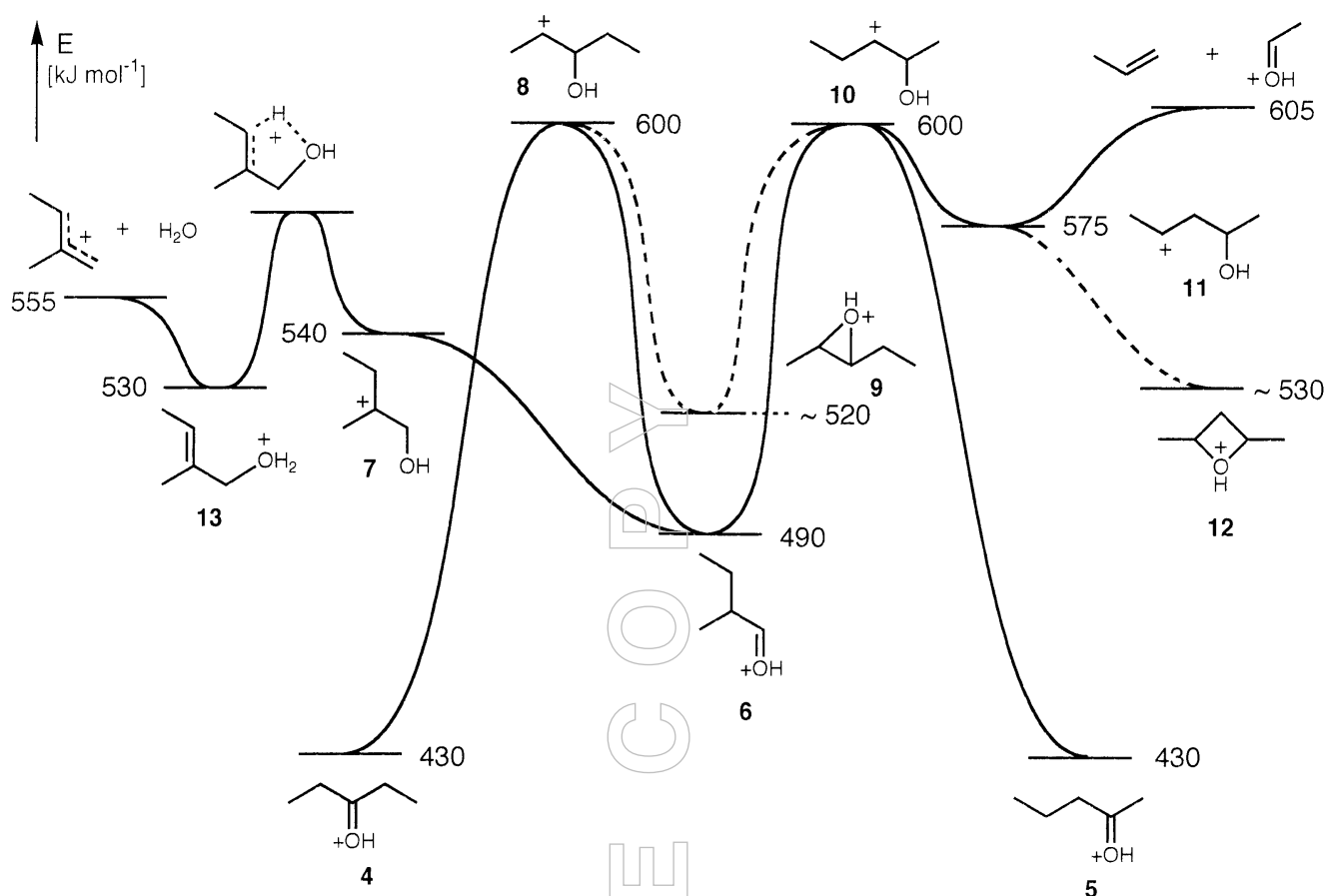


Figure 1. Potential energy profile for isomerisation and dissociation of $(\text{CH}_3\text{CH}_2)_2\text{C}=\text{OH}^+$, $\text{CH}_3\text{CH}_2\text{CH}_2(\text{CH}_3)\text{C}=\text{OH}^+$ and $\text{CH}_3\text{CH}_2\text{CH}_2(\text{CH}_3)\text{C}=\text{OH}^+$.

6 must occur more rapidly than the apparently favourable cyclisation to **9**. A similar argument suggests strongly that the 1,2-H shift by which **8** may revert to **4** must also take place more readily than ring closure to **9**. These trends may reflect the energetics of the relevant steps: both the 1,2- C_2H_5 and the 1,2-H shift in **8** lead to species (**6** and **4**, respectively) that are lower in energy than **9**. However, there may also be an additional effect discriminating against formation of **9** because the conformation of **8** that is best suited to cyclisation to **9** is one in which the C–O bond and the unoccupied p-orbital lie in a common plane. This conformation is one which maximises the unfavourable interaction between the hydroxyl substituent and the unoccupied p-orbital.¹⁸ In contrast, the conformations appropriate for the 1,2- C_2H_5 or the 1,2-H shifts bring the substituent that is about to migrate, rather than the C–O bond, into a common plane with the unoccupied p-orbital. Moreover, it is one of these rotamers which should be initially formed by the 1,2-H shift which converts **4** into **8**. These conformational considerations may also favour the 1,2- C_2H_5 or the 1,2-H shifts over cyclisation to form protonated oxiranes.

The major conclusions concerning the mechanism of C_3H_6 loss from **4** and **5** are reinforced by the behaviour of the higher

homologue $(\text{CH}_3\text{CH}_2\text{CH}_2)_2\text{C}=\text{OH}^+$, **14**. This species is known³³ to lose predominantly H_2O and C_3H_6 , together with smaller amounts of C_4H_8 and “ $\text{C}_3\text{H}_8\text{O}$ ” (actually sequential elimination³⁴ of H_2O and C_3H_6). Expulsion of C_4H_8 entails skeletal rearrangement and could occur via reorganisation of the carbon framework or by migration of the oxygen function. The loss of C_3H_6 and C_4H_8 with high selectivities (>99% and >95%, respectively), Table 3, establishes that the former is the case, Scheme 5. Any migration of the oxygen function from C-4 to C-3 or C-5 via protonated oxiranes would result in $\text{C}_3^{13}\text{CH}_8$ elimination from $(\text{CH}_3\text{CH}_2\text{CH}_2)_2^{13}\text{C}=\text{OH}^+$. Similarly, any involvement of protonated oxetanes would lead to C_5H_{10} loss from $(\text{CH}_3\text{CH}_2\text{CH}_2)_2\text{C}=\text{OH}^+$ and $\text{C}_4^{13}\text{CH}_{10}$ elimination from $(\text{CH}_3\text{CH}_2\text{CH}_2)_2^{13}\text{C}=\text{OH}^+$. However, none of these processes is observed to a measurable extent.

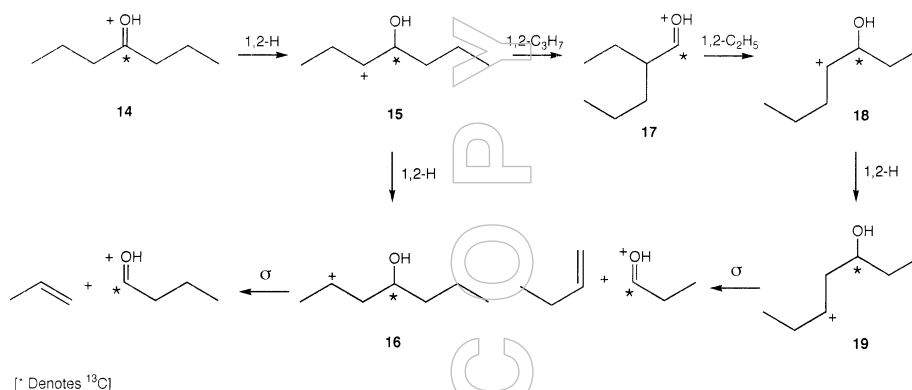
Conclusions

The skeletal isomerisations which often precede alkene expulsion from oxonium ions of general structure $\text{R}^1\text{R}^2\text{C}=\text{OH}^+$ normally involve reorganisation of the carbon framework via 1,2-H and 1,2-alkyl shifts. Migration of the

Table 3. Reactions of metastable $C_7H_{15}O^+$ and $C_6^{13}CH_{15}O^+$ ions.

	Neutral species lost											
	H ₂ O		C ₃ H ₆		C ₂ ¹³ CH ₆		C ₄ H ₈		C ₃ ¹³ CH ₈		C ₃ H ₈ O	
Ion structure	<i>RA</i> ^a	<i>T</i> ^b	<i>RA</i>	<i>T</i>	<i>RA</i>	<i>T</i>	<i>RA</i>	<i>T</i>	<i>RA</i>	<i>T</i>	<i>RA</i>	<i>T</i>
(CH ₃ CH ₂ CH ₂) ₂ C=OH ⁺	59 ^c	3.1	31 ^c	2.4			8 ^c	2.2			2 ^c	~3
(CH ₃ CH ₂ CH ₂) ₂ ¹³ C=OH ⁺	60 ^c	3.2	32.1 ^c	2.4	<0.5		7.5 ^c	2.5	<0.5		~2 ^c	

^{a,b,c}See footnotes to Table 1; values for alkene losses are quoted to one decimal place simply in order to avoid introducing rounding errors.



Scheme 5.

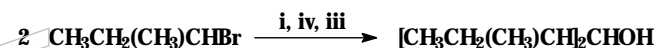
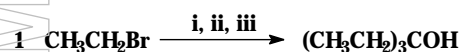
oxygen function rarely, if ever, occurs via protonated oxiranes and only occasionally via protonated oxetanes. The 1,2-alkyl shifts in the α -hydroxy cations occur more rapidly than cyclisation to the protonated oxiranes, even though formation of such three-membered rings is often considered to be a kinetically facile process. Since the enthalpies of formation of protonated oxiranes are lower than those of the relevant α -hydroxy cations, this finding suggests strongly that 1,2-H and 1,2-alkyl shifts are kinetically preferable to cyclisation in these systems.

Experimental

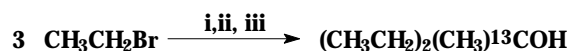
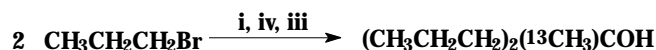
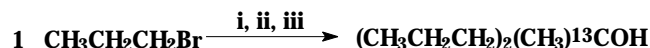
Most of the mass spectra were recorded on the VG Analytical ZAB-R mass spectrometer. Details of the geometry of this three-sector ($BE_1 \perp QE_2$) instrument have been reported elsewhere.³⁵ Data on the dissociation of metastable ions in the second field-free region were obtained by the MIKES technique.¹⁷ The quoted spectra are integrated data, compiled from 2–5 individual scans. Typical operating conditions were 70 eV ionising electron energy and 7910 V accelerating voltage. The KE releases were estimated from the width at half-height of the appropriate metastable peak, by means of the standard one-line equation^{17,36} after applying the usual correction³⁷ for the width at half-height of the main beam. The remaining new data reported in Table 2 were obtained with an AEI MS 902 double-focusing mass spectrometer, operating at an ionising electron energy of 70 eV, an accelerating voltage of 8 kV and a source pressure of $\sim 10^{-6}$ Torr. The KE releases for C_3H_6 loss were estimated from the width at half-height of the associated

peaks arising from dissociation of metastable ions in the second field-free region, by means of the usual one line equation,^{17,36} after applying the usual correction for the width at half-height of the main beam.³⁷ The quoted values are the means of 4–6 individual scans.

The oxonium ions studied in this work were generated by dissociative ionisation of the appropriate secondary or tertiary alcohols. These alcohols were either commercially available



Scheme 6. Reagents and conditions: i, 1.2 moles Mg, $(C_2H_5)_2O$; ii, 0.4 moles $CH_3CH_2CO_2CH_3$; iii, saturated aqueous $NH_4^+Cl^-$ solution; iv, 0.4 moles $HCO_2CH_2CH_3$.



Scheme 7. Reagents and conditions: i, 1.2 moles Mg, $(C_2H_5)_2O$; ii, 0.3 moles $CH_3^{13}COCl$; iii, saturated aqueous $NH_4^+Cl^-$ solution; iv, 0.3 moles $^{13}CH_3COCl$.

$[(\text{CH}_3\text{CH}_2)_2\text{C}(\text{CH}_3)\text{OH}]$ or synthesised by unexceptional methods via the routes shown in Scheme 6. The ^{13}C -labelled alcohols were prepared from commercial (Aldrich) samples of specifically labelled acetyl chlorides containing a high level (>99%) incorporation of ^{13}C via the routes shown in Scheme 7. Comparison of the 70 eV electron impact ionisation mass spectra of the labelled alcohols with those of the corresponding unlabelled analogues indicated that the label had been incorporated with high selectivities (99%) at the desired position.

Acknowledgements

Financial support from the Science and Engineering Research Council (UK), the Leverhulme Trust (Research Fellowship and Grant to RDB, 1992–3) the British Mass Spectrometry Society (funds for purchasing labelled starting materials) and the Natural Sciences and Engineering Research Council of Canada (NSERC) is gratefully acknowledged.

References

1. R.D. Bowen, A.W. Colburn and P.J. Derrick, *Org. Mass Spectrom.* **25**, 509 (1990), and references therein.
2. A.N.H. Yeo and D.H. Williams, *J. Am. Chem. Soc.* **93**, 395 (1971).
3. C.W. Tsang and A.G. Harrison, *Org. Mass Spectrom.* **7**, 1377 (1973).
4. A.W. Seigel, *Org. Mass Spectrom.* **3**, 1417 (1970).
5. C.W. Tsang and A.G. Harrison, *Org. Mass Spectrom.* **5**, 877 (1971).
6. R.D. Bowen, J.R. Kalman and D.H. Williams, *J. Am. Chem. Soc.* **99**, 5481 (1977).
7. J.L. Holmes, R.T.B. Rye and J.K. Terlouw, *Org. Mass Spectrom.* **14**, 606 (1979).
8. D.J. McAdoo and C.E. Hudson, *Int. J. Mass Spectrom. Ion. Processes* **88**, 133 (1989).
9. R.D. Bowen, D.H. Williams, G. Hvistendahl and J.R. Kalman, *Org. Mass Spectrom.* **12**, 721 (1978).
10. G. Hvistendahl, R.D. Bowen and D.H. Williams, *J. Chem. Soc., Chem. Commun.* 294 (1976).
11. A.G. Harrison, T. Gaumann and D. Stahl, *Org. Mass Spectrom.* **18**, 517 (1983).
12. S.J.A. Curtis and A.G. Harrison, *J. Am. Soc. Mass Spectrom.* **1**, 310 (1990).
13. H.E. Audier, R. Flammang, A. Maquestiau and A. Milliet, *Nouv. J. Chem.* **4**, 531 (1980).
14. J.V. Headley and A.G. Harrison, *Can. J. Chem.* **63**, 609 (1985).
15. S.G. Lias, J.E. Bartmess, J.F. Liebman, J.L. Holmes, R.D. Levin and W.G. Mallard, *J. Phys. Chem. Ref. Data* **17**, Suppl. 1 (1988).
16. The term “critical energy” corresponds conceptually to the expression “activation energy”, see: A. Maccoll, *Org. Mass Spectrom.* **15**, 109 (1980).
17. R.G. Cooks, J.H. Beynon, R.M. Caprioli and G.R. Lester, *Metastable Ions*. Elsevier, Amsterdam (1973).
18. L. Radom, J.A. Pople and P.v.R. Schleyer, *J. Am. Chem. Soc.* **94**, 5935 (1972).
19. R.D. Bowen and D.H. Williams, *Org. Mass Spectrom.* **12**, 475 (1977).
20. F.W. McLafferty and I. Sakai, *Org. Mass Spectrom.* **7**, 971 (1973).
21. For reviews of the PEP approach, see: D.H. Williams, *Acc. Chem. Res.* **10**, 280 (1977); D.H. Williams, *Philos. Trans. R. Soc. London Ser. A* **293**, 117 (1977); R.D. Bowen, D.H. Williams and H. Schwarz, *Angew. Chem. Int. Edn Eng.* **18**, 451 (1979); R.D. Bowen and D.H. Williams, in *Rearrangements in Ground and Excited States*, Ed. by P. DeMayo. Academic Press, New York, Volume 1, Chapter 2 (1980).
22. R.D. Bowen and A.G. Harrison, *Org. Mass Spectrom.* **16**, 159 (1981).
23. F.P. Lossing and G.P. Semeluk, *Can. J. Chem.* **48**, 955 (1970).
24. F.P. Lossing and J.C. Traeger, *Int. J. Mass Spectrom. Ion. Phys.* **19**, 9 (1976).
25. F.P. Lossing, *J. Am. Chem. Soc.* **99**, 7526 (1977).
26. F.P. Lossing and J.L. Holmes, *J. Am. Chem. Soc.* **106**, 6917 (1984), and references cited therein.
27. S.G. Lias, J.F. Liebman and R.D. Levin, *J. Phys. Chem. Ref. Data* **13**, 695 (1984).
28. J.D. Cox and G. Pilcher, *Thermochemistry of Organic and Organometallic Compounds*. Academic Press, New York (1970).
29. J.B. Pedley, R.D. Naylor and S.P. Kirby, *Thermochemical Data of Organic Compounds*, 2nd Edition. Chapman and Hall, London (1986).
30. J.L. Franklin, *Ind. Eng. Chem.* **41**, 1070 (1949); *J. Chem. Phys.* **21**, 2029 (1953).
31. S.W. Benson, *Thermochemical Kinetics*, 2nd Edition. Wiley, New York (1986).
32. J.L. Holmes, M. Fingas and F.P. Lossing, *Can. J. Chem.* **59**, 80 (1981); **60**, 2365 (1982).
33. U.I. Zahorszky, *Org. Mass Spectrom.* **17**, 253 (1982).
34. S. Chowdhury and A.G. Harrison, *Org. Mass Spectrom.* **23**, 79 (1988).
35. H.F. van Garderen, P.J. A. Ruttink, P.C. Burgers, G.A. McGibbon and J.K. Terlouw, *Int. J. Mass Spectrom. Ion Processes* **121**, 159 (1992).
36. K. Levsen, *Fundamental Aspects of Organic Mass Spectrometry*. Verlag Chemie, Weinheim (1978).
37. M.A. Baldwin, P.J. Derrick and R.P. Morgan, *Org. Mass Spectrom.* **11**, 440 (1976).

Received: 12 January 1995

Accepted: 24 January 1995

Time-dependent mass spectra and breakdown graphs. 18. pyrene

Yun Ling, Yehiel Gotkis and Chava Lifshitz^a

Department of Physical Chemistry and The Fritz Haber Research Center for Molecular Dynamics, The Hebrew University of Jerusalem, Jerusalem 91904, Israel.

Unimolecular fragmentations of the pyrene radical cation were studied by time-resolved photo-ionization in the VUV, RRKM/QET calculations and MS/MS with electron ionization. The major reactions observed are parallel H[•] and H₂ losses, as well as consecutive H[•] losses. Activation parameters were deduced for the reactions. Appearance energies were determined for the microsecond and millisecond time ranges. The reactions demonstrate large conventional and intrinsic shifts. The H[•] loss reactions are characterized by loose transition states and have no reverse activation energies. This has enabled the determination of new thermochemical data. The C–H bond energy in the pyrene radical cation was deduced to be 4.6 eV and the heat of formation of the pyrenyl cation, $\Delta H_{f0}^0(\text{C}_{16}\text{H}_9^+) = 1190 \text{ kJ mol}^{-1}$. The results are discussed in light of the possible role of pyrene-like ions in interstellar space.

Introduction

The photostability of polycyclic aromatic hydrocarbons (PAHs) is of importance in view of their astrophysical role.¹ PAHs are considered to be the most abundant free interstellar organic molecules known.² A large fraction of PAHs are expected to be ionized in the interstellar medium. The ionized PAHs are attractive candidates for the diffuse interstellar bands which have been known for some time. It has recently been demonstrated³ that a pyrene-like molecular ion may cause the 4430 Å diffuse interstellar absorption band. The importance of naphthalene and phenanthrene cations as interstellar species⁴ has led us recently to a detailed investigation of the energetics and dynamics of dissociation of these species.⁵ The present research effort is devoted to pyrene.

The special resilience of PAHs towards decomposition can be understood—it is due to their high bond energies and their large numbers of degrees of freedom. These attributes make them attractive candidates for study by time-resolved photo-ionization mass spectrometry (TPIMS), a technique which we have developed in recent years.⁶ Ions can be trapped in a Paul-type cylindrical ion trap (CIT) for up to several tens of milliseconds.⁷ This allows fragmentations at low energies and enables the determination of “kinetic shifts”.^{5–7} Owing to the long time-scale used, the experiment probes the energy region where fragmentation is in competition with radiative cooling.

This is the key region for the study of the survival of PAHs in the interstellar medium.⁸

Pyrene, as opposed to naphthalene and phenanthrene, is a compact PAH. As such it is less prone to acetylene loss,⁸ but loses hydrogen atoms. Nevertheless, appearance energies have recently been determined¹ for H loss, H₂ loss, as well as acetylene loss. When pyrene molecular ions undergo surface-induced dissociation,⁹ by far the most abundant peak is (M – 2H)^{•+}. Whether the unimolecular loss of 2H[•] atoms is consecutive,^{8,9} or due to H₂ loss as formulated by Jochims *et al.*,¹ is an open question of interest in interstellar chemistry.

We undertook a detailed study of the VUV photo-ionization and fragmentation of pyrene using our ion trapping device for time-resolved measurements. The data obtained, as well as their modelling by RRKM calculations, will be described here. This study was combined with an electron ionization MS/MS study, in order to decide between the consecutive 2H[•] and single step H₂ loss channels.

Experimental

The experimental technique of TPIMS has been described in detail recently,^{5–7, 10,11} and only a brief description will be given here. Photo-ionization is induced by a pulsed vacuum–UV light source, either the Hinteregger discharge in hydrogen, producing the many-line spectrum, or the Hopfield continuum in He. Photo-ions are trapped in a CIT. They are ejected into a quadrupole mass filter by a draw-out pulse, following a variable delay time. In this study ions were stored from ~20 μs to 10 ms. The radio frequency (RF) of the potential

^aArchie and Marjorie Sherman Professor of Chemistry.

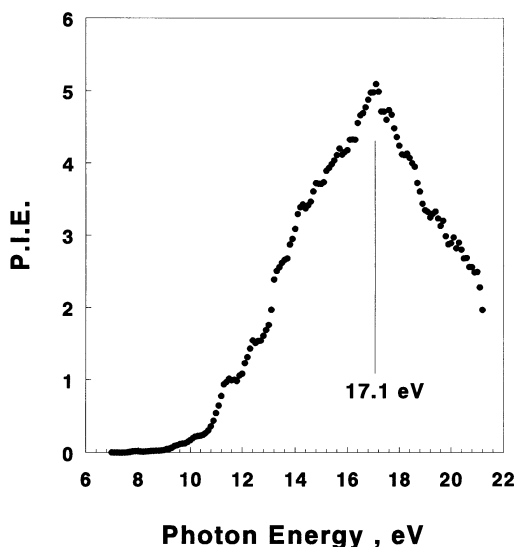


Figure 1. PIE curve for pyrene ions, without mass selection, in the 7–21.21 eV range.

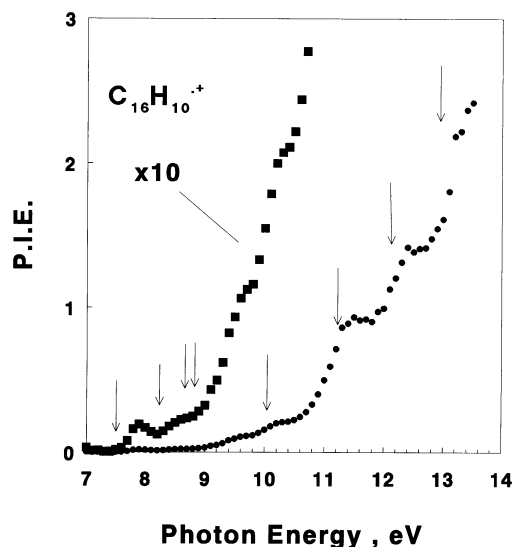


Figure 2. PIE curve for pyrene parent ion $C_{16}H_{10}^{+\bullet}$ in the 7–13.5 eV energy range. The arrows point to energies for which there are maxima in the photo-electron spectrum of pyrene.¹⁵

applied to the cylindrical barrel electrode of the CIT is 0.5 MHz ($\omega/2\pi$). The ion creation pulse is a train of short pulses applied to the light source. An ejection pulse is applied to the end-cap electrode of the CIT nearest the mass filter, and a detection pulse is gating the ion counter. The RF voltage is applied to the cylindrical electrode of the CIT throughout the whole cycle. The effective wavelength resolution employed is 5.0 Å. This corresponds to an energy resolution of ~ 0.02 eV near the ionization threshold of pyrene (~ 7.4 eV) and of ~ 0.1 eV near the fragmentation onsets.

A simple Knudsen-type molecular beam source for low-volatility compounds constructed earlier⁵ was used to study pyrene.

Mass-analyzed ion kinetic energy spectroscopy (MIKES) studies and high voltage (HV) scans were carried out on a VG ZAB-2F double-focussing mass spectrometer of reversed geometry.¹²

Pyrene was a commercial sample from Aldrich (99% stated purity) which was employed without further purification.

Results and discussion

Time-resolved photo-ionization efficiency curves.

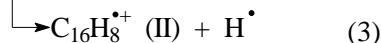
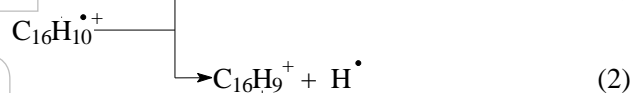
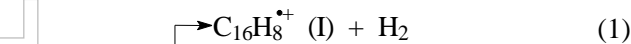
Experiment

The total ion photo-ionization efficiency (PIE) curve for pyrene was measured over the photon energy range 7–21.2 eV and the resultant curve is represented in Figure 1. It is dominated by a strong resonance with a maximum at 17.1 eV. C_{60} displays a similar resonance peak. This has been interpreted¹³ as being due to excitation of a collective plasmon resonance which is a bound state embedded in the ionization continuum.

The parent PIE curve between 7 and 13.5 eV is presented in Figure 2. The ionization energy, 7.40 ± 0.1 eV, is in excellent agreement with available literature data 7.45 ± 0.02 eV,³ 7.41 eV¹⁴ and 7.42 eV.¹⁵ Higher ionization energies are known

from photo-electron spectroscopy.¹⁵ The maxima of the photo-electron spectral bands are clearly discernible as pronounced changes in slope in the PIE curves (Figure 2).

We have studied three major reaction channels in pyrene namely, H^\bullet loss, H_2 loss and consecutive H^\bullet loss, Reactions (I)–(3),



The PIE curves for daughter ions $C_{16}H_9^{+\bullet}$ and $C_{16}H_8^{+\bullet}$ from pyrene are presented in Figure 3 for $t \sim 24 \mu s$. The PIE of $C_{16}H_8^{+\bullet}$ is much weaker than that of $C_{16}H_9^{+\bullet}$ below ~ 19 eV, but rises sharply above ~ 19 eV. From the experimental PIE curves, from RRKM/QET modelling (see below) and from MS/MS studies (see below), we conclude that the daughter ions $C_{16}H_8^{+\bullet}$ come from two different reaction channels—parallel H_2 loss in the low energy range and consecutive H -loss in the high energy range. The product ions were labeled $C_{16}H_8^{+\bullet}$ (I) and $C_{16}H_8^{+\bullet}$ (II), respectively. Figure 4 shows the threshold energy regions for these two reactions. There are four well-established reaction channels which the benzene ion undergoes: H^\bullet , H_2 , C_2H_2 and $C_3H_3^\bullet$ losses.¹⁶ Two major unimolecular reactions, H^\bullet loss and C_2H_2 loss have been studied by TPIMS in this laboratory⁵ for naphthalene and phenanthrene. Minor reaction channels in naphthalene are C_4H_2 and H_2 losses.^{5,17} The appearance energy (AE) of C_2H_2 loss from pyrene was published recently.¹ This reaction was also observed in our experiment, but was too weak for accurate time-resolved measurements to be made.

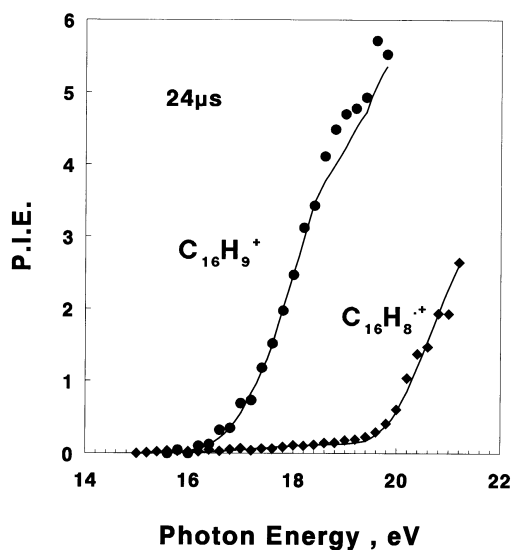


Figure 3. Experimental [(●) $\text{C}_{16}\text{H}_9^+$, (♦) $\text{C}_{16}\text{H}_8^{+\bullet}$] and calculated (lines) PIE curves for pyrene in the microsecond range ($\sim 24 \mu\text{s}$).

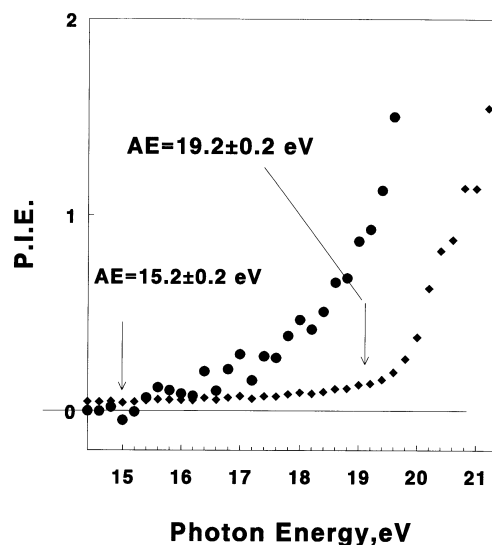


Figure 4. Experimental H_2 and 2H^\bullet loss PIE curves in the microsecond range.

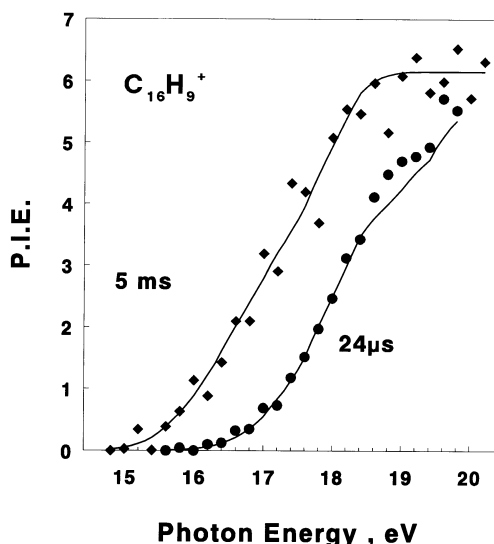


Figure 5. Time-resolved experimental [(●) $24 \mu\text{s}$, (♦) 5 ms] and calculated (lines) $\text{C}_{16}\text{H}_9^+$ daughter ion PIE curves for pyrene. The PIE curves are in arbitrary units to scale. The relative intensities of the experimental PIE curves of the parent served to scale the experimental daughter ion PIEs.

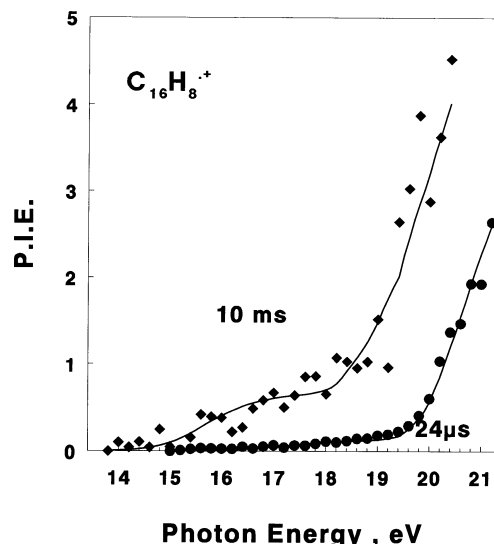


Figure 6. Time-resolved experimental [(●) $24 \mu\text{s}$, (♦) 10 ms] and calculated (lines) $\text{C}_{16}\text{H}_8^{+\bullet}$ daughter ion PIE curves. See caption to Figure 5 for normalization.

The AE s of daughter ions were measured from PIE curves with and without ion trapping. Time-resolved PIE curves for $\text{C}_{16}\text{H}_9^+$ at $24 \mu\text{s}$ and 5 ms are presented in Figure 5. We normalized all the daughter ion PIE curves by the ratio between parent and daughter at 21.2 eV . Because of mass resolution problems, contributions from the parent ions to the mass positions of $(M - \text{H})^+$ and $(M - 2\text{H})^+$ had to be subtracted at long ion trapping time. Time-resolved PIE curves for $\text{C}_{16}\text{H}_8^{+\bullet}$ at $24 \mu\text{s}$ and 10 ms are presented in Figure 6. Figure 7 displays time-resolved PIE curves for $\text{C}_{16}\text{H}_8^{+\bullet}$ (I) due to the H_2 loss reaction and Figure 8 shows time-resolved PIE curves for $\text{C}_{16}\text{H}_8^{+\bullet}$ (II) for the consecutive H^\bullet loss reaction. Fairly large

kinetic shifts are clearly observed. Pronounced AE s are summarized in Table 1. The AE for the H -loss channel in the microsecond time range is in good agreement with the value by Jochims *et al.*¹ The value for the H_2 loss channel is much lower than the literature value indicating that what was measured¹ is what we believe to be due to the consecutive loss of 2H^\bullet atoms.

The PIE curves for parent ($\text{C}_{16}\text{H}_{10}^{+\bullet}$) and daughter ($\text{C}_{16}\text{H}_9^+$) ions are shown for two storage times over similar energy ranges in Figure 9 (a, b). Several clear changes are observed upon extension of the ion storage time: (1) The rising onset for $\text{C}_{16}\text{H}_9^+$ shifts to lower energies (as noted before in Figure 5) and (2) the relative abundance of $\text{C}_{16}\text{H}_9^+$ versus $\text{C}_{16}\text{H}_{10}^{+\bullet}$

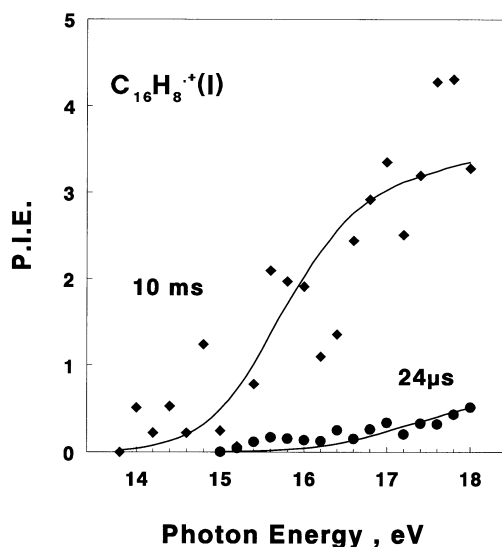


Figure 7. Same as Figure 6 but in the energy range up to 18 eV (H_2 loss only).

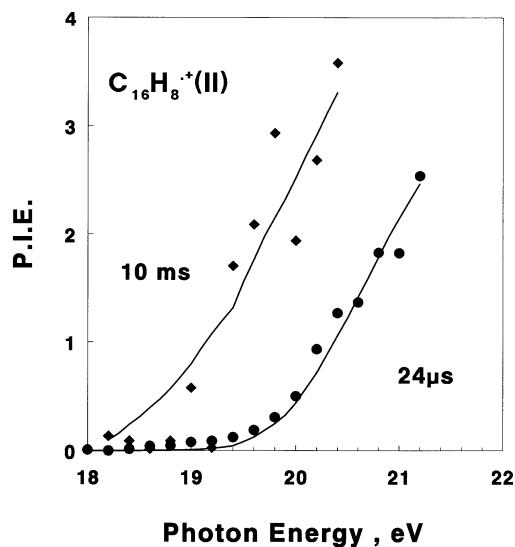


Figure 8. Time-resolved experimental [(●) 24 μ s, (♦) 10 ms] and calculated (lines) $C_{16}H_8^{++}$ (II) daughter ion ($2H^+$ loss) PIE curves. The experimental curves were obtained by subtracting the contribution from the H_2 loss reaction. See caption to Figure 5 for normalization.

Table 1. Time-resolved appearance energies (AEs) for ions from pyrene.

Ion	Reaction	AE in eV (time)
$C_{16}H_8^{++}$ (I)	(1)	15.2 ± 0.2 (24 μ s), 14.2 ± 0.2 (10 ms)
$C_{16}H_9^+$	(2)	16.2 ± 0.2 (24 μ s), 15.2 ± 0.2 (5 ms)
$C_{16}H_8^{++}$ (II)	(3)	19.2 ± 0.2 (24 μ s), 18.4 ± 0.2 (10 ms)

increases. Similar observations were made for the H_2 loss and consecutive $2H^+$ loss reactions.

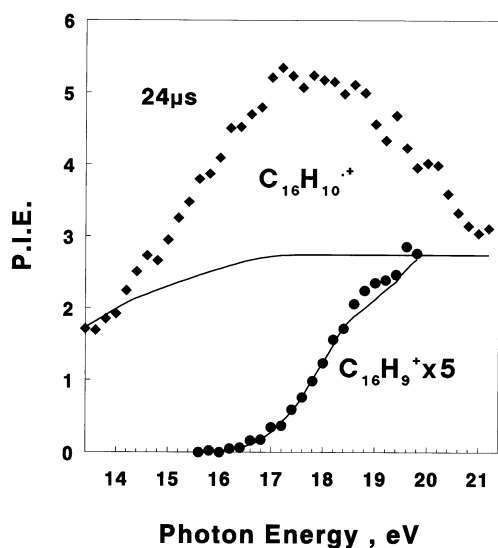


Figure 9 (a). Parent $C_{16}H_{10}^{++}$ (♦) and $C_{16}H_9^+$ daughter (●) ion PIE curves at 24 μ s. — experimental results; lines—calculated.

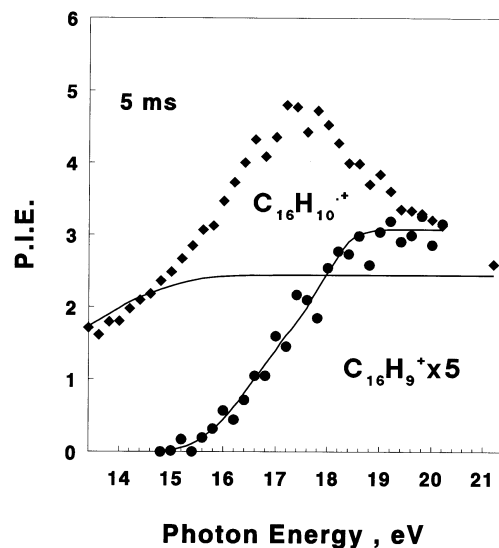


Figure 9 (b). Same as Figure 9 (a) but at 5 ms.

The similarity between the parent PIE curve (Figure 9) and the total ion PIE curve (Figure 1) indicates that only the parent ion contributes to the giant resonance peak around 17 eV.

RRKM/QET calculations

Time-resolved PIE curves were modeled by RRKM/QET calculations in a similar manner described before.⁵ The microcanonical rate coefficients $k(E)$ were calculated as a function of energy by an RRKM program.¹⁸ This was done for the three reactions (1)–(3). Figure 10 shows the schematic potential energy diagram for pyrene ion dissociation. The vibrational

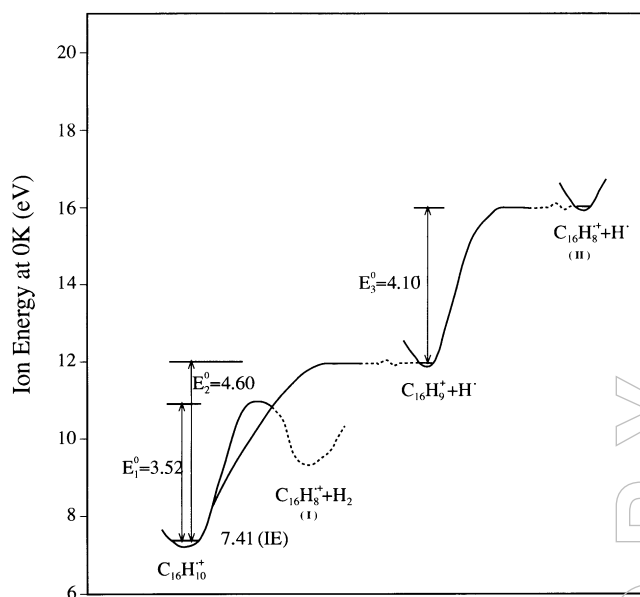


Figure 10. Schematic diagram of the postulated potential energy curves for the pyrene ion dissociation. (energy values in eV).

frequencies of the reactant ion $C_{16}H_{10}^{+\bullet}$ were taken equal to those of the corresponding neutral.^{19(a)} Using the vibrational frequencies of the ion^{19(b)} had no marked effect on the results. Vibrational frequencies of the transition states were varied to get the best agreement with experiment. It is widely accepted that the details of the frequency changes in the transition state are not very important,²⁰ the important factor is the degree of tightness or looseness of the transition state which is characterized by a single parameter—the activation entropy at 1000 K, ΔS_{1000}^\ddagger .

When we modeled the consecutive H^\bullet loss reaction we assumed that the H^\bullet atom does not carry any energy. The internal energy of $C_{16}H_9^+$ was taken as the excess energy above the H^\bullet loss activation energy E_2° (see Figure 10). Time-resolved parent and daughter ion breakdown curves were calculated from the rate-energy $[k(E)]$ dependences at 0 K; these give the internal energy dependences of the fractional abundances of the ions. The internal energy for the consecutive H^\bullet loss reaction was shifted by E_2° when calculating its breakdown curve. The breakdown curves can be converted into time-resolved curves as a function of photon energy by adding the ionization energy of the molecule to the internal energy. Calculated time-resolved breakdown graphs are presented in Figure 11. In these calculated breakdown curves an additional parallel energy independent rate process representing radiative decay in the infrared and/or collisional cooling was employed, together with the dissociative rates. A similar approach was applied previously.⁵ The radiative decay rate, which gave best agreement with all experimental PIE curves in this study, is 400 s^{-1} .

The 0 K breakdown curves were convoluted with the instrumental slit function, with the calculated thermal energy distribution at the temperature of the experiment and with the

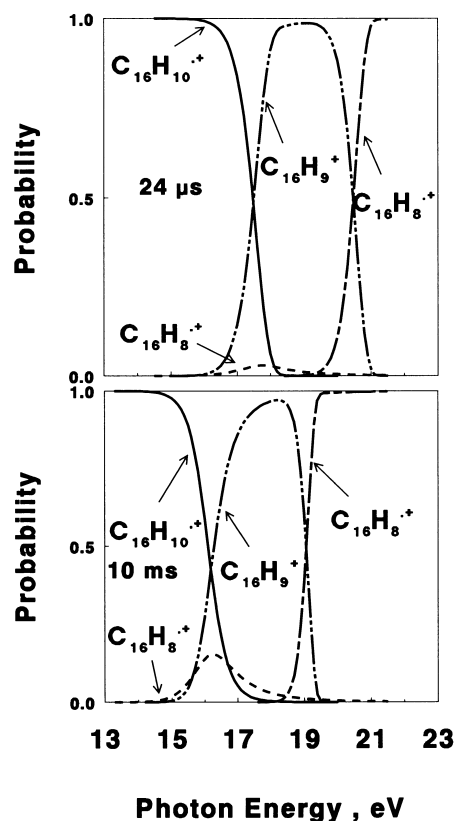


Figure 11. Calculated breakdown curves for pyrene parent and daughter ions at 24 μs and 10 ms. $C_{16}H_{10}^{+\bullet}$ —; $C_{16}H_9^+$ — — —, $C_{16}H_8^+$ (I) · · · · ·; $C_{16}H_8^+$ (II) — · —.

energy deposition function. The vibrational energy distribution of gaseous $C_{16}H_{10}$ at 425 K (the temperature of our experiment) is given in Figure 12. It is an almost symmetrical distribution with a maximum very near the average internal energy 0.49 eV (shown as a vertical line). This average internal energy may contribute to the appearance energy of daughter ions. The photo-electron spectrum of pyrene¹⁵ was employed as the first trial energy deposition function. This had to be modified somewhat. The HeI PES of pyrene¹⁵ shows a sharp drop in the high energy range in which all the fragmentation reactions take place. We found that we could not model the consecutive reaction with the HeI PES as the energy deposition function due to its very low probability in the threshold energy range of the consecutive reaction. A modified PES, to which assumed contributions from auto-ionization were added to the high energy range, was taken as the energy deposition function. Its fine details are related to the 1st derivative of the PIE and are of minor importance, but it was demonstrated to give better agreement with experiment. The energy deposition function employed is compared with the HeI PES in Figure 13.

The resultant curves following convolution of the 0 K breakdown curves, as explained above, represent the calculated first derivatives of the PIE curves of ions, provided the threshold law for photo-ionization is a step function.²¹ These curves were integrated to compare them with the experimental

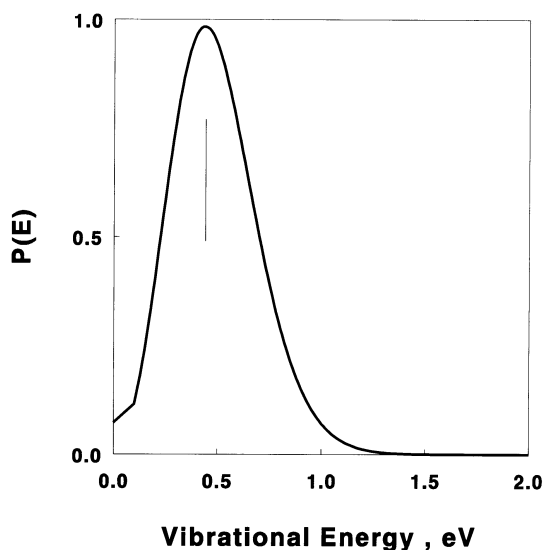


Figure 12. Vibrational energy distribution of gaseous $C_{16}H_{10}$ at 425 K. The vertical line denotes the average vibrational internal energy.

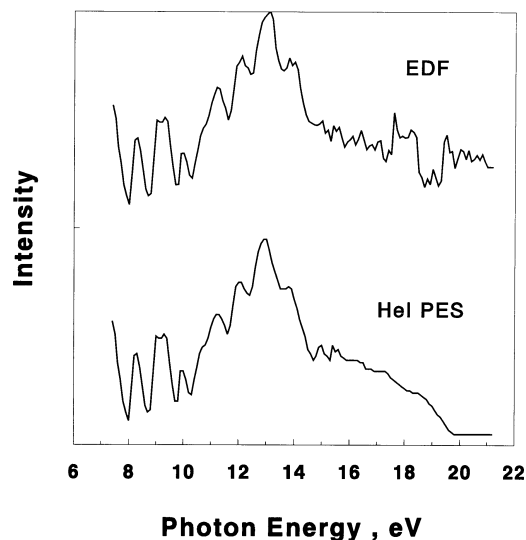


Figure 13. Comparison of energy deposition function (EDF) used in RRKM/QET modelling (upper) and HeI PES¹⁵ (lower).

time-resolved PIE curves and they are included in Figures 3 and 5–9.

The giant resonance peak in the parent ion PIE curves could not be fit with the theoretical calculation as shown in Figures 9 (a and b). It probably originates from an auto-ionization process of neutral superexcited states due to collective π electron excitation. Auto-ionization may lead to an isolated electronic state of the parent ion which does not internally convert to the ground state, but may radiatively decay. It is very difficult to assess the contribution of this auto-ionization process to the energy deposition function but from all the evidence we have it has a negligible contribution to the fragmentation processes.

The activation parameters—the critical energies E_0 and activation entropies $\Delta S^\ddagger_{1000\text{ K}}$, which best fit the whole set of experimental daughter PIE curves—are summarized in Table 2 together with the optimal values of the radiative (and collisional) decay constants as well as the σ values, which represent the number of equivalent reaction pathways. Figure 14 represents our calculated $k(E)$ dependences for the parallel and consecutive reactions in pyrene.

Table 2. RRKM/QET parameters for pyrene cation fragmentation.

Reaction	E_0 (eV)	$\Delta S^\ddagger_{1000\text{ K}}$ (eu)	k_{rad} (s^{-1})	σ
(1)	3.52	−12.7	400	4
(2)	4.60	+10.7	400	10
(3)	4.10	+13.3	400	9

Comparison of calculated and experimental kinetic shifts

The “conventional” kinetic shift (CS) is defined as the excess energy required to observe detectable (1%) dissociation within 10 μs , appropriate for conventional mass spectrometer appearance energy measurements.^{21,22} The “intrinsic” kinetic shift (*IS*) is taken as the energy needed for 10% fragmentation in competition with radiative relaxation of the excited ion.²² The latter definition is appropriate for an ion trap appearance energy experiment unlimited by ion containment time. Large kinetic shifts have been observed for naphthalene and phenanthrene⁵. *CS* for the acetylene loss from phenanthrene is 4.0, eV while *IS* is 3.25 eV.⁵ The kinetic shifts for pyrene were calculated from the $k(E)$ dependences of Figure 14. The appearance energies (*AEs*) expected for the 10 μs range and for an ion trap experiment with unlimited storage

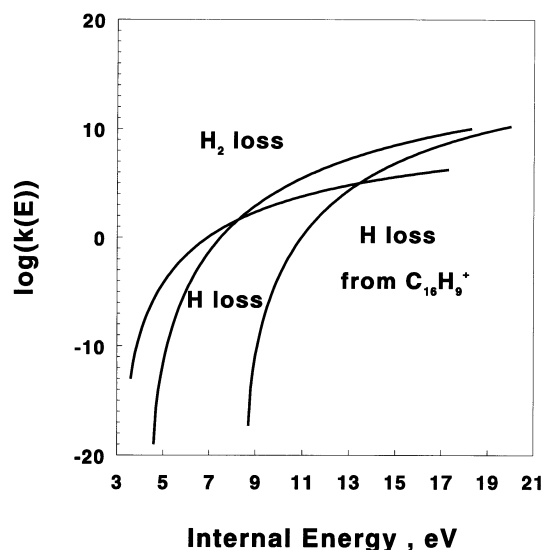


Figure 14. Calculated rate energy $k(E)$ dependence for pyrene ion dissociation.

Table 3. Kinetic shifts for pyrene dissociation (eV).

Reaction	CS	IS	AE (10 μ s calculated)	AE ($t \rightarrow \infty$, calculated)
(1)	6.29	4.71	17.22	15.64
(2)	4.45	3.64	16.46	15.65
(3)	3.52	2.86	19.63	18.97

time were calculated as well. The results are presented in Table 3. The experimental AEs (Table 1) are lower than the predicted limits. This is reasonable since the experimental values were obtained at 425 K and contain a compensating effect due to the internal thermal energy of the parent ion. There is comparatively good agreement between the predicted values and the experimental AEs for the H^\bullet loss and $2H^\bullet$ loss reactions. A key parameter for interstellar chemistry is the internal energy of the parent ion at the appearance energy of a particular fragment ion.¹ This internal energy was previously calculated¹ for $k = 10^4 \text{ s}^{-1}$ and for $k = 10^2 \text{ s}^{-1}$ and found to be 8.69 eV and 7.67 eV, respectively, for the H^\bullet loss reaction in pyrene. Calculations were carried out using the RRK theory rather than RRKM. Our calculated values are higher by 9.74 eV and 8.45 eV, respectively. In the RRK calculations¹ the critical energy E_0 was 2.8 eV, while our value is 4.6 eV (see Table 2), which is more plausible for the C–H bond energy.⁵ We have recently determined again the critical energy for C–H bond cleavage in naphthalene $^{\bullet+}$ and found it to be 4.48 eV.²³ The pyrene system thermochemistry will be discussed in greater detail below.

The breakdown curves allow one to calculate cross-over energies (the energies at which the parent has dropped to 50% abundance) and cross-over shifts (the shifts of these values between the microsecond range and the long storage time chosen). The cross-over energy for pyrene at 24 μ s is 17.47 eV and the cross-over shift is 1.37 eV for the 5–10 ms time range.

Thermochemical information and reaction mechanisms

The activation parameters deduced from the modelling allow us to draw the schematic potential energy diagram (Figure 10). The H^\bullet loss reactions were both drawn as having no reverse activation energies, i.e. loose transition state. In other words, the critical energies may be equated with the corresponding C–H bond dissociation energies. This information, combined with additional thermochemical data (Table 4), allows one to calculate the heat of formation of the fragment ions. The heat of formation of pyrene at 0 K was calculated from the 298 K value¹⁴ and from the pyrene frequencies¹⁹ using standard statistical mechanics methods: $\Delta H_{f0}^0(\text{C}_{16}\text{H}_{10}) = 246.9 \text{ kJ mol}^{-1}$. Employing the ionization energy gives $\Delta H_{f0}^0(\text{C}_{16}\text{H}_{10}^{\bullet+}) = 962 \text{ kJ mol}^{-1}$. Since $\Delta H_{f0}^0(H^\bullet) = 216.0 \text{ kJ mol}^{-1}$, we can calculate the heat of formation of pyrenyl cation $\text{C}_{16}\text{H}_9^+ - \Delta H_{f0}^0(\text{C}_{16}\text{H}_9^+) = 1190 \text{ kJ mol}^{-1}$; in addition $\Delta H_{f0}^0(\text{C}_{16}\text{H}_8^{\bullet+} \text{ [I]}) = 1369 \text{ kJ mol}^{-1}$.

Table 4. Thermochemical data.

Species	$\Delta H_{f0}^0 \text{ (kJ mol}^{-1}\text{)}$		IE (eV)
	0 K	298 K	
$\text{C}_{16}\text{H}_{10}$ (pyrene)	246.9 ^a	216 ± 1 ^b	7.41 ^b
$\text{C}_{16}\text{H}_{10}^{\bullet+}$ (pyrene)	962 ^a	931 ^b	
$\text{C}_{16}\text{H}_9^+$ (pyrenyl)	1190 ^a		
$\text{C}_{16}\text{H}_8^{\bullet+}$ (I)	<1301 ^a		
$\text{C}_{16}\text{H}_8^{\bullet+}$ (II)	1369 ^a		
H^\bullet	216.0 ^b	218.0 ^b	

^aPresent results.

^bReference 14.

Jochims *et al.*¹ have assumed that E_0 decreases for the H^\bullet loss reaction as the PAH size increases. This assumption is incorrect since E_0 (and the ionic C–H bond energy) is 3.88 eV in benzene²⁴ while being 4.48 eV in naphthalene.²³ We find that E_0 is 4.6 eV for pyrene (Table 2). The charge site is highly localized in closed shell $\text{C}_{16}\text{H}_9^+$ compared with parent radical cation $\text{C}_{16}\text{H}_{10}^{\bullet+}$ which has π -delocalization of the radical and the charge over the large aromatic system.²⁵ An effect of the positive charge which weakens the aromatic C–H bond has been noted, but as the aromatic framework is enlarged, this effect is attenuated.²³

The H_2 loss reaction has a low critical energy and a rather tight transition state with $\Delta S_{1000\text{ K}}^\ddagger = -12.7 \text{ eu}$ (Table 2). This indicates a four-center concerted reaction having a reverse activation energy. We can thus only estimate an upper limit for the heat of formation of $\text{C}_{16}\text{H}_8^{\bullet+}$ (I), $\Delta H_{f0}^0 \leq 1301 \text{ kJ mol}^{-1}$. This upper limit is lower than the value deduced for $\text{C}_{16}\text{H}_8^{\bullet+}$ (II) for either of two reasons: At least one of the values deduced is incorrect or the two ions have different structures. Further work is necessary in order to clarify this point.

MIKES and high voltage spectra

In the HV scans performed on our ZAB-2F we selected the ion $\text{C}_{16}\text{H}_8^{\bullet+}$ ($m/z = 200$) and ran a spectrum of its precursors. The result is presented in Figure 15. It demonstrates clearly that there are two precursor ions leading to $\text{C}_{16}\text{H}_8^{\bullet+}$ in the first field-free region of the instrument, one is the pyrene molecular ion ($m/z = 202$) $\text{C}_{16}\text{H}_{10}^{\bullet+}$ and the other is the parent minus one hydrogen atom, $\text{C}_{16}\text{H}_9^+$ ($m/z = 201$). The relative abundance of the two processes (corresponding to Reactions (1) and (3), respectively) is as expected from the PIE curves for $\text{C}_{16}\text{H}_8^{\bullet+}$ (I) and $\text{C}_{16}\text{H}_8^{\bullet+}$ (II), (see Figure 3).

The metastable peak shapes for the three reactions obtained by MIKES are given in Figures 16, 17 and 18. The peak shapes are not symmetrical because of mass resolution. The metastable peak shapes for H^\bullet loss from $\text{C}_{16}\text{H}_{10}^{\bullet+}$ (Figure 16) and from $\text{C}_{16}\text{H}_9^+$ (Figure 18) are sharp pseudo-Gaussian, in agree-

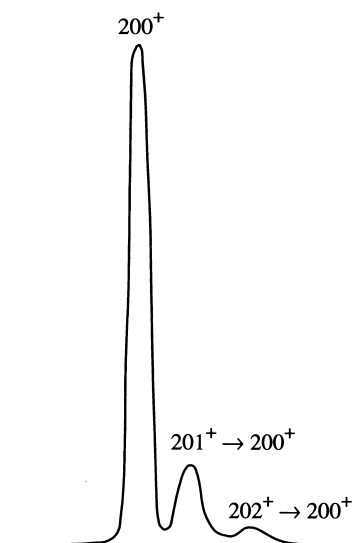


Figure 15. HV scan of m/z 200 from pyrene. The daughter ion $C_{16}H_8^{++}$ (m/z 200) has two precursors— $C_{16}H_{10}^{++}$ (m/z 202) and $C_{16}H_9^+$ (m/z 201).

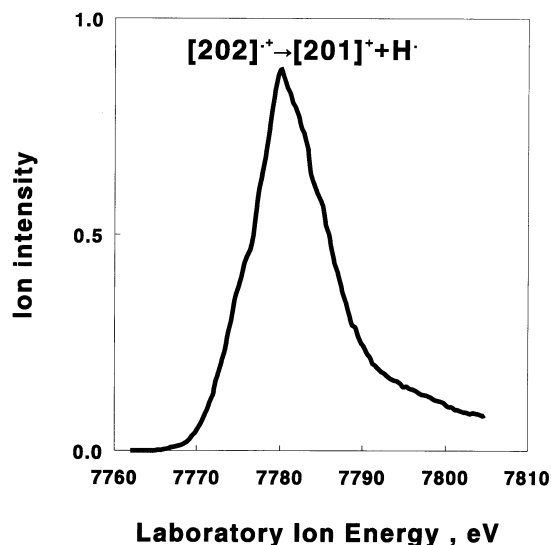


Figure 16. Metastable ion peak shape (second field-free region, ZAB-2F dissociation) for H^+ loss from pyrene. The normal parent beam passed at an energy of 7818 eV. The metastable peak is obtained by scanning the electrostatic energy analyzer (ESA) voltage.

ment with reactions having loose transition states with no reverse activation energy. The average kinetic energy releases for the H^+ loss reaction and for the consecutive H^+ loss reaction are 0.35 eV and 0.24 eV, respectively. These fairly high values are due to the large excess energy required for the dissociations to occur in the microsecond time range, characteristic of the second field-free region of our ZAB-2F instrument. The kinetic energy releases are in qualitative agreement with the relative values of kinetic shifts for the two reactions (Table 3).

The peak shape for the H_2 loss reaction (Figure 17) is characteristic of a reaction with a tight transition state and a reverse activation energy, since it is dish-topped. The kinetic energy release for this reaction is 0.61 eV.

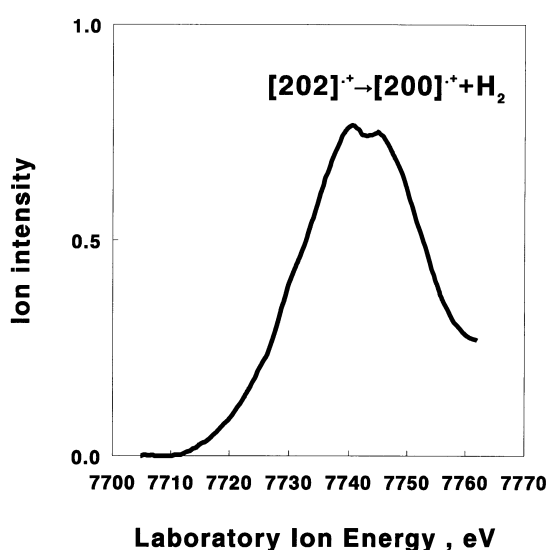


Figure 17. Metastable ion peak shape for H_2 loss from pyrene. See caption to Figure 16.

Conclusion

We believe this to be the first study to differentiate the H_2 loss reaction from the two consecutive H^+ losses in pyrene. We have deduced activation parameters for these reactions as well as thermochemical information concerning their daughter ions. The C–H bond energy deduced for the pyrene radical cation, 4.6 eV is in agreement with the rising trend of C–H bond energies with increasing PAH size. The value for

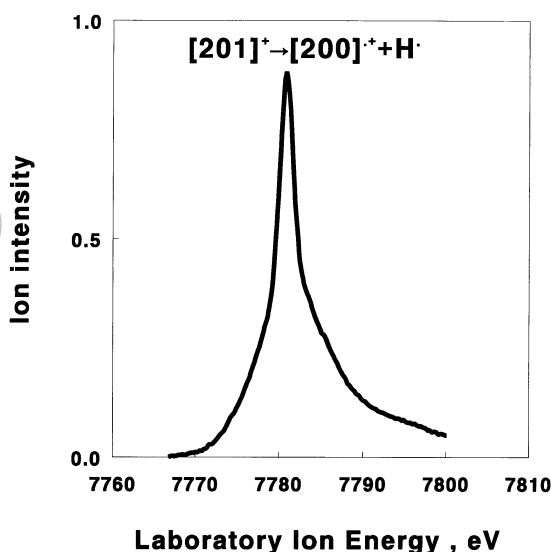


Figure 18. Metastable ion peak shape for consecutive H^+ loss from $C_{16}H_9^+$. The normal $C_{16}H_9^+$ passed at an energy of 7819 eV. See caption to Figure 16.

pyrene^{•+} is very nearly the same as the value for neutral PAHs, 4.8 eV.²³

References

1. H.W. Jochims, E. Rühl, H. Baumgärtel, S. Tobita and S. Leach, *The Astrophysical Journal* **420**, 307 (1994).
2. F. Salama and L.J. Allamandola, *J. Chem. Phys.* **94**, 6964 (1991).
3. F. Salama and L.J. Allamandola, *Nature* **358**, 42 (1992).
4. F. Salama and L.J. Allamandola, *J. Chem. Soc. Faraday Trans.* **89**, 2277 (1993).
5. Y. Gotkis, M. Oleinikova, M. Naor and C. Lifshitz, *J. Phys. Chem.* **97**, 12282 (1993).
6. C. Lifshitz, *Int. J. Mass Spectrom. & Ion Proc.* **106**, 159 (1991).
7. I. Gotkis and C. Lifshitz, *Org. Mass Spectrom.* **28**, 372 (1993).
8. P. Boissel, G. Lefèvre and Ph. Thiébot, *Physical Chemistry of Molecules and Grains in Space*, 50th International Meeting of Physical Chemistry: Mt. Ste Odile (France) 6–10 Sept. 1993.
9. S.J. Pachuta, H.I. Kenttämaa, T.M. Sack, R.L. Cerny, K.B. Tomer, M.L. Gross, R.R. Pachuta and R.G. Cooks, *J. Am. Chem. Soc.* **110**, 657 (1988).
10. N. Ohmichi, I. Gotkis, L. Steens and C. Lifshitz, *Org. Mass Spectrom.* **27**, 383 (1992).
11. I. Gotkis, M. Naor, J. Laskin, C. Lifshitz, J.D. Faulk and R.C. Dunbar, *J. Am. Chem. Soc.* **115**, 7402 (1993).
12. R.P. Morgan, J.H. Beynon, R.H. Bateman and B.M. Green, *Int. J. Mass Spectrom. Ion Phys.* **28**, 171 (1978).
13. I.V. Hertel, H. Steger, J. de Vries, B. Weisser, C. Menzel, B. Kamke and W. Kamke, *Phys. Rev. Lett.* **68**, 784 (1992).
14. S.G. Lias, J.E. Bartmess, J.F. Liebman, J.L. Holmes, R.D. Levin and W.G. Mallard, *J. Phys. Chem. Ref. Data* **17**, (Suppl. 1) (1988).
15. I. Akiyama, K.D. Li, P.R. LeBreton, P.P. Fu and R.G. Harvey, *J. Phys. Chem.* **83**, 2997 (1979).
16. H. Kühlewind, J.J. Neusser and E.W. Schlag, *J. Phys. Chem.* **88**, 6104 (1984); A. Kiermeier, H. Kühlewind, H.J. Neusser, E.W. Schlag and S.H. Lin, *J. Chem. Phys.* **88**, 6182 (1988).
17. E. Rühl, S.D. Price and S. Leach, *J. Phys. Chem.* **93**, 6312 (1989); H.W. Jochims, H. Rasekh, E. Rühl, H. Baumgärtel and S. Leach, *J. Phys. Chem.* **97**, 1312 (1993).
18. W.L. Hase and D.L. Bunker, *A General RRKM Program*. Chemistry Department, Indiana University: Bloomington, IN; QCPE No. 234.
19. (a) A. Bree, R.A. Kydd, T.N. Misra and V.V.B. Vilcos, *Spectrochimica Acta* **27A**, 2315 (1971); (b) M. Vala, J. Szczepanski, F. Pauzat, O. Parisel, D. Talbi and Y. Ellinger, *J. Phys. Chem.* **98**, 9187 (1994).
20. C. Lifshitz, *Adv. Mass Spectrom.* **11**, 113 (1989).
21. W.A. Chupka, *J. Chem. Phys.* **30**, 191 (1959).
22. F.-S. Huang and R.C. Dunbar, *J. Am. Chem. Soc.* **112**, 8167 (1990).
23. Y.P. Ho, R.C. Dunbar and C. Lifshitz, *J. Am. Chem. Soc.*, in press.
24. S.J. Klippenstein, J.D. Faulk and R.C. Dunbar, *J. Chem. Phys.* **98**, 243 (1993).
25. B.D. Nourse, K.A. Cox and R.G. Cooks, *Org. Mass Spectrom.* **27**, 453 (1992).

Received: 5 December 1994

Accepted: 31 January 1995

A mass spectral investigation of ethylenediaminetetraacetic acid

M.F. Duarte* and M.H. Florêncio

Faculdade de Ciências, Departamento de Química, Rua Ernesto de Vasconcelos, Edifício C1, Piso 5, 1700 Lisboa, Portugal.

Mass spectra of ethylenediaminetetraacetic acid (EDTA) were obtained using electron ionization (EI), chemical ionization (CI) and fast atom bombardment (FAB). Thermal degradation was observed in both EI and CI. It was nevertheless possible to obtain reproducible spectra and characteristic peaks at 125°C probe temperature. In FAB, protonated EDTA ions were observed only if the matrix was acidified. Selection of matrices also influences the $[M + H]^+$ signal in acidic solution, the best results being obtained with the matrix glycerol. The influence of pH becomes more evident for EDTA in HCl solutions of different concentration. These results seem to indicate an important role for protonated $[M + H]^+$ species in solution prior to gaseous ion formation by FAB. The main effect of acid seems to be a solubility effect, although surface activity may also play a role.

Introduction

Ethylenediaminetetraacetic acid is a well-known chelating agent with many applications in analytical procedures, agriculture, pharmacology and industry. The chemical and physical properties of EDTA and EDTA complexes as well as their applications have been extensively studied (see for example References 1–4). The unequivocal importance of the use of EDTA as an additive in many applications and a possible need for its identification explains our interest in studying the behaviour of this compound by mass spectrometry, using different ionization techniques. Mass spectrometry is known to be an extremely sensitive and versatile analytical tool. Studies of EDTA by this technique are, however, rare.^{5–8} The interpretation of the results has in fact been hampered in electron impact studies by a strong component of thermal degradation.⁵ With respect to fast atom bombardment (FAB) studies, these have been carried out either on EDTA complexes⁸ or using EDTA in its salt form.^{6,7}

First, we used electron impact, the most common ionization technique, and, due to the possible influence of thermal degradation, we examined its behaviour as a function of probe temperature. As expected, thermal degradation occurred when EDTA was studied in the positive chemical ionization mode. Fast atom bombardment mass spectrometry⁹ is still the technique most widely used for the characterization of non-volatile and thermally-labile compounds that are not amenable to electron impact or chemical ionization methods. The behaviour of EDTA was, therefore, also examined under FAB conditions. This technique proved to be the most suitable for the identification of this compound. The lack of solubility of

the intact EDTA molecule might be a drawback for obtaining high quality spectra. This solubility problem may partly be resolved by the use of acids.^{10,11}

A detailed investigation of the experimental conditions has been undertaken in order to optimize the experimental technique for this type of compound. It has been widely recognized that the nature of liquid matrices determines the sputtering and ionization yields and hence the overall characteristics of the spectra.¹² For some analytes, the addition of acids to the solvents under FAB conditions frequently enhances the generation of $[M + H]^+$ ions observed in the spectra.^{10,13} In order to study the influence of the matrix and the addition of acids, several widely used matrices have been selected and, in the case of glycerol, different experiments were carried out adding hydrochloric, oxalic and acetic acids.

Experimental

The experiments were performed on an AEI MS9 mass spectrometer which had been updated by VG Analytical. Electron ionization was performed with 70 eV electrons, 200 μ A trap current and a source housing pressure of 10^{-6} Torr. For the CI experiments a low electron energy of 45 eV was used since it proved to be the most suitable in agreement with previous reports in the literature.¹⁴ The emission current was 430 μ A and the source housing pressure was 10^{-4} Torr. The reagent gas used was NH_3 . The source temperature used was 200°C for both EI and CI.

The FAB mass spectra were obtained by bombardment of the target surface by a beam of energetic xenon atoms pro-

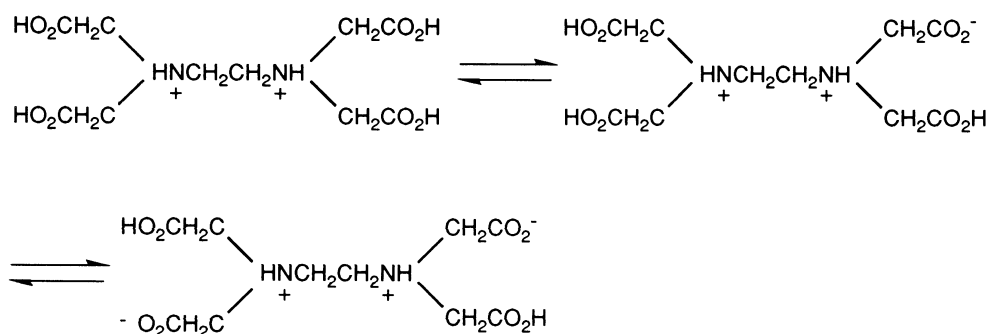
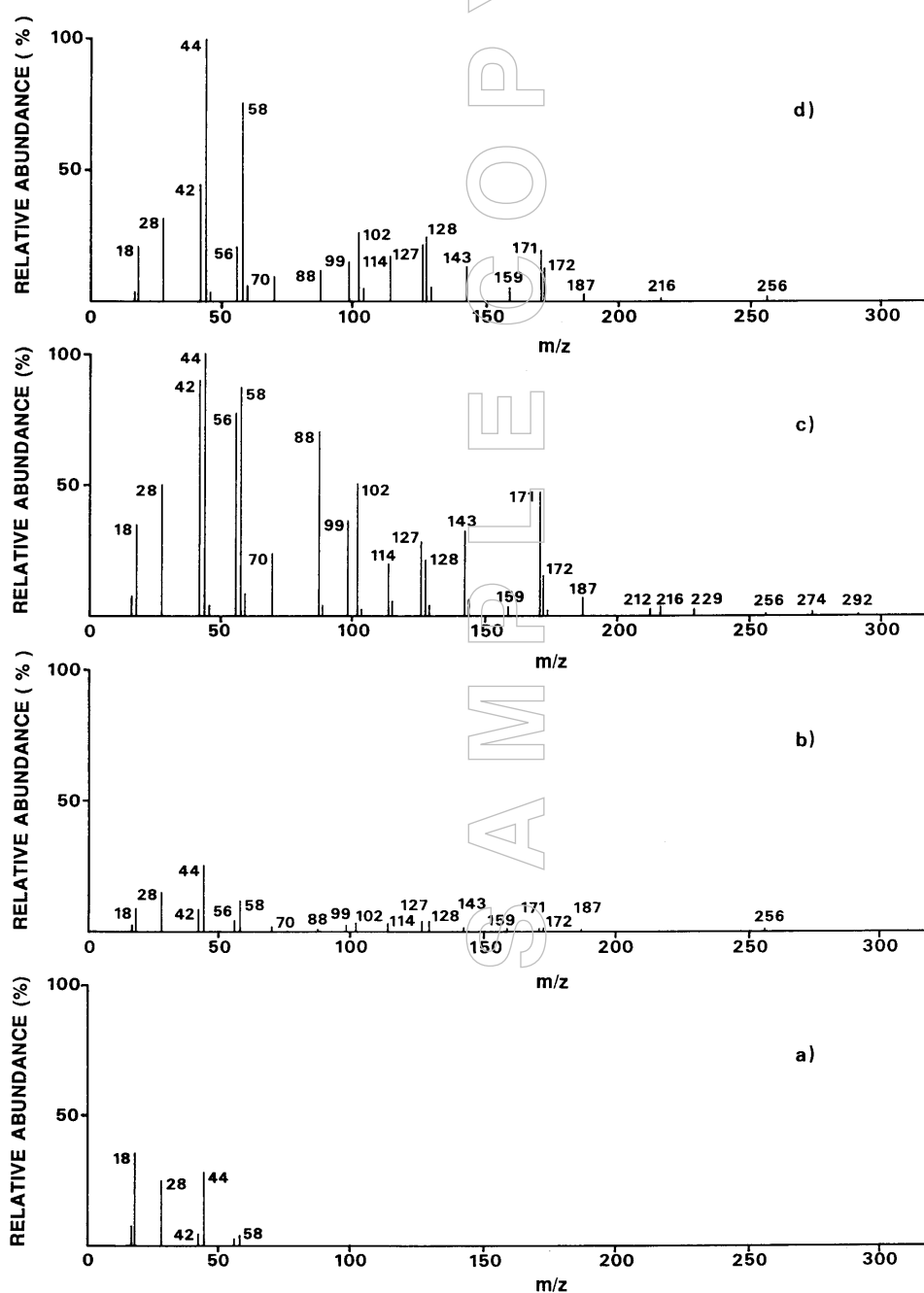
Figure 1. Mechanism for the ionization of H_6Y^{2+} and H_5Y^+ ions.

Figure 2. EI mass spectra of EDTA at probe temperatures of (a) 50°, (b) 100°, (c) 125° and (d) 150°C.

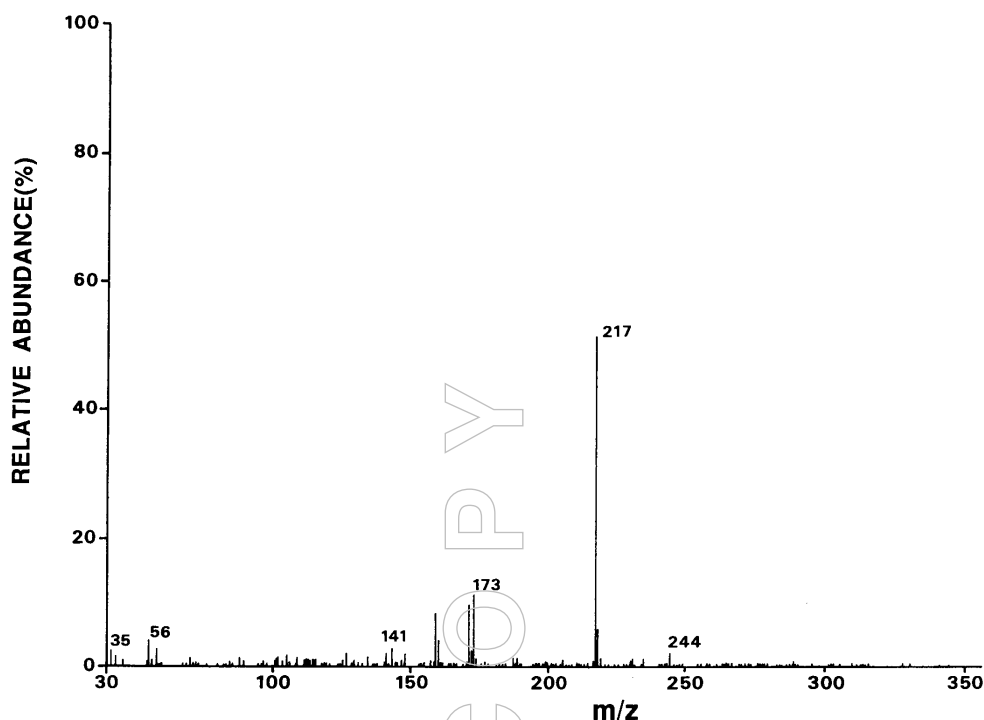


Figure 3. CI mass spectrum of EDTA. Reagent gas NH_3 .

duced by an Ion Tech FAB gun operated at 7 keV and 0.6 mA. The ion source was maintained at 70°C. Absolute amounts of about 10 μg EDTA were added to the matrix on the target. Where applicable, 10 μl of acid was added to the sample on the probe immediately before probe insertion.

In all the experiments the ions were accelerated through 8 kV.

The chemicals were obtained commercially and used without further purification.

Results and discussion

EDTA, commonly abbreviated as H_4Y , ionizes in acidic solution to the species H_5Y^+ and H_6Y^{2+} .¹¹ In strong acid solution both H_5Y^+ and H_6Y^{2+} species exist and the mechanism for the ionization of these species is represented in Figure 1.

Electron impact

In an attempt to study EDTA by electron impact mass spectrometry, we performed several experiments at different probe temperatures, since it has been proved that EDTA undergoes thermal degradation.⁵

The mass spectra recorded at four temperatures are shown in Figure 2. As it may be seen, at 50°C [Figure 2(a)] the most intense peaks are at m/z 18, 28 and 44. The peaks at m/z 18 and 44 corresponding to $[\text{H}_2\text{O}]^{+\bullet}$ and $[\text{CO}_2]^{+\bullet}$, respectively, are characteristic of thermal degradation. Nevertheless, mass spectrometric fragmentations cannot be ruled out. In addition

to the peaks obtained at 50°C, low intensity peaks at higher masses may be found at 100°C [Figure 2(b)]. With the probe temperature at 150°C [Figure 2(d)] peaks up to m/z 171 are more intense than at 100°C. The same does not apply for higher masses for which the ion abundance seems to be rather constant. At higher temperatures the compound did not come out. We tried therefore an intermediate temperature, 125°C [Figure 2(c)] which proved to be the best one. Reproducible spectra were obtained at this temperature and the peak corresponding to the molecular ion m/z 292, is observed in spite of being small. It is therefore possible to obtain useful information on EDTA using the electron impact technique under these experimental conditions and at a 125°C probe temperature.

Positive chemical ionization

The chemical ionization mass spectrum (Figure 3) obtained with ammonium as the reagent gas, does not show any

Table 1. Relative abundances (%) of EDTA ions in NH_3 CI mass spectra.

m/z	217	173	160	159
With probe	26.6	5.5	2.1	4.1
Without probe	24.2	5.0	2.4	4.9
Probe reinsertion	18.6	7.7	3.1	4.2

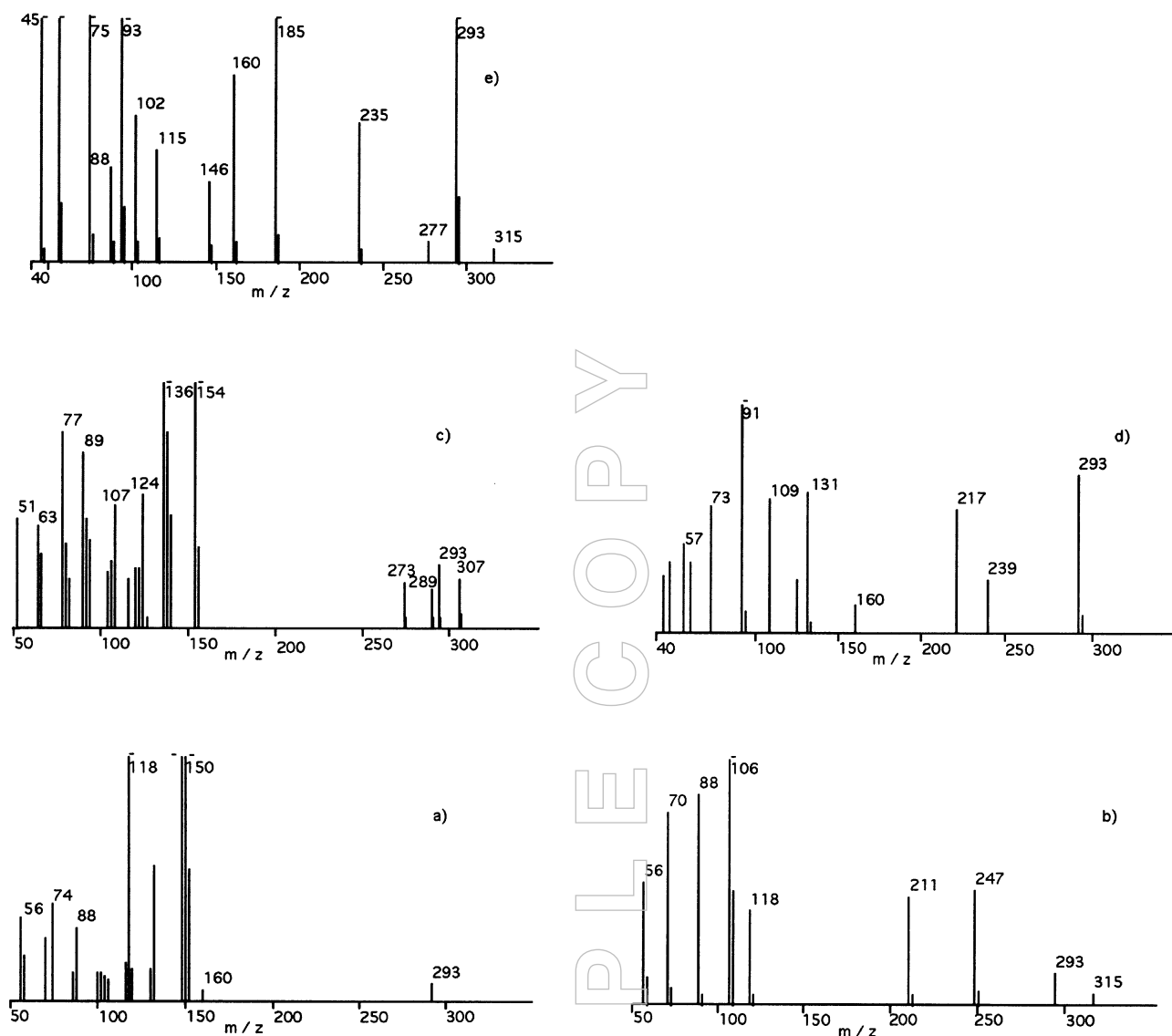


Figure 4. Positive-ion FAB mass spectra of EDTA in acidic matrices (a) triethanolamine, (b) diethanolamine, (c) *m*-nitrobenzyl alcohol, (d) thioglycerol and (e) glycerol.

peak at the characteristic masses of chemical ionization $[M + H]^+$, $[M - H]^+$ and $[M + NH_4]^+$. The more intense peak at m/z 217 appears to originate from protonation of the m/z 216 ion observed in all EI spectra.

In order to investigate a possible contribution from thermal degradation processes, a probe withdrawal experiment was performed. The intensities of the ions of m/z 159, 160, 173 and 217 were monitored whilst the probe was withdrawn and then reinserted with no further addition of compound. When the probe was reinserted, the intensity of the peak at m/z 217 never regained its value prior to withdrawal whereas the intensities of the peaks at m/z 173, 160 and 159 surpassed their original values (Table 1). These observations suggest that the m/z 217 ion is only formed in a mass spectrometric process. For the other ions, m/z 159, 160 and 173, a contribution from thermal degradation is operative.

Fast atom bombardment

FAB analyses of EDTA in several matrices do not yield $[M + H]^+$ ions or any ions indicative of the analyte molecule.

EDTA is barely soluble in water (0.5 g/100 ml at 80°C)¹ and usually insoluble in most solvents. We decided therefore to add some acid in order to overcome the solubility problem and to facilitate the protonation of this molecule.

Matrix liquids such as diethanolamine, triethanolamine, glycerol, thioglycerol and *m*-nitrobenzyl alcohol were tried with and without acid. The FAB mass spectra of EDTA in these matrices, acidified with concentrated HCl, are shown in Figure 4. A significant increase in $[M + H]^+$ ion abundance may be observed when the matrix is selected in what appears to be the following order triethanolamine < diethanolamine < *m*-nitrobenzyl alcohol < thioglycerol < glycerol. This order is in agreement with surface tension measurements performed

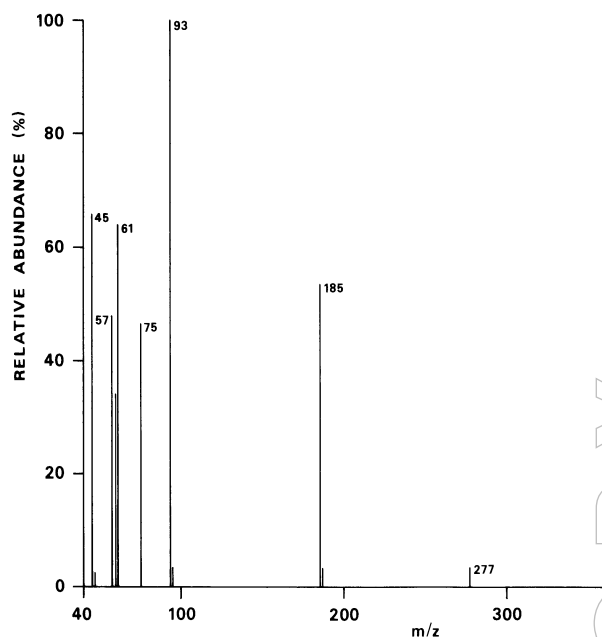


Figure 5. Positive-ion FAB mass spectrum of EDTA in glycerol with 1 M acetic acid.

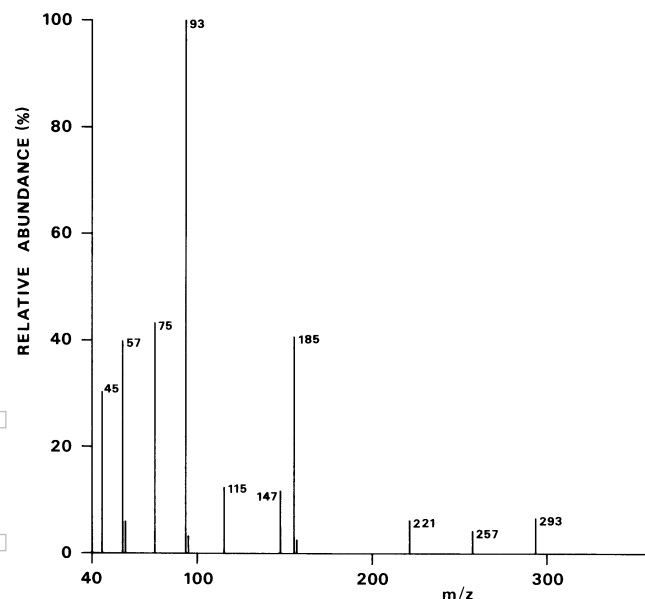


Figure 6. Positive-ion FAB mass spectrum of EDTA in glycerol with 1 M oxalic acid.

on EDTA solubilized in the acidified matrices.¹⁵ The surface tension decreased from glycerol to triethanolamine in the same order. The increased ion signal when the surface tension is raised suggests that surface activity effects may also play a role in the production of $[M + H]^+$. Our results agree with the findings of Takayama *et al.*,¹⁶ who suggest that the use of hydrophilic matrices favours $[M + H]^+$ production compared to the use of hydrophobic matrices such as *m*-nitrobenzyl alcohol.

Since the overall results obtained with glycerol in acidic solution were comparatively better than those with the other matrices with respect to the ion intensities from the analyte, the results presented here are only using glycerol as the matrix.

The effect of the addition of three acids of different strength to EDTA in glycerol was investigated. The mass spectrum of EDTA in glycerol when 1M acetic acid is added to the matrix may be seen in Figure 5. All the peaks observed are characteristic of glycerol whereas EDTA peaks are absent. The mass spectrum obtained with the addition of 1M oxalic acid is shown in Figure 6. Besides the characteristic peaks of glycerol and oxalic acid, the protonated molecule $[M + H]^+$ at m/z 293 may be found, although it was in small abundance. When the acid added was the stronger hydrochloric acid the mass spectrum in Figure 7 was obtained. The enhancement of the $[M + H]^+$ signal is evident. From these results it may be concluded that the protonation of the molecule is more effective in HCl than in oxalic acid and absent when acetic acid is used. It is reasonable to attribute this effect in part to a dependence on acid strength. A possible explanation could be the gen-

eration of protonated H_5Y^+ species in strong acid solutions.¹¹

The influence of pH becomes more evident from the results obtained for EDTA in HCl solutions at different concentrations. The addition of 0.1M HCl to the FAB matrix resulted in the appearance of m/z 293 ions corresponding to the protonated molecule. These ions were nevertheless not very abundant, as may be seen in Figure 8 where glycerol was the matrix compound used. When increasing the concentration of HCl up to 1M, the mass spectrum shown in Figure 7 was obtained. The relative $[M + H]^+$ signal improves by approximately a factor of 10. Figure 9 shows the result of adding concentrated HCl. When concentrated HCl is used the $[M + H]^+$ signal is enhanced two-fold with respect to 1M HCl.

These experiments seem to emphasize the important role of protonated $[M + H]^+$ species in solution prior to FAB analyses.

The known presence of H_6Y^{2+} species in strong acid solutions prompted us to investigate whether this doubly-charged species could be observed in the FAB mass spectra. The spectra do not provide, however, any evidence for the presence of the doubly-charged species H_6Y^{2+} , which is not unexpected since multiply charged ions have very seldom been observed.^{17,18} Moreover, it has been argued that FAB mass spectra should reflect solution composition but in the absence of side effects.¹⁹

The acid effect observed seems to be mainly a solubility effect whereas surface activity may also play a role. We intend to investigate further these aspects in the near future.

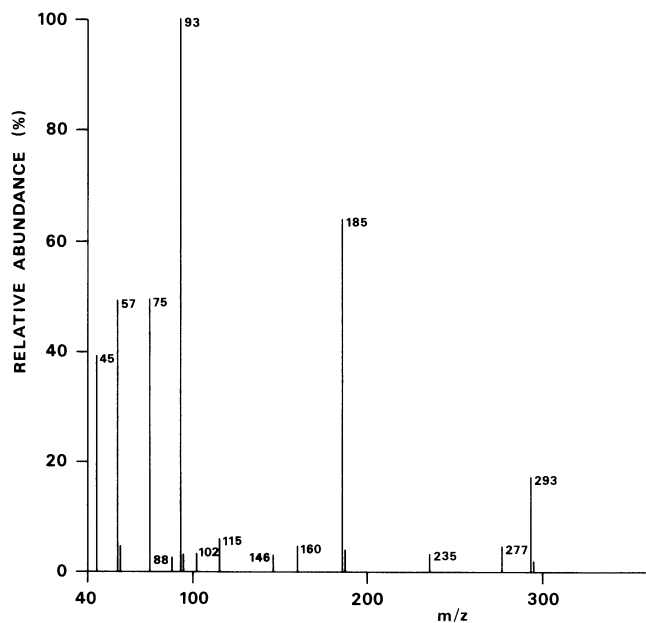


Figure 7. Positive-ion FAB mass spectrum of EDTA in glycerol with 1 M hydrochloric acid.

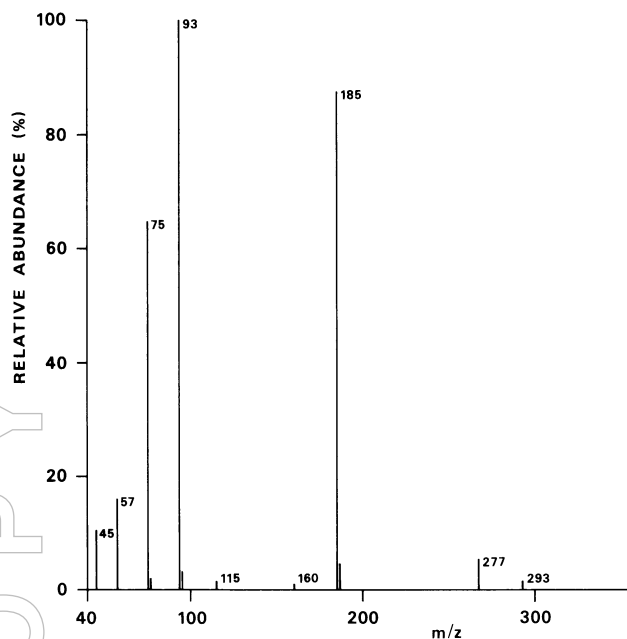


Figure 8. Positive-ion FAB mass spectrum of EDTA in glycerol with 0.1 M hydrochloric acid.

Conclusions

FAB mass spectrometry proved to be the more suitable technique for the identification of EDTA. Abundant $[M + H]^+$ ions and little fragmentation are obtained in acid solution by suitable choice of both the matrix compound and the acid. Optimized spectra were obtained with glycerol acidified with concentrated HCl.

With respect to EI and CI techniques it is possible to identify EDTA at a 125°C probe temperature in spite of the existence of a strong component of thermal degradation.

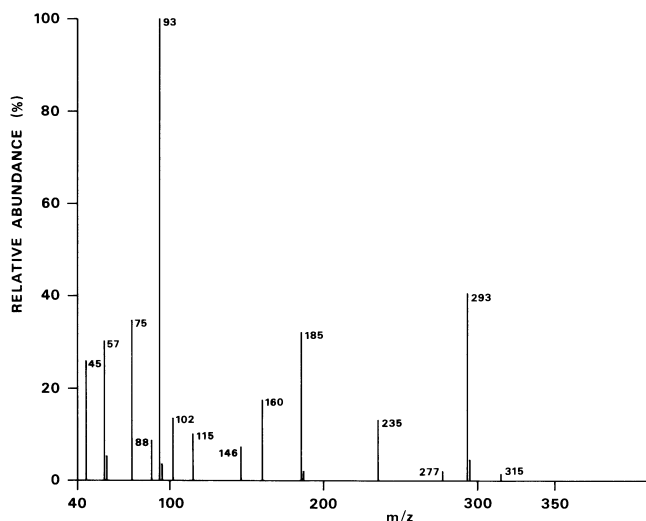


Figure 9. Positive-ion FAB mass spectrum of EDTA in glycerol with concentrated hydrochloric acid.

Acknowledgment

The authors thank Dr Benilde Saramago for the surface tension measurements and helpful discussions.

The authors thank Indalécio Marques for help with the mass spectrometer.

References

1. R. Pribil, *Analytical Applications of EDTA and Related Compounds*. Pergamon Press, Oxford (1972).
2. J.K. Hove and P.R. Tremaine, *J. Phys. Chem.* **89**, 5541 (1985).
3. J.K. Hove, L.G. Hepler and P.R. Tremaine, *Can. J. Chem.* **66**, 881 (1988).
4. P.G. Daniele, C. Rigano and S. Sammartano, *Anal. Chem.* **57**, 2956 (1985).
5. H.G. Langer and R.S. Gohlke, *Fortsch. Chem. Forsch.* **6**, 515 (1966).
6. A.W. Payne, *Int. J. Mass Spectrom. Ion Phys.* **46**, 555 (1983).
7. K.W.S. Chan and K.D. Cook, *Anal. Chem.* **55**, 1424 (1983).
8. A.S. Plaziak, S. Lis and M. Elbanowski, *Monatsh. Chem.* **123**, 225 (1992).
9. M. Barber, R.S. Bordoli, R.D. Sedgwick and A.N. Tyler, *Nature* **293**, 270 (1981).
10. S.A. Martin, C.E. Costello and K. Biemann, *Anal. Chem.* **54**, 2362 (1982).
11. D.C. Olson and D.W. Margerum, *J. Am. Chem. Soc.* **82**, 5602 (1960).
12. M. Barber, R.S. Bordoli, G.J. Elliott, R.D. Sedgwick and A.N. Taylor, *Anal. Chem.* **54**, 645A (1982).

13. C. Fenselau and R.G. Cotter, *Chem. Rev.* **87**, 501 (1987).
14. M.F.N. Duarte, D.W. Hutchinson and K.R. Jennings, *Org. Mass Spectrom.* **20**, 476 (1985).
15. A. Santos, M.F. Duarte, M.H. Florêncio and B. Saramago, submitted to *J. Chem. Soc. Faraday Trans.*
16. M. Takayama, Y. Tanaka and T. Nomura, *Org. Mass Spectrom.* **28**, 1529 (1993).
17. D.N. Heller, J. Yergey and R.J. Cotter, *Anal. Chem.* **55**, 1310 (1983).
18. J.M. Miller, K. Balasanmugam, J. Nye, G.B. Deacon and N.C. Thomas, *Inorg. Chem.* **26**, 560 (1987).
19. E. DePauw, A. Agnello and F. Derwa, *Mass Spectrom. Rev.* **10**, 283 (1991).

Received: 15 November 1994

Accepted: 28 January 1995

SAMPLE COPY

Fast atom bombardment and electrospray tandem mass spectrometry. Some fragmentation reactions in cyclic nitramines studied using collision-induced dissociation

Veronica Borrett*, Ian J. Dagley and Michael Kony

Aeronautical and Maritime Research Laboratory (AMRL)–DSTO, PO Box 4331, Melbourne, Victoria 3001, Australia.

Thomas Blumenthal

Department of Chemistry, The University of Adelaide, Adelaide, South Australia 5005, Australia.

The initial fragmentation pathways of some cyclic nitramines containing nitroguanidine and/or secondary nitramine groups were identified by fast atom bombardment (FAB) ionization mass spectrometry. Their partially nitrated analogues were analyzed as nitric acid salts using both FAB and electrospray (ES) ionization mass spectrometry. The ES technique gave simple mass spectra dominated by the more diagnostic higher molecular-mass species, which were ideal for tandem mass spectrometry (MS/MS) studies. Fragment-molecule adduct ions of the type $[\text{MH} + \text{NO}_2]^+$ and/or $[\text{MH} + \text{NO}]^+$ were observed in the FAB spectra in some cases. Fragmentation processes of these and the protonated molecules, together with some fragment ions, were elucidated. The main fragmentation processes were the loss of H_2O , NO_2 group(s) and to a lesser extent NO . Minor transitions involving ring fragmentations were more favorable for the nitric acid salts than their more highly nitrated analogues.

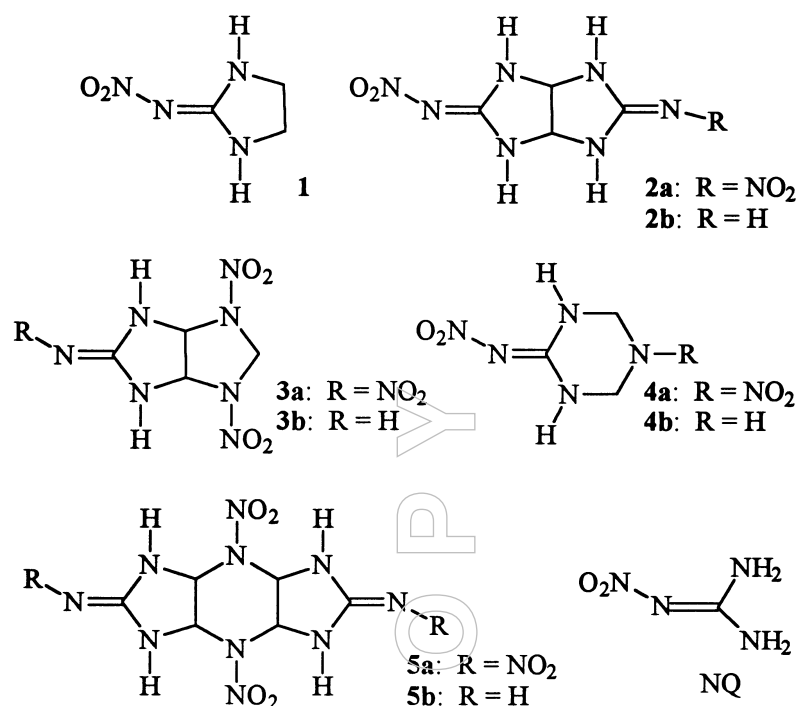
Introduction

The mass spectral fragmentation pathways of cyclic nitramines have been studied using a variety of techniques of varying analytical utility. Like most explosives, cyclic nitramines are heat-labile and are easily decomposed prior to ionization.¹ Their electron impact (EI) spectra are characterized by low abundances of molecular ions and many ions in the low mass region,² with the fragmentation pathways observed under these conditions^{1,3,4} of interest because of their possible correlation with thermal decomposition pathways.^{5,6} Fragmentation can be reduced using chemical ionization and pathways have been determined by recording mass analyzed ion kinetic energy (MIKES)/collision-induced dissociation (CID) spectra in both the positive and negative ion modes.^{1,4} Useful information on molecular mass and relatively simple spectra have also been obtained using field ionization and field desorption techniques.^{1,7}

We have found fast atom bombardment (FAB) a particularly useful technique for obtaining analytical information on the cyclic nitramines **1–5** (Scheme 1). These cyclic compounds contain nitro groups attached to secondary amines (secondary nitramines) and/or the imino group of guanidines

(nitroguanidines). The partially nitrated analogues **2b–5b** were examined as nitric acid salts. The acid salts are also suitable for analysis using electrospray ionization (ES) mass spectrometry. This technique^{8–11} has been recently developed, largely as a result of the pioneering work of Fenn *et al.*^{12–14} Its utility as a method for analyzing high molecular-mass biopolymers and, more recently metal complexes,^{15–17} has been demonstrated; however, few studies of low molecular-mass organic compounds have appeared. More recently the ESMS of some explosives, including HMX, have been obtained in the negative ion mode.¹⁸ An intrinsic feature of softer ionization techniques, such as ES, is that the mass spectra tend to be simple with most of the ion current in the more diagnostic higher mass fragments, facilitating MS/MS studies of these ions.

We now report the first tandem mass spectrometry (MS/MS) study using FAB and positive-ion ES ionization techniques with explosives, and the determination of some fragmentation reactions of molecule-fragment adducts, proton adducts and daughter ions of the cyclic nitramines (**1–5**) and nitroguanidine (NQ) which served as a useful model compound.



Scheme 1.

Experimental

Fast atom bombardment collision-induced mass spectra (FAB CID MS/MS) were obtained with a VG ZAB 2HF (VG Instruments) mass spectrometer. FAB conditions: current 1 mA, accelerating voltage 8 kV using argon gas. The pressure of argon in the second collision cell was measured outside the cell as 2×10^{-7} Torr which reduces the main beam by *c.* 10%, equivalent to single collision conditions for the purposes of this investigation. The samples for FAB were dissolved in an appropriate solvent and mixed with a matrix (glycerol or 3-nitrobenzyl alcohol).

Electrospray mass spectra were obtained using a VG Quattro mass spectrometer (VG Biotech, Altrincham, UK). The samples ($100 \text{ pmol } \mu\text{L}^{-1}$) were dissolved in water/acetonitrile/formic acid (50 : 50 : 1), which was also used as the mobile phase. The samples were injected directly into the spectrometer via an ISC (Lincoln, NE, USA) SFC-500 syringe pump at a flow rate of $5 \text{ } \mu\text{L min}^{-1}$. A dry nitrogen bath gas at atmospheric pressure was employed to assist evaporation of the electrospray droplets. The electrospray probe tip potential was 3.5 kV with 0.35 kV on the chicane counter electrode. The voltage of the first skimmer electrode (B1 voltage) was between 40 V and 60 V, as indicated. The second quadrupole of the triple quadrupole instrument was used as the collision region with argon used as the collision gas, at a pressure that gave approximately a 50% reduction in the parent ion abundance. The collision energy used for each experiment is indicated in Table 3.

Nitroguanidine was obtained from a commercial source, compounds **1**, **2** and **4** were prepared by literature methods^{19–21}

and the synthesis of compounds **3** and **5** is described elsewhere.²²

Results and discussion

FAB spectra of nitroguanidine (NQ) and cyclic nitramines **1**, **2a–5a**

The FAB mass spectra of nitroguanidine and the cyclic nitramines **1**, **2a–5a** all gave protonated molecules. The relative abundance of these ions varied from less than 4% for **2a** and **5a** to 31% for **3a**. The fragment-molecule adduct ions, $[\text{MH} + \text{NO}_2]^+$ (m/z 308) and $[\text{MH} + \text{NO}]^+$ (m/z 292), were observed in the FAB spectra of **3a**. Formation of fragment-molecule adduct ions for other cyclic nitramines have been previously observed^{4,23} in electron impact, and positive and negative chemical ionization modes. Daughter ions of the protonated molecules (Table 1), molecule-fragment adducts (Table 1) and some major fragment ions (Table 2) were determined by CID. The abundances of the daughter ions are expressed as a percentage of the most abundant fragment ion.

Fragmentation of the proton adduct of the model compound, nitroguanidine, commences predominantly by loss of H_2O , with competing smaller losses of NO and NO_2 . Under EI conditions the initial fragmentation of nitroguanidine involves only loss of NO and NO_2 ,²⁴ however, the analogous loss of OH is a minor pathway in the fragmentation of some secondary nitramines under EI conditions.²⁵

The initial fragmentation of the protonated monocyclic nitroguanidine **1** also involves competing loss of H_2O , NO_2 and to a lesser extent loss of NO. The loss of 14 u from this

Table 1. FAB daughter ions (CID) from molecule-adduct ions of NQ, **1** and **2a**–**5a**.

Compound	Parent ion (P)	Daughter ion	Relative abundance (%) FAB
NQ	[MH] ⁺ 105	87 [P – H ₂ O] ⁺ 75 [P – NO] ⁺ 67 [P – 38] ⁺ 59 [P – NO ₂] ⁺	100 13 14 13
1	[MH] ⁺ 131	117 [P – 14] ⁺ 113 [P – H ₂ O] ⁺ 101 [P – NO] ⁺ 85 [P – NO ₂] ⁺	100 75 35 75
2a	[MH] ⁺ 231	213 [P – H ₂ O] ⁺ 185 [P – NO ₂] ⁺ 141 [P – (NO ₂)N ₂ O] ⁺ 139 [P – 2NO ₂] ⁺	100 97 70 40
3a	[MH + NO ₂] ⁺ 308	248 [P – 2NO] ⁺ 216 [P – 2NO ₂] ⁺ 274 [P – H ₂ O] ⁺ 246 [P – NO ₂] ⁺ 233 [P – 59] ⁺ 200 [P – 2NO ₂] ⁺	15 100 18 18 15 100
	[MH + NO] ⁺ 292		
	[MH] ⁺ 263	217 [P – NO ₂] ⁺ 171 [P – 2NO ₂] ⁺ 129 [P – CH ₂ N ₄ O ₄] ⁺ 125 [P – 3NO ₂] ⁺	100 50 5 3
4a	[MH] ⁺ 191	176 [P – 15] ⁺ 173 [P – H ₂ O] ⁺ 161 [P – NO] ⁺ 145 [P – NO ₂] ⁺ 99 [P – 2NO ₂] ⁺	14 70 18 100 50
5a	[MH] ⁺ 377	360 [P – OH] ⁺ 347 [P – NO] ⁺ 331 [P – NO ₂] ⁺	100 44 30

ion is an unexpected result indicating the loss of N or CH₂, and requires further investigation. H₂O and NO₂ losses are also the dominant fragmentation pathways of the protonated bicyclic bis-nitroguanidine **2a**. The less intense fragment ion of *m/z* 139 arises from loss of two NO₂ fragments. The ion of *m/z* 141 probably results from loss of NO₂ and N₂O. The rearrangement reaction that results in the loss of N₂O would give the corresponding cyclic urea as the stable product ion.

Compounds **3a**, **4a**, and **5a** contain both nitroguanidine and secondary nitramine groups. In **3a** and **4a** the dominant fragmentation pathway of MH⁺ is loss of NO₂, with ions of half this abundance resulting from loss of two NO₂ groups; loss of NO₂ also occurs in **5a**, but as a minor pathway. The MH⁺ ion of **4a** shows a major fragmentation pathway involving loss of H₂O and to a lesser extent the loss of NO. In contrast, the major fragmentation pathway for compound **5a** was loss of OH. This compound (**5a**) was the most difficult to analyze using FAB and gave very weak high molecular-mass ions, however, duplicate analyses supported the observed loss of OH. Minor

Table 2. FAB daughter ions (CID) from major fragment ions.

Compound	Parent ion (P)	Daughter ion	Relative abundance (%) FAB
2b	[MH – NO] ⁺ 156	138 [P – H ₂ O] ⁺	88
		139 [P – OH] ⁺	100
		126 [P – NO] ⁺	32
		114 [P – HNC=NH] ⁺	20
		139 [P – H] ⁺	100
	[MH – NO ₂] ⁺ 140	126 [P – 14] ⁺	9
		123 [P – OH] ⁺	80
		113 [P – HCN] ⁺	17
		112 [P – 28] ⁺	12
		98 [P – HNC=NH] ⁺	85
3a	[MH – NO ₂] ⁺ 217	171 [P – NO ₂] ⁺	100
		125 [P – 2NO ₂] ⁺	40
		129 [P – CH ₂ N ₃ O ₂] ⁺	30
		199 [P – H ₂ O] ⁺	40
		98 [P – HCN ₃ O ₄] ⁺	20
	[MH – 2NO ₂] ⁺ 171	83 [P – CH ₂ N ₄ O ₄] ⁺	25
		125 [P – NO ₂] ⁺	100
		79 [P – 92] ⁺	25
	[MH – CH ₂ N ₄ O ₄] ⁺ 129	111 [P – H ₂ O] ⁺	100
		115 [P – CH ₂] ⁺	65
3b	[MH – NO ₂] ⁺ 172	155 [P – OH] ⁺	17
		145/146 [HCN] ⁺ /[CN] ⁺	80
		126 [P – NO ₂] ⁺	100
		109	100
		97/98	12
5b	[MH – OH] ⁺ 271	84 [P – CH ₂ N ₃ O ₂] ⁺	65
		253 [P – H ₂ O] ⁺	57
		241 [P – NO] ⁺	87
		225 [P – NO ₂] ⁺	100
		179 [P – 2NO ₂] ⁺	39

pathways from the protonated bicyclic compound **3a** are loss of all three NO₂ groups to give an ion of *m/z* 125, and loss of the O₂NNCH₂NNO₂ fragment to give a monocyclic ion of *m/z* 129. This latter decomposition route provides information useful in structural elucidation.

The [MH – NO₂]⁺ ion of *m/z* 217 in the spectrum of **3a** is formed by two competing pathways since its daughter ions of *m/z* 83 and 129 (Table 2) are due, respectively, to loss of O₂NNCH₂NNO₂ (from the ion formed by loss of NO₂ from the nitroguanidine group) and loss of NCH₂NNO₂ (from the ion formed by loss of NO₂ from a secondary nitramine group). Another low molecular-mass daughter ion (*m/z* 98) from the [MH – NO₂]⁺ ion probably arises from loss of two NO₂ groups and HCN. Other daughter ions are formed by loss of one and two NO₂ groups, and H₂O.

The molecule-fragment adduct ions, [MH + NO]⁺ and [MH + NO₂]⁺, observed in the spectrum of compound **3a** both fragment predominantly by loss of two NO₂ groups. The latter adduct ion fragments to a lesser extent with loss of two NO groups, and with H₂O and NO₂ losses occurring from the [MH + NO]⁺ ion.

Table 3. Daughter ions (CID) from molecule-adduct ions (FAB) and protonated molecules (FAB and ES) of the nitric acid salts of **2b**–**5b**.

Compound	Parent ion (P)	Daughter ion	Relative abundance (%)	
			FAB	ES ^a
2b	[MH + NO] ⁺ 216	198 [P – H ₂ O] ⁺ 186 [P – NO] ⁺ 170 [P – NO ₂] ⁺	100 38 16	
	[MH] ⁺ 186	168 [P – H ₂ O] ⁺ 156 [P – NO] ⁺ 143 [P – CH ₃ N ₂] ⁺ 142 [P – N ₂ O] ⁺ 140 [P – NO ₂] ⁺ 100 [P – NCNNO ₂] ⁺ 97 [P – NO CH ₃ N ₃] ⁺ 94 [P – 92] ⁺ 93 [P – 93] ⁺ 71 45	16 5 15 100 5 57 48	37 100 16 8 37
3b	[MH + NO ₂] ⁺ 264	172 [P – 2NO ₂] ⁺ 126 [P – 3NO ₂] ⁺ 109 84 [P – NO ₂ CH ₂ N ₄ O ₄] ⁺	100 4 3 3	
	[MH + NO] ⁺ 248	202 [P – NO ₂] ⁺ 156 [P – 2NO ₂] ⁺ 126 [P – NO 2NO ₂] ⁺ 84 [P – NO CH ₂ N ₄ O ₄] ⁺	100 85 4 4	
	[MH] ⁺ 218	172 [P – NO ₂] ⁺ 109 84 [P – CH ₂ N ₄ O ₄] ⁺ 126 [P – 2NO ₂] ⁺	100 3 4 4	100 19 19
4b	[MH] ⁺ 146	132 [P – 14] ⁺ 128 [P – H ₂ O] ⁺ 125 [P – 21] ⁺ 117 [P – H ₂ C=NH] ⁺ 100 [P – NO ₂] ⁺ 73 [P – NO ₂ HCN] ⁺ 42 [C ₂ H ₄ N] ⁺ 30 [NO] ⁺	8 15 7 25 100 15 15	6 100 20 55 15
5b	[MH + NO ₂] ⁺ 333	316 [P – OH] ⁺ 288 272 241 [P – 2NO ₂] ⁺ 195 [P – 3NO ₂] ⁺	20 11 21 100 10	
	[MH] ⁺ 287	270 [P – OH] ⁺ 241 [P – NO ₂] ⁺ 195 [P – 2NO ₂] ⁺ 99 [P – NO ₂ C ₃ H ₄ N ₅ O ₂] ⁺ 98 [P – NO ₂ C ₃ H ₅ N ₅ O ₂] ⁺	15 43 100 16	13 50 100

^aSkimmer voltage and MS/MS collision energy, respectively, for each compound are: **2b** (60 V, 20 eV); **3b** (40 V, 20 eV); **4b** (50 V, 50 eV); and **5b** (50 V, 20 eV).

FAB and ES spectra of the nitric acid salts of cyclic nitramines **2b**–**5b**

Both the FAB and ES mass spectra of the acid salts of **2b**–**5b** show abundant protonated molecules. The intensities

of the [MH]⁺ peaks in the FAB spectra varied from 100% for **3b** to around 50% for **2b**, **4b** and **5b**. Their relative abundance in the ES spectra of the acid salts varied from 35% for **2b** to 64% for **5b** and is dependent on the skimmer voltage which

is quoted in Table 3 (increasing the skimmer voltage may cause CID in its vicinity where the pressure is close to atmospheric). Typical examples of these are the mass spectra of **3b** obtained by (a) ES at $B1 = 40$ V and (b) FAB, given in Figure 1. The ES spectra are much simpler than the FAB spectra, showing less fragmentation and less chemical noise, with the FAB spectra being complicated by the ion current contribution of the matrix.

Molecule-fragment adduct ions were not detected in the ES spectra but $[MH + NO_2]^+$ and/or $[MH + NO]^+$ adduct ions are present in the FAB spectra of **2b**, **3b** and **5b**. The ion at m/z 256 in the spectrum of **3b** is presumably due to $[MK]^+$, from potassium ions incidental in the system. The daughter ions derived from the protonated molecules as well as the molecule-fragment adducts (Table 3) and some major fragment ions (Table 2) were determined from CID spectra. The abundances of the daughter ions are expressed as a percentage of the most abundant fragment ion.

The compounds contain cyclic nitroguanidine groups (**2b** and **4b**) or secondary nitramine groups (**3b** and **5b**) in combination with protonated cyclic secondary amine (**4b**) or cyclic guanidine groups. The FAB $[MH]^+$ ions and molecule-fragment adduct ions decompose largely by reactions of the cyclic nitramine groups. These reactions typically involve loss of nitro group(s), some losses of H_2O and less frequent examples of loss of nitroso groups (see discussion above). The cleavage of the $O_2NNCH_2NNO_2$ observed for **3a** is also a minor reaction of the structurally related salt (**3b**) and occurs in combination with loss of adducts to give the m/z 84 ion. A number of ring fragmentation reactions of $[MH]^+$ give rise to minor daughter ions and some examples are: loss of the H_2CNH fragment from the secondary amine **4b**, loss of NO and guanidine from **2b** to give the m/z 97 ion, decomposition of **3b** to m/z 109 (probably $C_3H_3N_5$) and **5b** to m/z 99 (probably $C_3H_7N_4$) which may be monocyclic guanidines.

Fragmentation reactions of some major daughter ions derived from some $[MH]^+$ ions, under FAB conditions, were also examined (Table 2). Significant new fragmentation reactions observed are: loss of $HNC = NH$ from the ions m/z 156 and 140 derived from **2b**, and loss of HCN from cyclic guanidine ions of m/z 140 (from **2b**) and 172 (from **3b**).

Daughter ions formed from the MH^+ ions of **2b–5b** under both ES and FAB conditions are compared (Table 3). The ES spectra differ significantly since no ions corresponding to losses of H_2O or NO were observed. An elimination of N_2O from the nitroguanidine in **2b** is observed in the ES spectrum and the similar fragmentation observed in the FAB spectrum for **2a** has been discussed. Loss of NO_2 is the dominant reaction under both ES and FAB conditions. Ring fragmentation of $[MH]^+$ ions was also observed under ES conditions. In particular, the major initial fragmentation pathway for **5b** involves the loss of 189 u, presumably due to fragmentation of the pyrazine ring ($P-C_3H_5N_5O_2$) together with loss of the second NO_2 group. A similar transition was observed as a minor peak in the FAB spectrum of **5b**. Some ring fragmentation reactions not observed under FAB conditions are loss

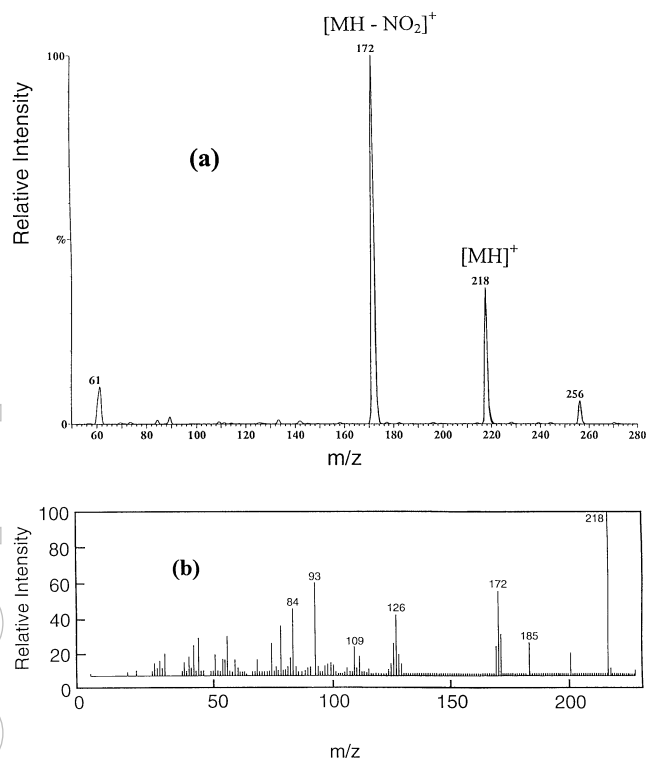


Figure 1. Mass spectrum of compound **3b** (a) ESMS, (b) FAB-MS.

of O_2NNCN from **2b**, and loss of both NO_2 and HCN to give the m/z 73 ion in the spectrum of **4b**.

Conclusions

Fast atom bombardment was found to be a useful technique for the characterization of several cyclic nitramines, including some examined as nitric acid salts of amines. Protonated molecules, and in some cases adduct ions with NO and/or NO_2 , were observed. The main fragmentation reactions of these ions and major fragment ions typically involve loss of nitro group(s), some losses of H_2O and less frequent examples of loss of nitroso groups. The minor ring fragmentation reactions compete more effectively with these nitramine decomposition reactions in the fragmentation reactions of the nitric acid salts. These nitric acid salts also give similar useful spectra under ES conditions. Differences arise because no NO or NO_2 adduct ions or losses of either H_2O or NO from MH^+ ions occur in the ES spectra. Some differences in some ring fragmentation reactions were also noted.

Acknowledgements

The assistance of Dr R. Colton (La Trobe University), and Dr M. Shiel and Mr Larry Hill (University of Wollongong), in performing the ES experiments is gratefully acknowledged.

References

1. J. Yinon, *Mass Spectrom. Rev.* **1**, 257 (1982).
2. R.G. Gillis, M.J. Lacey and J.S. Shannon, *Org. Mass Spectrom.* **9**, 359 (1974).
3. J. Yinon, W.C. Brumley, G.M. Brilis and S. Bulusu, *Org. Mass Spectrom.* **25**, 14 (1990).
4. J. Yinon, D.J. Harvan and J.R. Hass, *Org. Mass Spectrom.* **17**, 321 (1982).
5. J. Stals, *Trans. Faraday Soc.* **67**, 1768 (1971).
6. S. Bulusu, T. Axenrod and G.W.A. Milne, *Org. Mass Spectrom.* **3**, 13 (1970).
7. H.R. Schulten and W.D. Lehmann, *Anal. Chim. Acta* **93**, 19 (1977).
8. J.B. Fenn, M. Mann, C.K. Meng, S.F. Wong and C.M. Whitehouse, *Mass Spectrom. Rev.* **9**, 37 (1990).
9. M. Mann, *Org. Mass Spectrom.* **25**, 575 (1990).
10. R.D. Smith, J.A. Loo, C.G. Edmonds, C.J. Barinaga and H.R. Udseth, *Anal. Chem.* **62**, 882 (1990).
11. R.D. Smith, J.A. Loo, C.G. Edmonds, C.J. Barinaga and H.R. Udseth, *Mass Spectrom. Rev.* **10**, 359 (1991).
12. M. Yamashita and J.B. Fenn, *J. Phys. Chem.* **88**, 4451 (1984).
13. M. Yamashita and J.B. Fenn, *J. Phys. Chem.* **88**, 4671 (1984).
14. J.B. Fenn, M. Mann, C.K. Meng, S.F. Wong and C.M. Whitehouse, *Science* **246**, 64 (1989).
15. R. Colton and J.C. Traeger, *Inorg. Chim. Acta* **201**, 153 (1992).
16. R. Colton, J.C. Traeger and J. Harvey, *Org. Mass Spectrom.* **27**, 1030 (1992).
17. R. Colton, V. Tedesco and J.C. Traeger, *Inorg. Chem.* **31**, 3865 (1992).
18. R.F. Straub and R.D. Voyksner, *J. Am. Soc. Mass Spectrom.* **4**, 578 (1993).
19. A.F. McKay and G.F. Wright, *J. Am. Chem. Soc.* **70**, 430 (1948).
20. M. Kony and I.J. Dagley, *Heterocycles* **38**, 595 (1994).
21. D. Huang and R.R. Rindone, U.S. Patent 4 937 340 (1990).
22. I.J. Dagley and J.L. Flippen-Anderson, *Aust. J. Chem.* **47**, 2033 (1994).
23. E. P. Burrows, *Org. Mass Spectrom.* **26**, 1027 (1991).
24. J.H. Beynon, J.A. Hopkinson and A.E. Williams, *Org. Mass Spectrom.* **1**, 169 (1968).
25. J. Yinon, W.C. Brumley, G.M. Brilis and S. Bulusu, *Org. Mass Spectrom.* **25**, 14 (1990).

Received: 29 November 1994

Accepted: 16 January 1995

Fast atom bombardment mass spectrometry of new polydentate Schiff bases. 3. The case of mono- and bis aldimine containing benzo-5-crown-5 groups

Elvio Bullita, Sergio Tamburini, Pietro Alessandro Vigato

Istituto di Chimica e Tecnologie Inorganiche e dei Materiali Avanzati, Corso Stati Uniti 4, I-35020 Padova, Italy.

Massimo Carbini

Istituto di Chimica Industriale, Facoltà di Ingegneria, via Marzolo 9, I-35100 Padova, Italy.

Silvia Catinella and Piero Traldi*

CNR, Area di Ricerca, Corso Stati Uniti 4, I-35020 Padova, Italy.

The mass spectrometric behaviour of five polydentate Schiff bases derived from the condensation of formyl or diformyl precursors (2,3-dihydroxybenzaldehyde, 2-hydroxy-3-methoxybenzaldehyde, 4-methyl-2,6-diformylphenol, 2,6-diformylpyridine or 2,2'-(ethylenedioxy) dibenzaldehyde with 4-amino-benzo-5-crown-5 has been investigated by fast atom bombardment and metastable ion studies. The mass spectra mainly exhibit the results of decomposition processes related to the crown moiety. Only for two compounds have cleavages of the aldimine group been demonstrated. This behaviour is explained either by protonation on specific sites or by the occurrence of resonance phenomena.

Introduction

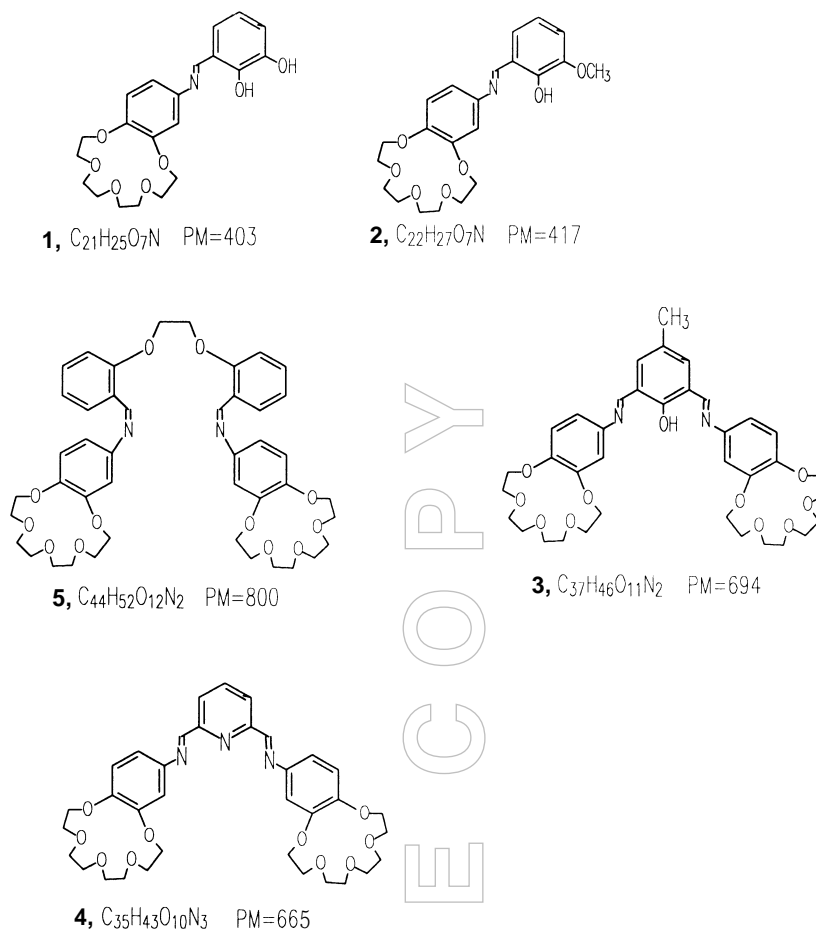
It is well known that Schiff bases can easily coordinate metal ions, giving rise to stable complexes. These ligands have been employed in the study of stereochemical, electronic, magnetic and catalytic properties of metal complexes.¹ Moreover they have successfully been proposed as models of the active sites of metal-enzymes.²

In the recent past macrocyclic, macrobicyclic and macroacyclic compartmental Schiff bases have been prepared in one-step multiple condensation reactions of suitable formyl or keto- and amine precursors.^{1,3} The insertion of additional donor atoms (S, P, O, N) into the coordination moiety of these systems can be tuned, in order to make them suitable and selective for particular ions, especially transition metal ions. Moreover emphasis was placed on ligands incorporating oxygen donor atoms, such as crown-ethers, which are considered good ligands for non-transition metal ions, especially alkaline or alkaline-earth ions.^{1,3}

Many papers have been published on the ability of these macrocyclic ligands to mimic ion encapsulation and transport of natural systems. The ability of these synthetic ligands to act

as suitable chelating agents for alkaline or alkaline-earth ions has been attributed to several factors, including the goodness of fit of the cation in the ligand cavity and the nature and the shape of the donor set.

The fusion of the Schiff base and crown-ether properties into a unique entity can give rise to polynucleating ligands with different coordination chambers in close proximity. These systems can incorporate suitable d-metal ions into the Schiff base sites and non-transition or f-metal ions into the crown-ether sites. The coordination of a metal ion into the crown-ether cavity can considerably modify the physico-chemical (electrochemical, optical, magnetic) properties of the metal ion bound to the Schiff base system and the mutual interaction through the ligand of the two metal ions can be applied to the development of molecular devices. To this end we have prepared a series of Schiff bases containing crown-ether by condensation of the appropriate formyl- or diformyl- precursors with 4-amino-benzo-5-crown-5. In particular the reaction of the formyl or diformyl derivatives 2,3-dihydroxy-benzaldehyde, 2-hydroxy-3-methoxy-benzaldehyde, 2,6-diformyl-4-methylphenol, 2,6-diformyl-pyridine and 2,2'-(ethylenedioxy) dibenzaldehyde with 4'-benzo-5-crown-



5 in methanol forms the compounds **1–5**, as white-yellow, yellow or red solids in high yield. The compounds are air stable and soluble enough to allow their characterization by 1H - and ^{13}C -NMR, using $CDCl_3$ or $DMSO-d_6$ as solvents, in addition to their identification by elemental analyses and IR spectroscopy.⁴ All these data agree with the formulation of pure mono- or bis-alimine derivatives, as proposed in Scheme 1.

Mass spectrometry has been proved to be a particularly valid analytical tool for the characterization of either Schiff bases or crown-ethers.⁵ In both cases fast atom bombardment proved to be the best ionization method, leading to the easy production of molecular species and fragment ions well related to the structure. Pursuing our interest in this field,⁶ we present here the mass spectrometric behaviour of compounds **1–5** as obtained under FAB conditions and by metastable ion studies.

Experimental

Mass spectrometry

All measurements were performed on a VG ZAB2F mass spectrometer⁷ (VG Analytical, Manchester, UK) operating under FAB conditions⁸ (8 keV xenon atoms bombarding a glycerol solution of the samples). Metastable transitions were

detected in the second field free region by MIKE spectrometry.⁹ Accurate mass measurements were performed by the peak-matching technique at 5000 resolving power (10% valley definition).

Compounds

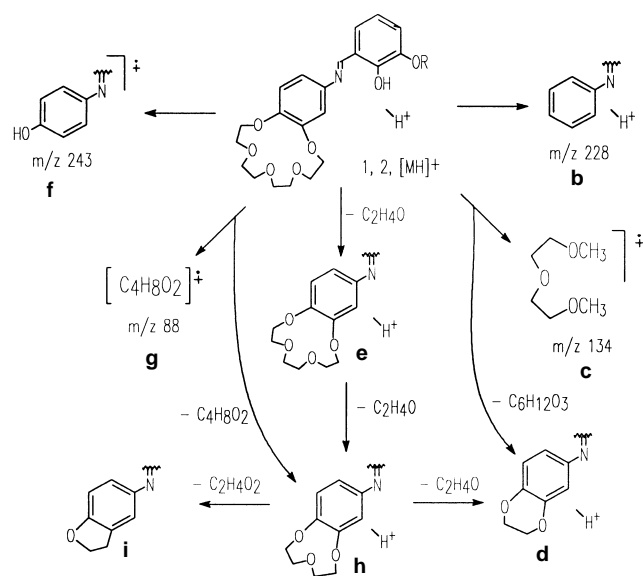
The formyl derivatives (2,3-dihydroxybenzaldehyde, 3-methoxysalicylaldehyde, 2,6-diformyl-pyridine, 2,2'-(ethylenedioxy)dibenzaldehyde, the amine 4-amino-benzo-5-crown-5 and the solvents were commercial products (Aldrich Chimica, Milan, Italy) used without further purification.

4-methyl-2,6-diformylphenol was prepared according to the literature.¹⁰ Its purity was checked by elemental analysis, IR and NMR spectroscopies and mass spectrometry.

Compounds **1–5** were prepared by the reaction in methanol of the appropriate formyl- or diformyl-precursor with 4-amino-benzo-5-crown-5, respectively, in a 1 : 1 or 1 : 2 (formyl : amine) molar ratio. The resulting white, yellow or yellow-orange or red solution was stirred for 30 min and refluxed for 20 min. Compound **1** precipitates as a red solid by partial evaporation of the solvent under reduced pressure. Compounds **2–4** precipitate from the methanol solution. The red-brown solution containing **5** was evaporated to dryness under reduced pressure. The oil obtained was dissolved in



Compounds	1		2		3		4		5	
Ionic species	FAB	MIKE	FAB	MIKE	FAB	MIKE	FAB	MIKE	FAB	MIKE
$[M + H]^+$	404 (38)		418 (100)		695 (11)		666 (34)		801 (100)	
$[M - C_2H_4O]^+$	360 (5)	360 (53)	374 (7)	374 (47)	651 (3)	651 (31)	622 (3)	622 (80)		
$[M - C_4H_8O_2]^+$	316 (2)	316 (100)	330 (5)	330 (100)	607 (2)	607 (31)	578 (4)	578 (100)		
$[MH - C_6H_{12}O_3]^+$	272 (5)	272 (90)	286 (9)	286 (92)	563 (5)	563 (100)	534 (4)	534 (72)		
$[MH - C_6H_{12}O_4]^+$	256 (4)	256 (5)	256 (3)	256 (40)						
$[MH - C_7H_{14}O_3]^+$					549 (4)	549 (52)	507 (2)	507 (21)		
$[MH - C_8H_{16}O_3]^+$					535 (2)					
$[MH - C_8H_{16}O_4]^+$					519 (3)					
$[MH - CH_2O]^+$					665 (5)	665 (30)				
1					428 (2)	428 (23)				
2					414 (2)	414 (72)	384 (3)	384 (83)		
3							373 (2)	373 (58)		
4 (a)									414 (56)	414 (100)
$[C_6H_{14}O_3]^{+*}$	134 (20)	134 (3)	134 (15)	134 (1)	134 (100)	134 (4)	134 (5)	134 (41)		
$[C_4H_8O_2]^{+*}$	88 (100)	88 (5)	88 (70)	88 (3)	88 (2)	88 (7)	88 (35)	88 (2)		
$[a-C_2H_4O]^+$									370 (7)	370 (14)
$[a-C_4H_8O_2]^+$									326 (6)	326 (31)
$[a-C_6H_{12}O_3]^+$									282 (3)	282 (19)



Scheme 2.

CHCl_3 and clarified by activated carbon. The solvent was evaporated under reduced pressure and the residue obtained was treated with ethanol and diethyl-ether. The compounds **1–5**, obtained as yellow or yellow-orange or red solids, were filtered, washed with methanol or ethanol and diethyl-ether and dried *in vacuo*. Their purity was inferred by elemental analysis, ^1H and ^{13}C NMR spectroscopy.⁴ Moreover the absence of absorptions due to $\text{C}=\text{O}$ or H_2N groups in the IR spectra of **1–5** confirm that full condensation reactions have taken place.

Results and discussion

The FAB mass spectra and the MIKE spectra of $[\text{MH}]^+$ ions obtained for compounds **1–5** are reported in Table 1. All the examined compounds exhibit particularly abundant protonated molecules, being responsible for the base peak of the spectra for **2** and **5**.

Compounds **1** and **2** show the common fragmentation pattern reported in Scheme 2. Fragment ions corresponding to losses of $\text{C}_2\text{H}_4\text{O}$, $\text{C}_4\text{H}_8\text{O}_2$, $\text{C}_6\text{H}_{12}\text{O}_3$ and $\text{C}_6\text{H}_{12}\text{O}_4$ are present in both FAB and MIKE spectra, but while in the latter case they are responsible for the most abundant ions, in the former spectra they are scarcely abundant. Such behaviour is good evidence that these fragmentation channels represent those at lower critical energy. On the contrary the $[\text{C}_4\text{H}_8\text{O}_2]^+$ and $[\text{C}_6\text{H}_{14}\text{O}_3]^+$ ions are particularly abundant in the FAB spectra (100% and 20%, 70% and 15% for **1** and **2**, respectively) and their high abundance could be rationalized by their high thermodynamic stability. Thus for the ions at m/z 88 the structure of the odd electron molecular ion of dioxane could be proposed. To confirm such hypothesis we compared the identical MIKE spectra of the $[\text{C}_4\text{H}_8\text{O}_2]^+$ species FAB-generated from compound **1** and **2** with that of the EI-generated M^{++} of dioxane. Such results are reported in Figure 1 and, as it can

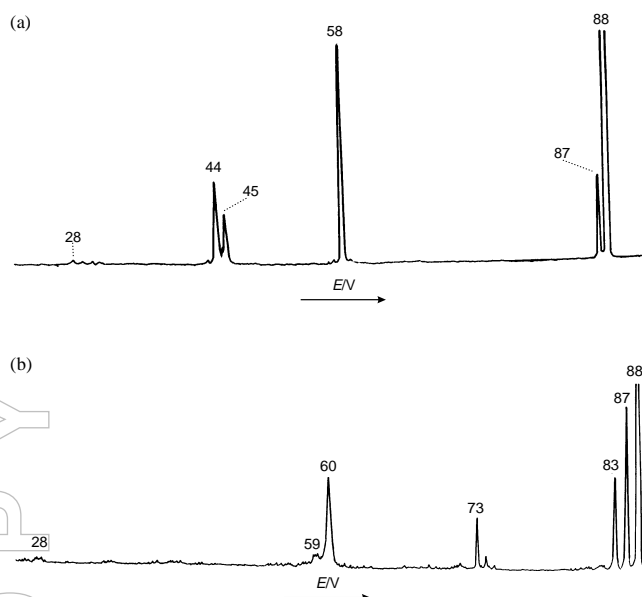
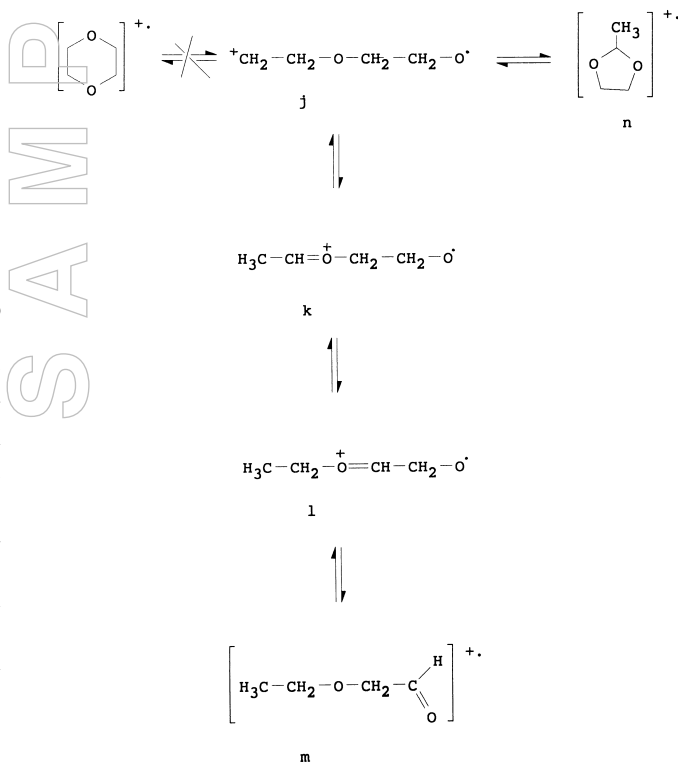


Figure 1. MIKE spectra of: (a) M^{++} of dioxane; (b) ions at m/z 88 FAB-generated from compound **1** (identical to that from compound **2**).

be easily seen, the spectra are very different. While in the case of M^{++} of dioxane the loss of CH_2O leading to ions at m/z 58 and the formation of $\text{C}_2\text{H}_4\text{O}$ and $\text{C}_2\text{H}_5\text{O}$ ions at m/z 44 and 45 lead to the most abundant peak in the MIKE spectrum [see Figure 1(a)], the $[\text{C}_4\text{H}_8\text{O}_2]^+$ ions observed for **1** and **2** give rise to fragment ions at m/z 73, 60 and 59, reasonably originating from methyl radical, ethylene and ethyl radical losses. Thus



Scheme 3.

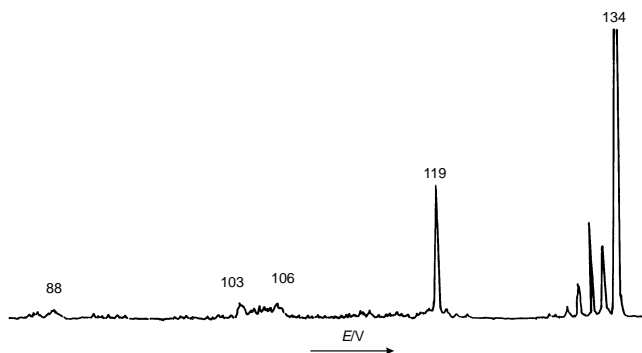
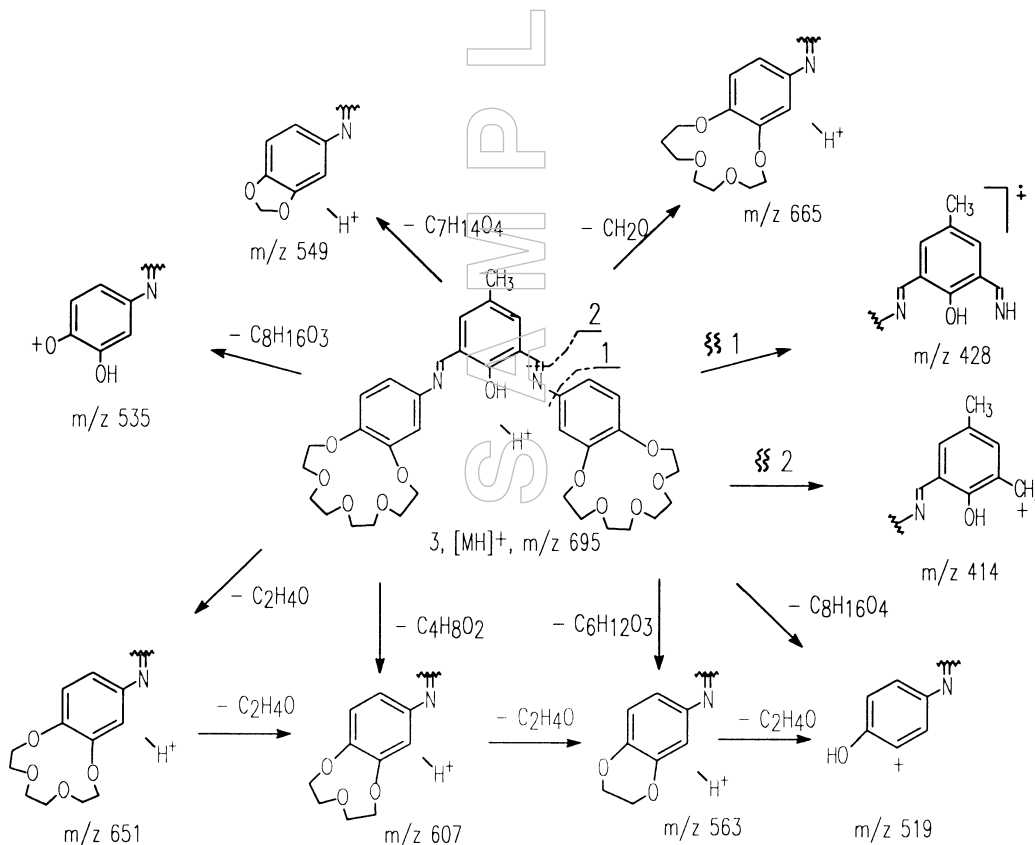


Figure 2. MIKE spectra of ionic species at m/z 134 generated by FAB of compound **1** (identical to that from compound **2**).

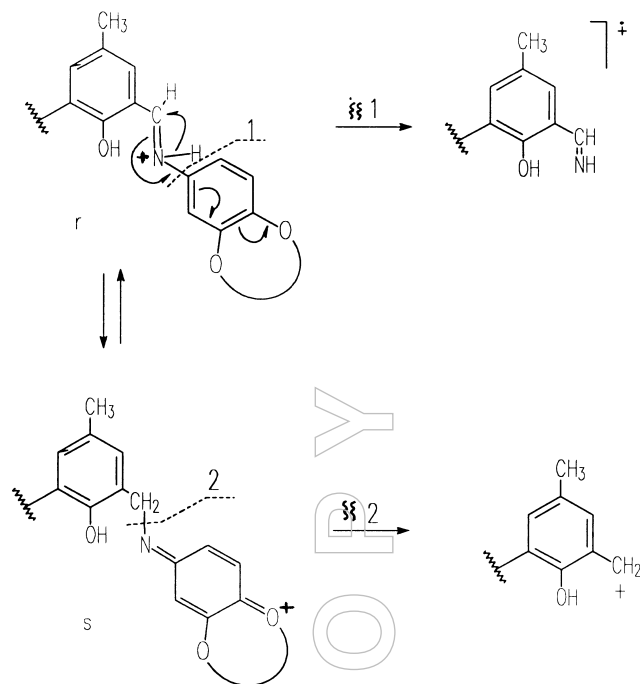
for the ions at m/z 88 originating from **1** and **2** the structure of $M^{+\bullet}$ of dioxane cannot be proposed. Some of the possible structures of these ions which are in agreement with the MIKE data are summarized in Scheme 3. The radical cation in distonic form **j**, originating from the cleavage of the crown moiety, can rearrange to species necessarily bearing a methyl group (thus explaining the methyl loss evidenced by MIKE spectrum) as the **k**, **l**, **m** and **n** ones reported in Scheme 3. The first two consist in γ distonic ions, while for **m** and **n** the rearrangement processes has led to an aldehyde and a five-membered cyclic moiety, respectively. We retain structures **l** and **m** as the more reasonable ones, because they give a better account for the unimolecular fragmentation pathways de-

tected by MIKE spectrometry. The ions at m/z 134 originate by the cleavage of the crown moiety with the rearrangement of two hydrogen atoms. The related MIKE spectrum, reported in Figure 2, shows losses of CH_3^\bullet , C_2H_4 , CH_3O^\bullet and C_2H_6O , leading to the ions at m/z 119, 106, 103 and 88, respectively. Hence, on the basis of the MIKE data, the structure reported in Scheme 2 can be reasonably proposed. Worth noting is the complete absence in the decomposition pattern of **1** and **2** of any fragment ions related to the aldimine chain, typical of the mass spectrometric behaviour of such a class of compounds. This result must be ascribed to the presence of the alternative, and energetically more favoured, processes related to the crown moiety and discussed above.

Compound **3** exhibits a fragmentation pattern more complex than that observed for compounds **1** and **2**. In fact, together with C_2H_4O , $C_4H_8O_2$, $C_6H_{12}O_3$ losses (leading to ions at m/z 651, 607 and 563, respectively) described above for compounds **1** and **2**, new fragmentation channels become operative. Some of them are still related to the crown moieties (i.e. those due to CH_2O , $C_7H_{14}O_4$ and $C_8H_{16}O_3$ losses, leading to ions at m/z 665, 549 and 535, respectively) while two decomposition routes are originated by cleavages of the aldimine chain (cleavages 1 and 2 of Scheme 4, giving rise to the ionic species at m/z 428 and 414, respectively). Such behaviour can suggest that in the case of **3** the protonation has taken place on the aldimine nitrogen with the formation of a quaternary nitrogen cation (structure **r** of Scheme 5), directly responsible for the formation of the ion at m/z 428. Through H



Scheme 4.



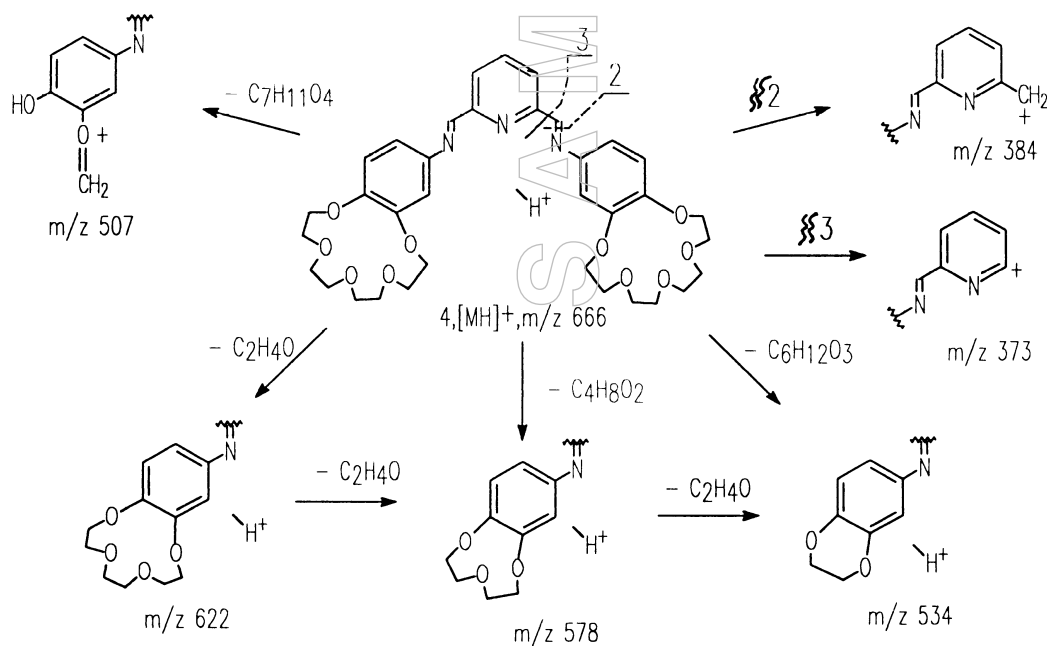
Scheme 5.

rearrangement and resonance phenomena, ions **r** can give rise to ions **s**, which account for the observed cleavage 2.

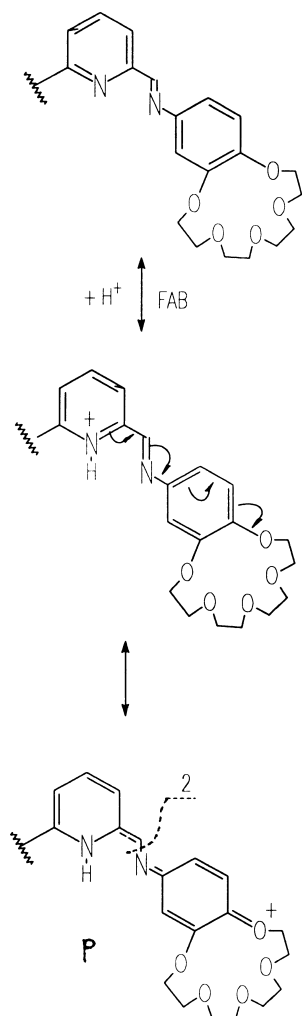
Compound **4** shows, together with the above described fragmentation routes related to the crown moiety (and leading to the ions at m/z 622, 578 and 534), the cleavage of the aldimine chain (cleavage 2 of Scheme 6, leading to the ions at m/z 384 and the unusual cleavage 3, in α position to pyridine giving rise to ions at m/z 373). In order to explain the easy formal cleavage of the $\text{CH}=\text{N}$ bonds (cleavage 2) molecular species in a structure different from that of a neutral molecule

must be hypothesized. As an alternative to the mechanism proposed for compounds **3** and reported in Scheme 5, in the present case we suggest the occurrence of the mechanism reported in Scheme 7, which hypothesizes the protonation on the pyridine nitrogen, followed by resonance phenomena leading to ions **p**. These ions easily account for the cleavage of the $\text{CH}-\text{N}$ bond.

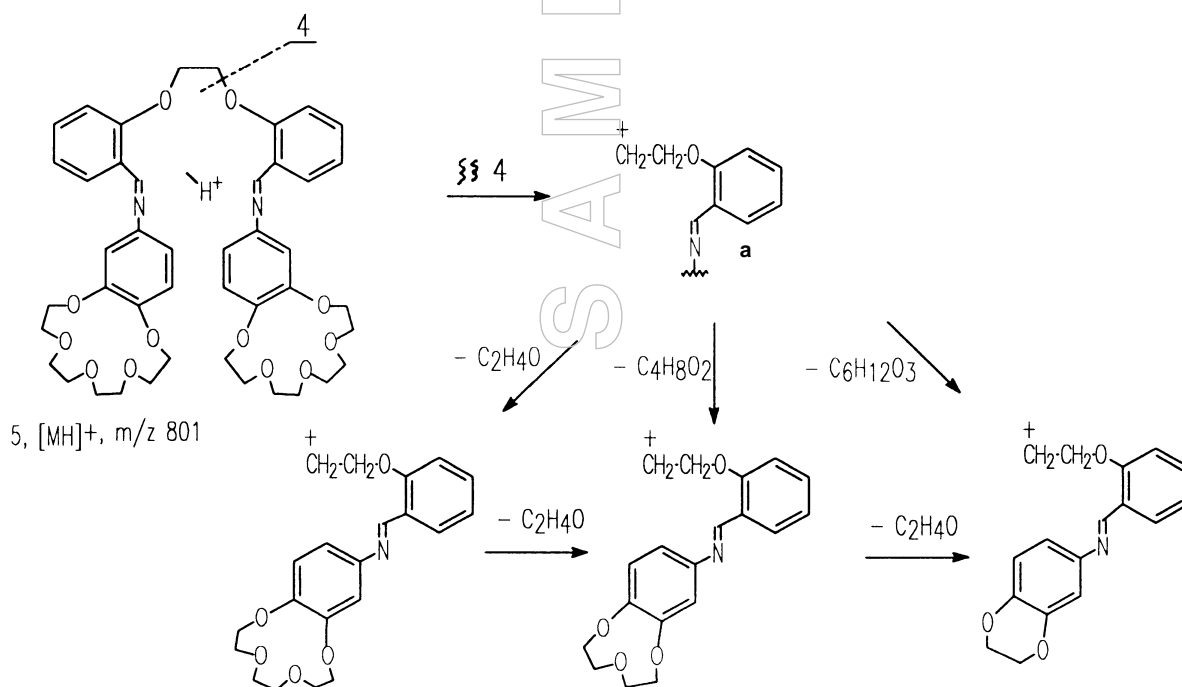
Finally, compound **5** shows an abundant protonated molecule at m/z 801 which undergoes only one fragmentation pathway, consisting of the cleavage 4 of Scheme 8. The ion so



Scheme 6.



Scheme 7.



Scheme 8.

formed, at m/z 414, is responsible for all the other ions present in the spectrum, through the fragmentation processes related to the crown moiety already described for the other compounds under study.

In conclusion the mass spectrometric behaviour of the title compounds is mainly governed by decomposition processes related to the crown moiety present in the molecules. The cleavages of the aldimine chain, evidenced for compounds **3** and **4** only, have been justified by the occurrence of protonation on aldimine or pyridine nitrogens, followed by resonance phenomena.

References

- (a) D.E. Fenton, U. Casellato, P.A. Vigato and M. Vidali, *Inorg. Chim. Acta* **95**, 187 (1984); (b) D.E. Fenton, U. Casellato, P.A. Vigato and M. Vidali, *Inorg. Chim. Acta* **62**, 57 (1982); (c) P. Guerriero, P.A. Vigato, D.E. Fenton and P.C. Hellier, *Acta Chemica Scand.* **46**, 1025 (1992); (d) R.D. Willet, D. Gatteschi and O. Kahn, *Magneto-structural Correlations in Exchange Coupled Systems*. Nato ASI Series, Reidel, Dordrecht (1983); (e) U. Casellato, P.A. Vigato, D.E. Fenton and M. Vidali, *Chem. Soc. Rev.* **8**, 199 (1979); (f) P. Zanello, S. Tamburini, P.A. Vigato and S.A. Mazzocchin, *Coord. Chem. Rev.* **77**, 165 (1987); (g) P.A. Vigato, S. Tamburini and D.E. Fenton, *Coord. Chem. Rev.* **106**, 25 (1990); (h) D.E. Fenton and P.A. Vigato, *Chem. Soc. Rev.* **17**, 69 (1988); (i) T.M. Sorrell, *Tetrahedron* **45**, 3 (1989); (j) J.-M. Lehn, *Pure Appl. Chem.* **50**, 871 (1978); (k) J.-M. Lehn, *Science* **227**, 849 (1985); (l) J.-M. Lehn,

- Angew. Chem. Int. Ed. Engl.* **27**, 89 (1988); (m) J.-M. Lehn, *Angew. Chem. Int. Ed. Engl.* **30**, 1304 (1990); (n) P. Guerriero, S. Tamburini and P.A. Vigato, *Coord. Chem. Rev.* in press.
2. (a) D. E. Fenton in *Advances in Inorganic and Bioinorganic Mechanisms*, Ed. by A.G. Sykes, Vol. 2. Academic Press, London, p.187 (1983); (b) K.D. Karlin and J. Zubieta, *Copper Coordination Chemistry and Biochemistry: Biochemical and Inorganic Perspective*. Adenine Press, New York, USA (1983); (c) K.D. Karlin and J. Zubieta, *Biological and Inorganic Copper Chemistry, Vols. 1,2*. Adenine Press, New York, USA (1986); (d) S.E. Groh, *Isr. J. Chem.* **15**, 277 (1976/1977); (e) F.L. Urbach, *Metal Ions in Biological Systems, No. 13. Copper Proteins*, Ed. by H. Sigel. Marcel Dekker, Basel, p.73 (1981), and references cited therein; (f) H. Adams, N.A. Bailey, W.D. Carlisle, D.E. Fenton and G. Rossi, *J. Chem. Soc., Dalton Trans.* 1271 (1990); (g) H. Adams, N.A. Bailey, M.J.S. Dwyer, D.E. Fenton, P.C. Hellier and P.D. Hempstead, *J. Chem. Soc., Chem. Commun.* 1297 (1991); (h) K.D. Karlin and Y. Gultneh, *Progress in Inorganic Chemistry Vol. 35*, Ed. by S.J. Lippard. Wiley, New York, p.19 (1987); (i) R. Menif, A.E. Martell, P.J. Squattrito and A. Clearfield, *Inorg. Chem.* **27**, 4723 (1990).
 3. (a) D. McDowell and J. Nelson, *Tetrahedron Lett.*, 347 (1988); (b) M.G.B. Drew, D. McDowell and J. Nelson, *Polyhedron* 2229 (1988); (c) V. McKee, D. McDowell and J. Nelson, *Polyhedron* 1143, (1989); (d) V. McKee, W. Robinson and D. McDowell, *Tetrahedron Lett.* 7453 (1989); (e) M.G.B. Drew, J. Hunter, C. Harding, M. McCann and V. McKee, *J. Chem. Soc., Dalton Trans.* 11 (1992); (f) M. Dorrity, J. Malone, D. Marrs, V. McKee and J. Nelson, *J. Chem. Soc., Chem. Commun.* 383 (1992); (g) M.G.B. Drew, J. Hunter, C. Harding, D. Marrs and J. Nelson, *J. Chem. Soc., Dalton Trans.* 3235 (1992); (h) N. Martin, V. McKee and J. Nelson, *J. Inorg. Chim. Acta* **218**, 5 (1994); (i) C. Harding, Q. Lu, V. McKee and J. Nelson, *J. Chem. Soc., Chem. Commun.* 1768 (1993); (j) Q. Lu, V. McKee, *J. Chem. Soc., Chem. Commun.* 1768 (1993); (k) J. Hunter, J. Nelson, C. Harding, M. McCann and V. McKee, *J. Chem. Soc., Chem. Commun.* 1198 (1990); (l) M. McCann, J. Nelson and Q. Lu, *Inorg. Biochem.* **51**, 633 (1993); (m) C. Harding, J. Nelson and V. McKee, *J. Am. Chem. Soc.* **113**, 9684 (1991); (n) D. Marrs, V. McKee, J. Nelson, C. Harding and Q. Lu, *Inorg. Chim. Acta* **211**, 195 (1993); (o) Q. Lu, J.-M. Latour, C. Harding, N. Martin, D. Marrs, V. McKee and J. Nelson, *J. Chem. Soc., Dalton Trans.* 1471 (1994); (p) G. Morgan, V. McKee and J. Nelson, *Inorg. Chem.* **33**, 4428 (1994).
 4. S. Tamburini and P.A. Vigato, unpublished results.
 5. B. Kiremire, R. Seraglia and P. Traldi, *Rapid Commun. Mass Spectrom.* **5**, 543 (1991).
 6. (a) P. Querriero, S. Tamburini, P.A. Vigato, R. Seraglia and P. Traldi, *Org. Mass Spectrom.* **27**, 231 (1992); (b) S. Catinella, P. Traldi, P. Guerriero, S. Tamburini and P.A. Vigato, *Rapid Commun. Mass Spectrom.* **8**, 111 (1994) and references therein reported.
 7. R.P. Morgan, J.H. Beynon, R.H. Bateman and B.N. Green, *Int. J. Mass Spectrom. Ion Phys.* **28**, 171 (1979).
 8. M. Barber, R.S. Bordoli, R.D. Sedgwick and A. N. Tyler, *J. Chem. Soc., Chem. Commun.* **7**, 325 (1981).
 9. R.G. Cooks, J.H. Beynon, R.M. Caprioli and G.R. Lester, *Metastable Ions*. Elsevier, Amsterdam (1973).
 10. (a) A. Zinke, F. Hanus and E. Ziegler, *J. Prakt. Chem.* **152**, 126 (1939); (b) S. Taniguchi, *Bull. Chem. Soc. Jpn.* **57**, 2683 (1984); (c) H. Fironzabadi and Z. Mostafavipoor, *Bull. Chem. Soc. Jpn.* **56**, 914 (1983); (d) R.S. Drago, M.J. Desmond, B.B. Carden and K.A. Miller, *J. Am. Chem. Soc.* **105**, 2287 (1983).

Received: 7 December 1994

Accepted: 16 January 1995

A new general fragmentation reaction in mass spectrometry: The hydrogen–carbon, carbon–carbon double rearrangement of 2-heteroalkyl substituted diphenylmethyl cations

Maria Concetta Natoli

Dipartimento di Chimica Organica, via Archirafi 20, I-90123 Palermo, Italy.

Pasquale Agozzino, Leopoldo Ceraulo,* Mirella Ferrugia and Liliana Lamartina

Dipartimento di Chimica e Tecnologie Farmaceutiche, via Archirafi 32, I-90123 Palermo, Italy.^a

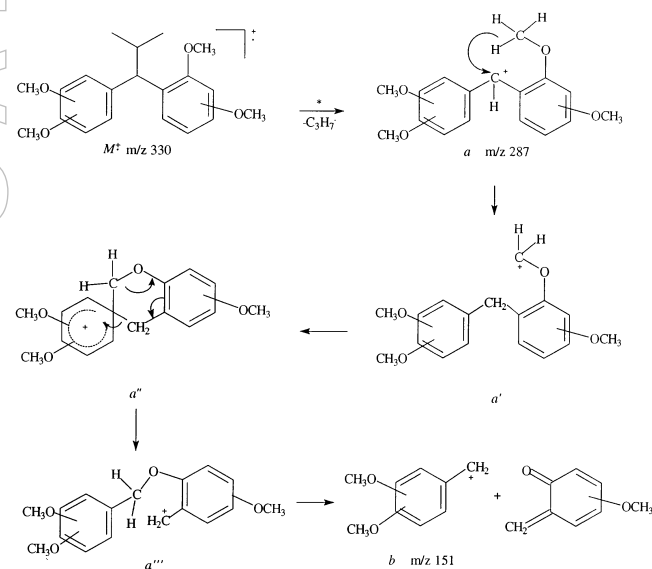
Diphenylmethyl cations formed by benzylic cleavage of the molecular ions of *ortho* heteroalkyl substituted 1,1-diphenylalkanes undergo the double rearrangement process (H to C followed by C to C) previously reported for *ortho*-methoxy derivatives. Hence the formation of substituted benzyl (or tropylium) ions allowing this double rearrangement process constitutes an interesting type of fragmentation reaction characteristic for 1,1-diphenylalkanes bearing *ortho* substituents (OMe, OEt, OiPr, SMe, NHMe, NMe₂) which are able to transfer a hydride to the charged benzyl carbon of diphenylmethyl cations formed by benzylic cleavage of the molecular ion.

Introduction

We reported¹ that the 70 eV mass spectrum of 1,1-bis(2,4-dimethoxyphenyl)-2-methylpropane **1** (Figure 1) bearing *ortho* methoxy groups shows an intense peak at m/z 151 corresponding to the dimethoxybenzyl or dimethoxytropylium ion **b** (Scheme 1), arising from $[M - iPr]^+$ ion **a**. The absence of the ion **b** in the spectrum of the isomer 1,1-bis(3,4-dimethoxyphenyl)-2-methylpropane **2** (Figure 2), together with the constant presence of intense peaks corresponding to methoxybenzyl or methoxytropylium ions in a large series of polymethoxy substituted 1,1-diphenylalkanes bearing *ortho* methoxy groups, led to the conclusion that such an ion is formed by *ortho* interaction between the methoxy group and the benzylic carbon.¹ The formation of ion **b** from ion **a** occurs through a double rearrangement (hydrogen–carbon followed by carbon–carbon: HC, CC-dr) process.¹

This has been unequivocally demonstrated by the use of ²H and ¹³C labelled compounds and principally by the observa-

tion that the m/z 151 ion observed in the mass spectrum of the compound **3** (Figure 3) is completely shifted to m/z 152 in the spectrum of the ¹³C isotopomer **4** (Figure 4). An isotopic effect $K_H/K_D \approx 1.4$ in the 70 eV spectra^{1,2} indicates that the hydrogen migration is the rate determining process.



Scheme 1.

^aThis work constitutes Part 4 of the series "Hydrogen–carbon, carbon–carbon double rearrangement induced by proximity effects" and Part 18 of the series "Studies in organic mass spectrometry", Parts 3 and 17 see Reference 2 and L. Ceraulo, P. De Maria, M. Ferrugia, S. Foti, R. Saletti and D. Spinelli, *J. Mass Spectrom.* **30**, 257 (1995).

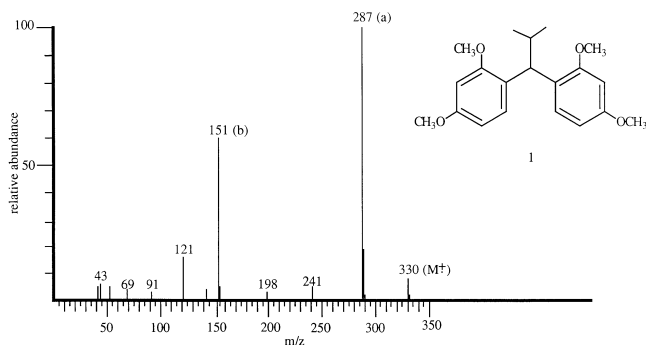


Figure 1. 70 eV electron impact mass spectrum of compound 1.

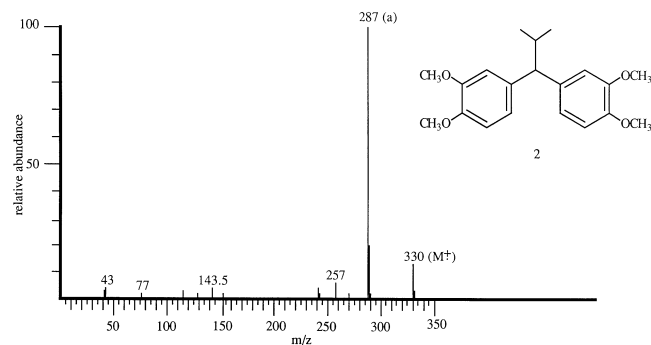


Figure 2. 70 eV electron impact mass spectrum of compound 2.

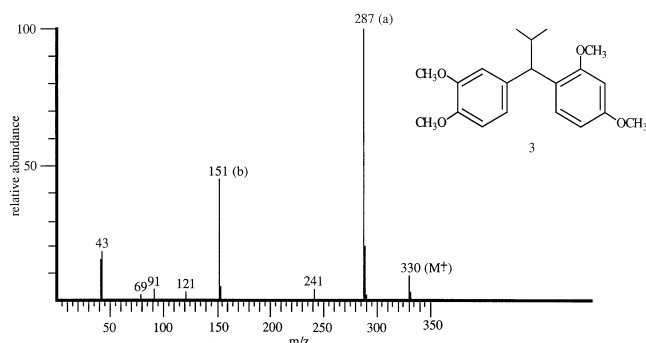


Figure 3. 70 eV electron impact mass spectrum of compound 3.

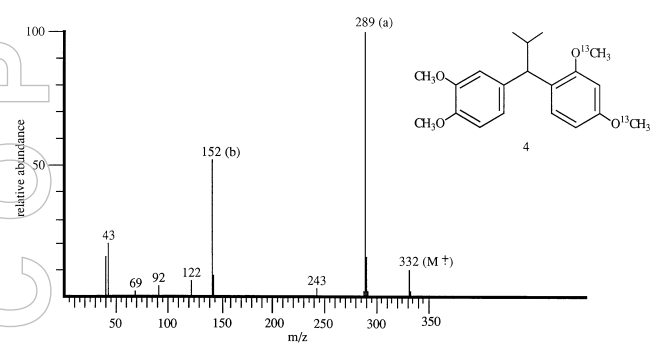


Figure 4. 70 eV electron impact mass spectrum of compound 4.

Further experiments with ^2H and ^{13}C labelled compounds showed that about 50% of the benzyl or tropylium ions present in the 70 eV spectrum of 2-methoxydiphenylmethane itself are formed through this double rearrangement reaction.^{2,3} All these findings give evidence that the *HC, CC-dr* process constitutes a generally occurring process for *ortho*-methoxy-substituted 1,1-diphenylalkanes, which had not been previously reported.^{4,5}

Hence, it seemed interesting to verify whether such a process could also occur with 2-substituents other than with the methoxy group. For this reason, we examined a series of 1,1-diphenylalkanes bearing *ortho* OEt, OiPr, SMe, NHMe and NMe_2 groups.

Results and discussion

Ethoxy derivatives

The mass spectrum of 2-ethoxydiphenylmethane **5** (Figure 5) is similar to that of 2-methoxydiphenylmethane.^{4,6} According to the easier loss of ethyl with respect to the methyl radical, in this case the base peak is at m/z 183 $[\text{M} - \text{Et}]^+$, and peaks at m/z 165 (fluorenyl cation) and m/z 91 (C_7H_7^+) are still observed. The peak at m/z 105 is a consequence of the *HC, CC-dr* process (Scheme 2). Its intensity ($I\% = 3.3$) is low, as is that of the precursor ion **a** $[\text{M} - \text{H}]^+$ ($I\% = 0.4$).

The peak at m/z 105 is completely shifted to m/z 109 for the pentadeutero derivative **6** (Figure 6). Its relative abundance of 1.8% indicates an isotope effect ($K_{\text{H}}/K_{\text{D}} \approx 1.5$) close to the

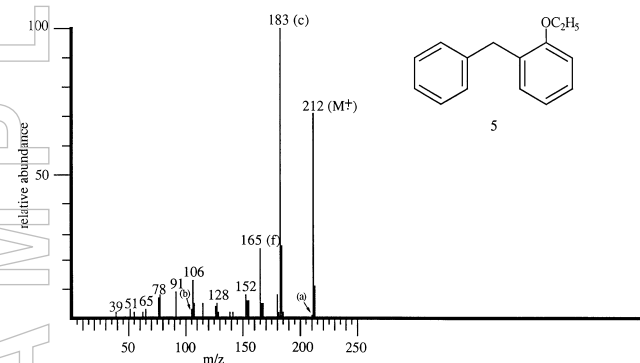
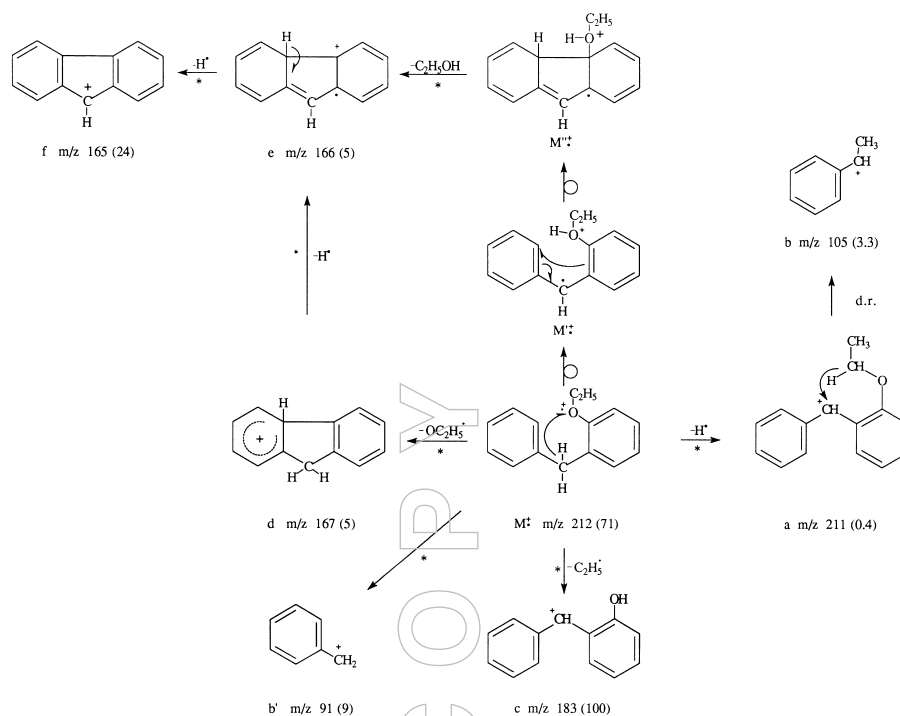


Figure 5. 70 eV electron impact mass spectrum of compound 5.

values previously found for both 1,1-bis(2,4-dimethoxyphenyl)-2-methylpropane¹ and 2-methoxydiphenylmethane.²

In order to increase the amount of the precursor ion **a**, by avoiding or decreasing other competitive fragmentation processes of the molecular ion, we examined the mass spectrum of the compound [1-(2-ethoxyphenyl)-1-(3,4-dimethoxyphenyl)-2-methylpropane] **7** (Figure 7). In fact the loss of the isopropyl group from the molecular ion (leading to the m/z 271 ion **a**) followed by the *HC, CC-dr* process constitutes the main fragmentation route for **7**. The resulting ion **b** (m/z 165) is responsible for the base peak and for 50% of the



Scheme 2.

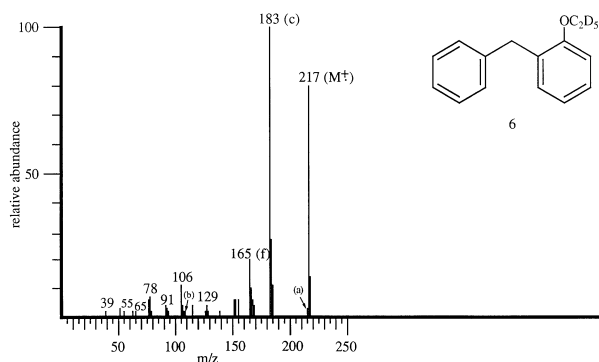


Figure 6. 70 eV electron impact mass spectrum of compound 6.

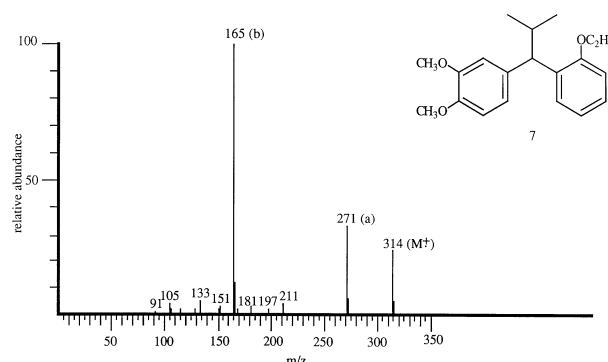


Figure 7. 70 eV electron impact mass spectrum of compound 7.

total ion current. The predominance of this process also agrees with the favoured hydrogen migration, as in this case the cation a' (Scheme 1) is stabilized by the inductive effect of the methyl group.

Isopropoxy derivatives

The m/z 119 ion **b**, expected for the HC,CC -*dr* process, is completely absent in the spectrum of the 2-isopropoxydiphenylmethane **8** (Figure 8). This is due to the occurrence of two major competitive reactions of the molecular ion, involving elimination of propene (m/z 184) and loss of isopropyl radical which affords the m/z 183 ion, in analogy to the corresponding 2-methoxy- or 2-ethoxy-diphenylmethane. Similar to the *ortho*-ethoxy derivative **7**, the easy formation of abundant precursor ion **a** (m/z 343) in the mass spectrum of compound **9** makes the peak at m/z 179 (ion **b** by the HC,CC -

dr process) one of the most abundant of the spectrum (Figure 9), even if a remarkable loss of propene is also occurring (m/z 344).

Methylthio derivative

The spectrum of the dimethylthio derivative **10** (Figure 10), in analogy to the corresponding 2,4,3',4'-dimethoxyderivative **3**,¹ is dominated by three peaks corresponding to the molecular ion, to the ion **a** (loss of isopropyl radical from M^+) and to the dimethoxybenzyl or dimethoxytropylium ion **b** at m/z 151, this latter arising again from the HC,CC -*dr* process.

Methylamino derivatives

The methylamino and dimethylamino derivatives **11** and **12** (Figures 11 and 12) give abundant ions **a** (m/z 316 and m/z 330, respectively) formed by loss of the isopropyl group.

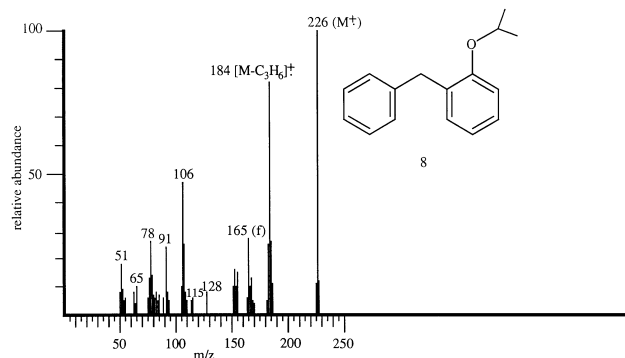


Figure 8. 70 eV electron impact mass spectrum of compound 8.

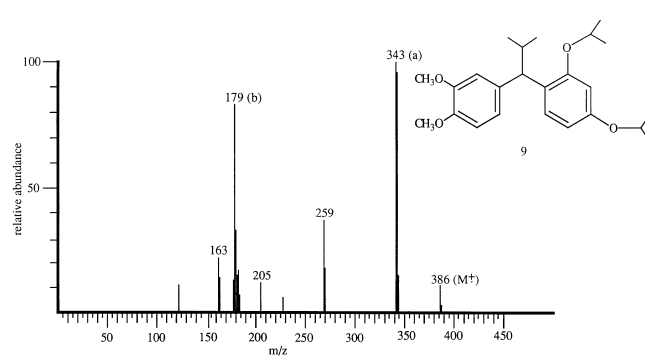


Figure 9. 70 eV electron impact mass spectrum of compound 9.

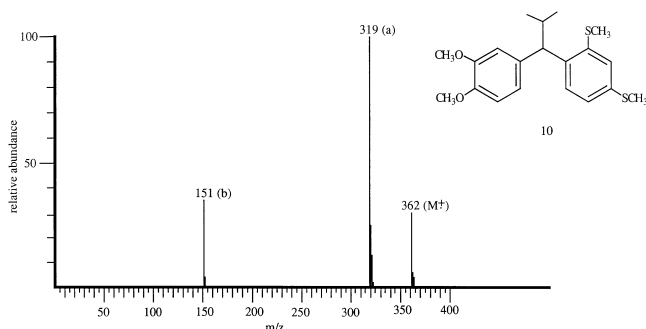


Figure 10. 70 eV electron impact mass spectrum of compound 10.

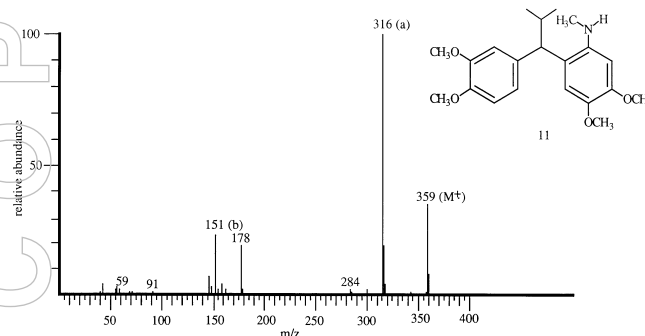


Figure 11. 70 eV electron impact mass spectrum of compound 11.

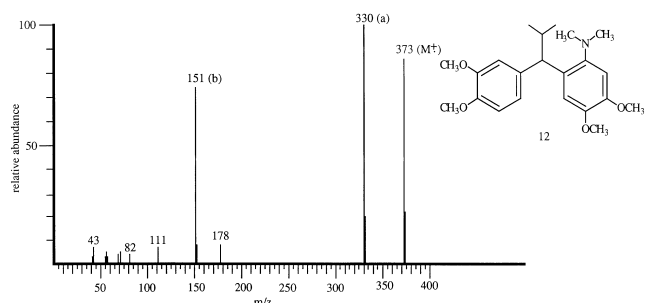


Figure 12. 70 eV electron impact mass spectrum of compound 12.

Subsequent fragmentation affords abundant ions **b** (m/z 151) arising from the *HC,CC-dr* process.

The higher relative abundance of the m/z 151 ion **b** for **12** with respect to **11** can be justified by the presence of two methyl groups linked to the nitrogen atom. Both statistical factors and stabilizing electronic effects of the second methyl group should enhance the *HC,CC-dr* reaction.

We investigated also 2-(*N*-methylamino)- and 2-(*N,N*-dimethylamino)-diphenylmethane **13** and **15**. Their mass spectra (Table 1) are closely related to those of both 2-methoxydiphenylmethane^{4,6} and 2-ethoxydiphenylmethane **5**. In particular the spectrum of the dimethyl derivative **15** was previously reported,⁷ but the presence of the $C_7H_7^+$ ion (m/z

91) was attributed exclusively to a simple benzylic cleavage reaction.

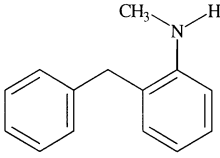
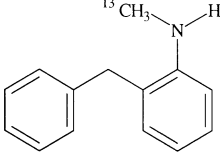
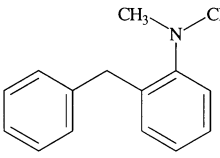
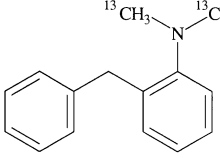
A comparison of the spectra of compounds **13** and **15** with those of the corresponding ^{13}C -labelled isotopomers **14** and **16** (Table 1) shows a partial shift (15% and 30%, respectively) of the peak at m/z 91 to m/z 92. This proves that the *HC,CC-dr* process also occurs for these simple compounds.

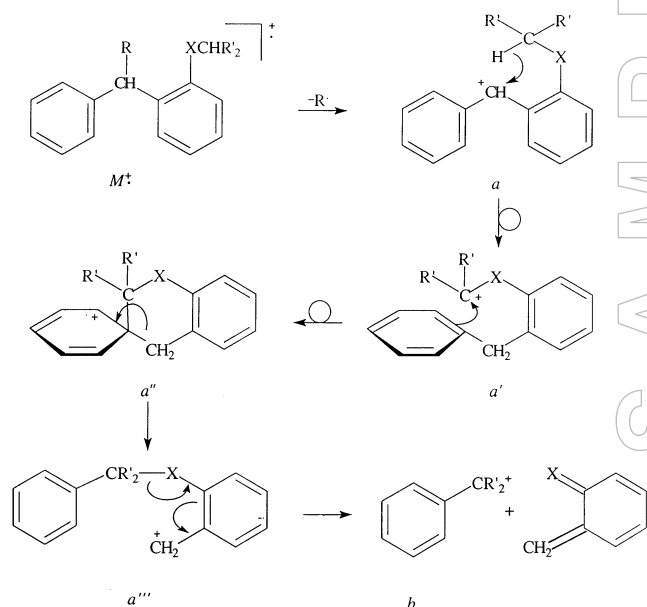
Conclusions

Our results show that the double rearrangement process (*HC,CC-dr*) occurs not only for variously substituted *ortho*-methoxy-1,1-diphenylalkanes, but it constitutes a generally occurring reaction for 1,1-diphenylalkanes bearing *ortho*-substituents -XR, which can transfer a hydride to the neighbouring benzylic carbenium ion through a six-centered transition state (Scheme 3).

It is worth noting that the *HC,CC-dr* process constitutes the main fragmentation route of the diphenylmethyl cation **a**. In fact, in the absence of competitive reactions of the molecular ion, which lower the relative abundance of ion **a**, the mass spectra of 2-XR substituted 1,1-diphenylalkanes (X = O, NH, NMe, S; R = Me, Et, *i*Pr) are essentially constituted by three peaks corresponding to the molecular ion $M^{+\bullet}$, to the diphenylmethyl cation **a** and to the rearrangement product ion **b**.

Table 1. Significant peaks in the 70 eV mass spectra of compounds 13–16.

<div style="display: flex; justify-content: space-around; align-items: center;"> <div style="text-align: center;">  <p>13</p> </div> <div style="text-align: center;">  <p>14</p> </div> </div> <div style="display: flex; justify-content: space-around; align-items: center;"> <div style="text-align: center;">  <p>15</p> </div> <div style="text-align: center;">  <p>16</p> </div> </div>								
Ions	M ⁺ m/z (%)	a m/z (%)	b m/z (%)	b' m/z (%)	c m/z (%)	d m/z (%)	e m/z (%)	f m/z (%)
Compound								
13	197 (100)	196 (23)	91 (19)	120 (11)	182 (81)	167 (12)	166 (6)*	165 (31)
14	198 (100)	197 (24)	91 (18) 92 (2.5)*	121 (12)	182 (82)	167 (13)	166 (8)*	165 (32)
15	211 (100)	210 (11)	91 (27)	134 (2)	196 (82)	167 (2)	166 (4)*	165 (17)
16	213 (100)	212 (12)	91 (16) 92 (9)*	136 (2)	197 (82)	167 (2)	166 (5)*	165 (15)

*Corrected for naturally occurring ¹³C isotopic contribution.

Scheme 3.

Experimental

Low resolution mass spectra were recorded on a VG-ZAB 2SE double focusing mass spectrometer operating under the

following conditions: ionization energy 70 eV; source temperature 200°C; sample temperature 30°C; accelerating voltage of 8 kV; trap current 100 µA; resolution 1500. Samples were introduced using the direct insertion probe.

The ¹H NMR spectra were recorded on a Bruker AC-250 F (250 MHz) spectrometer, using TMS as internal standard.

The IR spectra were performed using a Perkin-Elmer 257 spectrophotometer.

Melting points (uncorrected) were determined by a Büchi 510 apparatus.

Silica gel 60 (Merck, 0.05–0.2 mm) and silica gel plates (Merck F 254, 2 mm) were used for column chromatography and preparative TLC, respectively.

2-Ethoxydiphenylmethane (5) and **2-[ethoxy-²H₅]diphenylmethane (6)** were prepared from 2-hydroxydiphenylmethane (Aldrich) by reacting in alkaline solution with ethyl iodide (Janssen) and [ethyl-²H₅]iodide (Fluka), respectively. The degree of ²H incorporation for **6** was 99% by mass spectrometry.

1-(2-Ethoxyphenyl)-1-(3,4-dimethoxyphenyl)-2-methylpropane (7). By a Grignard reaction 2-ethoxybenzaldehyde (3.0 g) and isopropylmagnesium bromide (obtained from 3.5 g of magnesium and 14 g of isopropylbromide) in anhydrous Et₂O afforded 1-(2-ethoxyphenyl)-2-methylpropan-1-ol (2.3 g) as a yellow oil (yield 60%). A solution of this propanol (5 mmol) in AcOH (10 ml) was added drop-by-drop to a stirred solution of 1,2-dimethoxybenzene (25

mmol), AcOH (20 ml) and 70% H_2SO_4 (20 ml), while the temperature was maintained below 20°C . After standing at room temperature overnight, the mixture was poured on to crushed ice and the oil obtained was extracted with Et_2O . The ether solution was neutralized and brought to dryness. The residue was steam-distilled in order to remove any unreacted 1,2-dimethoxybenzene. The distillation residue was extracted with Et_2O , dried and evaporated. Crystallization of the crude product from ethanol affords compound **7** as white crystals (yield 96%), mp 62°C . ^1H NMR (CDCl_3), δ : 0.87 (3H, d, $J = 6.4$ Hz, CHCH_3), 0.88 (3H, d, $J = 6.4$ Hz, CHCH_3), 1.41 (3H, t, $J = 6.9$ Hz, OCH_2CH_3), 2.46 [1H, m, $\text{CH}(\text{CH}_3)_2$], 3.77 (3H, s, OCH_3), 3.83 (3H, s, OCH_3), 3.85–4.00 [3H, overlapped, $\text{CH}-\text{CH}(\text{CH}_3)_2$ and OCH_2CH_3], 6.70–6.85 (4H, m, 3-*H*, 5-*H*, 2'-*H* and 5'-*H*), 6.90 (1H, d, $J_{\text{ortho}} = 7.7$ Hz, 6'-*H*), 7.07 (1H, td, $J_{\text{ortho}} = 7.0$ Hz, $J_{\text{meta}} = 1.0$ Hz, 4-*H*), 7.34 (1H, dd, $J_{\text{ortho}} = 7.8$, $J_{\text{meta}} = 1.0$ Hz, 6-*H*).

2-Isopropoxydiphenylmethane (8) was prepared according to the literature.⁸

1-(2,4-Diisopropoxyphenyl)-1-(3,4-dimethoxyphenyl)-2-methylpropane (9) was synthesized as **7** using 1,3-diisopropoxybenzene⁹ and 1-(3,4-dimethoxyphenyl)-2-methyl-1-propanol.¹⁰ The mixture obtained was chromatographed on silica gel. Elution with cyclohexane-AcOEt (9 : 1) gave **9** as a yellow oil (yield 50%). ^1H NMR (CDCl_3), δ : 0.85 (3H, d, $J = 6.7$ Hz, CHCHCH_3), 0.88 (3H, d, $J = 6.7$ Hz, CHCHCH_3), 1.24 (3H, d, $J = 6.0$ Hz, OCHCH_3), 1.29 (3H, d, $J = 6.0$ Hz, OCHCH_3), 1.30 (3H, d, $J = 6.0$ Hz, OCHCH_3), 1.34 (3H, d, $J = 6.1$ Hz, OCHCH_3), 2.41 [1H, m, $\text{CHCH}(\text{CH}_3)_2$], 3.79 [1H, d, $J = 10.7$ Hz, $\text{CHCH}(\text{CH}_3)_2$], 3.80 (3H, s, OCH_3), 3.84 (3H, s, OCH_3), 4.46 [1H, hept, $J = 6.0$ Hz, $\text{OCH}(\text{CH}_3)_2$], 4.48 [1H, hept, $J = 6.0$ Hz, $\text{OCH}(\text{CH}_3)_2$], 6.36 (1H, d, $J_{\text{meta}} = 2.4$ Hz, 3-*H*), 6.42 (1H, dd, $J_{\text{ortho}} = 8.4$ Hz, $J_{\text{meta}} = 2.4$ Hz, 5-*H*), 6.72 (1H, d, $J_{\text{ortho}} = 8.5$ Hz, 5'-*H*), 6.81 (1H, d, $J_{\text{ortho}} = 8.5$ Hz, 6'-*H*), 6.82 (1H, s, 2'-*H*), 7.19 (1H, d, $J_{\text{ortho}} = 8.4$ Hz, 6-*H*).

1-(2,4-dithiomethylphenyl)-1-(3,4-dimethoxyphenyl)-2-methylpropane (10) was synthesized as **9** using 1,3-dithiomethylbenzene¹¹ instead of 1,3-diisopropoxybenzene. The obtained residue was chromatographed on silica gel. Elution with cyclohexane-Et₂O (9 : 1) gave **10** as a yellow oil (yield 80%). ^1H NMR (CDCl_3), δ : 0.87 (3H, d, $J = 6.5$ Hz, CHCH_3), 0.88 (3H, d, $J = 6.5$ Hz, CHCH_3), 2.40 (1H, m, $\text{CH}[\text{CH}_3]_2$), 2.42 (3H, s, SCH_3), 2.44 (3H, s, SCH_3), 3.80 (3H, s, OCH_3), 3.84 (3H, s, OCH_3), 3.92 (1H, d, $J = 10.9$ Hz, $\text{CHCH}(\text{CH}_3)_2$), 6.75 (1H, d, $J_{\text{ortho}} = 8.1$ Hz, 5'-*H*), 6.84 (1H, d, $J_{\text{meta}} = 1.9$ Hz, 2'-*H*), 6.87 (1H, dd, $J_{\text{ortho}} = 8.1$ Hz, $J_{\text{meta}} = 1.9$ Hz, 6'-*H*), 7.04 (1H, dd, $J_{\text{ortho}} = 7.1$ Hz, $J_{\text{meta}} = 1.8$ Hz, 5-*H*), 7.06 (1H, d, $J_{\text{meta}} = 1.8$ Hz, 3-*H*), 7.33 (1H, d, $J_{\text{ortho}} = 7.1$ Hz, 6-*H*).

1-(2-*N*-Methyl-4,5-dimethoxyphenyl)-1-(3,4-dimethoxyphenyl)-2-methylpropane (11) and **1-(2-*N,N*-dimethyl-4,5-dimethoxyphenyl)-1-(3,4-dimethoxyphenyl)-2-methylpropane (12)** A solution of 1,1-bis(2,4-dimethoxyphenyl)-2-methylpropane¹¹ (5 mmol) in Ac_2O (100 ml) was placed in a two-necked, round-bottomed flask fitted with a mechanical stirrer and a reflux condenser protected by a CaCl_2 tube. $\text{Cu}(\text{NO}_3)_2 \cdot 3\text{H}_2\text{O}$ was added to the stirred solution.

The mixture was heated at $40^\circ\text{--}60^\circ\text{C}$ for 1/2 h. After cooling at room temperature, the mixture was poured in water, neutralized and dried. After solvent evaporation, the residue was chromatographed by the flash method. Elution with petroleum ether (p.e. $40^\circ\text{--}60^\circ\text{C}$)- Et_2O (6 : 4) gave, in order, the following fractions: starting material (0.5 mmol), 1-(4,5-dimethoxy-2-nitrophenyl)-1-(3,4-dimethoxyphenyl)-2-methylpropane (yield 80%; pale yellow crystals from ethanol, mp 110°C) and 1,1-bis(4,5-dimethoxy-2-nitrophenyl)-2-methylpropane¹² (yield 10%).

To a solution of 1-(4,5-dimethoxy-2-nitrophenyl)-1-(3,4-dimethoxyphenyl)-2-methylpropane (1 g) in acetic acid (25 ml) was added 10% Pd-C (0.5 g). The mixture was hydrogenated in Parr apparatus for 96 h. Elimination of the catalyst and evaporation of the solvent at reduced pressure produced a mixture. The mixture was chromatographed on silica gel plates. Elution with cyclohexane-AcOEt (1 : 1) gave 1-(2-amino-4,5-dimethoxyphenyl)-1-(3,4-dimethoxyphenyl)-2-methylpropane as a brown oil (yield 43%).

Methyliodide (30 mmol) and K_2CO_3 (30 mmol) were added to a solution of 1-(2-amino-4,5-dimethoxyphenyl)-1-(3,4-dimethoxyphenyl)-2-methylpropane (6 mmol) in acetone (50 ml). The mixture was refluxed for 5 h. After cooling, the solid material was removed by filtration and the solution was diluted with water and then extracted with Et_2O . The ethereal extracts were treated with 10% aqueous sodium hydroxide solution, then neutralized, dried and evaporated. The residue obtained was chromatographed on silica gel employing cyclohexane-Et₂O (8 : 2) mixture as the eluant. The elution order of the separated compounds was: **12**, **11**.

Compound **11** was isolated as a brown oil (yield 30%). IR (CHCl_3): ν_{max} 3400 cm^{-1} (NH). ^1H NMR (CDCl_3), δ : 0.79 (3H, d, $J = 6.3$ Hz, CHCH_3), 0.95 (3H, d, $J = 6.2$ Hz, CHCH_3), 2.35 [1H, m, $\text{CH}(\text{CH}_3)_2$], 2.70 (3H, s, NCH_3), 3.30 [1H, d, $J = 10.1$ Hz, $\text{CHCH}(\text{CH}_3)_2$], 3.77 (6H, s, OCH_3), 3.80 (1H, broad, exchangeable with D_2O , NH), 3.82 (3H, s, OCH_3), 3.83 (3H, s, OCH_3), 6.26 (1H, s, 3-*H*), 6.67 (1H, s, 2'-*H*), 6.72 (2H, s, 5'-*H* and 6'-*H*), 6.98 (1H, s, 6-*H*).

Compound **12** was separated as a yellow oil (yield 70%). ^1H NMR (CDCl_3), δ : 0.75 (3H, d, $J = 6.4$ Hz, CHCH_3), 0.82 [3H, d, $J = 6.4$ Hz, CHCH_3], 2.27 [1H, m, $\text{CH}(\text{CH}_3)_2$], 2.50 (6H, s, $\text{N}(\text{CH}_3)_2$), 3.72 (3H, s, OCH_3), 3.74 (3H, s, OCH_3), 3.77 (3H, s, OCH_3), 3.78 (3H, s, OCH_3), 4.22 (1H, d, $J = 11.2$ Hz, $\text{CHCH}[\text{CH}_3]_2$), 6.66 (1H, s, 3-*H*), 6.68 (1H, d, $J_{\text{ortho}} = 8.2$ Hz, 5'-*H*), 6.82 (2H, s, $J_{\text{ortho}} = 8.2$ Hz, 6'-*H*), 6.83 (2H, s, 6-*H* and 2'-*H*).

***N*-Methyl-2-benzylaniline (13)**, ***N*-[^{13}C]methyl-2-benzylaniline (14)**, ***N,N*-dimethyl-2-benzylaniline (15)** and ***N,N*-di[^{13}C]methyl-2-benzylaniline (16)** were prepared from 2-benzylaniline (Aldrich) (6 mmol) by reacting in alkaline solution with methyliodide (Fluka) (18 mmol) and with [methyl- ^{13}C]iodide (Aldrich) (18 mmol), respectively. The mixtures obtained were chromatographed on silica gel plates, employing cyclohexane-Et₂O (8 : 2) mixture as the eluant. The elution order of the separated compounds was: **15** (or **16**) and **13** (or **14**), respectively. The yields are: 40% for **13** and **14**;

60% for **15** and **16**. The degree of ^{13}C incorporation for **14** and **16** was 99% by mass spectrometry.

Acknowledgements

The authors thank Professor S. Foti (Dipartimento di Scienze Chimiche, Università di Catania) for the use of a VG-ZAB 2SE mass spectrometer, Mr M. Cascino (Dipartimento di Chimica Organica, Università di Palermo) for technical assistance, the MURST and the CNR for financial support.

References

1. L. Ceraulo, M.C. Natoli, P. Agozzino, M. Ferrugia and L. Lamartina, *Org. Mass Spectrom.* **26**, 857 (1991).
2. L. Ceraulo, M.C. Natoli, P. Agozzino, M. Ferrugia and L. Lamartina, *Org. Mass Spectrom.* **27**, 1127 (1992).
3. P. Agozzino, L. Ceraulo, M. Ferrugia, L. Lamartina and M.C. Natoli. *Chim. & Ind. (Milan)*, **Suppl. 73**, (11), ms 28 (1991).
4. J.T. Bursey, M.M. Bursey and D.G. Kingston, *Chem. Rev.* **73**, 191 (1973) and references.
5. D. Kück. *Mass Spectrom. Rev.* **9**, 187 (1990) and references.
6. J.G. Liehr, A. Greth, J.H. Beynon and W.J. Richter, *Org. Mass Spectrom.* **16**, 139 (1981).
7. A.G. Giumanini and L. Plessi, *Chim. & Ind. (Milan)* **56**, 268 (1974).
8. B. Miller, M.P. McLaughlin and V.C. Marhevka, *J. Org. Chem.* **47**, 710 (1982).
9. H.H. Hodgson and H. Clay, *J. Chem. Soc.* 869 (1932).
10. P.C. Roberti, R.F. York and W.S. McGregor, *J. Am. Chem. Soc.* **72**, 5760 (1950).
11. E.V. Bell and G. McDonald Bennet, *J. Chem. Soc.* 3189 (1928).
12. M.C. Natoli, L. Ceraulo and L. Lamartina, *Gazz. Chim. Ital.* **113**, 145 (1989).

Received: 7 December 1994

Accepted: 28 January 1995

Dynamical parameters of ion ejection and ion formation in matrix-assisted laser desorption/ionization

Volker Bökelmann, Bernhard Spengler* and Raimund Kaufmann

Institute of Laser Medicine, University of Düsseldorf, PO Box 101007, 40001 Düsseldorf, Germany.

Molecular ejection and ionization processes in matrix-assisted laser desorption/ionization (MALDI) mass spectrometry are described. Angular resolved initial velocity distributions of matrix and analyte ions, obtained both from MALDI samples prepared normally and from peptide-doped single crystals of dihydroxybenzoic acid, are presented as ion density plots. The ejection distributions have been found to be bimodal, consisting of a slow, less forward peaked fraction and a fast fraction, which is directed more towards the surface normal. The ion plots show a significant quenching of matrix ions in areas of high peptide ion density. This effect is interpreted as the result of ion–molecule reactions in the gas phase leading to proton transfer from matrix ions to analyte molecules and is described by a simple kinetic overlap model. Additional effects of solid phase absorption, electronic excitation life times and fluorescence yield are discussed.

Introduction

Matrix-assisted laser desorption/ionization (MALDI) has soon after its invention has become one of the most versatile and widespread ionization methods in modern bioorganic mass spectrometry.^{1,2} Among its advantages are the almost unlimited mass range, the high sensitivity in the femtomolar range and the ability to analyze even poorly purified biological solutions or solids. Its recent extensions to structure analysis of biopolymers (“postsources decay MALDI”)^{3,4} using reflectron time-of-flight mass spectrometers is about to replace well-established methods such as collision-activated dissociation on four-sector tandem mass spectrometers.

The fundamental mechanisms of MALDI, however, are not understood sufficiently to perform, for example, instrumental optimization procedures other than by trial and error. Besides that, the MALDI ejection process of intact organic material by itself is of great scientific interest. It includes ion–molecule interactions in pulsed supersonic jet expansions, and is thus influenced by many factors such as gas phase acidities, excited states acidities and proton affinities of the interacting molecules and ions. The internal and external energetic parameters of colliding particles can be assumed to determine the resulting pathways of ionization and fragmentation.

Several recent investigations of velocity and angular distributions of MALDI ions have led to the idea that, after matrix excitation and sample desorption, analyte ions are

entrained in a supersonic jet of matrix ions and molecules,^{5–10} propagating with the speed of the carrier gas (the matrix molecules/ions) regardless of analyte mass. The “fine structure” of these pulsed jets as well as its dependence on sample structure and preparational parameters, however, have not been investigated yet. The purpose of this paper is to describe the ejection process in more detail and, by that, give some hints at the mechanisms of analyte ionization and fragmentation.

Several preparation techniques have been developed empirically for MALDI mass analysis so far. Almost all of them are based on mixing analyte and matrix solutions followed by an on-target drying procedure of a few μl , performed under various conditions. These “dried-droplet” methods have the advantage of easiness and usually sufficient ion yield. They are, however, far from being standardized, and success of analysis thus strongly depends on many parameters influencing sample crystallization. For investigation of the ejection and ionization process it is thus necessary to use a well-defined sample structure which, in its behavior, can then be translated to normally prepared samples. We therefore prepared single crystals of matrix material doped with a standard analyte. The use of single crystals in MALDI mass analysis has been described before.^{11–13} Investigations of ion ejection described in this paper were performed on these single crystals and, for comparison, on samples prepared using the dried-droplet method.

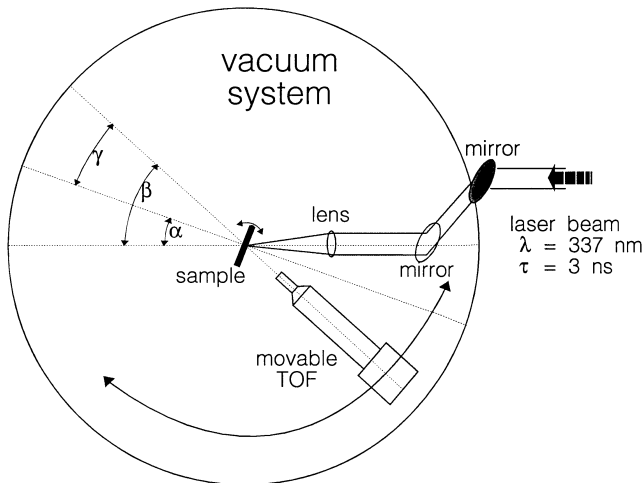


Figure 1. Scheme of the experimental set-up. α is the angle between laser beam axis and the surface normal ($0^\circ \leq \alpha \leq 90^\circ$), β is the angle between laser beam axis and TOF axis ($20^\circ \leq \beta \leq 180^\circ$), γ is the resulting angle between sample surface normal and TOF axis ($\gamma = \beta - \alpha$). The diameter of the vacuum system is 550 mm. The field-free distance between sample and TOF entrance is 25 mm.

Experimental

Instrumentation

Measurements were performed on a home-built instrument described in detail elsewhere.¹⁰ The apparatus has been designed for the investigation of initial kinetic parameters of laser desorbed ions and has the ability to measure ion abundances as depending on mass, velocity and angle.

In the center of a cylindrical vacuum chamber (Figure 1) a tiltable sample stage is positioned. A time-of-flight detector is revolvable around the central axis. All conductive surfaces inside the chamber are electrically grounded in order to avoid

any electric fields influencing the motion of ejected ions. The sample stage is mounted on a motor driven x-y manipulator which can be tilted by a stepper motor from perpendicular to parallel with respect to the irradiating laser beam. The nitrogen laser (LSI, Cambridge, MA, model VSL 337 ND, $\lambda = 337$ nm, $\tau = 3$ ns, not polarized) is guided on a fixed beam path and focused by a quartz lens (100 mm focal length) to a minimum diameter of ~ 80 μ m. The beam can be defocused by means of a beam expander outside the vacuum.

The detector is a pulsed Wiley-McLaren-type time-of-flight system¹⁴ (Figure 2), movable around the central axis under stepper motor control. The detection angle covers a section of 20° to 180° with respect to the laser beam axis.

The first grid of the detector system is permanently electrically grounded. At an adjustable time delay after the laser shot the second grid is pulsed from ground to negative potential (usually -250 V). The resistor layer of the tube forms a homogeneous field between the first and second grid. Ions located inside the tube at the pulsing event are accelerated to a kinetic energy correlated with their initial position in the tube. After final acceleration by the second stage ions of equal mass are time-focused on to the detector. The potential of the second stage has to be adjusted sensitively to fulfill the time focusing condition. For effective ion-to-electron conversion post acceleration to 3.1 kV is applied at the front of a pair of microchannel plates (active diameter 18 mm). The signal is recorded by a PC-based 40 MHz, 8 bit transient recorder (IMTEC GmbH, Backnang, Germany, model T 12840) and processed by the data system (Chips At Work GmbH, Bonn, Germany, "ULISSES 7.3"). Data transformation and plotting is performed by home-made software.

Mass resolving power $M/\Delta M$ attainable with this arrangement is about 150 for those ions located inside the extraction tube at the pulsing event. Each peak represents a certain range of initial velocities. By varying the time delay between the laser pulse and the extraction pulse we are able to calculate for every ion mass the entire initial velocity distribution with an

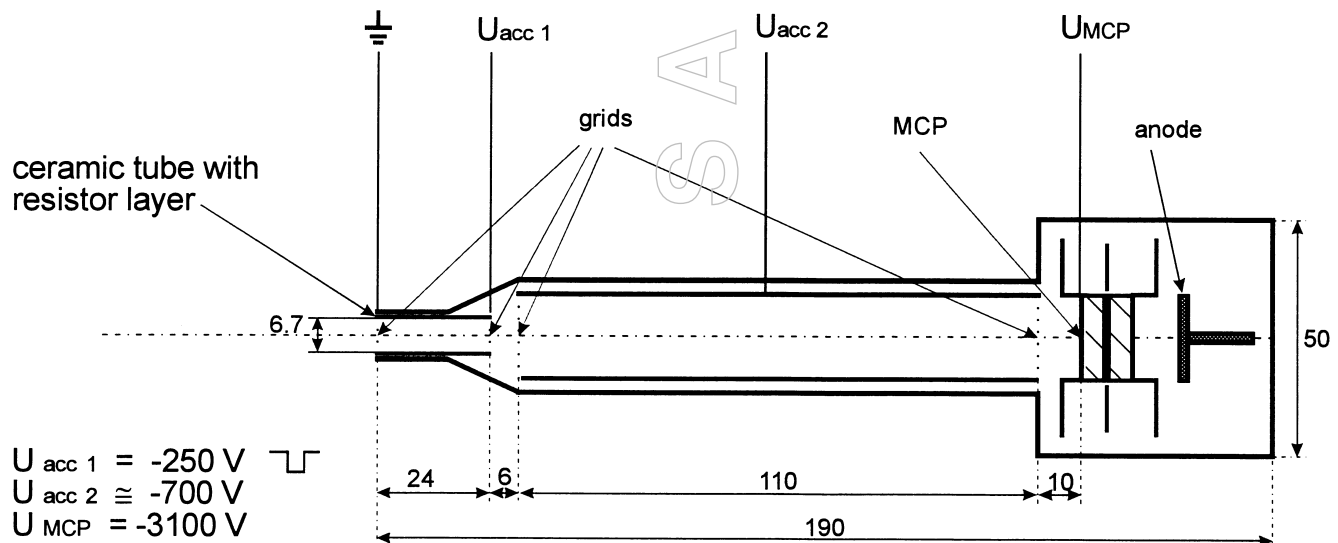


Figure 2. Schematic diagram of the movable time-of-flight system. See text for further explanations.

uncertainty depending on the probed velocity range and the length of the extraction tube. Numerical simulations indicated that an axial region of *c.* 10 mm is time-focused onto the detector, resulting in a velocity uncertainty of $\Delta v/v = 0.27$.

The angle of ion acceptance of the TOF system is 16° . To measure a complete angular distribution the detection angle is varied in steps of 8° . The delay between laser pulse and extraction pulse is increased in steps of $2.5 \mu\text{s}$ from $12.5 \mu\text{s}$ to $55 \mu\text{s}$ corresponding to a velocity range of 2960 m s^{-1} to 672 m s^{-1} . For each combination of angle and delay ten spectra are recorded.

Thus, a set of approximately 1000 spectra is recorded for the description of one complete angular resolved velocity distribution. The averaged signal areas of the masses of interest are processed from the stored data and listed in a matrix sheet. These data columns are not very easy to survey. For an instructive representation, we therefore prefer the illustration of an ion-density plot. The procedure for preparation of these ion-density plots is described below.

Each averaged mass spectrum acquired in our system contains ion abundances representative of a certain angular and velocity range. This two-dimensional range can be displayed as an element in an *x*–*y* diagram, where *x* and *y* are the cartesian coordinates relative to the sample surface (Figure 3). In order to transform velocity ranges into distance ranges an arbitrary “snapshot” time of $1 \mu\text{s}$ after the laser pulse has been chosen. For each of these elements a dot density is calculated from the intensities measured by the TOF system. In order to give a realistic image these dots are distributed randomly within each of the elements. As a result this transformation procedure leads to an *x*–*y* diagram which shows the ion cloud in the plane perpendicular to the sample surface, $1 \mu\text{s}$ after the laser shot. Each dot in this diagram represents a certain number of ions.

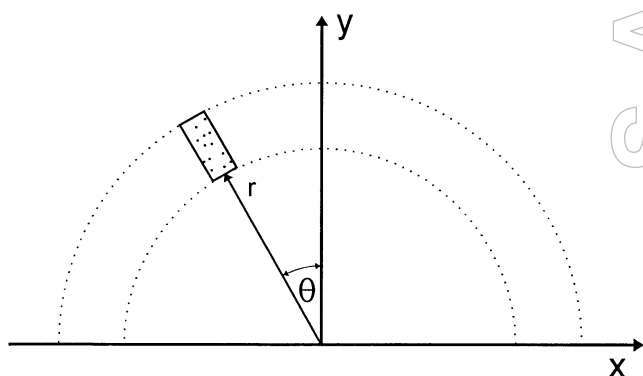


Figure 3. Transformation of measured ion abundances into ion-density plots. Ion abundances representative for a certain angular and velocity range are transformed into dot densities in a corresponding element in the *x*–*y* plane above the surface, choosing a snapshot time of $1 \mu\text{s}$ after the laser pulse.

Sample preparation

As an easy-to-use model system we chose the well-investigated peptide substance P (MW = 1347; Serva, Heidelberg, Germany) embedded in 2,5-dihydroxybenzoic acid (DHB, MW = 154; Neu-Ulm, Germany) as a matrix. For the dried-droplet preparation we mixed $10 \mu\text{l}$ of $10^{-2} \text{ mol l}^{-1}$ DHB/water and $10 \mu\text{l}$ of substance P dissolved in water. Peptide concentrations in the range of 1.3×10^{-4} to $1 \times 10^{-6} \text{ mol l}^{-1}$ have been prepared resulting in molar ratios DHB : substance P in the range of 80 : 1 to 10,000 : 1. Fast air drying with a hair-dryer of this droplet on an aluminum substrate gave samples with a diameter of *c.* 5 mm, consisting of a nearly homogeneous area inside a small rim of microcrystalline material. This inner region of the sample yielded better spectra of substance P ions than the rim. Approximately 15–20 laser shots could be positioned onto one spot at constant signal intensity.

Single crystals of neat DHB were prepared as described in Reference 12. Peptide-doped single crystals of DHB were prepared using the following procedure. A suspension of 50 mg DHB and 5 mg substance P in 1 ml water was carefully heated and the container was stirred in a water reservoir of 1 l until the DHB was dissolved at *c.* 55°C . The liquor was stored over night inside the reservoir in a thermally isolated box to achieve a low cooling rate. After cooling down to room temperature single crystals of doped DHB with dimensions up to $\sim 3 \times 2 \times 1 \text{ mm}^3$ had grown from the surface of the liquor and on the ground of the container. Crystals were washed with cold distilled water and mounted on the sample stage.

For dried droplet preparations a new spot on the nearly homogeneous inner region of the sample was used for any new combination of angle and delay to avoid complete ablation of material. For single crystals, however, all laser shots of one complete distribution were set to a single spot.

The applied irradiance was fine-tuned by monitoring the time-of-flight distribution of ejected ions prior to an angle delay scan. The TOF distribution of the total ion current is very sensitive to the irradiance¹⁰ and a good indicator for a certain laser power. For all measurements, a laser irradiance just slightly above the threshold of ion detection was chosen. The constance of laser irradiance was checked by scanning the angle in an alternating way during measurements. It was found that absolute ion intensities gave sufficiently reliable results. Thus no reference ion signal was needed.

Results

Dried-droplet samples

Mass spectra of samples prepared by the dried-droplet technique are characterized by mass peaks of sodium ($m = 23 \text{ u}$), potassium ($m = 39 \text{ u}$), the dehydrated DHB monomer ion ($m = 137 \text{ u}$), the protonated DHB ion ($m = 155 \text{ u}$), alkali-attached DHB ion peaks ($m = 177 \text{ u}$, 193 u), the dimer ion peak of dehydrated DHB ($m = 273 \text{ u}$), a DHB aluminum complex ($m = 333 \text{ u}$) (especially for hot-air dried samples),

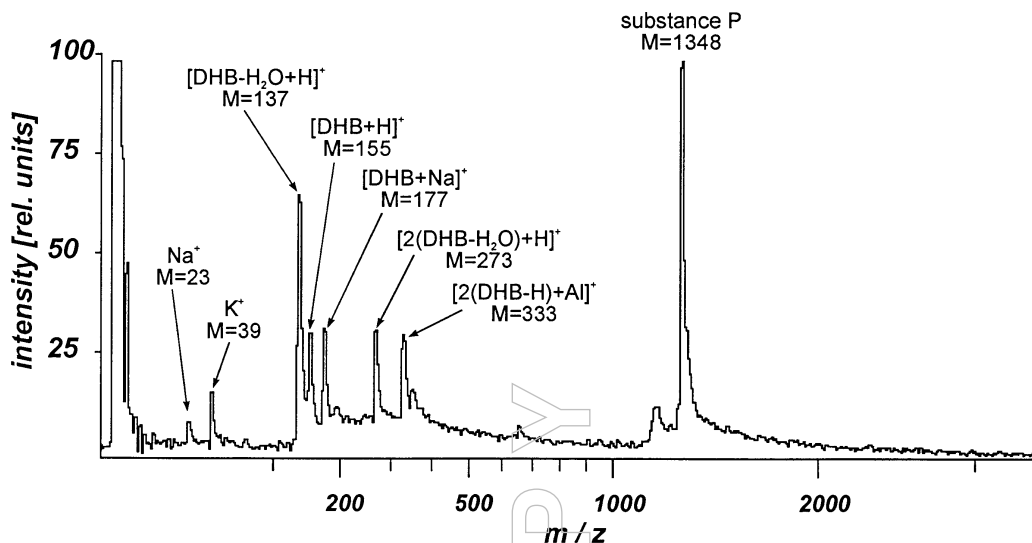


Figure 4. Summed spectrum (95 shots) of a dried-droplet sample of DHB/substance P, molar ratio 400 : 1. Single shot spectra were recorded under variation of the delay between laser shot and extraction pulse in order to cover the complete velocity range of different ions.

protonated substance P ($m = 1348$ u) and sodium-attached substance P ($m = 1370$ u). A typical spectrum is shown in Figure 4. It was acquired by summation of 95 single shot spectra. For this demonstration spectrum the delay time was varied during summation in the range of $15\ \mu\text{s}$ and $50\ \mu\text{s}$ in order to time-focus ions of the complete velocity range. The strong signal at the left edge of the spectrum is due to a perturbation by the extraction pulse. The molar ratio of DHB to substance P was 400 : 1, the incident angle of the laser beam was -20° and the detection angle 0° with respect to the surface normal. Mass resolution is slightly lower in this summed spectrum compared to single shot spectra due to non-adapted time focusing during summation at various time delays. Especially the peaks of protonated and sodium attached substance P are not resolved here which is possible for single shot spectra as used for distribution analyses. The small broad signal in front of the substance P peak has been found to originate from small secondary ions produced at the fourth grid just in front of the MCP detector.

No fragment ions of substance P are observed under these conditions. This is in good agreement with observations of decay behavior of MALDI ions under varied acceleration conditions¹⁵ (rate of post-source decay of analyte ions decreases with decreasing initial acceleration field strength).

Figure 5 shows an ion density plot obtained from a dried-droplet sample of neat DHB matrix. For this “snapshot” the ion signal of dehydrated DHB at $m = 137$ u was processed. The incident angle of the laser beam was -20° , the detection angle ranged from 0° (geometrical termination by the focusing lens) to 60° . For a better optical image, the measured distribution of the accessible angular sector (0° – 60°) is mirrored to negative angles at the crystal surface normal. Note that sharp edges between areas are due to the stepwise calculation of densities for each angle/delay element, not due to real inten-

sity jumps. The intensity cut-off at the low velocity end, however, is the result of a real intensity drop.

Figure 6 shows ion density plots obtained from a dried-droplet sample of substance P in DHB matrix. The molar ratio of DHB to substance P was 125 : 1. Ion signals of alkali ions (top), dehydrated DHB (middle) and substance P (bottom) were evaluated from the obtained mass spectra.

For both samples a multimodal ejection behavior has been observed in the density plots of DHB [Figures 5 and 6 (middle)]. The two main modes are a slow, spatially broad fraction with an average velocity below $1\ \text{mm}\ \mu\text{s}^{-1}$ ($= 1000\ \text{m}\ \text{s}^{-1}$) and a fast, forward directed distribution perpendicular to the sample surface with an average velocity of about $2\ \text{mm}\ \mu\text{s}^{-1}$. While alkali ions appear to be homogeneously distributed over

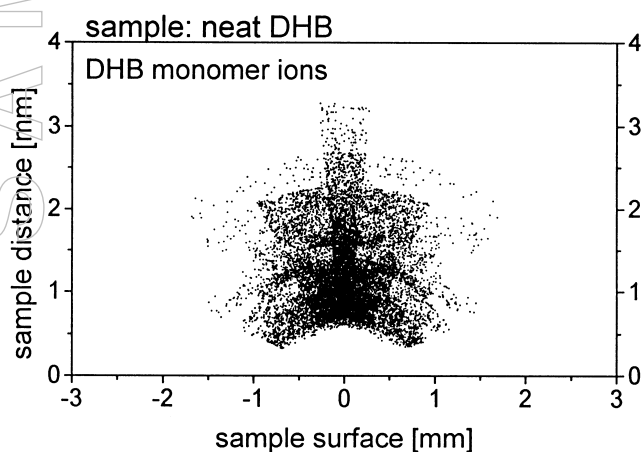


Figure 5. Ion-density plot, representing the spatial ion distribution $1\ \mu\text{s}$ after the laser shot. Displayed is the distribution of dehydrated DHB monomer ions ($m = 137$ u) obtained from a neat matrix sample (dried-droplet method). Angle of incidence of the laser beam was -20° with respect to the surface normal.

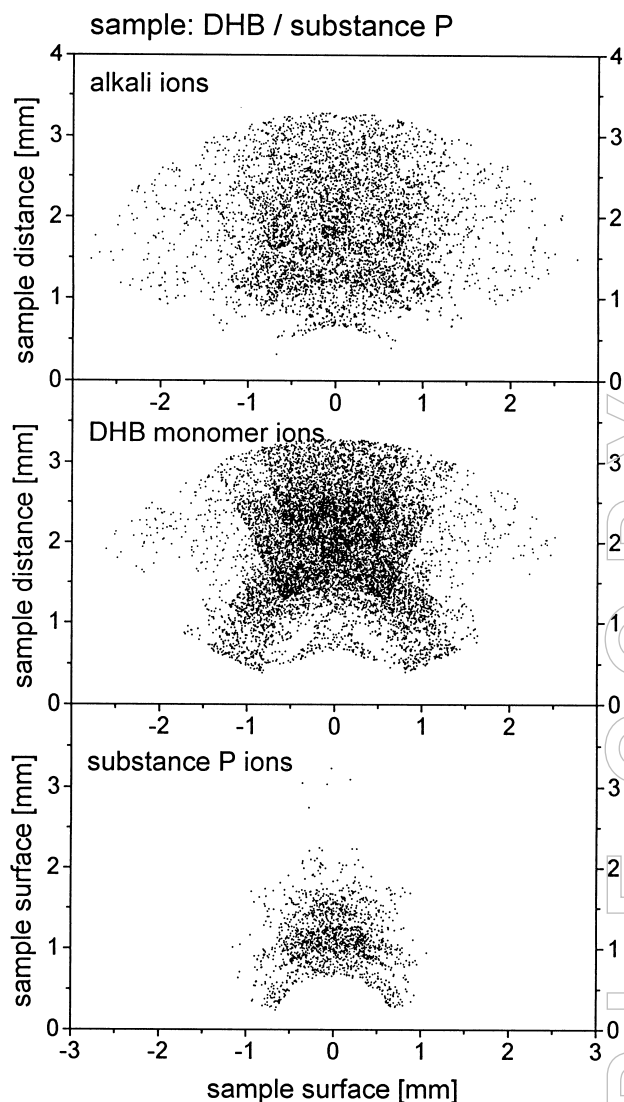


Figure 6. Ion-density plot, representing the spatial ion distribution 1 μ s after the laser shot. Displayed are the distribution of dehydrated DHB monomer ions (mid), substance P (bottom) and alkali ions (top) obtained from a substance P-doped DHB sample (dried-droplet method, molar ratio 125 : 1). Angle of incidence of the laser beam was -20° with respect to the surface normal.

the measured area, substance P ions seem to be entrained inside the DHB distribution of the slower mode. The most important observation is the suppression of matrix ions in sections where substance P ions occur in high concentrations. This effect is observed only when substance P is present in the sample but not for neat DHB preparations (Figure 5). The extent of this extinction phenomenon strongly depends on the molar ratio of DHB and substance P in the sample (Figure 7). While the extinction effect is obvious for preparations, where matrix is rather rare, it increasingly vanishes for higher ratios of matrix to analyte.

Measurement of single crystals

The appearance (color, shape) of substance P-doped DHB crystals is similar to that of neat DHB crystals. One notable difference, however, is that doped crystals are flatter than neat DHB crystals, giving an indication of a considerable perturbation of the crystal lattice. The plane of easiest cleavage is the plane parallel to the largest surface for both crystal species. According to crystal structure data DHB is crystallizing in space group $P2_1/a$ ¹⁶ and is characterized by formation of plane sheets of hydrogen-bonded molecules stacked in the *b* direction. It is assumed that hydrophobic molecules such as peptides or proteins are incorporated into the growing crystals between the sheets rather than in the other directions which are characterized by stronger hydrophilic interactions. The same behavior has been assumed for crystallization of the matrix sinapic acid.^{11,13}

Two main characteristics of mass spectra from substance P-doped single crystals of DHB have been observed in our free-expansion (no initial acceleration) mass spectrometer:

- 1) There is only a very weak substance P ion signal from the largest surface of the crystal in this non-accelerated expansion process. In contrast to that, both small surfaces provide stable and highly intense signals of substance P for several hundreds of shots under soft desorption conditions. In common laser mass spectrometers with initial ion acceleration the largest surface produced peptide ions as well.
- 2) Free-expansion experiments with a frequency quadrupled Nd:YAG laser at 266 nm wavelength have been completely unsuccessful. None of the surfaces yielding high analyte signals under N_2 laser irradiation gave any detectable substance P ion signal at 266 nm irradiation. Again, acceptable ion signals have been obtained at 266 nm in mass spectrometers with initial ion acceleration. Likewise, "dried-droplet" samples have been shown to produce substance P ions at 266 nm¹⁰ with low intensity.

A summed spectrum of a substance P-doped DHB single crystal is shown in Figure 8. A total of 500 shots was recorded at different delays. The extraordinary stability and strength of the mass signals allowed us to acquire and sum any number of spectra from a single spot on the long thin edge of the crystal (Figure 9).

By the 500 laser shots a crater of about 100 μ m in diameter and 10 μ m in depth was formed in the surface. The direction of the crater follows the direction of the incident laser beam (-30° to the surface normal). The crater contains small conical structures after moderate laser irradiation. These "Trulli" have been observed before,¹⁷ but their formation is not sufficiently explained yet. Consequently, the sample morphology of the crystal changes after a few laser shots, whereas the crystal structure should not be affected essentially. Measurements obtained exclusively from a defined intact crystal surface would require large doped crystals where the laser spot can be moved for every shot to a fresh site. Such large crystals have not been grown yet.

[DHB] :
[substance P] =

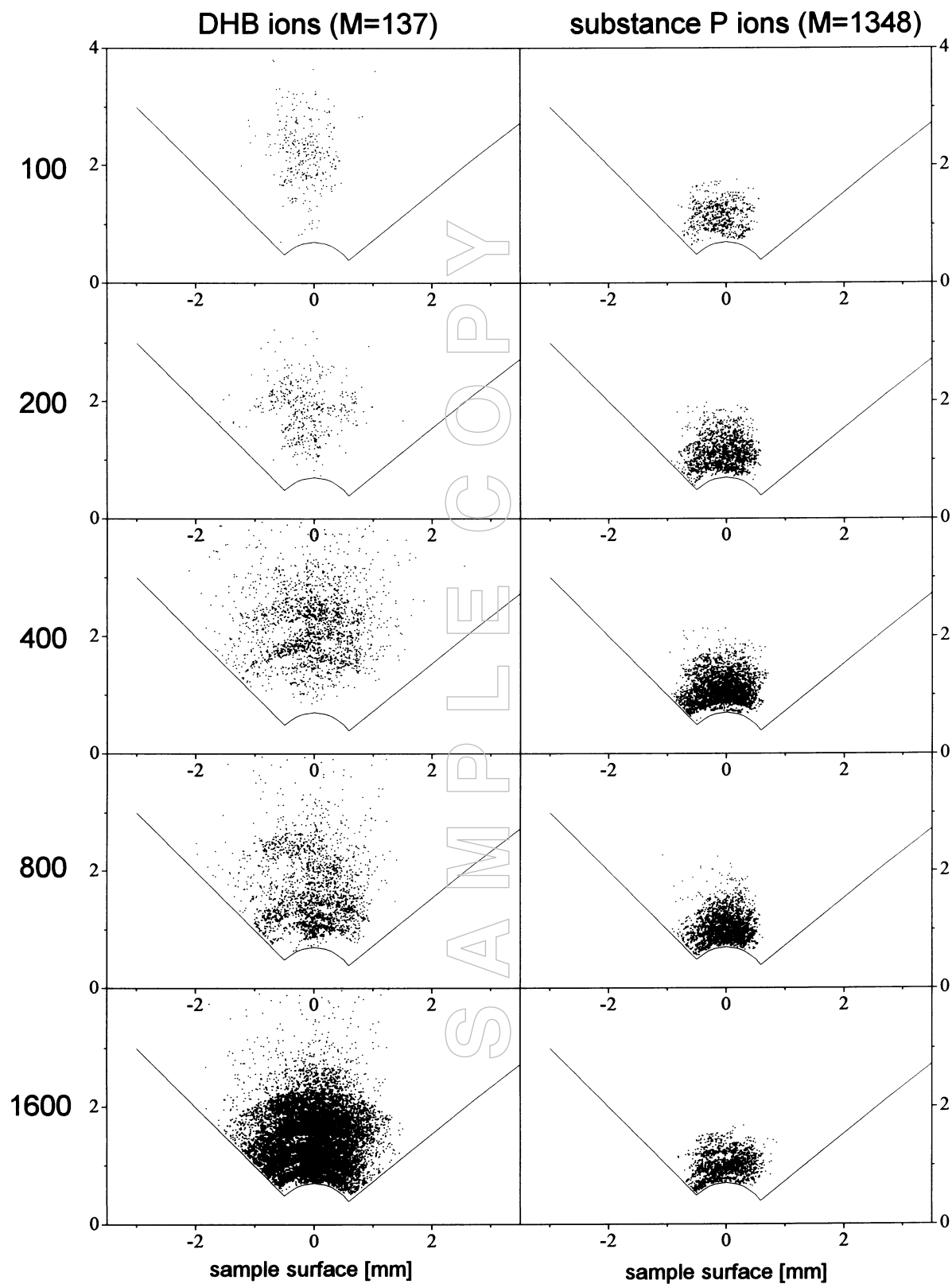


Figure 7. Ion-density plots of matrix and analyte ions obtained at various molar ratios of matrix to analyte (dried-droplet method). Angle of incidence of the laser beam was -60° with respect to the surface normal. The straight line marks the measured range.

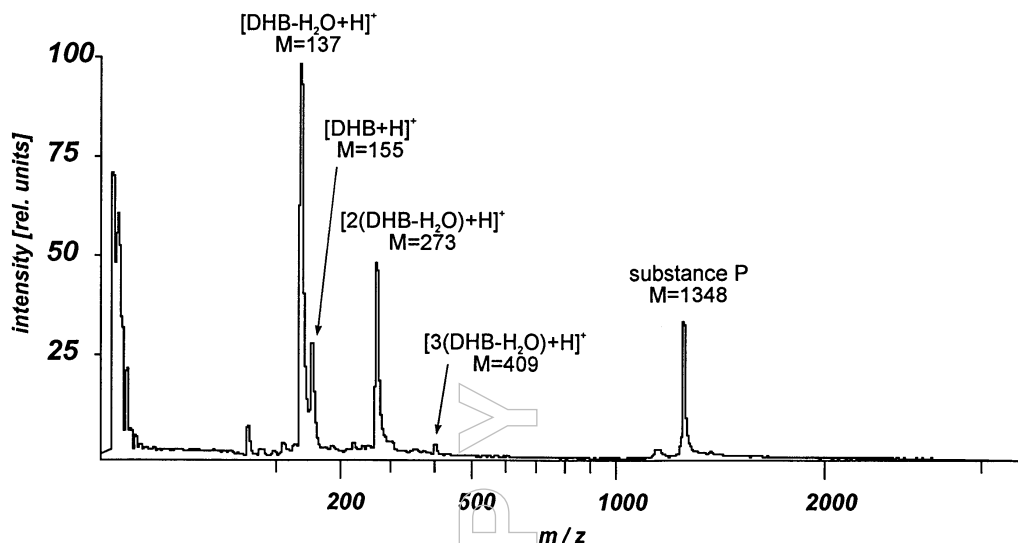


Figure 8. Summed spectrum (500 shots), obtained from a substance P-doped single crystal of DHB.

In contrast to dried-droplet samples mass spectra recorded from single crystals were characterized by a complete absence of any alkali ions and alkali attached molecule ions although the solution for growing the crystals was not free of alkali impurities. Crystallization is known to be a purification process so that alkali ions are phase separated from the growing crystal. This is much in contrast to macromolecular analyte molecules, which apparently are incorporated into the crystal lattice.^{11–13}

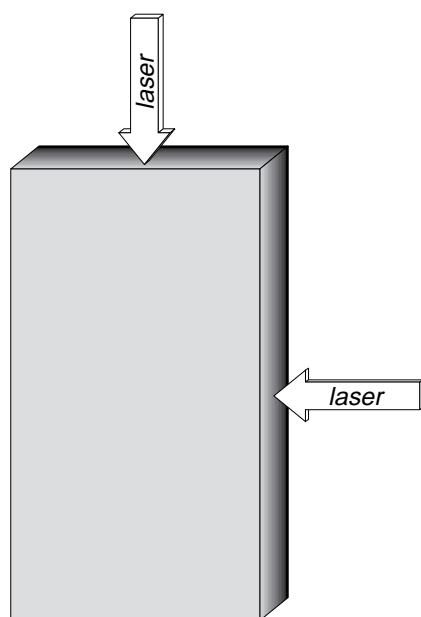


Figure 9. Typical shape of substance P-doped single crystals of DHB matrix. The surfaces yielding high analyte ion intensities under laser irradiation are signed.

The expansion pattern of the ion cloud desorbed from single crystals (Figure 10) is very similar to that of samples prepared by the dried-droplet procedure. As in Figure 6 DHB ions are largely depleted in the high-density region of substance P. This measurement was performed with an incident angle of -50° with respect to the surface normal. All laser shots have been set to one spot on the long narrow side of the crystal (Figure 9). The angular distribution shows an explicit preference of the high velocity part directed towards the incident laser beam. (Note that the cut-off at an angle of -30° on the side of the laser beam is due to the geometrical restriction and does not represent a true cut-off of ion emission.) Figure 11 (top) shows the evaluation of the distribution of radial velocities (averaged over all angles) of DHB monomer ions ($m = 137$ u, 155 u), DHB dimer ions ($m = 273$ u) and substance P ions ($m = 1348$ u) originating from the above measurement of the substance P-doped DHB crystal. For comparison, the DHB monomer velocity distribution measured from a pure DHB single crystal is added in Figure 11 (bottom). The latter distribution is bimodal with maxima at 900 m s^{-1} and 1500 m s^{-1} , respectively. The two ejection modes can be correlated with the two monomodal velocity distributions of DHB ions on the one hand and substance P ions on the other hand [see Figure 11 (top)]. While the velocity distribution of substance P corresponds to the slower mode observed for pure DHB, this mode is suppressed in the velocity distribution of DHB ions ejected from the peptide doped crystal, such that only the fast mode remains.

Discussion

Formation of protonated and deprotonated *matrix* ions is assumed to be a multi-step process which involves (1) two-photon excitation of matrix molecules (either direct, via two steps or via energy pooling), (2) radical ion formation by

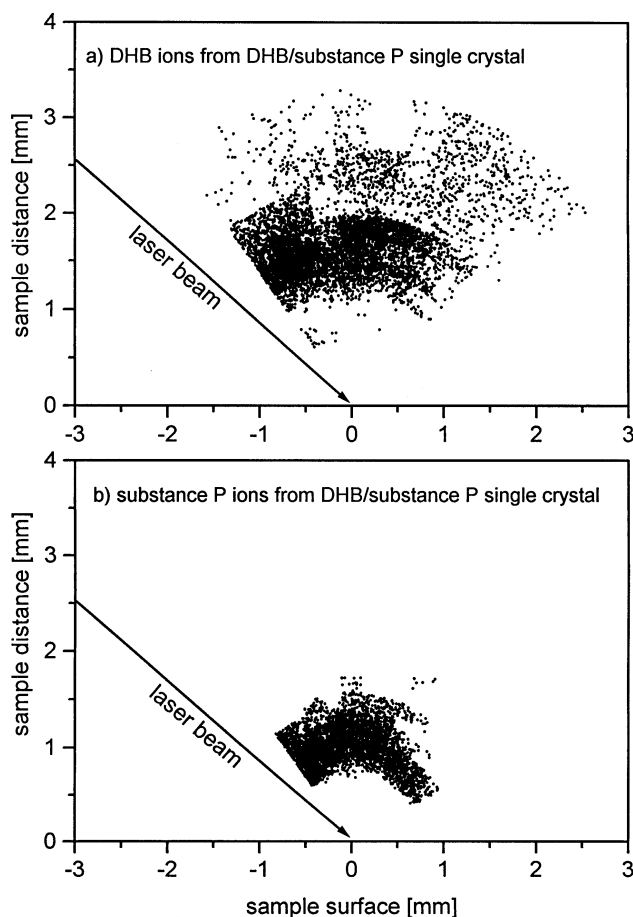


Figure 10. Ion density plots obtained from the long narrow side of a substance P-doped single crystal of DHB. The upper plot shows the distribution of matrix ions while the lower one shows the distribution of substance P ions. The angle of incidence was -50° . Consequently the measurable angular range is limited to -30° to 90° relative to the surface normal. The sharp radial cut-off signs the measured velocity range.

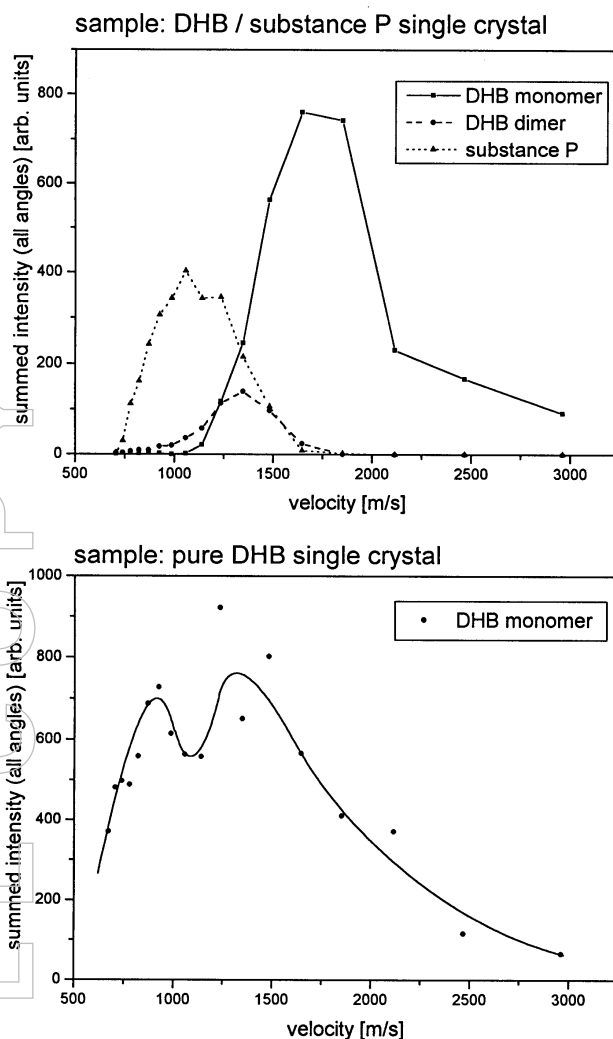


Figure 11. Velocity distribution (sum over all angles) of matrix and peptide ions from a substance P-doped DHB single crystal (top) and from a neat DHB single crystal (bottom). The distribution of substance P is related to the slow mode of the DHB ions from the pure DHB crystal.

electron abstraction/attachment and finally (3) multi-pathway proton transfer reactions.^{18,19} Formation of *analyte* ions, on the other hand, has been investigated much less. The main questions of interest in this field are:

- (1) Is analyte ion formation part of the matrix ion formation process as described above or is it a process taking place on a longer time scale (after formation of matrix ions) comparable to mechanisms known from chemical ionization mass spectrometry?
- (2) Where does analyte ion formation take place? Is it a gas-phase process or a condensed-phase process?

Prior to a discussion of the obtained data on ion kinetics we will try to outline a simple working model for the mechanism of analyte ionization in MALDI.

Kinetic overlap model

The most obvious observation from the obtained ion density plots is the lack of slow matrix ions in areas of high abundance of substance P ions. From this observation we deduce the following working model which then shall be

proved by discussion of the various experimental results. We suggest that ionization of analyte molecules takes place in the gas phase, driven only by a spatial overlap between a proton donor (in the positive-ion mode) and the molecule, which lasts long enough to reach a sufficient reaction probability. We further suggest that there is no need for energetic collisions but for a spatial overlap of isovelocic particles, and that there is no need to assume preformed or directly desorbed analyte ions. Ionization of analyte molecules is seen here as a secondary process taking place after formation of matrix ions.

Matrix ion quenching

There is no reasonable way to explain the observed lack of matrix ions other than by assuming a proton transfer from former matrix ions or electronically excited matrix molecules to neutral analyte molecules. A simple pressure-driven dislocation of matrix ions by analyte ions is rather unlikely, keeping

in mind that the total particle density is not dominated by the observed ions, but by neutral molecules which are present in much higher concentrations, and keeping in mind that coulomb repulsion does not play a major role since positive and negative charges should be balanced in particle clouds not subjected to an external electric field. There are, on the other hand, good reasons to believe that at least a considerable part of analyte ionisation takes place in the gas phase simply by transfer of protons from a proton donor (higher acidity) to an analyte molecule (the proton acceptor with lower acidity). This model is further supported by the fact that molecules like the common matrices tend to increase their acidity in the gas phase when they are electronically excited.^{20–23} Russell *et al.* have shown²⁴ that it is not an essential prerequisite for a matrix substance to contain a carboxylic group, and that all investigated matrix substances have a higher acidity in the excited state compared to the ground state. They concluded that MALDI involves proton transfer reactions between excited states of matrix molecules and ground states of the analyte.

An additional support of the above model is given by a very recent investigation of gas-phase proton affinities of common matrix substances by Jorgensen and coworkers.²⁵ They determined a decrease of proton affinities in the order nicotinic acid → sinapinic acid → ferulic acid → DHB → α -cyano-4-hydroxycinnamic acid. Thus for a given analyte molecule to become protonated α -cyano-4-hydroxycinnamic acid as donor has the highest release of excess energy upon protonation. A considerable part of this excess energy will contribute to an increase of internal energy of the protonated analyte and by that to an increase of post-source decay (PSD).¹⁵ An increase of this PSD fragmentation, if compared to DHB matrix, has indeed been observed for α -cyano-4-hydroxycinnamic acid in our instruments. This supports the assumption of a *gas-phase* ionization process as modelled above, since analyte ionization in the *condensed phase*, or even analyte ionization in parallel to the *dense-phase* matrix ion formation, would most probably, as a multi-particle process, not lead to a detectable change in internal energy uptake. A distinct increase of internal energy can only be expected from individual ion–molecule reactions taking place later in a low-density phase.

Effects of molar ratios

In MALDI mass analysis changing the molar ratio of matrix to analyte is known to affect the ionization probability. This is also observed under free-expansion (non-acceleration) conditions. Figure 7 shows ion density plots for various matrix/analyte ratios (substance P in DHB). As known from common MALDI instruments analyte ionization yield increases with increasing matrix concentration up to a maximum, due to an increase in ionization probability, and then decreases again, due to a decrease of analyte concentration in the matrix/analyte volume.

The quenching effect, as described above, is only observed when matrix ions are rare up to the ratio where the maximum analyte ion intensity is observed. This observation again supports the assumption of gas-phase acid/base reactions. Matrix

ions appear to become used up for protonation until the process is saturated and all accessible analyte molecules are ionized.

A similar effect of matrix suppression has been observed in mass spectrometers with accelerating ion sources,²⁶ for certain experimental conditions of laser irradiance and molar ratio between matrix and analyte.

Laser irradiance

The useful (with respect to analyte ion formation) range of laser irradiances has been found to be much narrower in the free-expansion system compared to common (accelerating) MALDI instruments. This observation is in good agreement with the kinetic overlap model. It has been found that the mean velocity of matrix ions strongly increases with laser irradiance.¹⁰ A change in initial velocity should strongly influence overlapping and, thus, ionization efficiency under free-expansion conditions. In accelerating instruments, on the other hand, there is another effect which might compensate for an increase of initial velocity, that is the dependence of acceleration-field shielding on the ion density in the cloud. It can be calculated that about 3×10^5 charges spread over an area of 100 μm in diameter are able completely to shield an electric field of 1000 V mm^{-1} . Only after a certain time shielding ions are extracted from the source region and the acceleration field is able to penetrate into deeper regions. An increase of laser irradiance will cause an increase in fast-mode ion density and by that to a prolonged field shielding. The result is a (compared to immediate acceleration) better kinetic overlap of slow-mode matrix ions and analyte molecules. In combination these two contrary effects (shielded acceleration field and increased proton-donor velocity) might cause a constant ionization yield over a rather broad irradiance range in accelerating instruments.

Detector saturation at high irradiances (and consequently high matrix ion yields) might as well contribute to the effect of vanishing peptide ion signals at higher mass. The detector problem probably plays a more important role in our small-size channelplate system (with less channels) compared to regular-size instruments.

Absorption and emission spectra of DHB

As an additional source of information on the fundamental energy uptake and transfer process it is helpful to have a brief look on to the spectral absorption and fluorescence of crystallized DHB, providing data on the excitation process and on typical life times of excited states.²⁷

Solid-state absorption was measured on a home-built micro spectral photometer. Fluorescence measurements were performed by modification of a “VISION 2000” MALDI mass spectrometer (Finnigan MAT, Bremen, Germany).

Absorption and fluorescence spectra are shown in Figure 12. An absorption spectrum of an aqueous solution of DHB is included for comparison.²⁸ Both wavelengths of interest, 337 nm and 266 nm, excite the same absorption band. The sym-

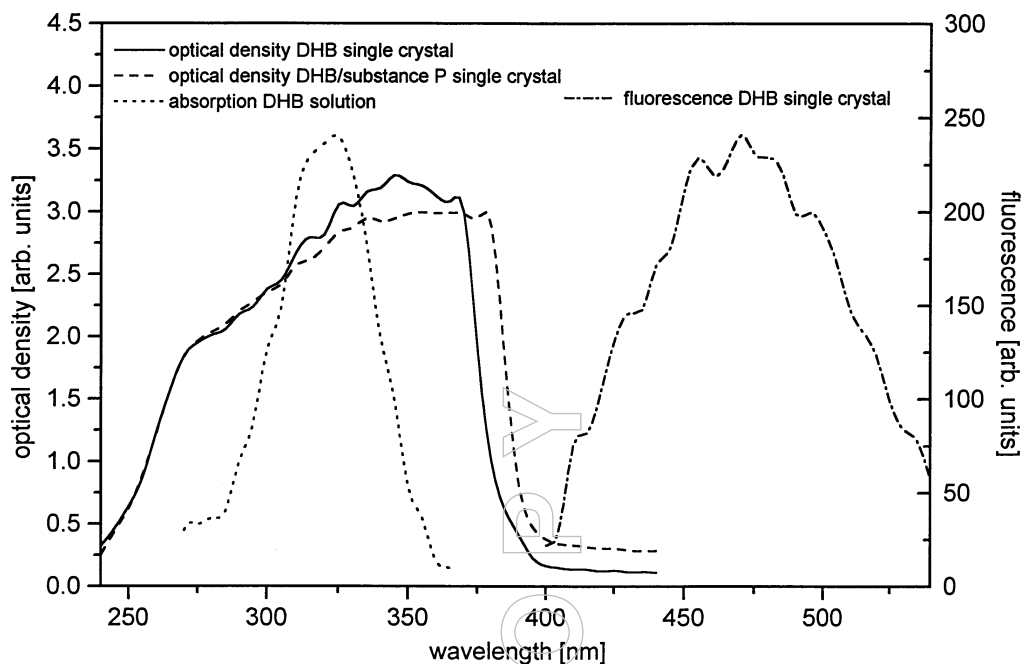


Figure 12. Spectral optical density of DHB solution and single crystal (doped and undoped) and spectral fluorescence of DHB single crystal. Fluorescence has been found to be identical within experimental errors for both, 337 nm and 266 nm excitation.

metrical splitting into two overlapping absorption bands (“Davydov splitting”)²⁹ in the crystal compared to absorption of the solution indicates that at least two absorbers (differently oriented) are present in the unit cell (the two molecules coupled via their carboxylic groups). Doped crystals show nearly the same spectral absorption except for a small shift of the long wavelength tail to the red. The fluorescence begins at the long wavelength tail of the absorption spectrum, as expected, leading to the (obvious) assumption that we are exciting higher vibrational S_1 states with both lasers. The vibrational energy dissipates into the crystal lattice and leads to relaxation of the molecules to the vibrational ground state of S_1 in the ps time scale (Figure 13). Within the fluorescence life time of this state, molecules emit a photon and relax to vibrationally excited S_0 states. Alternatively, excited molecules should be able to transfer their excitation energy to other molecules upon collision, undergo acid–base reactions with other molecules (driven by enhancement of acidity in the excited state^{20–23}) or transform their excitation energy into translational and vibrational energy. It has been found very recently, that less than 20% of the excitation energy of irradiated DHB is emitted by fluorescence at room temperature in the solid state.³⁰ A considerable amount of the excitation energy should thus be available for these alternative processes in the gas phase.

Fluorescence life times have been found to be in the range below 30 ns for DHB in our system and in Reference 30. Thus, for a mean velocity of matrix molecules or ions of 1000 m s⁻¹ ejected material is still considerably excited in an area of 30 μ m above the surface.

It can thus be assumed that excitation of matrix ions or molecules play a considerable role not just in the process of

self-chemical ionisation of the matrix but also in the process of analyte ionization.

Laser wavelength

The amount of vibrational energy released into kinetic energy within picoseconds after excitation should have some effect on the kinetic energy of the ejecting matrix ion jet. Comparison of observations at 337 nm and 266 nm laser wavelength supports this assumption. Photon absorption leads to a $S_0 - S_1$ transition in the DHB molecule with successive fluorescence from the lowest S_1 state. The exceeding energy above the lowest vibrational state of S_1 dissipates into dark (thermal) pathways, responsible for heating of the crystal and desorption of material. Different wavelengths between 250 and 380 nm will populate the same electronic state, but will deposit different quantities of thermal energy inside the crystal. The Nd:YAG laser with 266 nm wavelength (4.66 eV photon energy) is able to deposit 0.98 eV more thermal energy

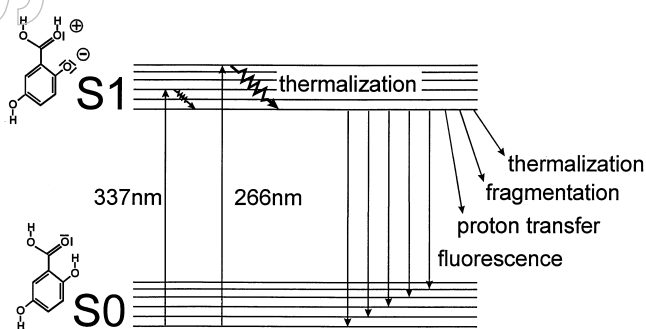


Figure 13. Scheme of excitation and relaxation processes of DHB at 266 nm and 337 nm.

in the crystal per absorbed photon than the N₂ laser with 337 nm wavelength (3.68 eV photon energy). The optical density of DHB, on the other hand, is almost one-half for 266 nm compared to 337 nm. Assuming a constant density of excited states (lowest vibrational S₁ states) necessary for inducing ionization of matrix molecules (see photochemical ionization model for matrix molecules^{18, 19}) the thermalized energy per volume due to relaxation of the higher vibrational states to the lowest S₁ state is thus higher at 266 nm compared to 337 nm. The result is a mismatch between kinetic properties and conditions for matrix ion formation, which then leads to a poor kinetic overlap between proton donors and analyte molecules. The fundamental independence of desorption and ionization of material in laser induced mass spectrometry has been described earlier.³¹ Increasing the laser irradiance will increase the density of matrix ions, but at the same time will increase their mean velocity and by that will even deteriorate the kinetic overlap. (This is the same effect as observed for 337 nm at higher irradiances.) It has to be noted that the above assumptions on the kinetic behavior cannot be proven directly by observation of a change in mean velocity of matrix ions, but can only be rationalized by the lack of analyte ion formation at 266 nm wavelength. An increase of velocity is induced to a much higher degree by just a slight change of irradiance, which cannot be measured precisely enough.

Single crystal analysis

The effect that analyte ions could only be observed from the small surfaces of the single crystals but not from the large surface cannot be explained sufficiently yet. Possible parameters which might influence this behavior are an anisotropic spectral absorption coefficient resulting from the fixed orientation of the absorbing aromatic rings in the crystal or mixing effects between ejected matrix and analyte molecules which might be different for stacked or neighboring orientation of the two different species. This question has to be left open here and shall be addressed in further crystallographic studies.

Effects of laser beam direction

Ion-density plots obtained from dried-droplet samples, which have been acquired by permanently changing the desorption spot, show a weak directional preference depending on the angle of incidence of the laser beam. Although we are not able to determine ion yields straight into the direction of the incident laser beam (the nearest detection angle with respect to the laser beam is 20°), it appears that ion clouds are shifted into the direction of irradiance (left side) in Figure 7. This observation is supported by recent investigations of Chaurand *et al.*³² They measured a mean ejection angle of 30° at a laser irradiance angle of 60° for proteins embedded in α -cyano-4-hydroxycinnamic acid. Their explanation was an arbitrary distribution of microcrystals, mainly excited at those surfaces facing the laser beam. Consequently, the mean ejection angle should follow the direction of the laser incidence.

Ion-density plots obtained from single crystals have been acquired from a single desorption spot. They exhibit a considerable directional preference into the direction of the incident laser beam. This observation can be explained by formation of an ablation crater (Figure 14). Irradiation of a surface by an oblique angle leads to an asymmetric distribution of absorbed energy per volume, as can be seen from Figure 14. The center of highest absorbed energy per volume is shifted to the right of the focal center. As a result ablation behavior of the material is asymmetric as well, finally (after several shots) resulting in a *mean ejecting surface* which is tilted towards the laser beam axis.

In general, there are no indications from our measurements that any other effects or mechanisms exist which would lead to an ejection behavior other than normal to the ejecting surface.

General behavior of ion plumes

There have been numerous investigations and theories about *angular* distributions of ions or neutrals under various conditions of thermal or laser excitation in the field of surface sciences and laser ablation (see, for example, Reference 33). In none of these studies has the angular distribution been found to be a simple cosine distribution as would be expected from a pure thermal model. In agreement with these more fundamental studies, the typical angular distribution of matrix ions ejected from MALDI samples has been found to be forward directed as well, described by $I \sim \cos^{2.4}$.¹⁰ The *temporal* distribution of laser desorbed ions has been found to be bimodal in certain cases, as observed in our case for matrix ions and earlier for ablation studies of PMMA³⁴ and other polymers,³⁵ for example. In the case of DHB matrix ions our investigations have shown that the slow mode has a broad (thermal-like) angular distribution, while the fast mode has a narrow (jet-like) angular distribution. The reason for this bimodal behavior has been described as the result of gas-phase collisions in a dense region, which leads to forward-peaked ejection plumes even in the case of thermal desorption processes.³⁶ A complete model of ejection modes in laser desorption/ablation, however, is still missing.

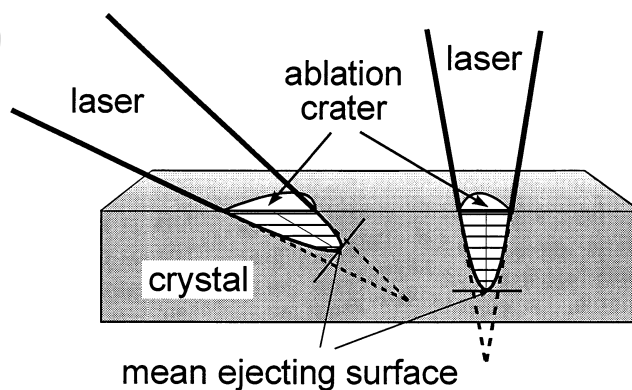


Figure 14. Scheme of ablation craters formed under laser irradiation at different incident angles.

The much more isotropic distribution of alkali ions, as observed in our measurements, indicates that these species might stem from separated areas of the sample, rather than from inside the matrix crystals, and that these ions not necessarily are entrained in the ion jet. Ion imaging studies of MALDI samples performed with a scanning laser microprobe support this model of separated areas of alkali and matrix/analyte location.³⁷

Implications for structure analysis of biopolymers

Post-source decay-matrix assisted laser desorption/ionization (PSD-MALDI) has been established recently as a method for structure analysis of biopolymers such as peptides, oligosaccharides and oligonucleotides.^{3,4} The principle of this new method is the mass analysis of product ions that are formed by unimolecular decay after ion acceleration. It has been found that the electric field strength effecting the ejecting ion cloud plays an important role for the extent of postsource fragmentation.¹⁵ In the light of the investigations presented in this paper the process of ion excitation is even clearer. Assuming that the densities of neutral matrix molecules are considerably higher than those of ions and assuming that the velocity distributions of ions and neutrals are comparable [meaning that Figure 6 (mid) holds for neutral matrix molecules as well] one can derive immediately from Figure 6 that analyte ions after formation in the gas phase have to pass a high density area of matrix molecules upon acceleration, that they will undergo a large number of low-energy collisions and that they will gain a considerable increase in internal energy, depending on the electric field strength, i.e. the collision energy. It is in good agreement with these interpretations that analyte ions undergo almost no fragmentations even at high laser irradiances, if the initial acceleration field is turned off.¹⁵

Conclusion

Investigations of the ejection behavior of matrix and analyte ions in MALDI mass spectrometry suggest a model of analyte ionization in the gas phase which is driven simply by the kinetic parameters and the difference in proton affinities of matrix and analyte. Ion-density plots obtained indicate that analyte ionization by proton transfer takes place in a region where fast and slow matrix ions have already separated in a way that they do not interfere with each other any more. Otherwise no localized matrix ion quenching would be observable. It is therefore assumed that analyte ionization takes place long after matrix ion formation. It appears that, for different systems of matrix/analyte combinations and wavelengths, different conditions of spatial and temporal overlapping of matrix ions and analyte molecules exist which can be more or less advantageous for effective ionization. Ionization behavior under non-accelerating conditions, as used in the experiments described here, is certainly different from ionization under accelerating conditions, and therefore results have to be translated carefully to MALDI analysis in common accelerating instruments. There is, however, no doubt that

ionization in accelerating instruments is affected by the observed mechanisms to the same extent and that a considerable part of limiting effects in MALDI, such as low mass resolving power, can be attributed to the way the ions are formed.

Acknowledgment

Financial support by the German Federal Ministry of Research and Technology, by the Ministry of Science and Research, NRW, and by the European Union is gratefully acknowledged. We like to thank Joachim Schwarzmaier and Kerstin Dienhardt for their help in measuring the optical density of the single crystals. This work is part of the dissertation of V.B. at the University of Düsseldorf.

References

1. F. Hillenkamp, M. Karas, R.C. Beavis and B.T. Chait, *Anal. Chem.* **63**, 1193A–1203A (1991).
2. B. Spengler and R. Kaufmann, *Analysis* **20**, 91–101 (1992).
3. B. Spengler, D. Kirsch, R. Kaufmann and E. Jaeger, *Rapid Commun. Mass Spectrom.* **6**, 105–108 (1992).
4. R. Kaufmann, B. Spengler and F. Lützenkirchen, *Rapid Commun. Mass Spectrom.* **7**, 902–910 (1993).
5. R.C. Beavis and B.T. Chait, *Chem. Phys. Lett.* **181**, 479 (1991).
6. Y. Pan and R.J. Cotter, *Org. Mass Spectrom.* **27**, 3–8 (1992).
7. T. Huth-Fehre and C.H. Becker, *Rapid Commun. Mass Spectrom.* **5**, 378 (1991).
8. (a) W. Ens, Y. Mao, F. Mayer and K.G. Standing, *Rapid Commun. Mass Spectrom.* **5**, 117–123 (1991).
(b) A. Verentchikov, W. Ens, J. Martens and K.G. Standing, *Proceedings of the 40th ASMS Conference on Mass Spectrometry and Allied Topics*, May 31–June 5, Washington, DC, pp. 360–361 (1992).
9. D. Kirsch, B. Spengler and R.D. Kaufmann, *Proceedings of the 41st ASMS Conference on Mass Spectrometry and Allied Topics*, May 31–June 4, San Francisco, CA, p. 670a (1993).
10. B. Spengler and V. Bökelmann, *Nucl. Instr. Meth.* **B82**, 379–385 (1993).
11. R.C. Beavis and J.N. Bridson, *J. Phys. D: Appl. Phys.* **26**, 442–447 (1993).
12. M. Karas, H. Ehring, E. Nordhoff, B. Stahl, K. Strupat, F. Hillenkamp, M. Grehl and B. Krebs, *Org. Mass Spectrom.* **28**, 1476–1481 (1993).
13. F. Xiang and R.C. Beavis, *Org. Mass Spectrom.* **28**, 1424–1429 (1993).
14. W.C. Wiley and I.H. McLaren, *Rev. Sci. Instrum.* **26**, 1150 (1955).
15. (a) B. Spengler, F. Lützenkirchen, D. Kirsch, A. Deppe and R. Kaufmann, *Proceedings of the 42nd ASMS Conference on Mass Spectrometry and Allied*

- Topics*, May 29–June 3, Chicago, IL (1994). (b) D. Kirsch, B. Spengler and R. Kaufmann, in preparation.
16. M. Haisa, S. Kashino, S.-I. Hanada, K. Tanaka, S. Okazaki and M. Shibagaki, *Acta Cryst.* **B38**, 1480–1485 (1982).
 17. J. Kampmeier, Diploma thesis, University of Münster (1993).
 18. H. Ehring, M. Karas and F. Hillenkamp, *Org. Mass Spectrom.* **27**, 472–480 (1992).
 19. B. Spengler, M. Karas, U. Bahr and F. Hillenkamp, *J. Phys. Chem.* **91**, 6502–6506 (1987).
 20. A. Weller, *Zeitschrift für Physikalische Chemie* **3**, 238–254 (1955).
 21. T. Förster, *Zeitschrift für Elektrochemie* **54**, 7531 (1950).
 22. A. Weller, *Zeitschrift für Elektrochemie* **60**, 1144 (1954).
 23. J. F. Ireland and P.A.H. Wyatt, (Ed. by V. Gold and D. Bethell), *Adv. Phys. Org. Chem.* **12**, 132–223 (1972).
 24. M.E. Gimón, L.M. Preston, T. Solouki, M.A. White and D.H. Russell, *Org. Mass Spectrom.* **27**, 827–830 (1992).
 25. T.J.D. Jorgensen, T. Vulpius and G. Bojesen, *13th International Mass Spectrometry Conference*, 29 August–2 September, Budapest, Hungary (1994).
 26. T.-W.D. Chan, A.W. Colburn and P.J. Derrick, *Org. Mass Spectrom.* **26**, 342–344 (1991).
 27. V. Bökelmann, A. Deppe, B. Spengler and R. Kaufmann, unpublished results.
 28. E.M. Kapp and A.F. Coburn, *J. Biol. Chem.* **145**, 556 (1942).
 29. D.P. Craig and P.C. Hobbins, *J. Chem. Soc.* **1**, 539 (1955).
 30. H. Ehring and B.U.R. Sundqvist, *13th International Mass Spectrometry Conference*, 29 August–2 September, Budapest, Hungary (1994).
 31. B. Spengler, U. Bahr, M. Karas and F. Hillenkamp, *Anal. Instr.* **17**, 173–193 (1988).
 32. P. Chaurand, S. Della Negra, C. Deprun, J. Hoyes, Y. Le Beyec and F. Aksough, *Proceedings of the 42nd ASMS Conference on Mass Spectrometry and Allied Topics*, May 29–June 3, Chicago, IL (1994).
 33. G. Comsa and R. David, *Surface Science Reports* **5**, 145–198 (1985).
 34. B. Danieizik, N. Fabrizius, M. Röwekamp and D. von der Linde, *Appl. Phys. Lett.* **48**, 212–214 (1986).
 35. S.G. Hansen, *J. Appl. Phys.* **66**, 3329–3336 (1989).
 36. I. Noorbach, R. Lucchese and Y. Zeiri, *Surface Science* **200**, 113–134 (1988).
 37. B. Spengler, M. Hubert and R. Kaufmann, *Proceedings of the 42nd ASMS Conference on Mass Spectrometry and Allied Topics*, May 29–June 3, Chicago, IL (1994).

Received: 19 January 1995

Accepted: 24 January 1995

Cluster formation of biomolecules in the gas phase

Michael Dey and Jürgen Grotemeyer

Institut für Physikalische Chemie, Universität Würzburg, Marcusstr. 9/11, D-97070 Würzburg, Germany.

Supersonic beam expansion with respect to the formation of neutral biomolecular clusters was investigated. Laser desorption (LD) into a supersonic beam was used to form neutral clusters of biomolecules in the gas phase. The internal degrees of freedom of laser desorbed neutral molecules were cooled, allowing for the formation of intermolecular bonds leading to neutral clusters of biomolecules. The clusters were post-ionized by either multiphoton ionization (MUPI), or photo-induced electron impact ionization (PEI), before detection in a reflectron time-of-flight mass spectrometer (RETOF-MS). Seeding small molecules, such as water and benzene, into the jet resulted in cluster formation during the supersonic expansion. Intermolecular forces strong enough to form and stabilize [biomolecule–biomolecule] clusters permitted the investigation of biologically relevant systems, such as [retinoid–amino acid] cluster interactions.

Introduction

Supersonic beams have been extensively studied since their first introduction in the early 1950s.^{1–3} They are widely used for many applications in physical and chemical experiments due to their unique features, such as cooling of the internal degrees of freedom of the molecular species and formation of clusters. In general, the carrier gas is expanded through a small orifice or nozzle.⁴ During the adiabatic expansion the translational degrees of freedom of the gas are effectively cooled. The cold translational modes then act as a refrigerant for the other degrees of freedom. The rotational and the vibrational modes of the analyte molecules are cooled by multiple collisions with the carrier gas in the expansion region.^{5–7}

Since the number of collisions decreases rapidly downstream from the nozzle, internal states of the molecules are “frozen”. A jet provides a powerful tool to generate isolated molecules in the gas phase with cooled internal degrees of freedom.⁸ Because of this feature, supersonic beams are widely used in spectroscopic applications.

In the mass spectrometric application of jets, the cooling of seeded molecules³ before post-ionization results in minimized fragmentation of labile molecules in the mass spectra since the internal energy of analyte molecules is decreased.^{9,10} To obtain the molecular ion peak in a mass spectrum, jet cooling is essential for many labile molecules.¹¹

Laser desorption of neutral organic molecules has been utilized by several groups.^{12–15} This technique allows for the transfer of non-volatile and thermally labile molecules into the gas phase. At low desorption laser power, significantly more neutrals than ions are produced during the desorption process.

Ratios of 10^5 – 10^3 neutrals to 1 ion generated by LD with IR lasers have been experimentally determined.^{18,19} Therefore, LD is a powerful tool to generate neutral gas phase molecules from non-volatile samples.

A general approach to obtain intact desorption of thermally labile polyatomic molecules such as biomolecules is to entrain the desorbed molecules into a jet.²⁰ This approach takes advantage of the features of both techniques, LD and supersonic expansion. Laser desorption of intact neutral molecules into a supersonic beam results in cooling of internal energies of the desorbed molecules. Combining LD of neutrals, supersonic jet expansion and soft post-ionization techniques allows for the detection of molecular ions of thermally labile molecules.²¹ In particular, resonant enhanced multi-photon ionization provides wavelength selective and sensitive detection of analyte molecular ions without fragmentation.

Besides their use for spectroscopic experiments utilizing the cooled internal degrees of vibrational and rotational freedom described here, supersonic jets are also used for the formation of gas-phase clusters. The unique features of similar velocities of all particles in a jet and multiple collisions enhance the probability of the formation of clusters with weak interaction forces. Therefore, molecules seeded into a jet form weakly bonded van der Waals clusters, which is one of the most interesting applications of supersonic beam expansions.²² Although van der Waals forces are weak, a supersonic beam provides a low temperature environment where the relative kinetic energy in a collision is less than the van der Waals binding energy. Therefore clusters remain intact once formed. Cluster formation in jets has been observed with different classes of analytes ranging from atomic clusters to

clusters of small molecules to metal clusters.²³ Interactions of molecules within clusters are of growing interest, especially interactions of biomolecules. Weak interactions such as van der Waals forces or hydrogen bonds are often an important factor in chemical properties and reactions within organisms. Many biological processes are governed by weakly bonded species, requiring demanding techniques for their study.

In this paper, the technique of laser desorption of neutral biomolecules into a supersonic beam is utilized to obtain neutral clusters of biomolecules in the gas phase. The idea was to combine LD producing a large amount of intact neutral biomolecules in the gas phase with a jet known for the capability of cluster formation enhancement. The features of supersonic beams have been examined and enhanced for the formation of clusters. Geometric parameters are crucial for the cluster formation of laser desorbed neutral molecules. Neutral [biomolecule–solvent] and [biomolecule–biomolecule] clusters were post-ionized with resonant enhanced multi-photon ionization (MUPI) for detection in a RETOF-MS. Post-ionization with photo-induced EI shows the relative high stability of jet-cooled clusters in respect to the post-ionization process. Mass spectra of [biomolecule–solvent] clusters such as [peptide–water] clusters are presented. Since retinoid–amino acid interactions are involved in biological processes such as vision and proton pumping through membranes, this system is presented as an example for biological relevant clusters of biomolecules in the gas phase.

Experimental

Experiments were performed in a reflectron time-of-flight mass spectrometer (RETOF-MS) described in detail elsewhere.²⁴ Desorption and post-ionization took place in separated areas of the instrument (Figure 1). Desorption was accomplished in the desorption chamber with a pulsed CO₂ laser. The characteristics of the infrared (IR) desorption laser are: wavelength 10.6 μm , pulse length 16 μs and pulse energy 40 mJ. The IR laser beam could be attenuated by an iris and was focused perpendicularly on to the probe tip by a 8 cm ZnSe lens. The desorption laser was focused on to the sample with a spot size of approximately 0.5 mm in diameter. Analyte molecules were desorbed from a 1 mm wide probe tip into a pulsed supersonic beam of argon or helium. Typical settings for the expansion into the vacuum were 2 bar back pressure of the gas behind the pulsed valve (Bosch valve, custom designed) and 10^{-5} to 10^{-6} mbar in the desorption chamber. The vacuum was maintained by three turbo pumps (Balzer, Wetzlar, desorption chamber: 330 l s^{-1} , ion source: 50 l s^{-1} , flight tube: 330 l s^{-1}).

The characteristics of the custom-made pulsed valve include a variable opening time and an immediate opening of the orifice by fast repulsion of a polyamide piston. Variable diameters for the opening were used, with a typical diameter of 100 μm . The geometric arrangement of the probe tip relative to the nozzle opening was found to be critical for the cluster formation. Probe tips with various designs were used

to vary distances and geometry of the solid sample and the laser impact relative to the orifice. Placing the probe tip close to the nozzle and about 1 mm below the opening, with the laser beam perpendicular to jet and sample, provided the best results for cluster formation. In this geometry neutrals are desorbed into the expansion region of the jet shortly after the opening, where most multiple collisions take place. By desorbing too close to the nozzle, the desorption plasma is affected and disturbs the expansion. By desorbing parallel with the jet, the desorbed neutrals would not reach the collision zone since the majority of desorbed molecules are desorbed straight from the surface.

The jet provides cooling of the internal degrees of freedom of the analyte molecules by multiple collisions with the carrier gas in the expansion region. During this time collisionally-cooled analyte molecules may form neutral clusters in the gas phase. Clusters of biomolecules and jet seeded molecules can only be formed in the expansion region. To exclude clusters of biomolecules possibly formed before or during the desorption process, different ratios of matrix : analyte were investigated. In the collision-free drift region after the expansion no further molecule–molecule reactions can take place. Neutral clusters formed in the jet pass a skimmer and are transported into the ion source. The skimmer allows only the effectively cooled centre of the jet to pass into the ion source while off-centre neutrals are quenched (Figure 1). Positive and negative ions produced during the desorption process are separated by a repeller plate set at +870 V, so they cannot pass into the ion source.

Neutral molecules and clusters were post-ionized in the ion source with MUPI or photo-induced electron ionization (PEI).²⁵ MUPI was achieved with the frequency doubled (BBO1) output of a XeCl excimer laser (LPX 110i, Lambda Physik Göttingen) pumped dye laser (FL 3002, Lambda Physik Göttingen) at variable wavelength with a 7 ns pulse width. Wavelengths typically used were in the range between 250 nm and 290 nm. This equals photon energies between 5 and 4.25 eV, so that ionization takes place after a two photon absorption process. Photo-induced electron ionization generates a pulse of electrons by an unfocused laser beam impact on to a tantalum wire. Electrons are emitted from the tantalum wire due to the photo-electrical effect occurring in tantalum at photon energies greater than 4.25 eV ($\lambda = 290 \text{ nm}$). Emitted electrons were accelerated in the electrostatic field of the ion source toward the repeller. The flight path of neutral molecules and clusters entering the ion source through the skimmer is in an opposite direction to the electrons. As the electrons traverse towards the repeller and the neutrals, they gain kinetic energy and ionize the neutrals. PEI was typically performed at electron energies between 50 and 70 eV, controlled by the reflector voltage.^{25b}

The ions formed were accelerated in a two-stage ion source with approximately 755 eV and detected in a RETOF-MS after a flight time of approximately 100–200 μs . Precise timing of the events-pulsed valve, desorption laser and ionization laser was achieved with a custom built trigger/delay unit. All

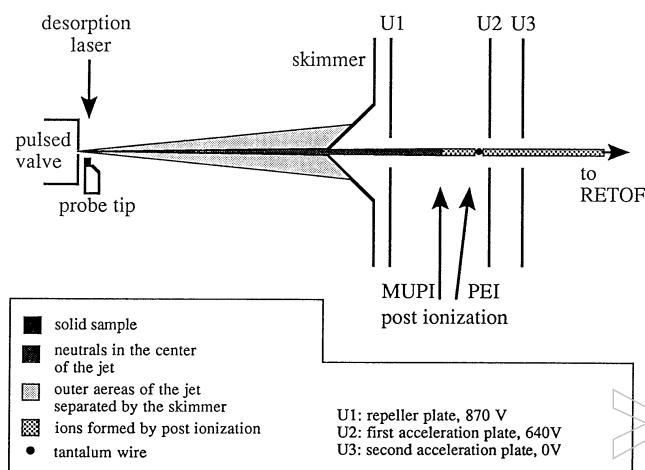


Figure 1. Experimental set-up with the desorption chamber and ion source of the RETOF-MS.

time-of-flight mass spectra in this paper represent the sum over 25 laser shots.

The peptide and retinol samples (Sigma, Munich) were used without further purification. Benzene and water were seeded into the jet by a reservoir connected to the carrier gas line. Samples containing the biomolecules were pressed into pellets prior to desorption. A mixture of the analyte molecules, a polyethylene matrix and a silver powder comatrix were mixed and pressed without using any solvent to prevent cluster formation due to interaction of the analyte molecules in solution.²⁶ The typically used ratio of 100 matrix molecules to 1 analyte molecule assured that the sample molecules were isolated in the matrix. A variety of matrix : analyte ratios ranging from 0 : 1 (no matrix) to 1000 : 1 were investigated. If cluster formation is related to the desorption process or clusters are already present in the solid sample, more clusters are expected to be detected at lower matrix : analyte ratios, due to the closer vicinity of analyte molecules in the sample. However, hetero cluster formation was observed up to a molar ratio of 1000 : 1, matrix : analyte indicating cluster gas-phase formation. Other evidence for the formation of clusters of laser desorbed molecules in the gas phase are the crucial geometric parameters for jet orifice, sample position and laser beam impact. Clusters formed by laser desorption without any interactions with the jet gas should be detected regardless of the position of the jet orifice relative to the solid sample. Clusters are, however, only detected at specific geometric arrangements. These observations suggest that cluster formation of laser desorbed neutral biomolecules takes place in the supersonic expansion in the gas phase.

Results and discussion

Since the term cluster is widely used for many different types of species, a short definition of the understanding of the term “cluster” as used in this paper and the types of clusters investigated is necessary. We adapt the definition of cluster from Haore,²⁷ which is a very general approach to the term

“cluster”. A particle has to fulfill two specifications to be considered a cluster: it has to consist of two or more sub-particles and most of the sub-particles have to be on the outside of the cluster. The first limitations exclude atoms and molecules, which are only one particle while the second limits a cluster in its size excluding solids. Within this definition many special types of clusters may be defined all fulfilling the main characteristics of a cluster.

In this paper different cluster types of biomolecules are presented. Homo clusters consist of only one kind of sub-particle while hetero clusters consist of at least two different sub-species. All clusters of biomolecules are weak bonded clusters²⁸ with interaction energies less than 1 eV. Within the category of weak bonded, clusters can be further distinguished by their interaction forces. Van der Waals clusters are bonded due to dispersive and weak electrostatic interactions up to 0.3 eV. Molecular clusters have binding energies between 0.3 and 1 eV from dispersive and electrostatic forces. Hydrogen bond clusters have binding energies between 0.3 and 0.5 eV.

Due to the weak attractive forces, a low internal energy of a cluster is required to avoid dissociation into sub-particles. However, to detect a cluster in a mass spectrometer, ionization is required. Neutral clusters need to be post-ionized in the gas phase. Post-ionization, however, allows for the detection of two different cluster distributions, which depend on experimental conditions. The detection of either the distribution of neutral clusters or ionized clusters depends on the interactions stabilizing neutral or ionized clusters, respectively. In addition, the most stable neutral cluster species are not necessarily the most stable ionic cluster species and *vice versa*. Here one has to consider the ionization conditions for the cluster distribution detected. Since only neutral clusters are transferred into the ion source, the distribution before ionization is due to the stability of neutral clusters. If ionization is achieved with little excess energy and the internal energy of the ionized cluster is below the appearance energy (*AE*) for dissociation the detected distribution is according to neutral stability [Figure 2(a)]. Ionization with higher excess energy, however, causes dissociation of clusters [Figure 2(b)] in the time-scale given by the instrument, which is about 100–200 μ s from ionization to detection. The observed distribution is then, according to stabilization, within the ionic species. Ionization with low and variable excess energy is required to obtain the neutral distribution, which is provided by MUPI.

There have been extensive studies of the features of supersonic beam expansions since they are widely used for physical and chemical experiments.²⁹ The purpose of this section is to summarize relevant properties of jet expansions and enhance the operating conditions to generate neutral clusters of biomolecules. A supersonic beam expansion is an adiabatic expansion of a gas through a nozzle into a vacuum. Generally a high back pressure of the gas (at least atmospheric range) P_0 , a small orifice or nozzle with a characteristic dimension D (in our experiment 100 μ m diameter) and an expansion volume at low background pressure P_{vac} are required to form a supersonic beam expansion. The gas may be expanded continu-

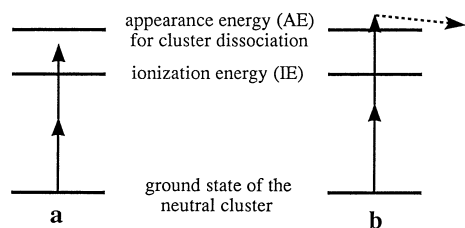


Figure 2. Scheme of multi-photon post ionization of neutral clusters.

ously or through a pulsed valve, which reduces the amount of carrier gas released into the vacuum system of the MS. We used a pulsed valve for the gas inlet, since we also used pulsed desorption, ionization and mass analysis. The criterion for a jet formation is:

$$\lambda_D \ll D \quad (1)$$

where λ_D is the mean free path of particles in the orifice and D is the diameter of the nozzle. If $\lambda_D \gg D$ there are no collisions of the gas in the nozzle and an effusive beam into the vacuum is formed. With $\lambda_D \ll D$, however, multiple collisions between the particles take place during the expansion. Due to the collisions a thermodynamic equilibrium of all particles is formed resulting in a supersonic beam. A directed beam is produced with a velocity greater than sound velocity. For an ideal mono-atomic gas the cooling during an adiabatic expansion equals:³⁰

$$T / T_0 = (P / P_0)^{(g-1)/g} \quad (2)$$

where $g = C_p / C_v$, the quotient of the heat capacities, T and P are the temperature and pressure after the expansion and T_0 and P_0 the temperature and pressure before the expansion.

The translational temperature T_{trans} of an ensemble is defined as the width of the velocity distribution of the particles, which is reduced significantly in a jet, since all particles have a similar flow velocity.³¹ The vibrational and rotational degrees of freedom are cooled by collisions with the “cold bath” translational degree of freedom. The probability of collisions decreases rapidly with distance from the nozzle. After multiple collisions in the expansion region, there is a collision-free drift region where all the internal degrees of freedom are frozen. The internal degrees of freedom are cooled in the order $T_{\text{trans}} < T_{\text{rot}} < T_{\text{vib}}$. Since the most effective cooling occurs in the core of the jet expansion, often a skimmer³ is used to separate the less cooled, off-centre neutrals, before probing.

The experimental necessity of a supersonic expansion for cooling the degrees of freedom of analyte molecules was investigated. The dipeptide leu-trp was laser desorbed and entrained into supersonic beams of argon and helium and compared to the situation without a jet (Figure 3). The desorbed neutral molecules were post-ionized with MUPI at 280 nm wavelength (4.43 eV) using soft ionization conditions. The use of argon as a carrier gas resulted in a mass spectrum where the molecular ion of leu-trp ($\text{C}_{17}\text{H}_{23}\text{N}_3\text{O}_3^+$, m/z 317) represents the base peak [Figure 3(a)]. Fragmentation due to

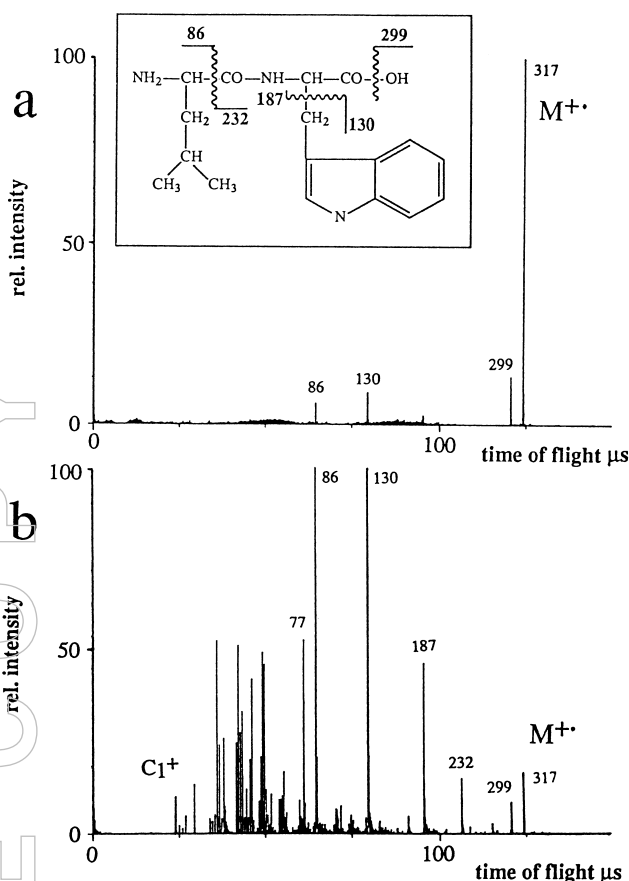


Figure 3. Time-of-flight mass spectra of the dipeptide leu-trp. LD of neutrals into a supersonic beam of argon results in the molecular ion as the base peak (a), while without a jet, increased fragmentation is observed (b). The insert shows the cleavage sites for leu-trp specific fragment ions.

the loss of water is minor as depicted by the abundance of the fragment ion $\text{C}_{17}\text{H}_{21}\text{N}_3\text{O}_2^+$ (m/z 299). The characteristic fragment ions of the amino acids trp, the methylen-indol ion ($\text{C}_9\text{H}_8\text{N}^+$, m/z 130), and leu, the $\text{C}_5\text{H}_{12}\text{N}^+$ ion (m/z 86) are detected.

Performing the experiment under the same conditions but without a supersonic beam results in tremendous changes in the TOF mass spectrum [Figure 3(b)]. Base peaks in the spectrum are the fragment ions $\text{C}_9\text{H}_8\text{N}^+$ (m/z 130) and $\text{C}_5\text{H}_{12}\text{N}^+$ (m/z 86). The intensity of the molecular ion has decreased significantly compared to the experiment with a supersonic beam of argon while the intensities of fragment ions have increased. In addition to the fragment ions $\text{C}_9\text{H}_8\text{N}^+$ (m/z 130) and $\text{C}_5\text{H}_{12}\text{N}^+$ (m/z 86), the fragment ions $\text{C}_8\text{H}_{15}\text{N}_2\text{O}_3^+$ (m/z 187) and $\text{C}_{12}\text{H}_{11}\text{N}_2\text{O}_3^+$ (m/z 232) were detected. These ions represent the same cleavages with the other part of the molecule retaining the charge. The charge is now found on both fragments resulting from the cleavage under conditions without a jet. In addition to the characteristic fragment ions of the dipeptide, fragmentation into small fragment ions down to C^+ (m/z 12) was detected. Spectra with helium (rmm 4) as the carrier gas show a decrease in the molecular ion signal and an

increase in fragmentation compared to the mass spectra using argon (rmm 40) as the carrier gas, yet not as extensive as without a jet. One can conclude that collisions with the heavier argon atoms were more efficient with respect to cooling the peptides than collisions with the lighter helium atoms. Only jet cooling with argon allowed for the detection of the molecular ion of the thermally labile dipeptide leu-trp as the base peak in the mass spectrum.

The observed increased fragmentation without a jet is the result of fragmentation occurring by two processes during the experiment: ionization and desorption. Fragmentation during ionization increases, since analyte molecules without jet cooling reach the ion source with higher internal energy. Post-ionization of molecules with high internal energy results in more fragment ions since appearance energies for fragmentation pathways are exceeded by ions with high internal energy. Fragmentation during desorption or shortly thereafter occurs due to the high internal energy of the analyte molecules after the desorption process. Without collisional cooling to decrease the high internal energies, fragmentation of the desorbed molecules into neutral fragments occurs, which are then post-ionized in the ion source.

There is strong evidence that cooling during both processes allows for detection of intact labile molecules and clusters. Ionization with EI, a hard ionization technique, allows only for the intact detection of jet cooled labile molecules and clusters. Without jet cooling of the internal degrees of freedom before post-ionization, only fragment ions are detected with EI. Fragmentation down to small fragment ions such as C^+ (m/z 12) as seen in the leu-trp spectrum without jet cooling, however, requires absorption of more than 10 photons by the molecules during MUPI,³² which is not likely under the soft ionization conditions. Therefore, since it is unlikely that these fragments are formed during the ionization process, it is concluded that the small fragment ions are most likely due to fragmentation of the peptide during the desorption process without jet cooling.

Cooling of both processes in a jet is also essential for the formation and detection of clusters. Cooling of the internal degrees of freedom of the analyte molecules, especially the translational temperature, results in similar velocities of all molecules in the jet. During multiple collisions in the expansion, clusters are formed by interactions between colliding molecules. High internal energies, however, result in an immediate dissociation of weakly bound species. The initially formed cluster is stable in the observation time of the experiment only if the attractive forces between the molecules forming a cluster is greater than the internal energy of the complex or if a cluster with high internal energy can be cooled by additional collisions. A cluster, formed and stabilized as neutral, also has to remain intact during post-ionization, which was only observed with jet cooling.

Of interest for cluster studies is the time distribution of clusters of different size in a supersonic beam. A time profile for the cluster distribution in a supersonic jet of argon was obtained for benzene homo clusters (Figure 4). Benzene was

seeded into the argon carrier gas and cluster formation took place during the expansion into the vacuum. The excess energy deposited during ionization for the non-resonant ionized benzene clusters was about 0.3 eV ($\lambda = 260$ nm, 2×4.77 eV = 9.54 eV). Non-resonant excitation with a wavelength significantly distant from the closest excited state for all cluster sizes is necessary to avoid resonant enhancement of one cluster size at specific conditions. Wavelengths close to a resonant state would result in increasing the signal of “warm” clusters with high internal energies, since some of them would be resonant enhanced ionized, while ionization with a resonant wavelength would enhance “cold” clusters with low internal energies. In both cases, not the time distribution in respect to the cluster size, but the conditions of the jet, at which most molecules are in a state to absorb resonantly the irradiated laser wavelength, would be probed. In the case of benzene, only with non-resonant conditions for all species is a time relevant distribution obtained.

This experiment indicates that the time at which the maximum intensities for clusters are detected is size independent. Homo clusters of up to nine benzene molecules have a similar time profile in the jet as the benzene dimer, as shown in Figure 4. The dimer time profile has a FWHM of 150 μ s, indicating that clusters are formed as long as the jet conditions are sufficient and neutral molecules are desorbed. The results also indicate multiple collisions between the molecules in the expansion and a collision-free drift region after the expansion. The characteristics of the pulsed valve are critical for the cluster formation, especially opening time and opening velocity. Therefore, if the conditions are sufficient for the formation of dimers, then they are also sufficient for the formation of larger clusters.

The location of the cluster formation is crucial for any study. Possibilities for the cluster formation are interaction in solution during sample preparation, interaction during the desorption and interaction between colliding molecules in the gas phase. Only the latter case, formation in the jet, allows for studying gas-phase interactions between molecules. Figure 5 shows a time-of-flight mass spectrum of the amino acid tryptophane (trp) desorbed into a supersonic beam of argon containing benzene molecules. Ionization was performed at 270 nm, a non-resonant wavelength of benzene at which trp shows good absorption. In addition to the molecular ion of trp (m/z 204), [trp-benzene]_x ($x = 1,2,3$) clusters are detected. The formation of the hetero clusters can only take place during the supersonic expansion shortly after the nozzle, since this is the only place where interactions between a seeded benzene and a desorbed trp can take place during the experiment. Formation due to the desorption process is not possible since there are no benzene molecules present in the solid sample. After the expansion region there is a collision-free drift region, where no interactions between the molecules take place. Clusters containing one trp molecule and up to three benzene molecules were detected. These clusters were formed during collisions of jet cooled molecules in the gas phase with less internal energy than the interaction forces. The observed clus-

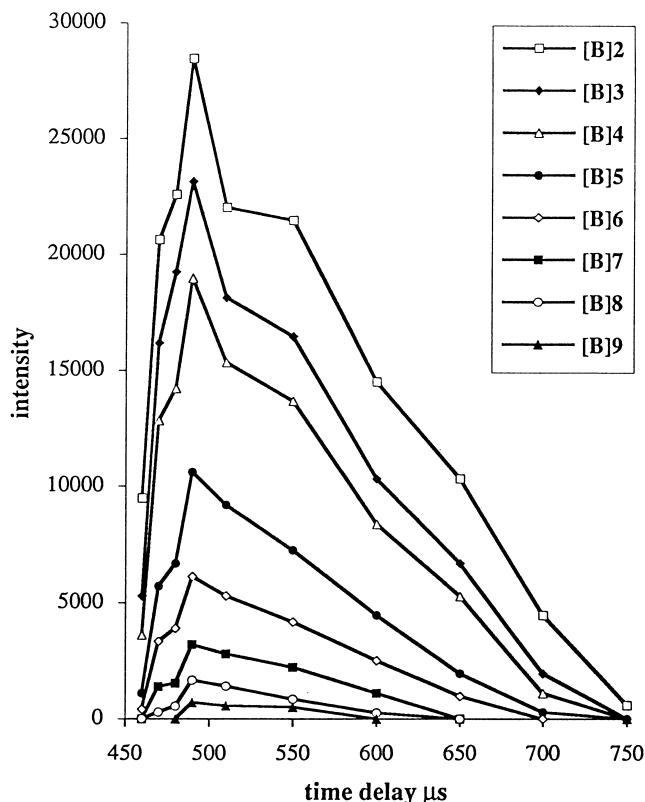


Figure 4. Time distribution of benzene homo clusters in a supersonic jet of argon.

ter formation of a laser desorbed and a seeded molecule proves that jet gas and desorbed molecules undergo multiple collisions until the velocities of both are similar enough to allow the formation of weak bonded clusters.

Optimized experimental parameters allowed for the detection of homo and hetero clusters of several types of biomolecules including amino acids, peptides and nucleosides. In Figure 6 this behaviour is demonstrated again by a TOF mass spectrum of the amino acid tryptophane (trp). Since the desorption process was optimized towards cluster formation, homo clusters of trp containing up to six trp molecules are detected. Jet cooling of the laser desorbed molecules provides an environment where neutral trp clusters up to $[\text{trp}]_6$ are formed although they are weakly bonded species. The weak attractive intermolecular forces between trp molecules are sufficient to stabilize the neutral clusters under jet conditions. Post-ionization of the neutral clusters in the gas phase with MUPI under soft conditions at 270 nm (4.6 eV) allows for the detection of the ionized clusters. The observation of trp clusters indicates, that our technique allows the formation of neutral clusters of biomolecules by multiple collisions in the gas phase.

Since jet cooling has been utilized to allow EI ionization of labile organic molecules,¹⁰ the dipeptide trp-gly (m/z 261) was ionized by PEI. Figure 7 is the time-of-flight mass spectrum of trp-gly ionized with PEI. The laser desorbed trp-gly was entrained into a jet of argon containing seeded water

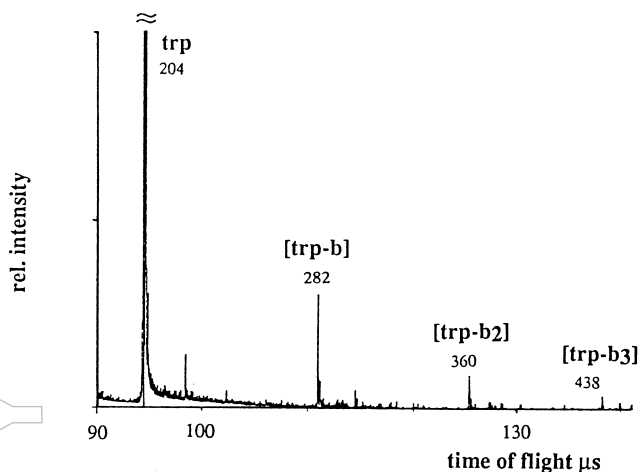


Figure 5. Time-of-flight mass spectrum of laser desorbed tryptophane into a seeded benzene argon jet. Hetero clusters are formed in the expansion region in the gas phase.

molecules. Jet cooling allows clusters of biomolecules to be ionized and detected, even when a hard ionization technique, such as EI, is employed, since the clusters are formed with low internal energy. The homo clusters of trp gly containing up to five dipeptides ($[\text{trp-gly}]_5$, m/z 1305) were detected. Beside the formation of peptide homo clusters, hetero clusters between peptide and water molecules are formed in the jet. However, a significant amount of [peptide-water] clusters are only detected for the monomer trp-gly with up to five water molecules. Attachment of up to three water molecules to trp-gly is detected with relative high abundance, while the attachment of the fourth and fifth water molecule is less intense. The dimer of trp-gly and larger clusters show only little evidence of the addition of water molecules. While the monomer is solvated in the gas phase by water molecules, the positions for water addition are probably blocked at the clusters due to peptide-peptide interactions. Since PEI is a non-selective ionization method, all molecules in the jet are

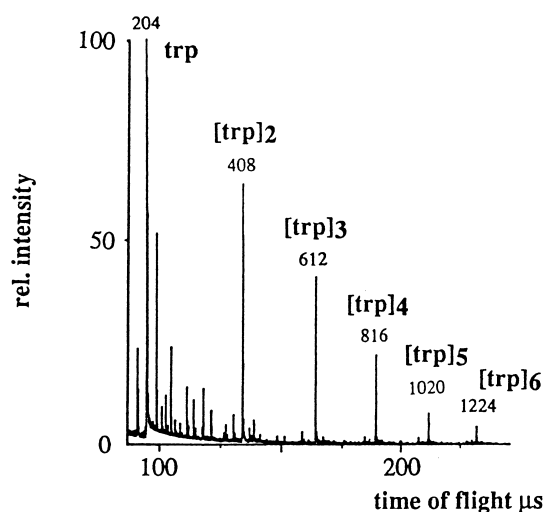


Figure 6. Time-of-flight mass spectrum of tryptophane homo clusters ionized with MUPI at 270 nm.

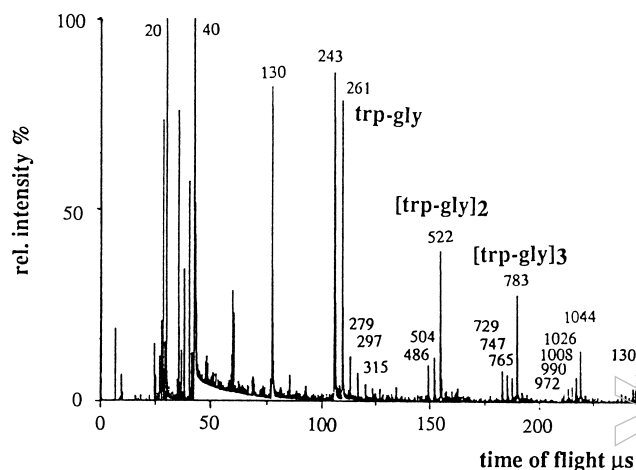


Figure 7. Time-of-flight mass spectrum of the dipeptide trp-gly. Homo clusters $[\text{trp-gly}]_x$ ($x = 1-5$) and hetero clusters $[\text{trp-gly} + (\text{H}_2\text{O})_y]$ ($y = 1-5$) are detected with photo-induced EI (PEI).

ionized. The peptide and its cluster as well as high abundant signals due to the jet gas argon (m/z 40) and the doubly charged argon (m/z 20) are detected. Also, water and other small molecules are observed in the mass spectrum.

Another interesting feature is the observed loss of water of the peptide monomer and clusters. All species lose up to as many water molecules as they contain dipeptides. Loss of one water molecule is observed for the peptide while loss of one, two, three and four water molecules is seen for the cluster $[\text{trp-gly}]_4$ (m/z 1044). In each case the fragment ions indicating the water loss are lower in intensity than the corresponding parent ion except in the case of the monomer. The signal at m/z 243 is significantly higher compared to the signals of cluster ions with one or more water loss. It should be noted that the water loss for peptides is a well-known mass spectrometric fragmentation.³³

After proving the ability to form clusters of biomolecules with this technique we applied the technique to form [retinoid-amino acid] clusters. Retinoids are involved in many photon-induced processes in organisms: Vision is initiated by a photo-induced *cis-trans* isomerization of retinal bound to a protein, and proton pumps through membranes contain a protein-bound retinoid, to mention only two examples. The photon energy is absorbed by the retinoid prior to the change in chemical energy. The environment of the retinoid in the protein is an important factor for these processes. Since the retinoids are surrounded by different amino acids of a protein, we were interested in the interaction and cluster formation of retinoids with different amino acids in the gas phase. All-*trans* retinol (ret, m/z 286) was used as the retinoid and tryptophane (trp, m/z 204) as an amino acid with a non-polar side group, tyrosine (tyr, m/z 181) as an amino acid with a polar side group and histidine (his, m/z 155) as an amino acid with a basic side group. The sample preparation avoided any interaction between the analyte molecules in solution. Ionization was per-

formed with MUPI at 270 nm wavelength ($2 \times 4.6 \text{ eV} = 9.2 \text{ eV}$), depositing an excess energy of less than 1.7 eV into the clusters during ionization. The time-of-flight mass spectra of the mixtures are summarized in Table 1. The formation of neutral clusters between retinol and the amino acids was observed in all spectra showing cluster formation of biological relevant molecules in the gas phase, due to weak molecule-specific attractive intermolecular forces.

A mixture of ret and trp results in a spectrum with the molecular ions of trp and ret as base peaks, since both molecules are resonant enhanced ionized at 270 nm. The homo cluster of the amino acid $[\text{trp-trp}]$ is detected with 18% abundance, while the cluster of interest, the hetero cluster $[\text{ret-trp}]$ is detected with 3% abundance. The hetero cluster $[\text{ret-trp}]$ is formed under the conditions of the jet expansion, however, there is no preference observed for formation of this cluster or special stabilizing interaction forces between ret and trp, since the homo cluster $[\text{trp-trp}]$ is detected with even higher abundance. The homo cluster $[\text{ret-ret}]$ was hardly detected in any of the mixtures, indicating that there are no substantial π -system or functional group stabilizing interactions between retinol molecules. Desorption of a mixture of ret and tyr also shows the molecular ions of ret and tyr as base peaks, both resonant enhanced ionized. The homo cluster $[\text{tyr-tyr}]$ is detected with the relatively high abundance of 30%, while the hetero cluster $[\text{ret-tyr}]$ is detected with the low abundance of 3%. Even the homo trimer of the amino acid $[\text{tyr-tyr-tyr}]$ is detected with higher intensity (6%) than the hetero cluster. Both the non-polar amino acid trp and the polar amino acid tyr show no preference in forming a hetero cluster with ret in the gas phase. These results indicate that there are no specific interactions between the amino acids trp and tyr and retinol molecules in the gas phase, which stabilize a cluster.

A mixture of ret and the base amino acid his, however, results in a different cluster formation. Since the resonant enhancement of absorption is weak for his at 270 nm, the abundance of the molecular ion is only 22%. The hetero cluster $[\text{ret-his}]$, however, has a relative abundance of 27%, even higher than the molecular ion of his. The hetero cluster $[\text{ret-his}]$ is the most abundant of all clusters detected within this mixture, indicating a preference of this cluster due to interactions between ret and his. Stabilization of a $[\text{ret-his}]$ cluster is due to attractive forces between the ret and the base side group of his. Theoretical calculations (QVFF, Insight Biosym³⁴) reveal several energetic stable geometric configurations for $[\text{ret-tyr}]$ and $[\text{ret-trp}]$ cluster while only one specific geometric configuration for the $[\text{ret-his}]$ cluster was found to be significantly stabilized. $[\text{ret-his}]$ clusters are formed in a specific geometry. The calculations also indicate strong stabilization forces within the ionic form of the $[\text{ret-his}]$ cluster. While $[\text{ret-trp}]$ and $[\text{ret-tyr}]$ clusters are detected only with low abundance, the $[\text{ret-his}]$ cluster is the most abundant cluster detected in a mixture of ret and his, indicating molecular recognition between ret and his. Specific interactions between retinoids and certain amino acids, that rule

Table 1. Summarized time-of-flight mass spectra ion abundances of mixtures of retinol and the amino acids trp, tyr and his, ionized with MUPI at 270 nm. Note the high abundance of the [ret-his] hetero cluster.

Mixture	Detected signals						
	A	B	[A-B]	[B-B]	[A-A]	[A-B-B]	[B-B-B]
ret, trp	ret ⁺ (<i>m/z</i> 286) 100%	trp ⁺ (<i>m/z</i> 204) 100%	[ret-trp] ⁺ (<i>m/z</i> 490) 3% ± 0.5%	[trp-trp] ⁺ (<i>m/z</i> 408) 18% ± 2.3%			
ret, tyr	ret ⁺ (<i>m/z</i> 286) 100%	tyr ⁺ (<i>m/z</i> 181) 80% ± 3.2%	[ret-tyr] ⁺ (<i>m/z</i> 467) 3% ± 0.7%	[tyr-tyr] ⁺ (<i>m/z</i> 362) 30% ± 2.1%	[ret-ret] ⁺ (<i>m/z</i> 572) 2% ± 0.2%		[tyr-tyr-tyr] ⁺ (<i>m/z</i> 543) 6%
ret, his	ret ⁺ (<i>m/z</i> 286) 100%	his (<i>m/z</i> 155) 22% ± 1.8%	[ret-his] ⁺ (<i>m/z</i> 441) 27% ± 1.3%	[his-his-H] ⁺ (<i>m/z</i> 311) 20% ± 1.7%		[ret-his-his] ⁺ (<i>m/z</i> 596) 8% ± 0.4%	

important organism processes, are detected between single molecules in the gas phase. Specific interactions and stabilizing attractive forces between ret and his molecules allow for high abundant detection of the hetero cluster [ret-his].

Conclusion

Supersonic expansion and LD of neutrals were combined to create a powerful tool to generate neutral clusters of biomolecules in the gas phase. Multiple collisions within the expansion region of a supersonic expansion provide sufficient cooling to create similar translational velocities of laser desorbed biomolecules. Collisional cooling after the desorption process and cooling of the internal degrees of freedom before post-ionization allow the detection of intact molecular ions and clusters of thermal labile molecules. The environment generated by a supersonic expansion allows the formation of weak bonded neutral clusters of biomolecules. Stable clusters are formed by collisions of jet cooled molecules if the velocity differences are less than the interaction forces.

In this paper the gas phase formation of hetero clusters of laser desorbed and seeded molecules have been studied with respect to analyte : matrix ratio studies, crucial geometric parameters for sample position. Jet cooling is essential for the formation and detection of the clusters. Cooling of the translational, rotational and vibrational degrees of freedom allows the formation of weak bonded neutral clusters with low internal energies. Using a soft ionization technique such as MUPI, weak bonded clusters of biomolecules were detected. Furthermore the jet cooling allows detection of clusters even with a "hard" ionization technique such as EI. An example of peptide clusters containing up to 5 dipeptide monomers, which were successfully post-ionized and detected with photo-induced EI, was presented.

The unique features of this technique allow the study of specific interactions between molecules in the gas phase, such as biomolecule-solvent and biomolecule-biomolecule inter-

actions. A mass spectrum of clustering between a dipeptide and water has been presented, demonstrating different affinities of the monomer and clusters to water molecules. Molecular interactions can be probed in the gas phase within the retinoid-amino acid cluster system. A specificity towards the formation of [ret-his] cluster was observed, indicating molecule specific intermolecular forces. The technique presented here can be used for the generation and detection of weak bonded neutral clusters of biomolecules in the gas phase, allowing for a wide range of promising applications.

Acknowledgement

This work has been supported by grants from the Deutsche Forschungsgemeinschaft (Gr 917/1-3 and Gr 917/9-1). The authors thank the Fonds der Chemischen Industrie for support.

References

1. A. Kantrowitz and J. Grey, *Rev. Sci Instrum.* **22**, 328 (1951).
2. G.B. Kistiakowsky and W.P. Schlichter, *Rev. Sci. Instrum.* **22**, 333 (1951).
3. E.W. Becker and K. Bier, *Z. Naturforsch. Teil A*, **9**, 975 (1954).
4. D.H. Levy, *Science* **214**, 263 (1981).
5. R. Campargue, A. Lebehot, J.C. Lemonier and D. Marette, in *Rarefield Gas Dynamics*, Volume 74 of *Progress in Astronautics and Aeronautics*, Ed. by S.S. Fischer (1981).
6. R. Campargue and J.P. Breton, *Entropie* **42**, 18 (1971).
7. G. Meijer, M.S. de Vries, H.E. Hunzicker and H.R. Wendt, *Appl. Phys. B*, **51**, 395 (1990).
8. D.H. Levy, *Ann. Rev. Phys. Chem.* **31**, 197 (1980).
9. H. K hlewind, H.J. Neusser and E.W. Schlag, *J. Phys. Chem.* **89**, 5593 (1985).

10. A. Amirav and A. Danon, *Int. J. Mass Spectrom. Ion Proc.* **97**, 107 (1990).
11. R.J.J.M. Steenvoorden, E.R.E. van der Haage, J.J. Boon, P.G. Kistemaker and T.L. Weeding, *Org. Mass Spectrom.* **29**, 78 (1994).
12. H.L. Selzle, H.v. Weysenhoff and E.W. Schlag, *Z. Naturforsch.* **40a**, 674 (1985).
13. J. Grotemeyer, U. Boesl, K. Walter and E.W. Schlag, *J. Am. Chem. Soc.* **108**, 4233 (1986).
14. J.H. Hahn, R. Zenobi and R.N. Zare, *J. Am. Chem. Soc.* **109**, 2842 (1987).
15. D. Lubman (Ed.), *Lasers in Mass Spectrometry*. Oxford (1990).
16. R.B. van Bremen, M. Snow and R.J. Cotter, *Int. J. Mass Spectrom. Ion Proc.* **49**, 35 (1983).
17. R.J. Conzemius and J.M. Capellan, *Int. J. Mass Spectrom. Ion Phys.* **34**, 197 (1980).
18. R. Stoll and F.W. Röhlgen, *Z. Naturforsch.* **37a**, 9 (1982).
19. R.J. Cotter, *Anal. Chem.* **52**, 1767 (1980).
20. J. Grotemeyer and E.W. Schlag, *Angew. Chem.* **100**, 461 (1988).
21. J. Grotemeyer and E.W. Schlag, *Acc. Chem. Res.* **22**, 399 (1989).
22. T.D. Märk, *Int. J. Mass Spectrom. Ion Proc.* **79**, 1 (1987).
23. L. Bewig, U. Buck, C. Mehlmann and M. Winter, *Rev. Sci. Instrum.* **63**, 3936 (1992).
24. U. Boesl, J. Grotemeyer, K. Walter and E.W. Schlag, *Anal. Instrum.* **16**, 159 (1987).
25. (a) E.R. Rohwer, R.C. Beavis, C. Köster, J. Lindner, J. Grotemeyer and E.W. Schlag, *Z. Naturforsch.* **43a**, 1151 (1988); (b) F. Moritz, M. Dey, K. Zipperer, S. Prinke and J. Grotemeyer, *Org. Mass Spectrom.* **28**, 1467 (1993).
26. G.R. Kinsel, J. Lindner and J. Grotemeyer, *Org. Mass Spectrom.* **26**, 1052 (1991).
27. M.R. Haore, *Adv. Chem. Phys.* **40**, 49 (1979).
28. J. Jortner, *Ber. Bunsenges. Phys. Chem.* **88**, 188 (1984).
29. D.H. Levy, *Science* **214**, 263 (1981).
30. H.W. Liepmann and A. Roshko, in *Elements of Gas Dynamics*. Wiley, New York, p. 40 (1957).
31. J.B. Anderson, R.P. Andres and J.B. Fenn, *Supersonic Nozzle Beams*, 275 (1965).
32. M. Dey and J. Grotemeyer, *Org. Mass Spectrom.* **29**, 659 (1994).
33. (a) J. Grotemeyer and E.W. Schlag, *Org. Mass Spectrom.* **23**, 388 (1988); (b) K. Walter, J. Lindner, J. Grotemeyer and E.W. Schlag, *Chem. Phys.* **125**, 155 (1988); (c) R. Tembreull, D.M. Lubman, *Anal. Chem.* **59**, 1003 (1987).
34. A. Meffert, M. Dey and J. Grotemeyer, in preparation.

Received: 29 November 1994

Accepted: 24 January 1995

Letter: Support for the proposed observation by ionspray mass spectrometry of piroxicam/ β -cyclodextrin and terfenadine/ β -cyclodextrin non-covalent inclusion complexes

Dear Sir

In recent years increasing effort has been directed to the investigation of guest–host non-covalent inclusion complexes by mass spectrometry. Almost all of the so-called “soft” mass spectrometric methods have been exploited in order to generate and characterise intact charged species in the gas phase of such weak supramolecular associations.

We are presently concerned^{1–3} with the study of the non-covalent inclusion complexes of guest-drug molecules in the hydrophobic cavity of host-cyclic oligosaccharides such as cyclodextrins (CDs). These complexes are of current interest to the pharmaceutical industry, as they are able to improve the solubility, stability and bioavailability of the guest-drug.⁴

We have reported recently¹ the first results of a study by ionspray (IS)⁵ mass spectrometry of the non-covalent inclusion complexes⁶ of the anti-inflammatory piroxicam⁷ (**1**), and also the antihistaminic terfenadine⁸ (**2**) with β -cyclodextrin (β -CD). Using this inherently mild technique we have been able to detect effectively the gaseous protonated and cationated 1 : 1 drug/ β -CD adducts from the diluted solutions (5–20 ppm in 50 : 50 (v : v) water/acetonitrile) of the **1** and **2**/ β -CD inclusion complexes. Tandem-mass spectrometry⁹ experiments supported these results,¹ and, very interestingly, they showed that collision-induced dissociation of the gaseous protonated or cationated 1 : 1 drug/ β -CD adducts did not generate protonated or cationated β -CD species. Hence, the abundant protonated or cationated β -CD species observed in the normal IS mass spectra might reasonably be considered to originate from free β -CD, which is present in the sample solution, due to the dissociation equilibrium of the complexes, according to the behaviour in water already investigated by NMR.³

Our previous results,¹ however, did not allow the question to be answered as to whether true inclusion complexes rather than 1 : 1 drug/ β -CD clusters were detected as protonated or cationated species by IS mass spectrometry. In the present paper we report further experimental results, which can cast some light on this point. In particular, operating with the same instrument and conditions used previously,¹ we have run the IS mass spectra of the mechanical mixtures of 10 ppm β -CD + 1.6 ppm of **1** or + 2.5 ppm of **2**, both dissolved in 1 : 1 water/acetonitrile containing ammonium acetate 5×10^{-2} M. Such concentrations correspond to a 1 : 2 drug/ β -CD molar

ratio as for the related inclusion complexes. In both these cases we have observed the peaks of the protonated 1 : 1 drug/ β -CD adducts at m/z 1466.7 and 1606.7, respectively. These results are in agreement with an equilibrium between the inclusion complexes and their components in solution, according to the behaviour already investigated in water.³ Further, we have injected separately the solutions of pure β -CD and of the drugs in the above concentrations through a coaxial capillary inlet, in which contact of the β -CD and drug solutions was allowed only just before the terminal tip. Also in this case we have observed the weak peaks of protonated 1 : 1 drug/ β -CD adducts at m/z 1466.7 and 1606.7, for **1** and **2**, respectively. While these results might suggest a rather fast formation of the inclusion complexes from their free components in our polar medium, they do not rule out the possibility of formation of the corresponding ion–molecule clusters. Therefore, in order to probe such a point, we have run the IS mass spectra of the mechanical mixtures of **1** or **2** and maltohexaose (MH) (Fluka, CAS 34620-77-4), a non-cyclic oligosaccharide, which, obviously, is not able to give inclusion complexes while it should not behave much differently from β -CD as regards the capability of producing ion–molecule clusters with **1** or **2**.

Very interestingly, operating in the same solvent and molar concentrations of MH plus drug and with addition of ammonium acetate, as with the β -CD + drug mechanical mixtures above, we did not observe the peaks of the protonated or cationated 1 : 1 drug/ β -CD adducts, and analogous negative results have been obtained even with 10 times more concentrated solutions. For instance, the IS mass spectrum of pure MH (see Figure 1) is analogous to that of β -CD¹ and shows the great predominance of the ammonium, with minor sodium, cationated species (m/z 1008.4 and 1013.4, respectively), while the protonated species (m/z 991.3) is practically absent.

In conclusion these results strongly support that the protonated or cationated 1 : 1 drug/ β -CD adducts we detected and characterised in the previous work¹ by IS mass spectrometry and MS/MS, were true host–guest inclusion complex species, rather than just ion–molecule clusters. Moreover, a rather fast equilibrium between complexes and free components in the polar solvent used is confirmed, and the free β -CD present in

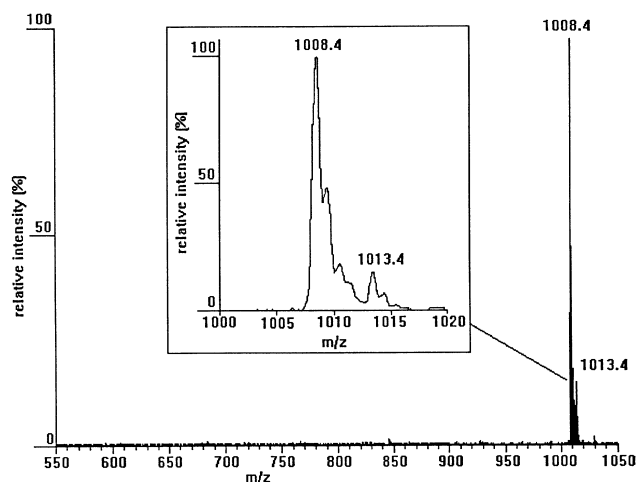


Figure 1. Ion spray mass spectrum of pure maltohexaose (MH).

solution can be detected by IS mass spectrometry only as ammonium or alkali cationated and not as protonated species.

Yours

Antonio Selva*

CNR-Centro di Studio sulle Sostanze Organiche Naturali,
c/o Dipartimento di Chimica, Politecnico, Via Mancinelli,
7, I-20131 Milano, Italy

Enrico Redenti, Margherita Zanol, Paolo Ventura

Chemical and Biopharmaceutical Department, Chiesi
Farmaceutici SpA, Via Palermo 26A, I-43100 Parma, Italy

Bruno Casetta

Perkin-Elmer Sciex ESSC, D-8011 Vaterstetten (Munich), Germany

References

1. A. Selva, E. Redenti, M. Zanol, P. Ventura and B. Casetta, *Org. Mass Spectrom.* **28**, 983 (1993), and references therein; A. Selva, E. Redenti, M. Zanol, P. Ventura and B. Casetta, *I° MS-Pharmaday*, Siena (Italy), 2–4 June 1993, book of abstracts, p. 40.
2. E. Redenti, A. Selva, M. Pasini, P. Ventura and B. Casetta, *7th International Cyclodextrins Symposium*, Tokyo, April 25–28 1994, book of abstracts, p. 65; A. Selva, E. Redenti, M. Pasini, P. Ventura and B. Casetta, *J. Mass Spectrom.* **30**, 219 (1995); A. Mele and A. Selva, *13th International Mass Spectrometry Conference*, Budapest, 29 August–2 September 1994, book of abstracts, p. 215; A. Mele and A. Selva, *J. Mass Spectrom.* (in press).
3. G. Fronza, A. Mele, E. Redenti and P. Ventura, *J. Pharm. Sci.* **81**, 1162 (1992); E. Redenti, M. Pasini, P. Ventura, A. Spisni, M. Vikmon and J. Szejtli, *J. Incl. Phenom.* **15**, 281 (1993).
4. J. Szejtli, *Cyclodextrins and their Inclusion Complexes*. Akadémiai Kiadó, Budapest (1982); K.H. Fromming and J. Szejtli, *Cyclodextrins in Pharmacy*. Kluwer Academic Publishers, Dordrecht (1994).
5. A.P. Bruins, T.R. Covey and J.D. Henion, *Anal. Chem.* **59**, 2642 (1987).
6. J. Szejtli, *Cyclodextrin Technology*. Kluwer Academic Publishers, Dordrecht (1988).
7. P.L. Boardman, M.J. Burke and A.V. Camp, *Eur. J. Rheumatology and Inflammation* **6**, 73 (1983).
8. D. McTavish, K.L. Goa and M. Ferrill, *Drugs* **39**, 552 (1990).
9. F.W. McLafferty, *Tandem Mass Spectrometry*. Wiley, New York (1983).

Received: 10 November 1994

Accepted: 19 February 1995

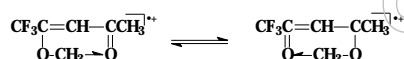
A reply to the comment on "Isodesmic reactions and thermochemistry of ions"

Dear Sir

Readers will be aware that it is scarcely possible to find a compound which does not produce rearrangement ions under electron impact (EI) (the processes of H- and C-scrambling are obviously included). There is a wealth of data collected by the international community of mass spectrometrists representing hydrogen and skeletal rearrangements. Often product ions formed after isomerisation of any precursor ions constitute the greater part of the total ion current. All this means that in such cases the rearrangement processes are accessible both energetically and kinetically. In this respect we are saying nothing new to practicing mass spectrometrists in our Account.¹ We give only the quantitative energetical grounds for both simple bond cleavage and rearrangement processes.

It would seem that some readers consider that we reject too easily such "respected" notions as kinetic shift, reverse critical energy E_R and others. That is just not the case. Seven years ago we measured appearance energies (AE s) of $[M-R']^+$ (or $[M-R]^+$) ions originating from more than 20 aliphatic and aromatic β -diketones.² In nearly all instances, we obtained ions of structure $RC(OH)=CHC\equiv O^+$. Although neutral molecules of β -diketones in the gas phase exist predominantly in one of two possible enol forms (with an admixture of keto-form and other enol), energetically accessible 1,3- (diketo-form \rightarrow enol) or 1,5- (one enol to another) hydrogen shifts in the molecule ion produce an ionized isomer which gives rise to the most stable fragment $RC(OH)=CHC\equiv O^+$. Even in isomers $CF_3C(OCH_3)=CHCOCH_3$ and $CF_3COCH=C(OCH_3)CH_3$ the AE s of $(M-CH_3)^+$ [and of $(M-CF_3)^+$] ions were nearly identical, manifesting a facile CH_3 - "tautomerization" in the molecule ion:²

$AE [M-CH_3]^+$	9.67 eV	9.66 eV
-----------------	---------	---------

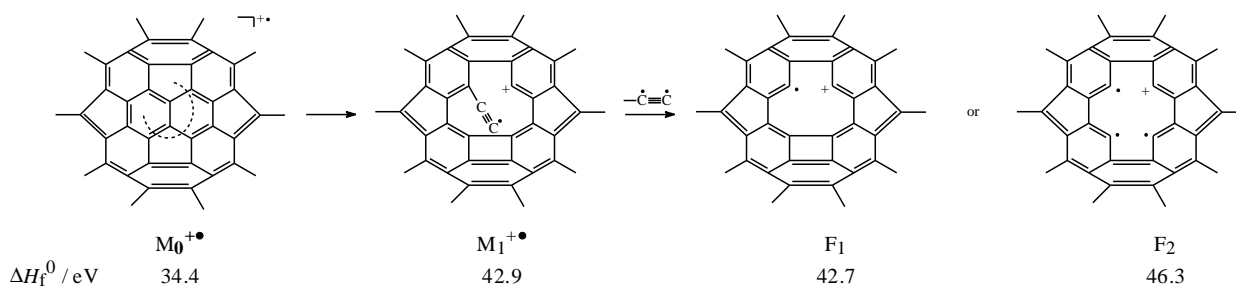


$AE [M-CF_3]^+$	9.71 eV	9.76 eV
-----------------	---------	---------

In $C_6H_5COCH_2COR'$ molecules ($R' = CH_3, C_2H_5, c-C_6H_{11}, CH_2C_6H_5, CF_3, n-C_3F_7, n-C_6F_{13}, \text{cyclo-}C_6F_{11}$) at the thresholds of $[M-R']^+$ formation, the ions of $C_6H_5C(OH)=CHC\equiv O^+$ structures were obtained. Similarly, $XC_6H_4C(OH)=CHC\equiv O^+$ ions were registered from $p-XC_6H_4COCH_2COCF_3$ ($X = CH_3, F, Br$ and H). But, surprisingly, in the case of $p-CH_3OC_6H_4COCH_2COR_f$ ($R_f = CF_3$ or $n-C_6F_{13}$), AE s $[M-R_f]^+$ values were by *c.* 0.9 eV higher than those expected for ions

of the $CH_3OC_6H_4C(OH)=CHC\equiv O^+$ structure. It was clear that neither kinetic shift nor reverse critical energy (at those times we, along with many other investigators, also admitted their importance) were responsible for the increase in AE , since both effects were virtually absent in nearly 20 structurally close compounds. The experimental AE values corresponded to an ion of structure $CH_3OC_6H_4COCH_2C\equiv O^+$, the heat of formation (ΔH_f) of the latter being estimated from the known heat of formation of the $CH_3C\equiv O^+$ ion. Only after several months of doubts and trials (the AE s of these ions were remeasured several times) could we answer the question of why in the case of diketones containing the $CH_3OC_6H_4$ -group, an ion in its diketo-form was produced despite being less stable by 90 kJ mol⁻¹ than its enol tautomer. The heats of isomerization ΔH_{iso} of ionized ketoenol to its diketo-form are 0.6–0.8 eV for aliphatic (compare with 0.6 eV for acetone)³ and 1.0–1.1 eV for aromatic β -diketones.² In most of the compounds studied the values of the critical energy E_0 for R' elimination from $[RC(OH)=CHCOR']^{+*}$ do not surpass the ΔH_{iso} values. But the introduction of the CH_3O -group drastically decreases the ionization energy (IE) of the molecule from 9.03 eV ($R = C_6H_5$) to 8.23 eV ($R = p-CH_3OC_6H_4$) and only slightly decreases the $AE [M-R_f]^+$, due to the remote position of the CH_3O -group from the breaking bond. Hence, the E_0 for R_f loss increases to *c.* 2.0 eV and the molecule ion gains an "energetical" opportunity to isomerize to an ionized diketo-form, spending only 1.0 eV as compared with 2.0 eV for simple bond cleavage. Now, a newly born isomer decomposes through its two most energetically favourable processes of simple bond cleavage giving $CH_3OC_6H_4COCH_2C\equiv O^+ + CF_3^\bullet$ and $CH_3OC_6H_4C\equiv O^+ + C^\bullet H_2COCF_3$ [but not $C^\bullet H=C(OH)CF_3$] fragments. This detailed analysis of the reasons and driving forces of rearrangement processes made in 1988 gave a start to the formation of the position expressed on a broader scale in our Account.¹

We consider that our Account¹ appeared at a proper time after reading the comments of McAdoo⁴ and the communication of Yoo *et al.*,⁵ in which a kinetic shift of 30 eV (!) or 2900 kJ mol⁻¹ was attributed to the decomposition of fullerene molecule ions $C_{60}^{+*} \rightarrow C_{58}^{+*} + C_2$ with an estimated E_0 of 6.0–6.5 eV for the latter process. We have made a quick (rather an approximate) estimate of the heats of formation of C_{58}^{+*} isomers (they should not be confused with ionized, stable C_{58} -fullerene similar to C_{60}).⁶ Of course, we represent only their fragments F_1 and F_2 (Figure 1) presuming the structure



$$\Delta H_f^\circ(M_0^{+\bullet}) = \Delta H_f^\circ(C_{60}) + IE(C_{60}) = 26.82 \text{ eV}^7 + 7.57 \text{ eV}^5 = 34.39 \text{ eV}.$$

$$\Delta H_f^\circ(M_1H_2 \text{ or } C_{60}H_2) = \Delta H_f^\circ(C_{58}H_2) - C_B(H) + C_B(C) + C_t(H) = 28.0 - 0.14 + 0.25 + 1.17 = 29.28 \text{ eV}.$$

$$\Delta H_f^\circ(M_1^{+\bullet}) = \Delta H_f^\circ(M_1) + \Delta H_f^\circ(HC \equiv C^\bullet) - \Delta H_f^\circ(HC \equiv CH) + \Delta H_f^\circ(C_6H_5^\bullet) - \Delta H_f^\circ(C_6H_6) = 29.28 + 5.23 - 2.35 + 11.62 - 0.86 = 42.92 \text{ eV}.$$

$$\Delta H_f^\circ(C_{58}H_2) = \Delta H_f^\circ(C_{60}) - 2[\Delta H_f^\circ(C_{60} : 60)] + 2[C_B(H)] = 26.82 \text{ eV} - 2(0.446) + 2(0.145) = 28.0 \text{ eV}.$$

$$\Delta H_f^\circ(F_1) = \Delta H_f^\circ(C_{58}H_2) + \Delta H_f^\circ(C_6H_5^\bullet) + \Delta H_f^\circ(C_6H_5^\bullet) - 2\Delta H_f^\circ(C_6H_6) + \Delta H_{\text{strain}}(\text{cyclobutene}) = 28.0 + 11.62 + 3.53 - 2(0.86) + 1.29 = 42.72 \text{ eV}.$$

$$AE(F_1) = \Delta H_f^\circ(F_1) + \Delta H_f^\circ(C \equiv C^\bullet) - \Delta H_f^\circ(C_{60}) = 42.72 + 6.16 - 26.82 = 22.1 \text{ eV}.$$

Figure 1. Heats of formation of $C_{60}^{+\bullet}$ and $C_{58}^{+\bullet}$ isomers. $C_B(H)$ and $C_B(C)$ signify benzene C atoms attached to the H and carbon of the triple bond, respectively; $C_t(H)$ indicates a carbon atom with triple bond attached to a H atom (see Reference 7).

of the rest of the molecule remains as in the C_{60} molecule (the thermochemical data were taken from References 7 and 8).

If an isomer F_2 is assumed, then its AE becomes 25.7 eV. We do not think that enclosure of the second four-membered ring is possible in F_1 . Any further opening of the benzene ring in $M_1^{+\bullet}$ will increase the heat of formation of both the isomeric molecule ion $C_{60}^{+\bullet}$ and the fragment ion $C_{58}^{+\bullet}$, since the $\Delta\Delta H_f$ contribution from $-C \equiv C-$ is higher than $C=C<$ in benzene, and will result in a further increase in the AE of the $C_{58}^{+\bullet}$ ion approaching the experimental value of AE $C_{58}^{+\bullet}$ ion. In this instance of fullerene fragmentation, it is not necessary to call for a kinetic shift of 30 eV.

We are compelled to discuss all these dull calculations (both in diketones and fullerene), because it is the only way to represent a reasonable energetical picture of any fragmentation process. It is much easier to suggest a kinetic shift and other effects than to estimate the heats of formation of possible isomers. Having measured the AEs $[M-CH_3]^+$ from compounds 1–3 and $[M-Cl]^+$ from compound 4 ($[C_9H_9O]^+$ being the only fragment at low energies), we estimated, instead, the heats of formation of 29 $[C_9H_9O]^+$ isomers using isodesmic reactions and found the structures of ions corresponding to

experimental AE values. We also suggested reasonable mechanisms of their formation (Figure 2).¹⁰

In the further example of compound 5, instead of obtaining $[M-CH_3]^+$ ions of the expected structures F_3 and F_4 with AEs (estimated) of 9.9 and 10.0 eV, respectively, we measured AE 9.0 eV for $[M-CH_3]^+$ ($IE = 8.84 \text{ eV}$) and estimated the heats of formation of 35 $C_5H_5O^+$ isomers rather than looking for “hot bands” (Figure 3).¹¹

In our Account¹ it was shown that elimination of HX from $[CH_2=CHX]^+$ ions ($X = H, CH_3, Br, Cl$) occurs with $E_R \approx 0$. Elimination of H_2 from $[CH_3CH_3]^+$ does not indicate a noticeable E_R value either: $AE(M-H_2)^+ = 12.1 \text{ eV}$ [by EI¹² and $AE_{\text{calc}} = 11.93 \text{ eV}$ (from $\Delta H_f^\circ C_2H_6, H_2$ and $C_2H_4^{+\bullet}$)]. In our discussion we omitted the processes of 1,1-elimination. Our analysis of data taken from References 12 and 13 indicates $AE_{\text{exp}} \approx AE_{\text{calc}}$ for $[M-H_2]^+$ ions coming from $PH_3, AsH_3, SiH_4, GeH_4$ for $FCH=C^+$ formation from $[FCH=CH_2]^+$, for HF loss from $[FCH=CH_2]^+$ giving $^+C=CH_2$. AEs only slightly higher than calculated AEs have been observed for HBr^+ (from CH_3Br), ^+NH (from NH_3), $^+CF_2$ (from CF_2Cl_2).¹² At the same time the high value of $AE H_2^+$ 15.42 eV ($AE_{\text{calc}} = 14.26 \text{ eV}$) originating from $CH_2O^{+\bullet}$ ¹² can be explained by the involvement of excited states at high values of AEs.¹⁴ Such a possibility was not discussed in our publication.¹ This involve-

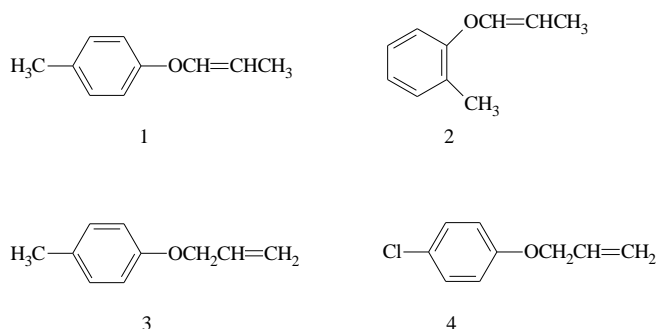


Figure 2. Compounds 1–4.

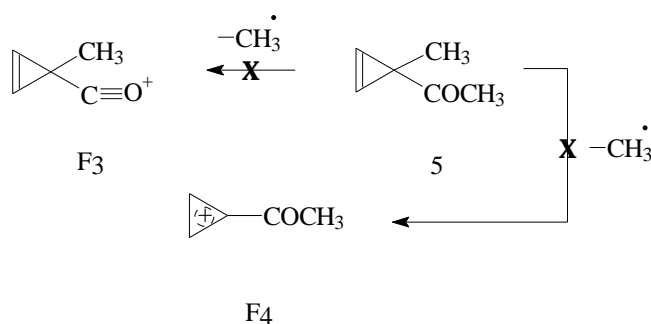
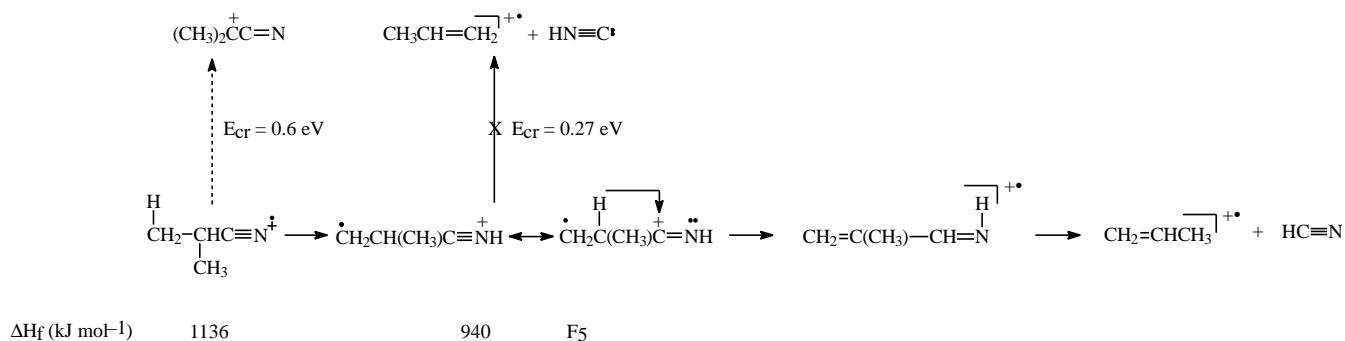


Figure 3. Compound 5 and fragments F_3 and F_4 .

Figure 4. Fragmentation of $(\text{CH}_3)_2\text{CHCN}$.

ment could explain the higher *AE* values for H_2 loss from $\text{H}_2\text{C}=\text{X}^+$ species ($\text{X} = \text{OH}, \text{NH}_2, \text{SH}$) although, to our knowledge, the experimental values of *AEs* for these processes are not available. An additional source of higher *AEs* in this case could originate from the contribution of the isomers $:\text{C}=\text{X}^+$ (having much higher heats of formation than their isomers $\text{HC}\equiv\text{O}^+$ and others) to the ionization efficiency curve.

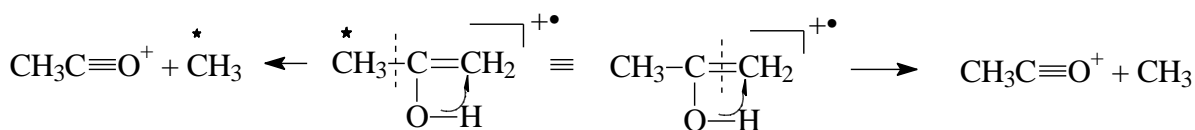
The energetical and kinetic accessibility of 1,2-, 1,3- and 1,4-H-shifts could be further illustrated by fragmentation of $(\text{CH}_3)_2\text{CHCN}$ molecules:¹⁵ $\text{IE} = 11.53 \text{ eV}$, $\text{AE} (\text{M}-27)^{\bullet+} = 11.52 \text{ eV}$, $\text{AE}_{\text{calc}} = 11.34 \text{ eV}$ [$\text{CH}_3\text{CH}=\text{CH}_2^{\bullet+} + \text{HC}\equiv\text{N}$], $\text{AE}_{\text{calc}} = 11.8 \text{ eV}$ [$\text{CH}_3\text{CH}=\text{CH}_2^{\bullet+} + \text{HN}\equiv\text{C}^{\bullet}$] (all thermochemical data necessary for these calculations are taken from References 8, 12 and 16). The mechanism of elimination of cyanic acid includes at least three rearrangement processes, all three occurring with zero E_0 and obviously possessing E_0 values below those necessary for simple bond cleavages, 0.6 eV and 0.27 eV in molecule ion and ion F_5 , respectively (Figure 4).

We quote Clark:¹⁷ "The above results not only suggest that suprafacial 1,3-hydrogen shifts in olefin radical cations should be facile processes but also hint at a general willingness of radical cations to undergo sigmatropic rearrangements that would be difficult in the neutral parent molecules". For the moment, we think, we demonstrate enough proofs and examples of accessibility of rearrangement processes in positively charged species. An explanation of an "asymmetric dissociation of the energized, structurally symmetric intermediate" (we quote McAdoo)⁴ can be made in two ways without suggesting the existence of "non-ergodic" processes. First, all possible isomers $[\text{C}_3\text{H}_6\text{O}]^{\bullet+}$ should be considered (and not only $[\text{CH}_3\text{COCH}_3]^{\bullet+}$ and its enol form $[\text{CH}_2=\text{C}(\text{OH})\text{CH}_3]^{\bullet+}$) as possible precursors for CH_3 loss. Second, non-equivalence of CH_3 groups lost could be explained by fragmentation of the ionized enol form (consistent with data in Reference 18) (Figure 5).

In our Account¹ we did not reject completely the involvement of isolated states or participation of processes with high-energy demands. Thus, we mentioned¹ that in our experience a small proportion of ions (1% or less) could be involved in highly energetical processes. This could be probably referred to some (but not all) metastables whose behaviour is the main source of data on high values of critical energies for reverse processes. Hence we propose to Professor McAdoo to come to a consensus that 99% of the processes taking place in both ion source and field free regions behave in an "ergodic" manner, whereas the behaviour of the rest is governed, possibly, by other driving forces. Returning to β -diketones (see above), we remind the reader that the structure of $p\text{-XC}_6\text{H}_4\text{C}(\text{OH})=\text{CHC}\equiv\text{O}^+$ was established for $[\text{M}-\text{CF}_3]^+$ ions originating from $p\text{-XC}_6\text{H}_4\text{COCH}_2\text{COCF}_3$ molecules ($\text{X} = \text{H}, \text{CH}_3, \text{Br}, \text{F}$) at low energies. But defocusing of metastable ions at 70 eV ionizing energy gave a linear correlation for the I_{m^*}/I_{M^+} ratio and $\% \Sigma [\text{M}-\text{CF}_3]^+$ ($\text{X} = \text{H}, \text{CH}_3, \text{C}(\text{CH}_3)_3, \text{F}, \text{Br}$ and OCH_3). This indicates the common structure of those molecule ions which lose CF_3 in the field-free region, and since for $\text{X} = \text{OCH}_3$ the structure $\text{CH}_3\text{OC}_6\text{H}_4\text{COCH}_2\text{C}\equiv\text{O}^+$ was proved (see above), the diketo-form should be attributed to the whole series. The latter structure for $[\text{M}-\text{CF}_3]^+$ ions formed in the field-free region is further supported by observation of the linear correlation of $I_{m^*}/I_{3(\text{M}-\text{CF}_3)^{\bullet+}}$ ratio and $\% \Sigma [\text{M}-\text{CF}_3-\text{CH}_2=\text{C}=\text{O}]^+$ for all X except $\text{N}(\text{CH}_3)_2$.²

References

1. V.V. Takhistov and D.A. Ponomarev, *Org. Mass Spectrom.* **29**, 395 (1994).
2. V.M. Orlov, Y.V. Rashkes, T.V. Siretskaya and V.V. Takhistov, *Zh. Obshch. Khim. (Russ.)* **58**, 429 (1988).

Figure 5. Non-equivalence of CH_3 groups.

3. J.L. Holmes and F.P. Lossing, *J. Am. Chem. Soc.* **102**, 1591 (1980).
4. D.J. McAdoo, *J. Mass Spectrom.*, in press.
5. R.K. Yoo, B. Ruscic and J. Berkowitz, *J. Chem. Phys.* **90**, 911 (1992).
6. B.L. Zhang, C.Z. Wang, K.M. Ho, C.H. Xu and C.T. Chan, *J. Chem. Phys.* **97**, 5007 (1992).
7. S.W. Benson, *Thermochemical Kinetics*. Wiley, New York (1968).
8. V.V. Takhistov, *Organic Mass Spectrometry*. Nauka, Leningrad (1990) (in Russian).
9. W.V. Steele, R.D. Chirico, N.K. Smith, W.E. Billups, P.R. Elmore and A.E. Wheeler, *J. Phys. Chem.* **96**, 4731 (1992).
10. V.V. Takhistov, D.A. Ponomarev, A.D. Misharev, V.M. Orlov and K. Pihlaja, *Zh. Obshch. Khim. (Russ.)* **64**, 110 (1994).
11. I.N. Domnin, V.V. Takhistov and V.M. Orlov, in preparation.
12. R.D. Levin and S.G. Lias, *Ionization Potential and Appearance Potential Measurements, 1971–1981*. National Bureau of Standards, Washington, DC.
13. J. Berkowitz, G.B. Ellison and D. Gutman, *J. Phys. Chem.* **98**, 2744 (1994).
14. K. Levsen, *Fundamental Aspects of Organic Mass Spectrometry*. Verlag Chemie, Weinheim (1978).
15. V.V. Takhistov and V.M. Orlov, unpublished results.
16. J.B. Pedley, R.D. Naylor and S.P. Kirby, *Thermochemical Data of Organic Compounds, 2nd Edn.* Chapman and Hall, London (1986).
17. T. Clark, *J. Am. Chem. Soc.* **109**, 6838 (1987).
18. J.H. Beynon, R.M. Caprioli and R.G. Cooks, *Org. Mass Spectrom.* **9**, 1 (1974).

V.V. Takhistov
Chemical Faculty,
St Petersburg State University,
Stary Petershof,
198904 St Petersburg
Russia
D.A. Ponomarev*
Faculty of Chemical Engineering,
St Petersburg Forest Technical Academy
Institutski 5,
194018 St Petersburg
Russia

Received: 15 November 1994

Accepted 5 January 1995